VOLUME 78 DECEMBER 19, 1974 NUMBER 26

JPCHAx

THE JOURNAL OF
PHYSICAL CHEMISTRY

PUBLISHED BIWEEKLY BY THE AMERICAN CHEMICAL SOCIETY

THE JOURNAL OF PHYSICAL CHEMISTRY

BRYCE CRAWFORD, Jr., *Editor*
WILMER G. MILLER, *Associate Editor*
ROBERT W. CARR, Jr., FREDERIC A. VAN-CATLEDGE, *Assistant Editors*

EDITORIAL BOARD: A. O. ALLEN (1970–1974), C. A. ANGELL (1973–1977),
F. C. ANSON (1974–1978), V. A. BLOOMFIELD (1974–1978), J. R. BOLTON (1971–1975),
L. M. DORFMAN (1974–1978), M. FIXMAN (1970–1974), H. S. FRANK (1970–1974),
R. R. HENTZ (1972–1976), W. J. KAUZMANN (1974–1978), R. L. KAY (1972–1976),
D. W. McCLURE (1974–1978), R. M. NOYES (1973–1977), J. A. POPLE (1971–1975),
B. S. RABINOVITCH (1971–1975), H. REISS (1970–1974), S. A. RICE (1969–1975),
F. S. ROWLAND (1973–1977), R. L. SCOTT (1973–1977), A. SILBERBERG (1971–1975),
J. B. STOTHERS (1974–1978), W. A. ZISMAN (1972–1976)

AMERICAN CHEMICAL SOCIETY, *1155 Sixteenth St., N.W., Washington, D. C. 20036*

Books and Journals Division

JOHN K CRUM *Director*
RUTH REYNARD *Assistant to the Director*

CHARLES R. BERTSCH *Head, Editorial Processing Department*
D. H. MICHAEL BOWEN *Head, Journals Department*
BACIL GUILEY *Head, Graphics and Production Department*
SELDON W. TERRANT *Head, Research and Development Department*

©Copyright, 1974, by the American Chemical Society. Published biweekly by the American Chemical Society at 20th and Northampton Sts., Easton, Pa. 18042. Second-class postage paid at Washington, D. C., and at additional mailing offices.

All manuscripts should be sent to *The Journal of Physical Chemistry,* Department of Chemistry, University of Minnesota, Minneapolis, Minn. 55455.

Additions and Corrections are published once yearly in the final issue. See Volume 77, Number 26 for the proper form.

Extensive or unusual alterations in an article after it has been set in type are made at the author's expense, and it is understood that by requesting such alterations the author agrees to defray the cost thereof.

The American Chemical Society and the Editor of *The Journal of Physical Chemistry* assume no responsibility for the statements and opinions advanced by contributors.

Correspondence regarding accepted copy, proofs, and reprints should be directed to Editorial Processing Department, American Chemical Society, 20th and Northampton Sts., Easton, Pa. 18042. Department Head: CHARLES R. BERTSCH. Assistant Department Head: MARIANNE C. BROGAN. Assistant Editor: CELIA B. McFARLAND. Editorial Assistant: JOSEPH E. YURVATI.

Advertising Office: Centcom, Ltd., 50 W. State St., Westport, Conn. 06880.

Business and Subscription Information

Send all new and renewal subscriptions *with payment* to: Office of the Controller, 1155 16th Street, N.W., Washington, D. C. 20036. Subscriptions should be renewed promptly to avoid a break in your series. All correspondence and telephone calls regarding changes of address, claims for missing issues, subscription service, the status of records, and accounts should be directed to Manager, Membership and Subscription Services, American Chemical Society, P.O. Box 3337, Columbus, Ohio 43210. Telephone (614) 421-7230.

On changes of address, include both old and new addresses with ZIP code numbers, accompanied by mailing label from a recent issue. Allow four weeks for change to become effective.

Claims for missing numbers will not be allowed (1) if loss was due to failure of notice of change in address to be received before the date specified, (2) if received more than sixty days from date of issue plus time normally required for postal delivery of journal and claim, or (3) if the reason for the claim is "issue missing from files."

Subscription rates (1974): members of the American Chemical Society, $20.00 for 1 year; to nonmembers, $60.00 for 1 year. Those interested in becoming members should write to the Admissions Department, American Chemical Society, 1155 Sixteenth St., N.W., Washington, D. C. 20036. Postage to Canada and countries in the Pan-American Union, $5.00; all other countries, $6.00. Air freight rates available on request. Single copies for current year: $3.00. Rates for back issues from Volume 56 to date are available from the Special Issues Sales Department, 1155 Sixteenth St., N.W., Washington, D. C. 20036.

Subscriptions to this and the other ACS periodical publications are available on microfilm. Supplementary material not printed in this journal is now available in microfiche form on a current subscription basis. For information on microfilm or microfiche subscriptions, write Special Issues Sales Department at the address above.

Notice to Authors last printed in the issue of June 6, 1974

THE JOURNAL OF

PHYSICAL CHEMISTRY

Volume 78, Number 26 December 19, 1974

JPCHAx 78(26) 2637–2726 1974
ISSN 0022-3654

Photochemistry of 7-Ketonorbornane in Vapor Phase and Solution . . . **Timothy F. Thomas,* Bogdan Matuszewski, and R. S. Givens*** 2637

Ion–Molecule Reactions in Monosilane–Acetylene Mixtures . . **T. M. Mayer and F. W. Lampe*** 2645

Kinetic Isotope Effects in the Reactions of Hydrogen and Deuterium Atoms with Dimethyl Ether and Methanol . . . . . **James F. Meagher, P. Kim, J. H. Lee, and Richard B. Timmons*** 2650

Comparison of General-Acid-Catalyzed Ethyl Vinyl Ether Hydrolysis in 80% Dimethyl Sulfoxide with that in Water . . . . **Robert Eliason* and Maurice M. Kreevoy** 2658

Pulse Radiolysis Study of Aqueous Hydrogen Cyanide and Cyanide Solutions . . . . . **D. Behar** 2660

Thermal Decomposition of Three Crystalline Modifications of Anhydrous Copper(II) Formate . . . **Andrew Knox Galwey,* David M. Jamieson, and Michael Ewart Brown** 2664

The Copper|Copper Oxide|Carbonate Electrode at 350° in Fused Potassium Nitrate–Sodium Nitrate . . . . **A. G. Keenan* and Carlos G. Fernandez** 2670

Dependence of the Glass Transition Temperature on Heating and Cooling Rate . . . **Cornelius T. Moynihan,* Allan J. Easteal, James Wilder, and Joseph Tucker** 2673

The Four Electron (or Hole) Noncubic Ligand Field Spectrum. I. Tetragonal Energy Levels . . . **Jayarama R. Perumareddi** 2678■

Approximate Molecular Orbital Study of Organic Positron and Positronium Complexes . . . **W. J. Madia, J. C. Schug, A. L. Nichols, and H. J. Ache*** 2682

Conductance Behavior of Some Ammonium and Partially Substituted Ammonium Tetraphenylborates in 3-Methyl-2-oxazolidone and 3-*tert*-Butyl-2-oxazolidone at 25° . . . **Barbara J. Barker and Paul G. Sears*** 2687■

Conductance Behavior of Tetraalkylammonium Salts in 3-*tert*-Butyl-2-oxazolidone at 25° . . . **Barbara J. Barker, Hugh L. Huffman, Jr., and Paul G. Sears*** 2689■

Heats of Transport of Gases. III. Thermoosmosis of Ternary Gaseous Mixtures . . . **R. P. Rastogi* and A. P. Rai** 2693

COMMUNICATIONS TO THE EDITOR

On the Carcinogenicity of Bis(chloromethyl) Ether and Chloromethyl Methyl Ether . . . **Lloyd D. Taylor* and Myron S. Simon** 2696

Scavenging of Electrons in 3-Methylpentane Glass at 77 K . . . **J. Kroh,* J. Mayer, E. Wojciechowska, and J. Grodkowski** 2696

Additions and Corrections 2698

Author Index to Volume 78, 1974 2699

Keyword Index to Volume 78, 1974 2715

ห้องสมุด กรมวิทยาศาสตร์

■ Supplementary and/or miniprint material for this paper is available separately, in photocopy or microfiche form. Ordering information is given in the paper.

* In papers with more than one author, the asterisk indicates the name of the author to whom inquiries about the paper should be addressed.

AUTHOR INDEX

Ache, H. J., 2682

Barker, B. J., 2687, 2689
Behar, D., 2660
Brown, M. E., 2664

Easteal, A. J., 2673
Eliason, R., 2658

Fernandez, C. G., 2670

Galwey, A. K., 2664
Givens, R. S., 2637
Grodkowski, J., 2696

Huffman, H. L., Jr., 2689

Jamieson, D. M., 2664

Keenan, A. G., 2670
Kim, P., 2650
Kreevoy, M. M., 2658
Kroh, J., 2696

Lampe, F. W., 2645
Lee, J. H., 2650
Madia, W. J., 2682
Matuszewski, B., 2637
Mayer, J., 2696
Mayer, T. M., 2645
Meagher, J. F., 2650
Moynihan, C. T., 2673

Nichols, A. L., 2682

Perumareddi, J. R., 2678

Rai, A. P., 2693
Rastogi, R. P., 2693
Schug, J. C., 2682
Sears, P. G., 2687, 2689
Simon, M. S., 2696

Taylor, L. D., 2696
Thomas, T. F., 2637
Timmons, R. B., 2650
Tucker, J., 2673

Wilder, J., 2673
Wojciechowska, E., 2696

THE JOURNAL OF PHYSICAL CHEMISTRY

Volume 78

JANUARY—JUNE 1974

PAGES 1-1338

BRYCE CRAWFORD, Jr., *Editor*
Wilmer G. Miller, *Associate Editor*
Robert W. Carr, Jr., Frederic A. Van-Catledge, *Assistant Editors*

EDITORIAL BOARD

A. O. Allen
C. A. Angell
F. C. Anson
V. A. Bloomfield
J. R. Bolton
L. M. Dorfman
M. Fixman
H. S. Frank
R. R. Hentz
W. J. Kauzmann
R. L. Kay
D. W. McClure
R. M. Noyes
J. A. Pople
B. S. Rabinovitch
H. Reiss
S. A. Rice
F. S. Rowland
R. L. Scott
A. Silberberg
J. B. Stothers
W. A. Zisman

AMERICAN CHEMICAL SOCIETY, BOOKS AND JOURNALS DIVISION

John K Crum, *Director*
Ruth Reynard, *Assistant to the Director*

Charles R. Bertsch, *Head, Editorial Processing Department*
D. H. Michael Bowen, *Head, Journals Department*
Bacil Guiley, *Head, Graphics and Production Department*
Seldon W. Terrant, *Head, Research and Development Department*

Joseph E. Yurvati, *Editorial Assistant*

THE JOURNAL OF PHYSICAL CHEMISTRY

Volume 78

JULY—DECEMBER 1974

PAGES 1339-2726

BRYCE CRAWFORD, Jr., *Editor*
Wilmer G. Miller, *Associate Editor*
Robert W. Carr, Jr., Frederic A. Van-Catledge, *Assistant Editors*

EDITORIAL BOARD

A. O. Allen
C. A. Angell
F. C. Anson
V. A. Bloomfield
J. R. Bolton
L. M. Dorfman
M. Fixman

H. S. Frank
R. R. Hentz
W. J. Kauzmann
R. L. Kay
D. W. McClure
R. M. Noyes
J. A. Pople
B. S. Rabinovitch

H. Reiss
S. A. Rice
F. S. Rowland
R. L. Scott
A. Silberberg
J. B. Stothers
W. A. Zisman

AMERICAN CHEMICAL SOCIETY, BOOKS AND JOURNALS DIVISION

John K Crum, *Director*
Ruth Reynard, *Assistant to the Director*

Charles R. Bertsch, *Head, Editorial Processing Department*
D. H. Michael Bowen, *Head, Journals Department*
Bacil Guiley, *Head, Graphics and Production Department*
Seldon W. Terrant, *Head, Research and Development Department*

Joseph E. Yurvati, *Editorial Assistant*

THE JOURNAL OF
PHYSICAL CHEMISTRY

Registered in U. S. Patent Office © Copyright, 1974, by the American Chemical Society

VOLUME 78, NUMBER 26 DECEMBER 19, 1974

Photochemistry of 7-Ketonorbornane in Vapor Phase and Solution

Timothy F. Thomas,*

Department of Chemistry, University of Missouri—Kansas City, Kansas City, Missouri 64110

Bogdan Matuszewski,[1] and R. S. Givens*

Department of Chemistry, University of Kansas, Lawrence, Kansas 66044 *(Received March 25, 1974; Revised Manuscript Received August 21, 1974)*

Publication costs assisted by the University of Missouri—Kansas City

The photochemistry of 7-ketonorbornane (1) has been studied in both vapor phase and solution. The products formed in primary processes are 3-cyclohexenecarboxaldehyde (2), 1,5-hexadiene (3), bicyclo[2.2.0]hexane (4), and carbon monoxide. Quantum yields of product formation are the following: $\phi_2 = 0.16$, $\phi_3 = 0.008$, and $\phi_4 = 0.001_7$ in ether solution at 307 nm; $\phi_2 = 0.090_5$, $\phi_3 = 0.091_5$, and $\phi_4 = 0.018$ in ~0.9 Torr of the vapor at 313 nm; and $\phi_2 = 0.097$, $\phi_3 = 0.137$, and $\phi_4 = 0.027$ in ~0.85 Torr of the vapor at 302.5 nm. Fluorescence lifetime of the vapor has been found to be 1.2×10^{-8} sec for λ_{ex} 337 nm, leading to a value of 6.6×10^{-5} sec for the natural radiative lifetime (Υ_0) of the fluorescence. Fluorescence quantum yields of the vapor decrease from 1.7×10^{-4} for λ_{ex} 334 nm to $\approx 1 \times 10^{-6}$ at 291 nm. A reaction mechanism featuring an acyl–alkyl biradical (vibrationally excited in the vapor phase system) is proposed. Comparison with previously published results for acyclic and cyclic ketones, and interpretation of additional fluorescence quantum yield data obtained for cyclobutanone and acetone, leads to the suggestion that the reaction proceeds *via* the triplet n,Π* state at longer wavelengths but that predissociation from the singlet state predominates at the shorter wavelengths.

Introduction

Although the photochemistry of monocyclic ketones has been the subject of considerable investigation in recent years, only a few bicyclic ketones have been studied[2-5] and in no case has a complete determination of product quantum yields been made for the same parent compound in both vapor phase and solution. Such a determination is clearly essential to ascertain the effects of the bicyclic structure on the rates of competing photochemical and photophysical processes. 7-Ketonorbornane (1) was chosen for a complete study for several reasons. First, it can be compared with the well-studied cyclic ketones such as cyclopentanone, to which it is structurally related. Second, it was hoped to examine the rates of unimolecular reaction of vibrationally hot products formed in the primary photodissociation, as has been done in the case of other cyclic and bicyclic ketones and azo compounds.[5,6-8] Finally, the compound has been synthesized only relatively recently and its photochemistry has not (to our knowledge) been examined before.

Experimental Section

Materials. 7-Norborneol was synthesized from 7-norbornadienyl acetate in 58% yield by the method of Story.[9] The alcohol was then oxidized in a CrO_3–pyridine slurry after the method of Gassman and Pape.[10] Following extraction and removal of solvent a mixture containing 63% of the desired 7-ketonorbornane plus 21% of the alcohol and 16% other products was obtained. The ketone was purified either by preparative gas chromatography using a 5 ft × ⅛ in. column of Ucon 50HB (15% on Chromosorb G, DMCS/A-W, at 80° and a He flow of 15 cc/min) followed by vacuum sublimation, or by recrystallization from acetone. Samples used in the vapor-phase photolyses were further purified by distilling off traces of volatile impurities on a high vacuum line at −23° and discarding the distillate. Analytical gas chromatograms of the purified ketone showed <0.1% total impurities with retention times less than that of the parent ketone; no impurities of longer retention times were detected. The melting point of the purified ketone was 74.0–75.0° and its vapor pressure was 35 mTorr at −22.8° and 365 mTorr at 0°.

The infrared absorption of the purified 7-ketonorbornane in CCl_4 solution showed three peaks in the carbonyl region at 1845 (w), 1783 (s), and 1742 (m) cm^{-1}, in complete agreement with literature values.[10] In the vapor phase at 1.4 Torr the following absorption peaks were observed: 3002 (m), 2968 (ms), 2880 (m), 1844 (m), 1795 (s), 1742 (mw), 1461 (w), 1256 (?, vw), 1134 (mw), 1058 (w), 852 (w), 771 (vw), and 702 (vw). The vapor-phase frequencies, determined on a Perkin-Elmer 621 spectrophotometer, are ± 4 cm^{-1} above 2000 cm^{-1} and ± 2 cm^{-1} below 2000 cm^{-1}. The mass spectrum of the ketone, scanned on a Nuclide 12-90-G mass spectrometer operating at an ionizing voltage of 70 eV and an ion accelerating voltage of 8 kV, showed the following principal peaks and abundances: 110 (54%), 111 (4.5%), 81 (19%), 67 (100%), 54 (76%), 41 (32%), 39 (23%).

The *cis*-butene-2 (Phillips Research Grade; 0.015% trans), oxygen (Matheson Research Grade), *n*-heptane (Phillips Pure Grade), and acetone (Chemical Samples Co., 99.9% purity) were used without further purification. Cyclobutanone, from Aldrich Chemical Co., was purified by trap-to-trap distillation on a high vacuum line. Cyclooctane, from Eastman Kodak Co. was purified by vacuum distillation to remove a yellow impurity. Quinine sulfate was used as obtained from K and K Laboratories, Inc. Azomethane was synthesized from dimethylhydrazine dihydrochloride by the method of Renaud and Leitch[11] and purified by trap-to-trap distillation through zeolite on a high vacuum line.

Sample Preparation and Photolysis Procedure. Solutions for photolysis were made up in pentane (6.1×10^{-2} *M* in **1**) and in diethyl ether (4.8×10^{-2} *M* in **1**), with a known amount of cyclooctane added as internal standard. Samples were placed in a 1-cm quartz photolysis cell, degassed with oxygen-free nitrogen for 5–10 min, and then irradiated at 307 nm using a HBO 200-W high-pressure xenon arc followed by a Bausch and Lomb high-intensity monochromator and quartz collimating lenses. The light intensity was monitored before, during (to determine the fraction of light absorbed), and after each run using a uranyl oxalate actinometer.[12] The uv spectrum of the sample was recorded before and after a run and showed a slight increase in absorbance with time around 290 nm, probably due to formation of the isomeric aldehyde **2**. Aliquots were taken at 2-hr intervals for analysis by gas chromatography, except in the case of the ether solution, for which the results of single analyses for two separate runs are reported.

Vapor-phase samples were made up on a standard mercury-free high vacuum line, using a Texas Instruments Model 144 pressure gauge readable to 1 mTorr and calibrated volumes to measure out the desired amount of each component. The mixtures were prepared by freezing all condensible components successively into a small sidearm on the photolysis *cell* then rapidly vaporizing the solid mixture. The resulting gas mixture was allowed from 0.75 to 3 hr mixing time before photolysis except in the runs with added *cis*-C_4H_8 or O_2 when 12–17 hr was allowed to ensure complete mixing. The photolysis cells were 10 cm in length and 1.9 cm o.d., and were sealed by a Martin/Kontes Kel-F high vacuum stopcock which showed a leak rate of ≤ 0.7 mTorr of air per hour into the cell. Identical photolysis blanks were made up routinely, principally to measure the level of the trace impurities present, since no dark reactions were observed. The light source used in both the photochemical and fluorescence quantum yield studies was a Bausch and Lomb Super Pressure mercury arc, whose output was passed through filter cells of distilled water and of bromine gas, into a Bausch and Lomb high-intensity monochromator (33-86-25-01) with a uv grating, slits selected for $\Delta\lambda_{1/2} = 4.8$ nm. The output of the monochromator was formed into a parallel beam approximately 1.2 cm in diameter, passed through a CS-7-54 filter and the photolysis cell, and monitored by an RCA No. 935 vacuum photodiode operated at 67.5 V. This detector was calibrated using gaseous azomethane as an actinometer,[13] assuming $\phi_{C_2H_6} + \frac{1}{2}\phi_{CH_4} + \frac{3}{2}\phi_{C_3H_8} = 1.0$ (C_2H_6 ranged from 97.4 to 99.5% of the total hydrocarbon products, increasing with the incident light intensity). Because of the low vapor pressure of **1**, the fraction of light absorbed by photolyzed samples had to be calculated from measured extinction coefficients rather than measured directly. Extinction coefficients for **1** were determined by freezing a known amount into a optical cell which was then sealed and raised to a temperature high enough to vaporize all the solid ($\simeq 70°$), in a thermostated cell compartment of a Cary 14 spectrophotometer. The resulting spectrum is shown in Figure 1. The measured extinction coefficients of azomethane, used in calculating the photochemical quantum yields at 313, 302.5, and 291 nm were ϵ_{313} 2.89 M^{-1} cm^{-1}, $\epsilon_{302.5}$ 1.878 M^{-1} cm^{-1}, and ϵ_{291} 0.768 M^{-1} cm^{-1}.

The spectral purity of the irradiation system (Hg arc + filters + monochromator) used in the vapor-phase studies was checked by scanning its wavelength distribution, for the various settings of the Bausch and Lomb monochromator, using a McPherson 0.3-m scanning monochromator (Model 218) equipped with a sodium salicylate coated photomultiplier tube as the detector. The following percentages of total light intensity were found within the indicated bandwidth of the set wavelengths (corrected): 334 nm, 98.6%, ± 0.55 nm; 324.5 nm, 92.6%, ±5.2 nm; 313 nm, 99.84%, ±2.2 nm; 302.5 nm, 96.0%, ±1.8 nm; 291 nm, 64.2%, ±2.4 nm. Rough calculations showed the effects of stray light outside the indicated ranges on the measured photochemical and fluorescence quantum yields to be less than the total experimental error for all wavelengths used, except for 291 nm. Because of the rapid variation in quantum yields and extinction coefficients at wavelengths greater than 291 nm and uncertainties in the relative intensities in the stray light "spectra," it was not possible to make exact corrections to the quantum yields for this effect. Rough calculations indicate that at 291 nm the absolute product quantum yields obtained for 7-ketonorbornane and ϕ_f for acetone may be somewhat low, and ϕ_f for hexafluoracetone may be slightly high, because of irradiation by stray light. Preliminary data obtained at 280 nm are not included in this report, as only ~17% of the output light was found within ±3.7 nm of that setting.

Product Analyses. Products of the photolyses in pentane were analyzed by gas chromatography, using two different columns. Amounts of 1,5-hexadiene (**3**) and cyclohexene (**5**) formed were determined using a Varian 1200 chromatograph with an 8 ft × ⅛ in. porapak Q column at 165°: N_2 flow = 40 cc/min. 3-Cyclohexenecarboxaldehyde (**2**) and the parent ketone were analyzed in a Hewlett-

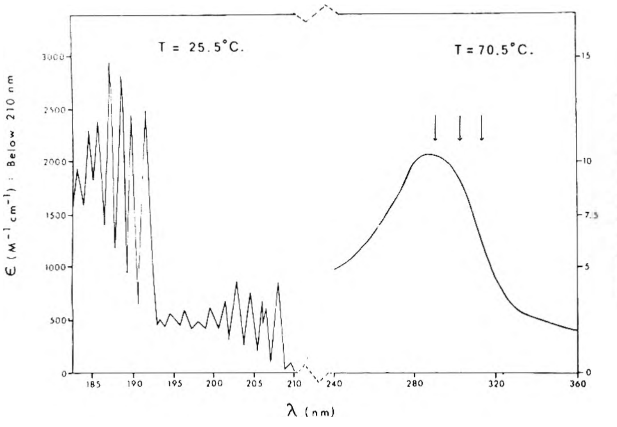

Figure 1. Vapor-phase absorption spectrum of 7-ketonorbornane (resolution $\simeq$ 0.1 nm). Only major progressions are shown below 210 nm, for clarity.

Packard 5750 chromatograph with a 50 ft × ⅛ in. LAC-728 column at 150°: He flow = 15 cc/min. The product peaks were identified by comparing retention times with known samples and also by combined gc–mass spectrometric analysis.

Products of the vapor-phase photolyses and the two photolyses of ether solutions were analyzed with a Varian 2400 series gas chromatograph, using a 50 ft × ⅛ in. Ucon 50HB (10% on Chromosorb G) column held at 89 ° until all C_6 hydrocarbons were eluted (21 min) then raised to 170 ° to obtain the peaks corresponding to 2 at 44 min and 1 1.3 min later. This column succeeded in resolving three peaks in the C_6H_{10} region, two of which were confirmed to be 1,5-hexadiene and cyclohexene as in the pentane solution. The third peak was identified as bicyclo[2.2.0]hexane (4) by injection of a photolyzed sample of 2,3-diazabicyclo[2.2.2]oct-2-ene vapor, which is reported to have 3 and 4 as the principal photolysis products.[14] The hydrogen flame detector sensitivity was calibrated relative to either *n*-heptane or cyclooctane; the internal standard used for each run is specified in Table II. The concentration of 1 before and after each photolysis was checked by scanning the sharply structured absorption band beginning at 210 nm on the Cary 14 (see Figure 1) but the data obtained were not sufficiently precise to give reliable values for ϕ_1, because of the low conversions and because of a slow adsorption of 1 on the cell walls which apparently occurred to a small extent after filling the cells.

Fluorescence Measurements. Fluorescence yield and lifetime measurements were carried out on gaseous samples in a 3.7-cm o.d. cylindrical quartz cell with a 15.0-cm pathlength, a 2.5-cm o.d. viewing port midway down the cell, and a Wood's Horn light trap facing the viewing window. The entire cell was painted with a flat black paint except for the entrance, exit, and viewing windows. The cell was equipped with a freezing tip for use both in making up gas mixtures and for freezing down samples while measuring the intensity of "scattered" light. Light emerging through the viewing window was collimated by a 2 in. diameter f/1.5 Pyrex lens, passed through a Corning CS-0-52 filter, and detected by an RCA No. C31025C photomultiplier tube (commercial No. 4832) operated at 1440 V. The anode current pulses of the photomultiplier were amplified in an SSR Model 1120 amplifier discriminator and counted in an SSR Model 1110 digital synchronous computer, operated in a "chop" mode for automatic subtraction of background counts. Excitation of fluorescence was done in the same way as for the photolyses, except that the light beam was interrupted by a mechanical chopper operating at 42 Hz, synchronized to the photon-counting system. By simultaneously recording the intensity of light transmitted through the fluorescence cell and the number of photons reaching the PMT through the viewing window (accumulated for 210 cycles), repeating the measurements 3 to 10 times for each value of λ_{ex}, it was possible to determine I_{em}/I_{ex} to a fractional standard deviation of 0.5% or better. Such high precision was essential for samples of low optical density and ϕ_f because of the relatively large correction for "scattered light" in these cases. In the case of 7-ketonorbornane, the "worst case" because of the low vapor pressure at room temperature, the "scattered light" contribution to the observed ratio of I_{em}/I_{ex} increased from 80% at 334 nm to 97.9% at 291 nm. This factor is a major source of the estimated uncertainties in the ϕ_f's indicated in Table III.

The fluorescence quantum yields were calculated from the equation

$$\phi_f = \left(\frac{k_n}{k_{n,r}}\right) \frac{\epsilon_r c_r}{\epsilon c} \frac{\langle I_{em}/I_{ex}\rangle}{\langle I_{em}/I_{ex}\rangle_r} \phi_{f,r} \tag{1}$$

in which the subscript r refers to the reference sample, a $4.7_2 \times 10^{-7}$ *M* solution of quinine sulfate in 0.1 *N* aqueous H_2SO_4. The effect of the refractive index of the medium on the fraction of emitted light reaching the detector was corrected by the k_n which were calculated according to the analysis of Hermans and Levinson,[15] taking $n = 1.000$ for the gases and $n_r = 1.341$ for the reference solution. The ratio of these correction factors was 0.633 for the geometry of the system used here. Extinction coefficients used in eq 1 were measured in the Cary 14 except for the case of cyclobutanone whose sharply structured absorption required direct measurements of absorbance (for 32.8-Torr sample) in the photochemical–fluorescence irradiation system. The quantities in brackets were corrected for scattered light contributions, as indicated above, and for slight difference in reflection losses of gaseous and reference samples. The fluorescence quantum yield of the reference samples, $\phi_{f,r}$, was taken to be 0.563 (a compromise between the two best literature values) and independent of the λ_{ex}.[16,17] It was judged unnecessary to correct for small differences between the fluorescence spectra of the various samples because of the flat spectral response of the photomultiplier tube used to measure I_{em} (<±18% variation in quantum efficiency between 400 and 600 nm, with good sensitivity extending to ≈850 nm, claimed). The emission spectrum of 7-ketonorbornane vapor ($\simeq$2.2 Torr in a 1-cm rectangular fluorescence cell) was scanned using an Aminco-Bowman Model No. 4-8911 spectrophotofluorimeter with λ_{ex} 332 nm and all slits at the maximum value of 5 mm. Because of the low fluorescence intensity and the relatively large scattered light correction (≈65% of total light at λ_{em} (max)) it was not possible to obtain a complete spectrum. However, the maximum emission intensity of the vapor lies close to 500 nm (±30 nm) and the spectrum extends from below 430 nm to above 560 nm. A rough excitation spectrum (uncorrected for spectral output of the Xenon arc) shows a maximum at $\lambda_{ex} \simeq 340$ nm (±5 nm). An emission spectrum run on a portion of the quinine sulfate solution mentioned above showed a maximum emission at 465 nm (±10 nm), compared with a reported value of 460 nm.[17]

TABLE I: Photochemical Quantum Yields in Solution[a]

Solvent	% reaction	ϕ_1	ϕ_2	ϕ_3	ϕ_4	ϕ_5
*n*Pentane	19	0.28	0.20	0.006	n.d.	0.0
n-Pentane	33	0.25	0.18	0.008	n.d.	0.002
n-Pentane	41	*0.20*	*0.15*	*0.010*	n.d.	0.006
	Av	0.24	0.18	0.008	n.d.	0.000[b]
Ethyl ether	11.4	0.20	0.15	0.007_8	0.001_8	0.001_7
Ethyl ether	48.5	0.25	0.17	0.007_7	0.001_4	0.005_7
	Av	0.22	0.16	0.007_6	0.001_7	0.000[b]

[a] λ_{irr} 307 nm, $T \simeq 23°$. [b] Extrapolated value.

Fluorescence lifetimes were measured using an Avco-Everett Model C950 pulsed nitrogen laser as the excitation source (λ 337.1 nm), the same sample cell as used in the ϕ_f determinations, and an RCA 1P28 photomultiplier tube as the fluorescence detector. The laser, which emits ≃50 kW per pulse, was operated at 16 kV and 70 pulses per second. The voltage pulses developed across a 50 Ω resistor connected between the anode of the PMT and ground were transmitted *via* a 25-ft cable to Hewlett-Packard Model 141 B storage oscilloscope equipped with a 1410 A sampling vertical amplifier, a 1425 A time base module, and a Polaroid camera. The PMT was operated with the photocathode at −1180 V (in the case of samples of 1) or at −1040 V (for cyclobutanone vapor). The time profile of the exciting light, $I_{ex}(t_j)$, was obtained by directing a small amount of reflected light (highly attenuated) from a quartz plate toward the PMT. The time profile of light emitted by a sample, $I_{em}(t_i)$, was obtained by subtracting the emission obtained when the sample was frozen down to 78°K from the emission when the sample was vaporized. Fluorescence decay times (ϒ) were evaluated by finding the best fit of the experimental $I_{em}(t_i)$ to the equation[18]

$$I_{em}(t_i) = \propto \sum_{j=0}^{i} I_{ex}(t_j) \exp\left[-\left(\frac{t_i - t_j}{\Upsilon}\right)\right] \quad (2)$$

Both I_{em} and I_{ex} profiles for one sample of 1 are shown in Figure 2.

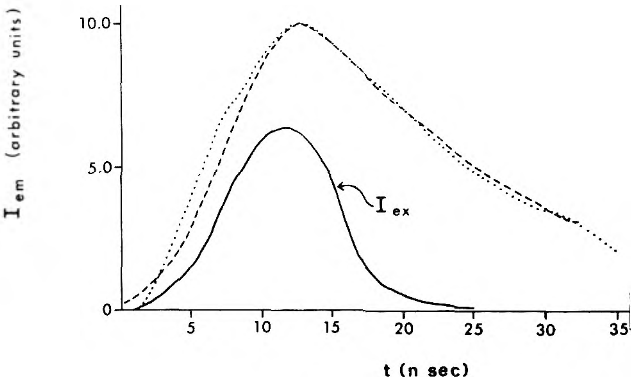

Figure 2. Fluorescence decay curves, 7-ketonorbornane vapor at 1.29 Torr and ≃25°: experimental (· · · ·); eq 2 with ϒ = 14 nsec (- - - -).

Results

In Solution. Irradiation of 7-ketonorbornane (1) in either ether or pentane solvent at 307 nm yielded a mixture of 3-cyclohexenecarboxaldehyde (2), 1,5-hexadiene (3), bicyclo[2.2.0]hexane (4), and CO as primary prducts (eq 3).

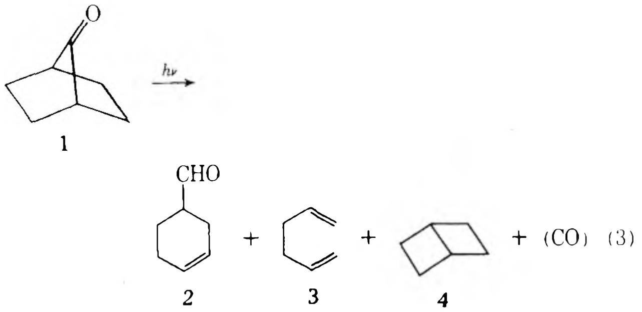

An additional product, cyclohexene (5), was found to result from a secondary process, the photolysis of 2 (eq 4). This

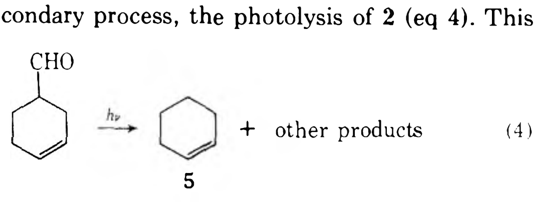

was demonstrated both by examining the time dependence of the quantum yield for formation of 5 from 1 (see Table I) and by irradiation of a solution of 2 in ether. "Other products" in eq 4 includes an unidentified gas chromatographic peak shown by GC-MS to be isomeric with 1 and 2, but not further identified.

Quantum yields for decomposition of the parent ketone, ϕ_1, and formation of the products, ϕ_2 through ϕ_5, are reported in Table I. Although ϕ_1 and ϕ_2 should both show some time dependence (the former due to competition for the incident light with 2, and the latter due to the secondary photolysis of 2) the trend is not clearly discernible above the random scatter of the data. Therefore only ϕ_5 is extrapolated to 0% conversion in the table. The results shown indicate no significant effect of a change in solvent upon the photochemical quantum yields. The near equality between ϕ_1 and the sum of the product ϕ's indicates that substantially all the products have been accounted for. Clearly 2 is the predominant product in solution.

In Vapor Phase. Quantum yields for the products formed upon irradiation of samples of 7-ketonorbornane vapor at the wavelengths designated by arrows in Figure 1 are given in Table II. Because of the low per cent conversions it was not necessary to extrapolate the experimental ϕ's to t = 0. The formation of cyclohexene occurred to an insignificant extent except in a few early runs carried to higher conversions which are not included in the table. The sum of the product quantum yields at 313 nm (0.20) is within experimental error of the value of the same sum for the photolyses in solution (0.19 in pentane, 0.17 in ether). The distribution of products is greatly changed, however; the aldehyde 2 which comprised 94% of the identified products in ether solution accounts for only 45% in the vapor phase at 313 nm. A clear wavelength dependence is seen in the ratio ϕ_3/ϕ_2 (1.01 at 313 nm, 1.40 at 302.5 nm, and 3.6 at

TABLE II: Vapor Phase Photochemical Quantum Yields ($T \simeq 23°$)

λ, nm	P_1, Torr	P_R, Torr	P_Q, Torr	% reaction	ϕ_2	ϕ_3	ϕ_4
313	1.08	0.185[a]		3.12	0.094	0.109	0.022
313	0.87	0.229[a]		1.35	0.107	0.109	0.022
313	0.87	0.218[a]		0.66	0.130	0.094	0.017
313	0.88	0.133[a]	10.1[c]	1.34	0.062	0.066	0.011
313	0.92	0.302[b]	10.0[d]	1.34	0.069	0.085	0.017
313	0.79	0.152[b]	21.4[d]	2.72	0.081	0.086	0.017
					Av 0.090_5	0.091_5	0.018
					(±0.016)	(±0.010)	(±0.002)
302.5	0.934	0.278[b]		1.67	0.067	0.134	0.025
302.5	0.875	0.261[b]		1.36	0.127	0.140	0.029
					Av 0.097	0.137	0.027
					(±0.020)	(±0.002)	(±0.001)
291	0.75	0.278[b]		0.63	0.059	0.214	0.046

[a] R ≡ C_7H_{16}. [b] R ≡ c-C_8H_{16}. [c] Q ≡ *cis*-C_4H_8. [d] Q ≡ O_2.

291 nm) and in the sum of product ϕ's (0.20 at 313 nm, 0.26 at 302.5 nm, and 0.32 at 291 nm), for the vapor phase. The ratio ϕ_4/ϕ_3, however, is surprisingly independent of both irradiation wavelength and phase, being ~0.2_1 under all conditions.

In quoting average values above, it is assumed that the added oxygen and *cis*-butene-2 shown in Table II had no quenching effect. Excluding the runs with added *cis*-butene-2 or oxygen would reduce the probable error (50% confidence limit; shown in parentheses) of the runs at 313 nm by nearly a factor of 2 and raise the average product quantum yields by an average of 16%. However the difference between the two sets of average ϕ's is only slightly greater than the scatter of values within each set and the values with added oxygen do not show increased quenching with increased P_{O_2}. Also, analysis of the photolyzed sample of 1 plus *cis*-C_4H_8 gave an upper limit for isomerization of the butene of $\phi_{c\to t} < 0.007$, indicating that no significant quenching of a triplet state of 1 occurred.[19] Because of the short lifetime of the excited singlet state produced directly by the irradiation (see below), quenching of this state is unlikely. The small difference in quantum yields noted above may represent effectively complete trapping of some other intermediate in a relatively minor pathway, may be an experimental artifact related to the method of sample preparation, or may reflect a simple pressure effect (*i.e.*, due to collisional removal of vibrational energy).

Vapor-Phase Fluorescence Studies. Fluorescence quantum yields obtained by methods described in the Experimental Section are presented in Table III; these may be considered as absolute quantum yields if the quinine sulfate solution is accepted as a universal standard for the range of λ_{ex} employed. As a test of the reliability of the techniques used and for comparison of the dependence of the ϕ_f's on λ_{ex}, experimental results for acetone, hexafluoroacetone, and cyclobutanone are included and compared with corresponding literature values. The experimental results include an indication of the "probable error," estimated by a statistical analysis of $\langle I_{em}/I_{ex}\rangle$ after making the correction for scattered light. Despite the inescapably large estimated range of error at the two lower wavelengths in the case of 7-ketonorbornane, a fairly rapid decline of ϕ_f with decreasing λ_{ex} is clearly shown. For cyclobutanone the variation of ϕ_f with λ_{ex} (from 324 nm down) is even faster, while acetone and hexafluoroacetone show a more gradual dependence on λ_{ex}.

Comparing the present results with previous ones listed in the table, one sees approximate agreement in most cases. Certainly no systematic errors in the present procedure are indicated: for hexafluoroacetone the present results show a slightly more rapid variation of ϕ_f with λ_{ex} than previously reported;[20] while for cyclobutanone the variation is less strong than at least one recent report indicates.[21] There is a clear qualitative difference in the case of acetone vapor, the present results conflicting with earlier work which indicated ϕ_f to be virtually wavelength independent from 313 to 280 nm.[22] More recently a thorough study of the detailed mechanism and rates of photolysis of actone[23] has shown that the quantum yield for photodissociation *via* the singlet state increases rapidly with increasing temperature (thus presumably with decreasing wavelength); and ϕ_f must decrease as ${}^1\phi_{CO}$ increases. Recent theoretical and experimental[24,25] reevaluations of the acetone system support the conclusion that ϕ_f is wavelength dependent in this case also.

In the case of cyclobutanone the results at excitation wavelengths above 313 nm lie within experimental error of those previously reported, while at lower wavelengths they lie roughly between the two sets of data given by Lee, *et al.*[21,25] Both the precision and the absolute accuracy of the present results appear to be better, however; use of the quinine sulfate standard *via* eq 1 eliminates the major uncertainty introduced by using an uncalibrated phototube to measure I_{ex} as a function of wavelength (or relying upon manufacturers' spectral response curves for a general class of tubes), as was done by Lee, *et al.*, and earlier by Heicklen.[22] In eq 1 unknown sensitivity factors contained in I_{ex} cancel out; errors in these sensitivity factors may have seriously distorted the apparent wavelength dependence of previous ϕ_f values.

The reason for the differences between the present and previous fluorescence quantum yields of hexafluoroacetone is uncertain, since the experimental methods were essentially the same, except that I_{em} was measured with a different PMT and with photon-counting apparatus. The higher pressure of quencher (for phosphorescence) used in the present case might partly explain the larger values of ϕ_f given here for the longer wavelengths, since the high-pressure limit of ϕ_f found by Gandini and Kutschke[20] was 0.018_5 at λ_{ex} 313 nm. At the two shorter wavelengths the cited values for ϕ_f were obtained by a nonlinear interpolation between Gandini and Kutschke's data at 313 and 265 nm; the resultant uncertainties may account for part of the apparent discrepancies.

TABLE III: Fluorescence Quantum Yields of Gaseous Ketones[a] ($T \simeq 23°$)

Ketone	P, Torr	λ_{ex}, nm 334	324	313	302.5	291	Ref
I	0.89	$1.7 \pm 1.3 \times 10^{-4}$		$5.2 \pm 2.8 \times 10^{-5}$	$7 \pm 21 \times 10^{-6}$	$1 \pm 16 \times 10^{-6}$	This work
Cyclobutanone	17.4	$2.5 \pm 0.3 \times 10^{-3}$	$1.99 \pm 0.09 \times 10^{-3}$	$1.86 \pm 0.05 \times 10^{-4}$	$1.4 \pm 0.5 \times 10^{-5}$	$2.4 \pm 5.3 \times 10^{-6}$	This work
Cyclobutanone	18		1.9×10^{-3} [b]	$<1.4 \times 10^{-4}$ [c]	$<2.7 \times 10^{-5}$ [d]		25
Cyclobutanone	20	2×10^{-3} [e]		6×10^{-5}			21
Acetone	23.3 (+11.7 Torr O_2)	$1.9 \pm 0.1 \times 10^{-3}$	$1.36 \pm 0.02 \times 10^{-3}$	$2.08 \pm 0.01 \times 10^{-3}$	$1.22 \pm 0.01 \times 10^{-3}$	$4.68 \pm 0.04 \times 10^{-4}$	This work
Acetone	24.8 (+ ? Torr O_2[f])			2.03×10^{-3} [g]	1.89×10^{-3}	2.06×10^{-3}	22
Hexafluoroacetone	0.97 (+ 5.41 Torr O_2)	$2.25 \pm 0.03 \times 10^{-2}$		$2.48 \pm 0.02 \times 10^{-2}$	$1.37 \pm 0.01 \times 10^{-2}$	$6.5 \pm 0.2 \times 10^{-3}$	This work
Hexafluoroacetone	~0.97 (+0.02 → 0.1 Torr isobutene)	1.38×10^{-2}		1.06×10^{-2}	0.94×10^{-2} [h]	8.2×10^{-3} [h]	20

[a] Based on the following extinction coefficients for quinine sulfate: ϵ_{334} 5372 ± 25; ϵ_{324} 4915 ± 30; ϵ_{313} 4941 ± 35; $\epsilon_{302.5}$ 3629 ± 30; ϵ_{291} 2081 ± 40; ϵ_{280} 1117 ± 50 (all in M^{-1} cm^{-1}). [b] λ_{ex} "310–320" nm. [c] λ_{ex} 310 nm. [d] λ_{ex} 300 nm. [e] λ_{ex} 327 nm. [f] T = 40°, O_2 pressure not specified. [g] P_{ace} = 77 Torr. [h] Interpolated values.

[NOTE ADDED IN PROOF: Redetermination of ϕ_f for 0.137 Torr of hexafluoroacetone + 0.098 Torr of isobutene shows there was only a small pressure effect at the longer λ_{ex}'s: $\phi_{334} = 2.14 \times 10^{-2}$; $\phi_{313} = 1.98 \times 10^{-2}$; $\phi_{302.5} = 1.15 \times 10^{-2}$; $\phi_{291} = 6.4 \times 10^{-3}$.]

Typical data used in determining the exponential decay time of the fluorescence emitted from 7-ketonorbornane vapor are shown in Figure 2. The best fit of the computer-generated curve to the experimental $I_{em}(t_i)$ was obtained in the case shown for $\Upsilon = 1.4 \times 10^{-8}$ sec. Averaging this result with others obtained under slightly different instrumental conditions leads to a final value of $\Upsilon = 1.2 \pm 0.3 \times 10^{-8}$ sec for λ_{ex} 337.1 nm and a sample pressure of 1.29 Torr. As a test of the apparatus the same procedures used for 1 were applied to a 20-Torr sample of cyclobutanone. The result was a fluorescence decay time of $\Upsilon = 3.9 \pm 0.8 \times 10^{-9}$ sec, compared with a previously reported value of 4.7 ± 0.3×10^{-9} sec for λ_{ex} ~320 nm and 30 Torr.[26]

Combining the fluorescence decay time obtained here for 1 and the fluorescence quantum yield data from Table III, the natural radiative lifetime (Υ_0) of 1 in its (n, II*) state can be calculated from

$$\Upsilon = \phi_f \Upsilon_0 \qquad (5)$$

A short extrapolation of the ϕ_f values in Table III yields $\phi_f = 1.8 \pm 1.3 \times 10^{-4}$ at λ_{ex} 337.1 nm, and the experimental value for $\Upsilon_0 = 6.6 \pm 5.1 \times 10^{-5}$ sec. It is of interest to compare this result with the natural radiative lifetime calculated *via* the equation of Strickler and Berg[27]

$$\Upsilon_0 = \langle \tilde{\nu}_f^{-3} \rangle / (2.88 \times 10^{-9} \int \epsilon \, d \ln \tilde{\nu}) \qquad (6)$$

For the incomplete emission data reported in the Experimental Section the average emission frequency (in cm^{-1}) in the numerator of eq 6 can only be estimated by setting $\langle \tilde{\nu}_f^{-3} \rangle^{1/3} \simeq \lambda_{em}(\max) = 5.00 \times 10^{-5}$ cm ($\pm 0.3 \times 10^{-5}$). Using this approximation and carrying out the indicated integration, the following "theoretical" value of Υ_0 is obtained: $\Upsilon_0 = 1.67 \pm 0.32 \times 10^{-5}$ sec. Although the large estimated limits of error weaken the comparison, the factor of 4 discrepancy between the two Υ_0's is in the range of discrepancies found recently for acetone, acetone-d_6, and hexafluoroacetone in various phases.[28] In these, however, "theoretical" values of Υ_0 were too long rather than too short.

Discussion

The data of the preceding section are consistent with the mechanism shown in Scheme I.

The intermediacy of several biradicals is proposed, based on good, albeit indirect, evidence for the formation of similar species upon photolysis of several cyclic ketones.[29–32] The asterisks indicating vibrational excitation are used where the rate constants for an elementary process appear to be energy dependent. Thus, the increase of the total of product quantum yields with decreasing wavelength of irradiation in the vapor phase suggests that $k_5^* + k_6^*$ increases more rapidly with vibrational energy than does k_{ic}^* (which probably changes slowly with $E_{vib} = \nu_{ex} - \nu_{CO}$).

The proposed intermediacy of the acyl-alkyl biradical in the process of internal conversion is similar in concept to the proposed role of valence isomers in internal conversion of electronically excited benzene molecules.[33] The lack of any clear effect of the added gases indicates steps 4* through 6* must occur in $<10^{-8}$ sec. Other pathways for

Scheme I

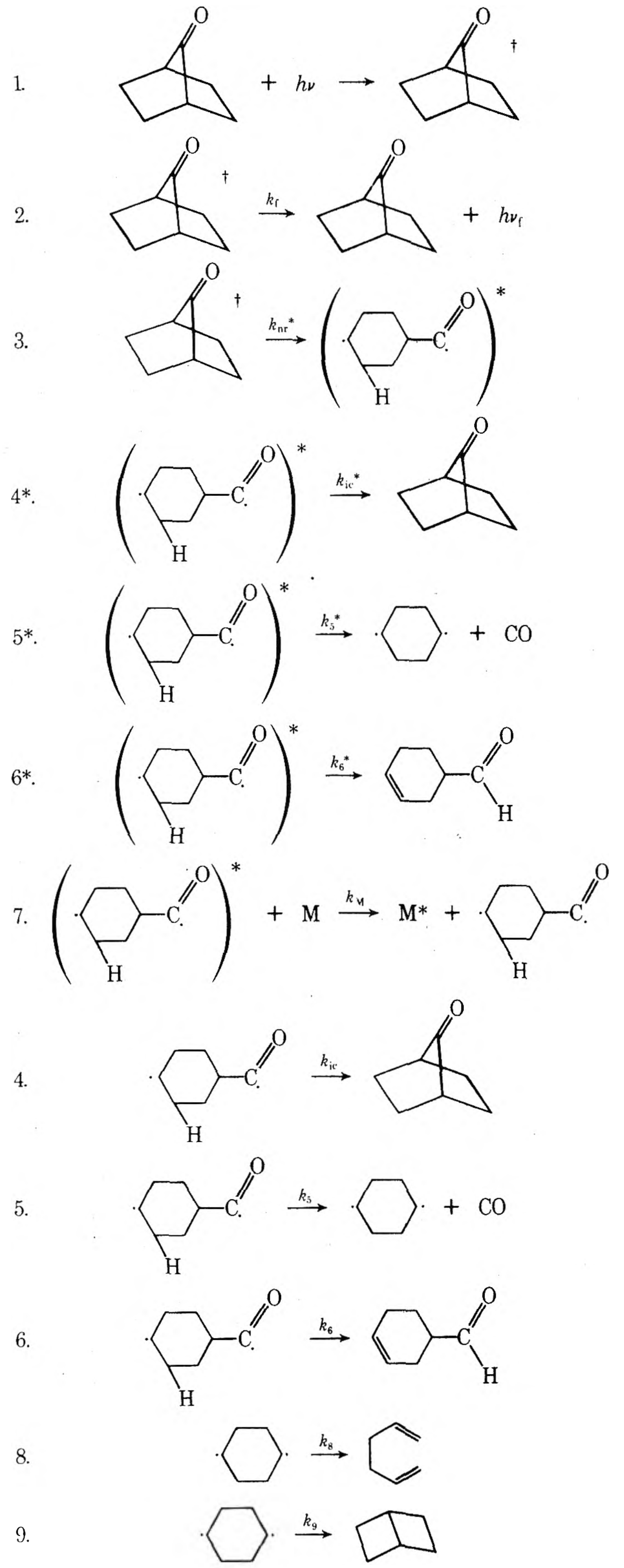

conversion of electronic to vibrational energy cannot, of course, be ruled out by the present data.

The wavelength dependence of ϕ_3/ϕ_2 corresponds to k_5^*/k_6^* increasing with vibrational energy, or the decarbonylation process (step 5) having a higher activation energy than the internal hydrogen transfer (step 6). Similar behavior has been observed in the cyclopentanone system for which $\phi_{CO}/\phi_{pentenal}$ has been found to increase with decreasing wavelength[34] and with increasing temperature[35] (Srinivasan estimated the energy of activation for decarbonylation to be ≈2.5 kcal/mol greater than for isomerization).

Steps 7, 4, 5, and 6 are included to account for the difference between the product quantum yields found in vapor phase and in solution. Step 7, which is assumed to occur with an insignificant rate at the pressures used in the vapor phase, produces a vibrationally "cold" intermediate, characterized by a much reduced value of k_5. Thus the isomeric aldehyde 2 becomes the highly favored product in solution, which is similar to results reported for cyclic ketones.[36,37]

Relative values for several of the rate constants appearing in the proposed mechanism, calculated from the data in Tables I and II, are shown in Table IV. The small effect of the change in phase on $k_{ic}/(k_5 + k_6)$ suggests that k_{ic} and k_6 have nearly the same dependences on E_{vib}, a somewhat surprising conclusion since steps 4 and 4* are internal radical recombinations. The activation energy for this recombination should not exceed the relatively small strain energy of the parent ketone. The phase and wavelength independence of ϕ_4/ϕ_3 is more compatible with k_9/k_8 being independent of E_{vib} (in the present mechanism) than with intermediacy of

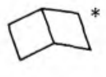

which was proposed at the outset of this study.

The greater than 20-fold increase in the probability of decarbonylation (*i.e.*, in k_5/k_6) on going from solution to vapor phase agrees remarkably well with the report that ϕ_{CO} for camphor rises from 0.005 in ethyl ether to ≥0.1 in vapor phase.[38] Available quantum yield data for this and other related compounds are compared with the results for 7-ketonorbornane in Table V.

Except for the case of bicyclo[3.1.0] hexane-3-one, whose behavior is apparently dictated by the special properties of the cyclopropane ring, the similarities among the results listed above are rather striking. Apparently cyclopentanone is a good model for the photochemical behavior of the bicyclic ketones listed above, all of which include a cyclopentanone ring. The only change with molecular structure apparent (with one exception already noted) is a decline in quantum yields with increasing molecular complexity, very likely due to an increasing k_{ic} (or decreasing $k_4 + k_5$), in the proposed mechanism.

The wavelength dependence noted for the fluorescence quantum yields of 1 is attributed to an increase in k_{nr}^* with the vibrational energy content of the ^{1}(n,Π*) state. Values of this rate constant were calculated from

$$k_{nr}^* = (\phi_f^{-1} - 1)/\Upsilon_0 \tag{7}$$

and plotted in Figure 3, along with corresponding results for cyclobutanone and acetone. The value of Υ_0 used for cy-

TABLE IV: Relative Rate Constants for Biradical Intermediates

	In Solution		Vapor Phase		
	Ether	Pentane	313 nm	302.5 nm	291 nm
$k_{ic}/(k_5 + k_6)$	3.5	3.2	4.0	2.8	2.1
k_5/k_6	0.058		1.21	1.69	4.4
k_9/k_8	0.22		0.20	0.20	0.21

TABLE V: Quantum Yields of Cyclic and Bicyclic Ketones (λ_{irr} 313 nm, $T \approx 25°$)

Compd	In solution		Vapor	
	ϕ_{enal}	Φ_{CO}	ϕ_{enal}	ϕ_{CO}
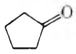	0.24[a]	<0.01[a]	0.22[b]	0.23[b]
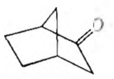	0.28[c] 0.40[d]	n.d. n.d.	n.d.	n.d.
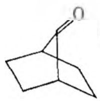 [e]	0.16	0.010	0.090	0.11
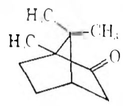	0.12[f] 0.06[g]	n.d. 0.005[g]	n.d.	≥0.1[g]
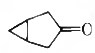 [h]	n.d.	n.d.	n.d.	0.79

[a] Reference 39; in C_6H_6. [b] Reference 34; 2.5 Torr. [c] Reference 40; in C_6H_6. [d] Reference 41; in C_6H_{14}. [e] This work; solvent ether, λ 307 nm; vapor: ~0.9 Torr. [f] Reference 4; in C_7H_{16}. [g] Reference 38; solvent diethyl ether; vapor: ~0.3 Torr. [h] Reference 5; 2 → 36 Torr, 118°.

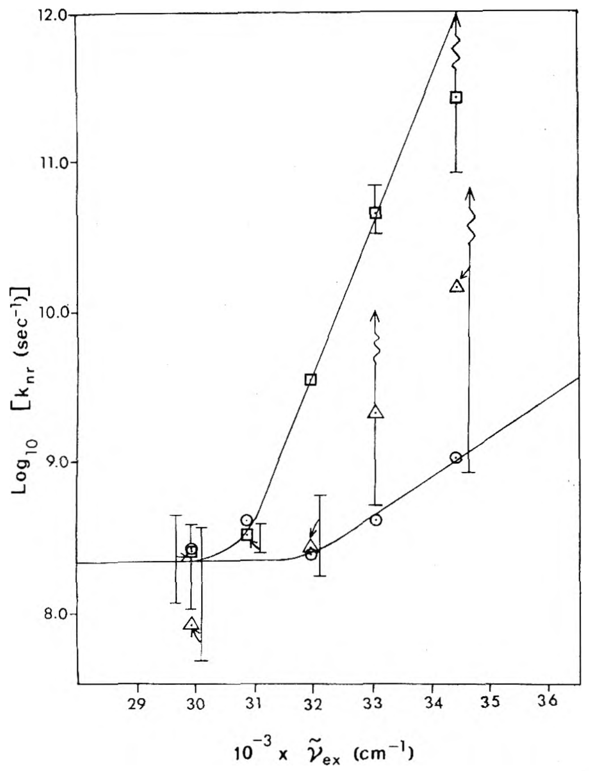

Figure 3. Nonradiative rate constant k_{nr}^* *vs.* excitation energy $\tilde{\nu}_{ex}$ for acetone (O); cyclobutanone (□); and 7-ketonorbornane (Δ). Error bars (including probable error in ε's) are shown when probable error range exceeds size of symbols. Best fit curves are drawn through points for acetone and cyclobutanone.

clobutanone is 1.56×10^{-6} sec, based on data obtained in this study, while $\tau_0 = 2 \times 10^{-6}$ sec for acetone is taken from the work of Halpern and Ware.[28] As discussed earlier, k_{nr}^* for 7-ketonorbornane shows an energy dependence intermediate between acetone and cyclobutanone. More striking, however, is the indication that k_{nr}^* approaches a common limiting value of $\simeq 2.1 \pm 0.5 \times 10^8$ sec^{-1} for all three compounds, as $E_{vib} \rightarrow 0$. Since the quantum yield for intersystem crossing (ϕ_{isc}) to the ^{3}(n,Π*) state is generally thought to be ≥0.98[23,42] for acetone vapor, it is tempting to conclude that the limiting value for k_{nr}^* is identical with k_{isc} for all three compounds. Breuer and Lee[26] have reached a similar conclusion by comparing the fluorescence lifetimes of a series of cyclic ketones for $\lambda_{ex} \approx 320$ nm, obtaining $k_{isc} \approx 3 \times 10^8$ sec^{-1}. The rapid increase of k_{nr}^* with ν_{ex} is probably due largely to an increasing contribution from predissociation, although k_{isc} is known to increase with E_{vib}.[43]

The involvement of the triplet n,Π* state in the photochemistry of cyclic ketones has been shown by quenching studies in solution,[36] and has been suggested (but not proven) by use of triplet sensitizers in the vapor phase.[44,45] The absence of any clear effect of quenchers prevents a firm decision on whether step 3 proceeds *via* the triplet state to be made in the present case, but similar attempts made in the case of cyclopentanone have also been unsuccessful.[34] If it is formed, the elusive triplet must have a very short lifetime, certainly $<10^{-8}$ sec.

It is implicit in the preceding discussion that the spin state of the biradical reacting in steps 4–6 (and 4*–7) does not effect the values of k_4–k_6 (k_4^*–k_7). This is contrary to an earlier suggestion, based on the virtually exclusive 4-pentenal formation from cyclopentanone sensitized by triplet benzene,[44] that internal hydrogen abstraction (steps 6* and 6 here) is greatly favored when the molecule is in a triplet state. Other evidence obtained with a triplet sensitizer of higher energy,[46] however, indicates that the vibrational energy content of the intermediates is more important than spin state in determining the distribution of reactants between competing reaction paths. Actually, the biradical reacting in steps 4–6 (and 4*–7) should be close to the "ultimate biradical" in which the two electrons are independent of each other.[47] In such a case the spin correlation is zero and it should make no difference (in terms of reactivity) whether the biradical is formed from a molecule in the triplet or in the singlet state.

Acknowledgments. We are indebted to Professor Marvin Querry of the Department of Physics at the University of Missouri—Kansas City for making available the N_2 laser and storage oscilloscope used in this work and to the National Science Foundation for partial support of the vapor phase experiments (through Grant No. GP-9578) and to the National Institutes of Health for support of the solution phase experiments (Grant No. GM16611). The assistance of Mr. J. C. Chang of UMKC in a portion of the vapor-phase experiments is gratefully acknowledged.

References and Notes

(1) On leave from A. Mickiewicz University, Poznan, Poland, Grunwaldska 6.
(2) Bicyclo[3.2.0]heptanone-3: S. Cremer and R. Srinivasan, *Tetrahedron Lett.*, **No. 21**, 24 (1960); J. C. Dalton, *et al.*, *J. Amer. Chem. Soc.*, **92**, 2565 (1970).
(3) Norcamphor: R. Srinivasan, *J. Amer. Chem. Soc.*, **83**, 2590 (1961).
(4) Camphor: W. C. Agosta and D. K. Herron, *J. Amer. Chem. Soc.*, **90**, 7025 (1968).
(5) Bicyclo[3.1.0]hexanone-3: L. D. Hess and J. N. Pitts, Jr., *J. Amer. Chem. Soc.*, **89**, 1973 (1967).
(6) R. F. Klemm, D. N. Morrison, P. Gilderson, and A. T. Blades, *Can. J. Chem.*, **43**, 1934 (1965).
(7) R. J. Campbell and E. W. Schlag, *J. Amer. Chem. Soc.*, **89**, 5103 (1967).
(8) T. F. Thomas, C. I. Sutin, and C. Steel, *J. Amer. Chem. Soc.*, **89**, 5107 (1967).

(9) P. R. Story, *J. Org. Chem.*, **26**, 287 (1961).
(10) P. G. Gassman and P. G. Pape, *J. Org. Chem.*, **29**, 160 (1964).
(11) R. Renaud and L. C. Leitch, *Can J. Chem.*, **32**, 545 (1954).
(12) C. R. Masson, V. Boekelheide, and W. A. Noyes, Jr., *Tech. Org. Chem.*, **2**, 295 (1956).
(13) M. H. Jones and E. W. R. Steacie, *J. Chem. Phys.*, **21**, 1018 (1953).
(14) W. D. Clark and C. Steel, *J. Amer. Chem. Soc.*, **93**, 6347 (1971). We are grateful to Professor Steel for providing the sample of diazabicyclooctene.
(15) J. J. Hermans and S. Levinson, *J. Opt. Soc. Amer.*, **41**, 460 (1951).
(16) W. H. Melhuish, *J. Phys. Chem.*, **65**, 234 (1961).
(17) J. W. Eastman, *Photochem. Photobiol.*, **6**, 55 (1967).
(18) C. Steel and T. F. Thomas, *Chem. Commun.*, 900 (1966); J. B. Birks and I. H. Munro, *Progr. React. Kinet.*, **4**, 271 (1967).
(19) R. B. Cundall, F. J. Fletcher, and D. J. Milne, *Trans. Faraday Soc.*, **60**, 1146 (1964).
(20) A. Gandini and K. O. Kutschke, *Proc. Roy. Soc., Ser. A.*, **306**, 511 (1968).
(21) J. C. Hemminger and E. K. C. Lee, *J. Chem. Phys.*, **56**, 5284 (1972).
(22) J. Heicklen, *J. Amer. Chem. Soc.*, **81**, 3863 (1959).
(23) R. B. Cundall and A. S. Davies, *Proc. Roy. Soc., Ser. A*, **290**, 563 (1966).
(24) H. E. O'Neal and C. W. Larson, *J. Phys. Chem.*, **73**, 1011 (1969).
(25) R. G. Shortridge, C. F. Rusbult, and E. K. C. Lee, *J. Amer. Chem. Soc.*, **93**, 1863 (1971).
(26) G. M. Breuer and E. K. C. Lee, *J. Phys. Chem.*, **75**, 989 (1971).
(27) S. J. Strickler and R. A. Berg, *J. Chem. Phys.*, **37**, 814 (1962).
(28) A. M. Halpern and W. R. Ware, *J. Chem. Phys.*, **54**, 1271 (1971).
(29) R. L. Alumbaugh, G. O. Pritchard, and B. Rickborn, *J. Phys. Chem.*, **69**, 3225 (1965).
(30) P. Dowd, A. Gold, and K. Sachdev, *J. Amer. Chem. Soc.*, **92**, 5724 (1970).
(31) J. A. Barltrop and J. D. Coyle, *Chem. Commun.*, 1081 (1969).
(32) H. A. J. Carless, J. Metcalfe, and E. K. C. Lee, *J. Amer. Chem. Soc.*, **94**, 7221 (1972).
(33) D. Phillips, J. LeMaire, C. S. Burton, and W. A. Noyes, Jr., *Advan. Photochem.*, **5**, 329 (1968). E. K. C. Lee *et al.*, have also proposed a chemical mechanism for internal conversion involving biradical intermediates in several cyclic ketones: *J. Amer. Chem. Soc.*, **94**, 1 (1972).
(34) C. Y. Mok, *J. Phys. Chem.*, **74**, 1432 (1970).
(35) R. Srinivasan, *Advan. Photochem.*, **1**, 92 (1963).
(36) J. C. Dalton and N. J. Turro, *Annu. Rev. Phys. Chem.*, **21**, 499 (1970).
(37) P. Dunion and C. N. Trumbore, *J. Amer. Chem. Soc.*, **87**, 4211 (1965).
(38) R. Srinivasan, *J. Amer. Chem. Soc.*, **81**, 2604 (1959).
(39) P. J. Wagner and R. W. Spoerke, *J. Amer. Chem. Soc.*, **91**, 4437 (1969).
(40) J. C. Dalton, *et al.*, *J. Amer. Chem. Soc.*, **92**, 2564 (1970).
(41) R. S. Givens, *et al.*, "Mechanistic Studies of the Type I Photorearrangement for Bicyclic Ketones," to be submitted for publication.
(42) R. F. Borkman and D. R. Kearns, *J. Chem. Phys.*, **44**, 945 (1966).
(43) S. Fischer and E. W. Schlag, *Chem. Phys. Lett.*, **4**, 393 (1969); E. W. Schlag, S. Schneider, and S. F. Fisher, *Annu. Revs. Phys. Chem.*, **22**, 465 (1971).
(44) E. K. C. Lee, *J. Phys. Chem.*, **71**, 2804 (1967).
(45) H. O. Denschlag and E. K. C. Lee, *J. Amer. Chem. Soc.*, **90**, 3628 (1968).
(46) C. C. Badcock, M. J. Perona, G. O. Pritchard, and B. Rickborn, *J. Amer. Chem. Soc.*, **91**, 545 (1969).
(47) S. P. McGlynn, T. Azumi, and M. Kinoshita, "Molecular Spectroscopy of the Triplet State," Prentice-Hall, Englewood Cliffs, N.J., 1969, p 106.

Ion-Molecule Reactions in Monosilane-Acetylene Mixtures[1]

T. M. Mayer and F. W. Lampe*

Davey Laboratory, Department of Chemistry, The Pennsylvania State University, University Park, Pennsylvania 16802

(Received April 29, 1974)

Publication costs assisted by the U. S. Atomic Energy Commission

The reactions of Si^+, SiH^+, $SiH_2{}^+$, and $SiH_3{}^+$ with C_2H_2 and the reactions of $C_2H_2{}^+$ with SiH_4 have been studied as a function of collision energy in the range of 0.3-2.5 eV in the center-of-mass system by tandem mass spectrometry. Phenomenological rate constants have been measured in the low-energy region 0.3-0.9 eV and appear to be independent of energy throughout this range. High-pressure mass spectrometry in the range 0.04-0.3 Torr for a mixture containing 10% of acetylene indicates that acetylene has a striking effect on the ionic chemistry of monosilane. Above 0.05 Torr, the principal reaction of acetylene with ions derived from monosilane appears to be that of simple association, leading to ionic polymerization of acetylene.

Introduction

In a previous study of ion-molecule reactions in monosilane-acetylene mixtures[2] rate constants were reported for a number of reactions of $C_2H_2{}^+$ with SiH_4 and of $SiH_2{}^+$ with C_2H_2. In this investigation, which was carried out in a single-source mass spectrometer, reaction identification was made principally on the basis of appearance potential measurements of product ions and rate constants were determined by the pulse technique[3-5] for ion-source pressures below 0.006 Torr. In view of the fact that application of the same apparatus and technique to the monosilane-methane system[6] has been shown by ion-cyclotron resonance studies,[7] tandem mass spectrometry,[8] and high-pressure mass spectrometry[8] to have yielded incomplete and/or misleading results, a reinvestigation of this system was felt to be desirable. Accordingly we have carried out a tandem mass-spectrometric study of ion-molecule reactions in the monosilane-acetylene system. Our results are in qualitative accord with the earlier report[2] but we have identified a number of additional secondary processes in this system not reported earlier and have measured phenomenological rate constants or cross sections for them. In addition, a limited high-pressure mass-spectrometric study (up to 0.3 Torr) was carried out in order to define the fates of the major secondary ion products in this system.

Experimental Section

The tandem mass spectrometer used in these studies permits the injection of mass-selected reactant ions, having kinetic energies variable down to about 1 eV, into a collision chamber containing the neutral reactant molecule. The apparatus, which has been described previously,[9] consists of two quadrupole mass filters separated by the collision chamber and ion lenses, and mounted in the "in-line" configuration. Retarding field measurements indicate that the energy spread (full-width at half-maximum) of the reactant ion beam entering the collision chamber is about 1 eV.

In addition to identification of the reactions of Si^+, SiH^+, SiH_2^+, and SiH_3^+ with C_2H_2 and of $C_2H_2^+$ with SiH_4, the various relative reaction cross sections were studied as a function of collision energy in the range 0.4–3 eV. As described previously[8,10] the shapes of the cross section *vs.* energy curves were used to differentiate between exothermic and endothermic processes. Since our major interest in this system pertains to the effect of acetylene on the radiolysis of monosilane[11] and therefore is concerned with monosilane-rich mixtures, we did not study reactions of the low-abundant C_2H^+ with SiH_4.

Phenomenological rate constants were determined by direct comparison of relative reaction cross section for 1.4 eV ions (laboratory system) with the cross sections for reactions

$$CH_4^+ + SiH_4 \longrightarrow SiH_3^+ + CH_3 + H_2 \qquad (1)$$

and

$$CH_3^+ + SiH_4 \longrightarrow SiH_3^+ + CH_4 \qquad (2)$$

whose rate constants had been determined previously.[8] Since (1) and (2) are hydride-ion transfer reactions that may form product ions that contain very little momentum of the reactant ion, one must be concerned about the effect of differing ionic collection efficiency on the rate constants for ions of the condensate type, *i.e.*, $SiC_xH_y^+$. Comparison[12] of the total depletion rate constants for reaction of Si^+, SiH^+, SiH_2^+, and SiH_3^+ with Si_2H_6 as determined by high-pressure mass spectrometry with those determined in our tandem mass spectrometer indicates no significant trend even though the percentage of condensation reaction undergone by each reactant ion varies from 29% in the case of SiH_2^+ to 98% in the case of Si^+. We conclude that differences in collection efficiency do not introduce error exceeding ±20% into our phenomenological rate constants. Collision chamber pressures of the order of 10^{-3} Torr and ionization chamber pressures in the range of $1\text{–}5 \times 10^{-3}$ Torr were employed.

Measurements of the dependence of ionic abundances on ion-source pressures in the range 0.04–0.3 Torr for a 90–10% SiH_4–C_2H_2 mixture were carried out in a Nuclide Associates 12-90G sector-field mass spectrometer, an instrument that has been described previously.[9] The energy of the ionizing electron beam was 100 eV, the trap current was very small and not measured, and the ion-accelerating voltage was 2500 V. In all experiments the ion-exit energy was 1.9 eV. The ion-source temperature was 100°.

Ion-source pressures in the Nuclide mass spectrometer were measured with a Granville-Phillips capacitance monometer that had been calibrated using a McCleod gauge. The calibration was checked by observation of CH_5^+ formation in methane. We estimate our source pressures to be accurate to ±10%.

Monosilane, purchased from the Matheson Co., was purified by fractionation on a vacuum line prior to use. Research grade acetylene, also purchased from the Matheson Co., was used as received.

Results and Discussion

1. Nature of the Elementary Reactions. The ion-molecule reactions found to be exothermic on the basis of the dependence of reaction cross section on kinetic energy are tabulated in Table I. Also shown in Table I are standard enthalpy changes, calculated from available thermochemical data,[13,14] and phenomenological rate constants determined at 1.4-eV ion-kinetic energy in the laboratory system. For comparison the rate constants reported previously are shown in the last column of Table I. With the exception of reaction 3, the neutral products are written arbitrarily as those that yield the maximum exothermicity.

One may note immediately from Table I, that the most rapid of all reactions with monosilane is hydride ion abstraction leading to formation of SiH_3^+; the predominance of this process in the reactions of positive ions with silanes[8,9,15] is undoubtedly due to the hydridic character of hydrogen in the Si–H bond.[16,17] Recent studies in this laboratory[18] have shown that the process of transfer of the hydride ion from SiH_4 occurs with very little if any momentum transfer from the reactant ion to the product SiH_3^+. In other words, the SiH_3^+ species acts as a spectator to the pick-up of its bound H^- by the reactant ion.

In the remainder of this section we discuss the characteristics of the reactions that occur when the various reactant pairs are brought together.

(*a*) *$C_2H_2^+ + SiH_4$.* When $C_2H_2^+$ ions are injected into SiH_4, reactions 3–11 (Table I) are observed as exothermic processes in that the cross sections decrease with increasing collision energy over the entire range studied. With the exception of reaction 4 the calculated enthalpy changes for 3–7 are in agreement with the experimental conclusion that the reactions are exothermic processes. Enthalpies of formation are not available for the $SiC_2H_x^+$ ions. Thermochemical calculations using available data[13,14] indicate reaction 4 to be endothermic by 8 kcal/mol, in contradiction to our experimental observations. This contradiction is undoubtedly due to the value $\Delta H_f°(SiH^+) = 308$ kcal/mol[13] being too high. This value was determined from the appearance potential of SiH^+ from SiH_4 and processes involving the breakage of so many bonds are notorious for yielding high values. In fact, Potzinger and Lampe[13] state that the ionization-efficiency curve for SiH^+ from SiH_4 showed a long tail indicating processes involving excess energy. Therefore, we believe reaction 4 to be, in fact, exothermic or thermoneutral which places an upper limit of 300 kcal/mol on the standard enthalpy of formation of SiH^+.

The rate constants obtained in this work for the reactions of $C_2H_2^+$ with SiH_4 are in qualitative agreement with those of Beggs and Lampe[2] for reactions 5, 7, and 9–11 but are in general smaller by a factor of 3–4. Our rate constants for reaction 8 cannot be considered to be in even qualitative agreement since it is smaller by a factor of 30 than that reported by Beggs and Lampe.[2] Moreover, the fastest of all the reactions of $C_2H_2^+$ with SiH_4, namely, formation of SiH_3^+, could not be observed with the single-source technique of Beggs and Lampe,[2] since SiH_3^+ is a reactant ion as well as a product ion in this system. Since the rate constants of Beggs and Lampe[2] refer to thermal-energy ions and in this work were determined at a center-of-mass energy of 0.77 eV, it is conceivable that the former values could be correct. However, we do not think so because normally the phenomenological rate constants at low energies are not very sensitive to collision energy;[19] secondly, the total reaction rate constant of $C_2H_2^+$ with SiH_4 obtained by Beggs and Lampe,[2] when increased by the contribution of reac-

TABLE I: Exothermic Ion–Molecule Reactions in SiH_4–C_2H_2 Mixtures

Reaction no.	Reaction	$\Delta H°$, kcal	$10^{10}k$, cm³/sec This work	$10^{10}k$, cm³/sec Ref 2
3	$C_2H_2^+ + SiH_4 \rightarrow Si^+ + C_2H_4 + H_2$	−15	1.1 ± 0.4	Not observed
4	$\rightarrow SiH^+ + C_2H_5$	+8	0.73 ± 0.30	Not observed
5	$\rightarrow SiH_2^+ + C_2H_4$	−30	4.1 ± 1.6	14 ± 4
6	$\rightarrow SiH_3^+ + C_2H_3$	−21	10 ± 4	Not observed
7	$\rightarrow SiCH_3^+ + CH_3$	−16	0.32 ± 0.13	1.1 ± 0.3
8	$\rightarrow SiC_2H^+ + 2H_2 + H$		0.10 ± 0.04	3.0 ± 0.8
9	$\rightarrow SiC_2H_3^+ + H_2 + H$		0.49 ± 0.19	3.5 ± 0.9
10	$\rightarrow SiC_2H_4^+ + H_2$		0.18 ± 0.07	0.8 ± 0.2
11	$\rightarrow SiC_2H_5^+ + H$		0.89 ± 0.35	2.6 ± 0.7
12	$Si^+ + C_2H_2 \rightarrow SiC_2H^+ + H$		1.8 ± 0.7	Not observed
13	$SiH^+ + C_2H_2 \rightarrow SiC_2H^+ + H_2$		1.5 ± 0.6	Not observed
14	$\rightarrow SiC_2H_2^+ + H$		1.7 ± 0.7	Not observed
15	$SiH_2^+ + C_2H_2 \rightarrow SiC_2H^+ + H_2 + H$		0.44 ± 0.17	Not observed
16	$\rightarrow SiC_2H_2^+ + H_2$		0.63 ± 0.25	Not observed
17	$\rightarrow SiC_2H_3^+ + H$		3.2 ± 1.2	11 ± 3
18	$SiH_3^+ + C_2H_2 \rightarrow SiC_2H^+ + 2H_2$		0.1 ± 0.04	Not observed
19	$\rightarrow SiC_2H_3^+ + H_2$		0.26 ± 0.10	Not observed

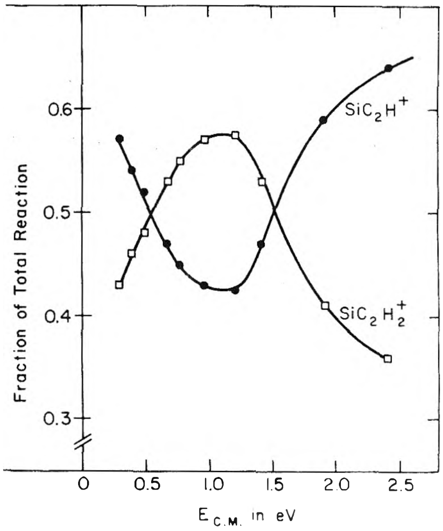

Figure 1. Kinetic energy dependence of reactions of SiH^+ with C_2H_2. Contribution of the two reaction channels to the total cross section as a function of center-of-mass energy: ●, SiC_2H^+; □, $SiC_2H_2^+$.

tion 6, which they could not observe, is far in excess of the Langevin polarization theory rate constant[20] for this reactant pair of 14.4 × 10^{-10} cm³/sec. On the other hand, the total reaction rate constant for $C_2H_2^+$ with SiH_4 determined in this work is 17.9 × 10^{-10}, a much more plausible result.

In view of the above discussion we believe that our present results supercede those of Beggs and Lampe[2] and demonstrate once again[4,8] the inadequacy of low-pressure, single-source mass-spectrometric techniques for detailed studies of ion–molecule reactions in systems containing more than one neutral reactant.

(*b*) *$Si^+ + C_2H_2$*. The only product ion observed when Si^+ ions were injected into the collision chamber containing C_2H_2 was SiC_2H^+. The reaction is exothermic, as indicated by the dependence of cross section on collision energy, and has a phenomenological rate constant of 1.8 ± 0.7 × 10^{-10} cm³/sec. For purposes of comparison the low-energy Langevin rate constant for this reactant pair is 1.2 × 10^{-9} cm³/sec. Beggs and Lampe[2] were unable to observe this reaction in their apparatus.

(*c*) *$SiH^+ + C_2H_2$*. Two product ions are observed when 1.4-eV SiH^+ ions react with C_2H_2, namely, SiC_2H^+ and $SiC_2H_2^+$. Both reactions are exothermic since all cross sections decrease with increasing collision energy. The total phenomenological rate constant for this reactant pair is 3.2 × 10^{-10} cm³/sec as compared with the Langevin orbiting rate constant of 1.1 × 10^{-9} cm³/sec.

In Figure 1 is shown the relative contributions of the two channels of reaction of SiH^+ with C_2H_2 as a function of collision energy. The increase in relative abundance of the SiC_2H^+ product above 1.2 eV is due to an increase in the actual cross section for SiC_2H^+ formation which is probably the result of the opening of the endothermic channel depicted by

$$SiH^+ + C_2H_2 \longrightarrow SiC_2H^+ + 3H \qquad (20)$$

Neither of the reactions of SiH^+ with C_2H_2 could be detected in the apparatus used by Beggs and Lampe.[2]

(*d*) *$SiH_2^+ + C_2H_2$*. Collision of SiH_2^+ with C_2H_2 produces SiC_2H^+, $SiC_2H_2^+$, and $SiC_2H_3^+$ ions by reactions 15–17 shown in Table I. All reactions exhibit exothermic behavior in the dependence of cross section on collision energy. The cross section of reaction 15 goes through a minimum at 1.2-eV collision energy, similar to that of reaction 13. The most probable explanation for this behavior is the opening of the endothermic channel shown by

$$SiH_2^+ + C_2H_2 \longrightarrow SiC_2H^+ + 3H \qquad (21)$$

Reaction 17 was reported by Beggs and Lampe[2] to occur with a rate constant in qualitative agreement with that obtained in this work; if one assumes the rate constants in the two investigations to be the same for reaction 5, one obtains values for reaction 17 that are in excellent agreement.

(*e*) *$SiH_3^+ + C_2H_2$*. Collision of SiH_3^+ with C_2H_2 results in the formation of SiC_2H^+ and $SiC_2H_3^+$ by reactions 18 and 19 shown in Table I. Both reactions are quite slow, such behavior being quite typical of second-order reactions of SiH_3^+ with hydrocarbons,[7,8,21] Beggs and Lampe[2] were not able to observe any reactions of SiH_3^+ in their apparatus. The cross-section dependence on energy indicates both reactions 18 and 19 to be exothermic.

(*f*) *Endothermic Reactions*. All of the reactions in Table I are observed to be exothermic, and the onset of the two endothermic processes 20 and 21 has already been mentioned. In addition to these latter reactions

$$C_2H_2^+ + SiH_4 \longrightarrow SiC_2H_2^+ + (4H) \qquad (22)$$

and

$$C_2H_2^+ + SiH_4 \longrightarrow SiCH_2^+ + (C + 4H) \qquad (23)$$

where the state of aggregation of the products in parentheses is not known, were also observed as endothermic processes. The threshold of (22) lies above 1.1 eV and that of (23) above 1.4 eV, both energies being in the center-of-mass system.

(2) *High-Pressure Mass Spectra.* The variation of abundance of the major product ions of Table I with ion-source pressure for an SiH_4-C_2H_2 mixture containing 10% C_2H_2 is shown in Figures 2 and 3. Inspection of these figures and comparison with similar plots for pure SiH_4 demonstrate that the presence of 10% of C_2H_2 has a major effect on the ionic chemistry of monosilane.

In pure monosilane the intensity of SiH_3^+ increases with pressure initially but passes through a maximum of about 50% of the total ionization at a source pressure of 0.06 Torr. Subsequent to this maximum, $Si_2H_7^+$, which is formed by the termolecular association of SiH_3^+ with SiH_4, increases with increasing pressure and attains a maximum at about 0.19 Torr that represents about 35% of the total ionization. The major secondary ions in SiH_4, typified by $Si_2H_4^+$, attain maxima in the range 0.10–0.15 Torr, with $Si_2H_4^+$ reaching 19% of the total ionization.

This situation is drastically altered by the presence of 10% of acetylene as can be seen in Figure 2. Here one sees that the expected maximum in SiH_3^+ intensity must lie below 0.04 Torr and that the maximum abundance of its' association product with monosilane, namely, $Si_2H_7^+$, is less than 6%. Both effects are undoubtedly due to a very effective competition of C_2H_2 with SiH_4 for SiH_3^+, even though SiH_4 is ninefold more abundant. The bimolecular reactions of SiH_3^+ with C_2H_2 (Table I) and those of SiH_3^+ with SiH_4,[9] while partially accounting for these facts, are not sufficient. Figure 3 shows that above 0.04 Torr $SiC_2H_5^+$ appears in much greater abundance relative to SiC_2H^+ and $SiC_2H_3^+$ than expected from the bimolecular rate constants of Table I. It is thus suggested that SiH_3^+ undergoes rapid termolecular association with C_2H_2 as shown by

$$SiH_3^+ + C_2H_2 \xrightarrow{M} SiC_2H_5^+ \qquad (24)$$

This association reaction could not be detected at the low pressures obtaining in the tandem experiments. The fact that the maximum in $SiC_2H_5^+$ occurs at higher pressures than do those for SiC_2H^+ and $SiC_2H_3^+$ is consistent with the formation of $SiC_2H_5^+$ from (24), since the SiH_3^+ is still very abundant at 0.10 Torr.

In the SiH_4-C_2H_2 mixture the maximum abundance of $Si_2H_4^+$ (Figure 2) must be considerably lower than that in pure monosilane (19% of total ionization) and it is shifted from about 0.15 Torr in the pure compound to a pressure of less than 0.04 Torr. This is typical also of the behavior of $Si_2H_2^+$ and $Si_2H_5^+$ and indicates that these secondary ions of pure monosilane react rapidly with acetylene although the products of these reactions are at the moment somewhat obscure. $Si_2H_3^+$ appears to behave in the mixture identically with that in the pure compound, namely, it appears to be quite unreactive, its abundance remaining essentially constant over the pressure range 0.04–0.3 Torr.

The major secondary organosilicon ions formed by the reactions in Table I and by (25) are also reactive in this system as shown by Figure 3. While we are not certain of the details of their fates, we believe that a major cause of their depletion as well as of $Si_2H_5^+$ and $Si_2H_7^+$ is association with C_2H_2. The basis of this contention is Figure 4 which shows the relative intensities of *m/e* 53–57, *m/e* 61, and *m/e* 63 as well as the relative intensities of ions with *m/e* increased by 26, respectively, for several pressures. The observed similarity of the patterns leads us to suggest that these secondary ions in question react primarily by association with acetylene. There is a suggestion in the spectra that at masses even higher this addition of successive units of C_2H_2 continues, analogously to the observed ionic polymerization of acetylene.[22-24]

It has been reported[11] that in the γ-ray radiolysis of monosilane at 0.5 atm pressure, the addition of acetylene results in an increase in $G(H_2)$, apparently from a value of 22.8 to 52.7. This is a rather startling effect since the radiolysis of acetylene[25] produces very little hydrogen and the reactions of free radicals derived from SiH_4 would not be expected to produce hydrogen upon reaction with acety-

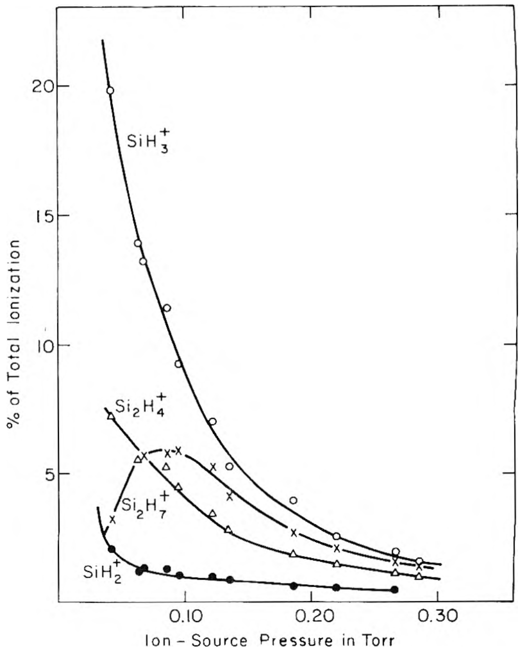

Figure 2. Pressure dependence of relative intensities of major siliconium ions in a 90% SiH_4–10% C_2H_2 mixture: ○, SiH_3^+; ●, SiH_2^+; △, $Si_2H_4^+$; X, $Si_2H_7^+$.

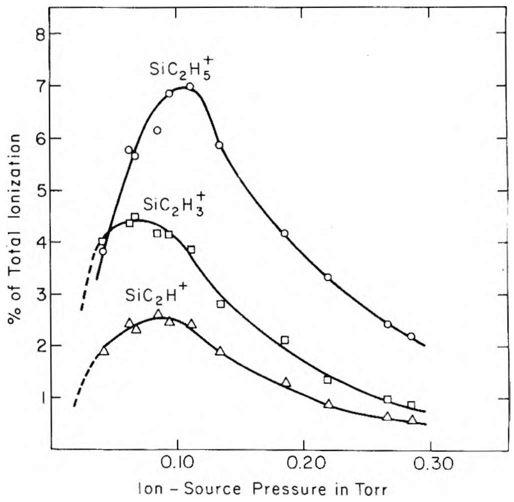

Figure 3. Pressure dependence of relative intensities of major organosilicon ions in a 90% SiH_4–10% C_2H_2 mixture: △, SiC_2H^+; □, $SiC_2H_3^+$; ○, $SiC_2H_5^+$.

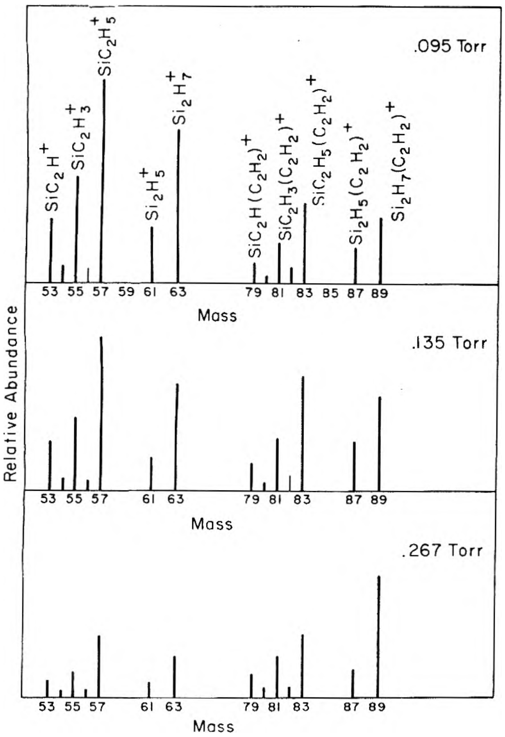

Figure 4. High-pressure spectra of major ions in a 90% SiH_4–10% C_2H_2 mixture. Similarity of the ion intensity patterns for the mass regions 53–63 and 79–89 suggests reaction by association with an acetylene molecule.

lene.[26-28] While the details remain unclear, we suggest that the striking effect of acetylene on $G(H_2)$ in the radiation chemistry[11] is associated with this very marked effect that acetylene has on the ionic chemistry of SiH_4. Thus in a radiolysis system containing an excess of monosilane we would expect increased H_2 production because of reactions 3, 8–12, 18, and 19 and neutralization of the association complexes of C_2H_2 with SiH_3^+; reactions of Si^+, SiH^+, and SiH_2^+ with C_2H_2 will not be of importance in a system containing an excess of SiH_4. Hydrogen atoms formed in reactions 8, 9, 11, and 12 are known[29] to react very efficiently with SiH_4 to form H_2 and SiH_3.

Acknowledgment. This work was supported by the U. S. Atomic Energy Commission under Contract No. AT(11-1)-3416. We also wish to thank the National Science Foundation for providing funds to assist in the original purchase of the Nuclide Associates mass spectrometer and the Gulf Oil Corporation for a grant that assisted in the construction of the tandem mass spectrometer.

References and Notes

(1) U. S. Atomic Energy Commission Document No. COO-3416-14.
(2) D. P. Beggs and F. W. Lampe, *J. Phys. Chem.*, **73**, 3307 (1969).
(3) V. L. Tal'roze and E. L. Frankevich, *Zh. Fiz. Khim.*, **34**, 2709 (1960).
(4) C. W. Hand and H. von Weyssenhoff, *Can. J. Chem.*, **42**, 195 (1964).
(5) G. G. Hess and F. W. Lampe, *J. Chem. Phys.*, **44**, 2257 (1966).
(6) D. P. Beggs and F. W. Lampe *J. Phys. Chem.*, **73**, 4194 (1969).
(7) G. W. Stewart, J. M. S. Henis, and P. P. Gaspar, *J. Chem. Phys.*, **57**, 990 (1972).
(8) T. M. H. Cheng, Tung-Yang Yu, and F. W. Lampe, *J. Phys. Chem.*, **77**, 2587 (1973).
(9) T-Y. Yu, T. M. H. Cheng, V. Kempter, and F. W. Lampe, *J. Phys. Chem.*, **76**, 3321 (1972).
(10) T. M. H. Cheng and F. W. Lampe, *Chem. Phys. Lett.*, **19**, 532 (1973).
(11) W. Ando and S. Oae, *Bull. Chem. Soc. Jap.*, **35**, 1540 (1962).
(12) T. M. H. Cheng, T-Y. Yu, and F. W. Lampe, unpublished results.
(13) P. Potzinger and F. W. Lampe, *J. Phys. Chem.*, **73**, 3912 (1969); **74**, 719 (1970).
(14) J. L. Franklin, J. G. Dillard, H. M. Rosenstock, J. T. Herron, K. Drexl, and F. H. Field, *Nat. Stand. Ref. Data Ser., Nat. Bur Stand.*, **No. 26** (June 1969).
(15) T. M. H. Cheng and F. W. Lampe, *J. Phys. Chem.*, **77**, 2841 (1973).
(16) A. G. MacDiarmid, *Advan. Inorg. Radiochem.*, **3**, 216 (1961).
(17) E. A. V. Ebsworth, "Volatile Silicon Compounds," Pergamon Press, London, 1963 p 16.
(18) T. M. Mayer and F. W. Lampe, *J. Phys. Chem.*, **78**, 2195 (1974).
(19) D. Hyatt and K. Lacmann, *Z. Naturforsch. A*, **23**, 2080 (1968).
(20) G. Gioumousis and D. P. Stevenson, *J. Chem. Phys.*, **29**, 294 (1958).
(21) D. P. Beggs and F. W. Lampe, *J. Phys. Chem.*, **73**, 3315 (1969).
(22) M. S. B. Munson, *J. Phys. Chem.*, **69**, 572 (1965).
(23) G. A. Derwish, A. Galli, A. Giardini-Guidoni, and G. G. Volpi, *J. Amer. Chem. Soc.*, **87**, 1159 (1965).
(24) J. H. Futrell and T. O. Tiernan, *J. Phys. Chem.*, **72**, 158 (1968).
(25) S. C. Lind, D. C. Bardwell, and J. W. Perry, *J. Amer. Chem. Soc.*, **48**, 1556 (1926).
(26) D. G. White and E. G. Rochow, *J. Amer. Chem. Soc.*, **76**, 3897 (1954).
(27) G. Rabilloud, *Bull. Soc. Chim. Fr.*, 2152 (1965).
(28) J. F. Schmidt and F. W. Lampe, *J. Phys. Chem.*, **73**, 2706 (1969).
(29) D. Mihelcic, P. Potzinger, and R. N. Schindler, *Ber. Bunsenges. Phys. Chem.*, **78**, 82 (1974).

Kinetic Isotope Effects in the Reactions of Hydrogen and Deuterium Atoms with Dimethyl Ether and Methanol

James F. Meagher, P. Kim, J. H. Lee, and Richard B. Timmons*

Department of Chemistry, The Catholic University of America, Washington, D.C. 20017

(Received December 12, 1973; Revised Manuscript Received August 16, 1974)

Publication costs assisted by The Catholic University of America

The kinetics and mechanism of the reactions of H and D atoms with CH_3OCH_3 and CH_3OH have been investigated using flow discharge methods. The specific rate constant for the reaction $H + CH_3OCH_3 \rightarrow H_2 + CH_2OCH_3$ was found to be $(1.3 \pm 0.5) \times 10^{13} \exp(-4700 \pm 100/RT)$ cm^3 mol^{-1} sec^{-1}. The specific rate constant for the corresponding reaction with methanol $H + CH_3OH \rightarrow H_2 + CH_2OH$ is recommended to be $6.5 \times 10^{12} \exp(-5440 \pm 150/RT)$ cm^3 mol^{-1} sec^{-1}. This value is based on an assumed preexponential factor obtained from the CH_3OCH_3 results. Major emphasis was placed on comparing the magnitude of the kinetic isotope effects in the reactions of H and D atoms with CH_3OCH_3 and CH_3OH. The temperature dependence of the kinetic isotope effects of these two molecules was found to be equal, within experimental error. From this it is concluded that the reactive intermediates formed in the attack of H atoms on CH_3OCH_3 or CH_3OH must be nearly identical with respect to bond breakage and bond formation in the activated complex. Thus, the substitution of an H atom for the CH_3 group in going from CH_3OCH_3 to CH_3OH results, apparently, in relatively little effect on the reaction dynamics in the case of H atom attack reactions studied in this work.

Introduction

In considering a bimolecular abstraction reaction of the type

$$H + RX \longrightarrow H_2 + R'X\cdot$$

one would like to know what effect, if any, the substituent group, X, might exert on the structure of the activated complexes formed in these reactions. In order for any reasonable comparison to be made it is, of course, essential that varying the substituent group not change the reaction mechanism.

In this paper, we wish to report on the reactions of H and D atoms with dimethyl ether (DME) and methanol, in which the X group above becomes $-OCH_3$ and $-OH$, respectively. These are reactions in which we feel that valid comparisons are justified in that the reaction mechanisms are the same and the heats of reaction are approximately equal. The C–H bond strengths in CH_3OCH_3 are comparable in magnitude and the C–H bond strength in methanol is much weaker than the O–H bond strength.Thus, in the methanol reaction, the abstractive reaction from the C–H bonds will predominate as in the DME reaction.

In order to assess the relative influence of the $-OCH_3$ or $-OH$ group on the activated complexes formed, we have studied the kinetic isotope effects in the reactions of H and D atoms with CH_3OCH_3 and CH_3OH over a fairly extended temperature range. The magnitude of the kinetic isotope effect can be used to assess the extent of bond breaking and bond formation in the activated complexes and thus is a useful probe in comparing the reaction dynamics of these two molecules in this particular type reaction.

In addition, it might be noted that there appear to be few quantitative gas phase kinetic data available in the literature on the kinetics and mechanism of the reactions of hydrogen atoms with ethers or alcohols. Therefore, the kinetic results reported here are an added contribution in that respect. The kinetic parameters obtained in this work can be compared with other molecular systems, particularly the reactions of H atoms with alkanes.

Experimental Section

The experimental studies were carried out using fast flow methods. Atomic species were generated by a microwave electrodless discharge of H_2 or D_2 in inert helium or argon carrier gas. Most of the kinetic data were obtained by esr studies of the decay rate of H or D atoms as functions of the various reaction variables. In addition, a number of experiments were carried out on a separate flow apparatus using mass spectrometric detection to follow the consumption rate of the stable reactant. The esr spectrometer employed was a Varian Model 4503 instrument equipped with a Varian Model V-4535 large sample access cavity. A Varian-MAT Model CH5 mass spectrometer was employed in our mass spectrometric studies. It was coupled to the flow apparatus through an all-glass inlet port, including a glass leak into the ion source.

The details of the experimental procedures involved in both the esr and mass spectrometric work have been discussed previously.[1] For the present purpose, it is sufficient to state that the kinetic data are obtained under pseudo-first-order conditions employing a large excess of the stable reactant in the esr work, whereas a large excess of the atomic species is employed in the mass spectrometric studies. The integrated first-order rate expressions then predict a linear plot of the logarithm of the atomic or stable molecule decay *vs.* time of reaction. Such plots were obtained in the present studies with excellent precision. An example of these decay plots is shown in Figure 1 for the $H + CH_3OH$ reaction. The overall approach and procedure involved in this work is virtually identical with the method developed by Westenberg and de Haas in applying esr spectroscopy as a tool in measuring atom–molecule reaction rates.[2] The setup we employed was similar to the modified version of their original apparatus as described in 1969.[3]

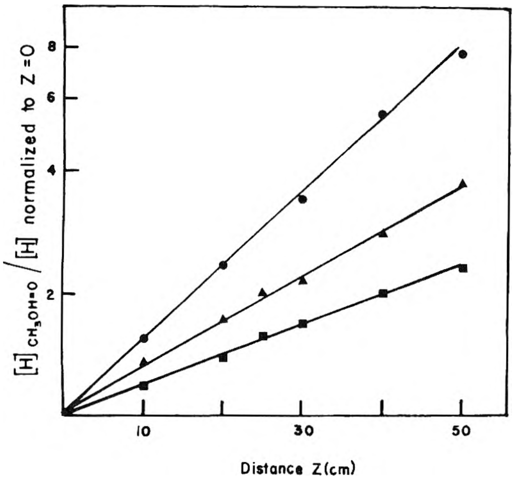

Figure 1. Typical atom decay plots observed in the reaction of H + CH_3OH at 491°K: (●) total pressure = 2.13 Torr, v = 1262 cm sec^{-1}, $[CH_3OH] = 3.42 \times 10^{-10}$ mol cc^{-1}; (▲) pressure = 1.78 Torr, v = 1523 cm sec^{-1}, $[CH_3OH] = 6.68 \times 10^{-10}$ mol cc^{-1}; (■) pressure 1.78 Torr, v = 1530 cm sec^{-1}, $[CH_3OH] = 3.05 \times 10^{-10}$ mol cc^{-1}.

Unfortunately, we were unable to obtain any kinetic data on the reactions of H and D atoms with CH_3OH using mass spectrometry to follow the CH_3OH concentration. Since the reactant ratio required for the mass spectrometric work is [atom] ≫ CH_3OH, the partial pressure of the CH_3OH is extremely low. When the CH_3OH flow was diverted to a bypass position, the mass peak at m/e 31, used to monitor the CH_3OH concentration, decreased very slowly requiring 15–20 min to reach an equilibrium value. Thus, it was apparent that quantities of the highly polar CH_3OH, significant in comparison with that in the gas phase, must be adsorbed on the walls of the flow tube. As such, we would be unable to distinguish between the homogenous and heterogenous contributions to the reaction rate. For this reason, we were not successful in obtaining mass spectrometric data on these reactions. This particular problem did not seem to present any difficulties in the esr studies in which the methanol concentrations involved are very much larger than those employed in the mass spectrometric work. Experimentally we observed that diverting the CH_3OH flow to a bypass position, at temperatures above 298°K, resulted in an increased H or D atom esr signal intensity, as expected, and this signal remained constant with time. It is also worth noting, that we did not encounter any complications arising from reaction products and/or surface effects in either the DME or methanol esr studies. Flowing the stable molecule through the reactor at a fixed injector position, for a long period of time, resulted in an atom signal intensity which remained constant with time. This observation can be contrasted with the experiences we have encountered in other systems, for example, the $O(^3P) + C_6H_6$ reaction, in which a slow decrease in atom intensity was noted with prolonged flow of the stable reactant.[4] In view of the lack of any such complications, the precision of the rate measurements obtained in the present study are sufficiently good to obtain the data necessary to distinguish between the small differences in reactivity of H and D atoms in reactions with these stable molecules.

The mass spectrometric studies require a knowledge of the absolute atom concentrations in order to obtain the desired specific rate constant. In this work, the hydrogen and deuterium atom concentrations were determined using NO_2 as the titrant gas. A reaction stoichiometry of two hydrogen atoms per three molecules of NO_2 was employed.[5] More recent kinetic investigations of H + NO_2 have shown it to be a complex reaction in which the exact reaction stoichiometry depends on the nature of the wall conditioning as well as the relative concentrations of NO_2 and H atoms.[6] Since titrations in the present study were carried out in the presence of a five or sixfold excess of NO_2, the assumed reaction stoichiometry of $\Delta NO_2/\Delta H = 1.5$ seems reliable, particularly in view of the recent esr studies by Westenberg and de Haas[7] on this system. However, one should bear in mind that any uncertainty in the atom concentration will be reflected in the reported rate constants.

Unfortunately, it is not possible to detect the presence of hydrogen atoms using our mass spectrometric apparatus. For that reason the mass spectrometric studies were limited to reaction mixtures containing an excess of atoms over stable reactants. It would have been useful to follow the formation of reactant products such as CH_4 or C_2H_6 etc. However, under the conditions of low DME or CH_3OH concentration involved in these studies, the background peaks in the low mass ranges (arising from cracking of the polyphenyl diffusion pump oil) obscured our attempts at quantitative measurement of reaction products.

Results and Discussion

H (and D) + DME Reactions. The esr data obtained from studies of H and D atoms with CH_3OCH_3 are shown in Tables I and II, respectively. The mass spectrometric results from these same reactions are shown in Table III. Plots of these data in terms of an Arrhenius' equation are shown in Figure 2. It is apparent that, although the higher temperature data fit an Arrhenius type plot, there is significant curvature obtained at the lowest temperatures. Discussion of this curvature along with possible reasons for its existence is deferred until a later section.

Over the temperature range of 251–365°K, linear least-squares treatment of the data gives values of $(2.61 \pm 0.13) \times 10^{13} \exp(-4700 \pm 50/RT)$ and $(4.14 \pm 0.73) \times 10^{13} \exp(-4430 \pm 100/RT)$ $cm^3\ mol^{-1}\ sec^{-1}$ for the H + DME and D + DME, respectively, based only on the esr data. The higher preexponential factor for the D atom reaction is contrary to theoretical predictions, however, we feel it is consistent with the following mechanism proposed for this system

$$H + CH_3OCH_3 \longrightarrow H_2 + CH_2OCH_3 \tag{1}$$

$$H + CH_2OCH_3 \longrightarrow CH_3OCH_3^* \tag{2}$$

$$CH_3OCH_3^* \longrightarrow CH_3 + OCH_3 \tag{3}$$

$$H + OCH_3 \longrightarrow CH_3 + OH \tag{4}$$

$$\longrightarrow CH_2O + H_2 \tag{5}$$

followed by radical recombination reactions. A similar mechanism would apply to the D + DME reactions with the important addition that we must include reactions involving isotope exchange with the methyl radicals

$$D + CH_3 \longrightarrow CH_2D + H \tag{6}$$

$$D + CH_2D \longrightarrow CHD_2 + H \text{ etc.} \tag{7}$$

Such exchange reactions are rapid processes and they have been shown to occur under flow tube conditions in other reactions in which methyl radicals are formed.[8,9] As a result of the occurrence of reactions 6 and 7, the mechanism pre-

ห้องสมุด กรมวิทยาศาสตร์

TABLE I: Experimental Results Obtained in the Esr Study of the H + CH_3OCH_3 Reaction

T, °K	p, Torr	v, cm/sec	$10^{10}[CH_3OCH_3]$, mol/cc	(DME)/(H_2)	k,[a] cc/mol sec
207	1.60	819	3.85	4.52	7.72×10^8
	1.69	791	8.29	9.41	8.06
	2.63	504	13.59	9.85	9.24
	2.67	512	9.09	6.67	8.52
					k_{av} 8.38×10^8
211	2.40	615	1.89	1.60	1.17×10^9
	3.61	394	2.76	1.54	0.95
	2.41	606	6.89	5.76	0.81
	5.40	264	5.59	1.99	0.76
					k_{av} 9.22×10^8
231	1.42	901	3.21	4.26	1.60×10^9
	1.46	888	4.76	6.30	1.40
	2.52	520	8.08	6.18	1.95
	1.50	884	6.15	8.15	1.58
					k_{av} 1.63×10^9
251	2.34	653	3.05	2.69	2.64×10^9
	2.34	653	3.13	2.76	2.84
	2.32	659	4.78	4.25	2.48
	2.39	640	6.07	5.25	2.46
	2.45	671	8.24	7.46	2.45
					k_{av} 2.57×10^9
273	2.80	772	1.88	2.04	4.52×10^9
	2.86	758	2.95	3.14	4.70
	2.82	770	3.90	4.22	4.60
	2.90	757	5.59	6.11	4.07
	2.93	545	1.26	0.97	4.07
					k_{av} 4.39×10^9
298	1.80	731	0.63	0.74	8.17×10^7
	2.75	478	0.96	0.74	8.62
	1.79	740	1.26	1.50	9.96
	2.05	767	2.26	3.82	9.51
	2.05	736	1.66	2.70	9.43
	2.05	738	2.11	2.20	8.83
	2.05	810	9.27	1.06	11.13
					k_{av} 9.38×10^9
343	1.50	1230	0.46	0.91	3.54×10^{10}
	1.51	1220	0.79	1.53	2.45
	1.51	1230	1.22	2.41	2.44
	1.60	1210	2.14	3.55	2.45
	2.51	779	1.02	1.09	2.51
					k_{av} 2.68×10^{10}
365	1.60	1242	0.49	0.87	4.29×10^{10}
	1.60	1245	0.65	1.22	3.42
	1.66	1214	0.33	0.60	3.76
					k_{av} 3.82×10^{10}

[a] Specific rate coefficients are uncorrected for any reaction stoichiometry.

dicts a higher preexponential factor for the deuterium atom reactions, as observed experimentally. It might be mentioned, that H atom esr signals were observed in the D + DME studies with the H atoms arising, presumably, from reactions such as (6) or (7).

Obviously, the above mechanism predicts that the *A* factors from both reactions are too high as a result of additional atom consumption after the initial abstraction reaction. In order to obtain a measure of this stoichiometric factor, the mass spectrometric results shown in Table III and Figure 2 are useful. Since we are monitoring the disappearance of DME, the subsequent reactions of H or D atoms will not influence the rate measurements as the atom concentration is present in large excess. We are excluding from consideration the reaction of CH_3 with DME as the specific rate constant for this reaction is, in all probability, much smaller than the corresponding H (or D) + DME reaction. For example, the rate constant for H + CH_4 is 6×10^7 cm^3 mol^{-1} sec^{-1} at 425°K[5] whereas that for CH_3 + CH_4 is 1×10^5 cm^3 mol^{-1} sec^{-1} at 425°K.[10] Furthermore, under the mass spectrometric conditions the ratio of atom/CH_3 is exceedingly large and therefore abstraction by CH_3 radicals from DME must be negligible compared to that by H or D atoms. If OH(or OD) radicals are generated in this system, we must consider the reaction of OH + DME → H_2O + CH_2OCH_3 as it would be a reasonably fast reaction. However, under the mass spectrometric conditions, the concentration of H_2 or D_2 is of the order of 200–400 times larger than that of DME. AT 352°K, the midpoint in the mass spectrometric studies, the reaction OH + H_2 → H_2O + H has a reported specific rate constant of 1.06×10^{10} cm^3 mol^{-1} sec^{-1}.[11] Therefore, even if the OH + DME reaction has a specific rate constant as high as $\sim 5 \times 10^{11}$ cm^3 mol^{-1} sec^{-1}, the reaction of OH + H_2 would still predominate. For these reasons, we feel that our mass spectrometric measurements are reasonably free from stoichiometric factors with respect to DME consumption. The specific rate constant we obtain from linear least-squares treatment of the mass spectrometric data is $(1.3 \pm 0.5) \times 10^{13} \exp(4600 \pm 200/RT)$ cm^3 mol^{-1} sec^{-1}. The activation energy is in close

TABLE II: Experimental Results Obtained in the Esr Study of the D + CH_3OCH_3 Reaction

T, °K	p, Torr	v, cm sec^{-1}	$10^{10}[CH_3OCH_3]$, mol cc^{-1}	$CH_3OCH_3/[D_2]$	k,[a] cm^3 mol^{-1} sec^{-1}
198	2.34	490	9.57	5.42	1.59×10^9
	1.50	773	6.05	5.52	1.22
	1.62	761	8.91	7.85	1.25
	1.72	766	10.84	9.62	1.26
					k_{av} 1.33×10^9
211	2.40	592	2.42	3.69	1.99×10^9
	2.40	593	3.65	5.58	2.00
	2.40	594	4.96	7.60	1.70
	2.43	602	7.47	11.6	2.04
					k_{av} 1.93×10^9
230	1.40	903	7.22	3.42	4.13×10^9
	1.41	930	4.88	5.26	4.80
	1.41	886	2.57	2.64	3.48
	2.28	563	4.44	2.90	4.38
					k_{av} 4.20×10^7
250	2.11	629	3.12	3.61	6.02×10^7
	2.11	653	2.11	2.55	5.74
	2.11	645	1.52	1.82	5.59
	2.11	642	0.88	1.05	5.56
					k_{av} 5.73×10^9
273	2.84	763	0.85	1.48	1.03×10^{10}
	2.89	745	2.28	3.88	1.19
	2.90	747	1.61	2.75	1.69
	2.84	752	1.17	2.00	1.52
	2.83	749	0.51	0.87	0.92
					k_{av} 1.27×10^{10}
298	2.04	698	0.88	11.1	2.13×10^{10}
	2.03	701	0.47	5.8	1.66
	2.25	634	0.21	3.6	1.38
	2.23	651	1.47	11.3	2.34
	2.23	650	1.13	12.4	2.29
					k_{av} 1.96×10^{10}
332	1.52	1184	0.25	0.78	6.92×10^{10}
	2.20	818	0.36	0.78	4.94
	1.59	1136	0.52	1.57	5.16
	1.60	1127	0.38	1.14	5.18
					k_{av} 5.55×10^{10}
363	1.60	1202	0.30	0.94	7.56×10^{10}
	1.60	1200	0.14	0.43	11.52
	1.61	1193	0.20	0.62	9.19
	1.61	1196	0.37	1.18	8.12
					k_{av} 9.10×10^{10}

[a] Specific rate coefficients are uncorrected for any reaction stoichiometry.

agreement with the esr result, whereas the preexponential factor is approximately a factor of 2 lower than H + DME from the esr work. However, such a difference in A factors is expected in terms of the proposed reaction mechanism and indicates that, on the average, an extra H atom is consumed each time reaction 1 occurs. With respect to the D + DME results, the A factor from the esr studies is approximately a factor of 3 higher than the mass spectrometric result and we feel this added difference can be accounted for satisfactorily by the occurrence of reactions 6 and/or 7.

A number of mass spectrometric experiments on the D + DME reaction gave specific rate constants in close agreement with the mass spectrometric H + DME studies, as shown in Figure 2. This result is in accord with the proposed mechanism. Of greater significance in the D + DME work was the complete absence of any increase in the mass peak at 47 which would indicate the formation of CH_2DOCH_3. For that reason, we have concluded that the lifetime of the chemically activated species formed in reaction 2 must be short compared with collisional relaxation. Thus atomic cracking predominates under our reaction conditions of low total pressure and a flow mixture in which the major components are helium and H_2 or D_2 (inefficient molecules from the energy transfer point of view). As a result of the lack of detection of measurable amounts of CH_2DOCH_3, we have not included the collisional stabilization reaction of excited CH_3OCH_3* or CH_2DOCH_3* in the reaction mechanism.

The specific rate constants reported above were calculated using data above 251°K, above which temperature reasonable linear Arrhenius' plots were obtained. However, definite curvature is observed in these Arrhenius' plots at low temperatures. It is tempting to ascribe this increased reaction rate at low temperatures simply to a heterogenous component of the reaction, having a lower activation energy, and thus, a more noticeable effect only at the lower temperatures. However, with respect to this suggestion, it is important to note that we did not observe any unusual effects in taking the low-temperature esr data. For example, if reactions of adsorbed DME molecules become more significant at lower temperatures, we might have anticipated that diverting the DME to a bypass position would result in a sluggish return of the hydrogen or deuterium atom esr signal up to constant value. In point of fact, diverting the ether to a bypass position resulted in an essentially instantaneous return of the atom signal to constant

TABLE III: Experimental Results Obtained in the Mass Spectrometric Studies of the Reactions of H and D Atoms with CH_3OCH_3

T, °K	p, Torr	v, cm sec^{-1}	$[H]/[CH_3OCH_3]$	k, cm^3 mol^{-1} sec^{-1}
		$H + CH_3OCH_3$		
300	0.61	1744	40.8	7.55×10^9
	0.61	1760	41.3	6.44
	0.63	1689	30.1	4.92
				k_{av} 6.30×10^9
327	0.59	2482	46.0	1.42
	0.61	2590	42.5	1.18
	0.66	2219	30.1	1.66
	0.66	2219	35.6	1.73
	0.68	2120	30.5	1.17
				k_{av} 1.43×10^{10}
385	0.69	2160	19.6	3.86×10^{10}
	0.43	2025	18.7	3.98
	0.65	2079	16.5	3.89
				k_{av} 3.91×10^{10}
404	0.47	966	10.8	4.75×10^{10}
	0.62	2413	14.4	5.29
	0.40	1065	15.3	5.38
	0.48	1545	11.4	4.79
				k_{av} 5.05×10^{10}
		$D + CH_3OCH_3$		
300	0.72	1849	32.8	6.95×10^9
	0.89	2125	29.2	7.54
	0.93	2150	28.7	7.49
				k_{av} 7.33×10^9
404	0.41	1275	12.8	3.95×10^{10}
	0.47	1083	15.2	4.81
	0.69	1378	10.4	4.21
				k_{av} 4.32×10^{10}

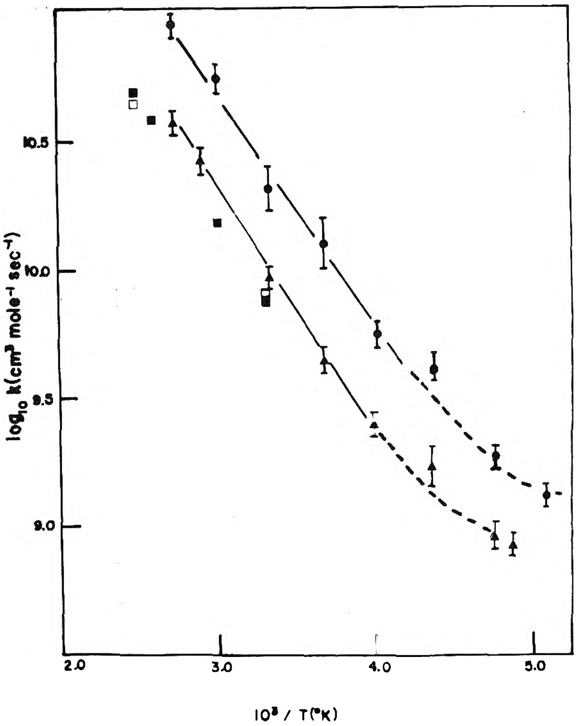

Figure 2. Arrhenius plot of the data obtained in kinetic studies with CH_3OCH_3. (●) esr results of the $D + CH_3OH$ reaction (uncorrected for any reaction stoichiometry); (▲) esr results of the $H + CH_3OH$ reaction (uncorrected for any reaction stoichiometry); (■) mass spectrometric results from the $H + CH_3OCH_3$ reaction; (□) mass spectrometric results from the $D + CH_3OCH_3$ reaction.

intensity, the time requirement being essentially the same as that observed at higher temperatures. These observations, of course, do not rule out completely the possibility of a heterogeneous reaction, but they do, in our estimation, make this explanation seem somewhat less likely.

Actually, the curvature observed in these studies is of the type usually attributed to quantum mechanical tunneling in chemical reactions. There are different formulations for estimating the importance of such tunneling in reactions, and all methods have in common the fact that any such tunneling contribution would become more noticeable, from the experimental standpoint, at lower temperatures. In order to obtain an estimate of the importance of such tunneling, one needs, as a minimum, the potential energy barrier height and the imaginary frequency along the reaction coordinate leading to decomposition. This latter quantity is obtained from a potential energy surface, usually employing some semiempirical approach, such as the LEPS method, to construct the surface. In view of the complexity of the stable reactant in the present case, we did not carry out any direct calculations based on an LEPS surface as such calculations involve the use of a three-atom model in constructing the potential energy surface. However, it is possible to obtain a rough estimate of such tunneling corrections by estimating a frequency for the assymetric stretch along the reaction coordinate. This stretching motion involves, presumably, a H $\cdots\cdot$ H $\cdots\cdot$ C vibration leading to H_2 formation. By analogy with other systems involving an assymetric H $\cdots$ H $\cdots$ C stretch (for example, $H + CH_4$[12]), a frequency of 1400 i cm^{-1} would represent a reasonable lower limit. This value, when coupled with a barrier height of 5.00 kcal/mol, can lead to rather large tunneling corrections. For example, based on an unsymmetrical Eckart barrier we calculate a ratio of tunneling factors at 210 and 250°K of $\tau_{210}/\tau_{250} \approx 3$, using the procedures outlined by Johnston.[13] The use of a higher imaginary frequency along the reaction coordinate would result in slightly higher tunneling ratios. Although this treatment is obviously very qualitative, it does emphasize the point that, at least from the theoretical standpoint, rather large tunneling corrections might be expected in the present case.

Actually, the H + DME reaction reported here is one of the few studies involving a hydrogen atom transfer in which the temperature range studied has been extended down as low as 200°K. It is precisely under such conditions of H atom transfer and low temperatures where one might expect to observe quantum mechanical tunnel effects from the experimental standpoint. In this connection it is important to mention that the $D + H_2$ and $H + D_2$ reactions represent one other system for which quantitative gas-phase kinetic data are available at low temperatures.[14,15] In this particular case, reliable data now extend down to 167°K.[15] Only very slight curvature of the Arrhenius plots is noted and the experimental data are such as to discount the importance of tunneling in these reactions. In view of these results, plus the added reaction complexities in our present study, it is clear that one cannot simply ascribe the observed curvature to quantum mechanical tunneling processes. However, the result obtained does emphasize the need for additional low-temperature data on reactions involving hydrogen atom transfer.

Finally, it might be acknowledged that transition state theory predicts that over an extended temperature range (and even in the absence of tunneling effects) one should observe nonlinearity in an Arrhenius type plot. For example, such an effect was observed recently in the reactions of

CO + OH and H_2 + OH.[11] In such cases, the nonlinearity results from the fact that the vibrational partition function for the activated complex decreases somewhat faster than that of the reactants, as the temperature increases, as a result of the lower vibrational frequencies present in the activated complex. However, this effect cannot be of much importance at temperatures below 400°K, and thus, should not be a factor in the present studies.

H (and D) + CH_3OH Reactions. The data obtained in the esr studies of H and D atoms with CH_3OH are shown in Tables IV and V, respectively. Arrhenius' plots of these data are shown in Figure 3. We were not able to extend the CH_3OH studies to temperatures below 298°K. Unlike the situation with DME, we did encounter an apparent problem with CH_3OH at temperatures below 298°K. Diverting the CH_3OH to a bypass position at $T < 298°K$ resulted in a rather slow increase of the atom signal with time. This effect became more pronounced as the temperature was lowered. Thus, it appears that significant amounts of CH_3OH are absorbed on the surface of the flow tube at lower temperatures. Because of this difficulty, no attempt was made to obtain kinetic data below room temperature. On the other hand, the CH_3OH reactions are somewhat slower than the corresponding DME reactions, and for that reason, we were able to extend the high temperature limit in the methanol work up to 575°K.

Treatment of the data in Tables IV and V, in the usual way, leads to the specific rate constant expressions of $(1.80 \pm 0.33) \times 10^{13} \exp(-5440 \pm 130/RT)$ and $(2.82 \pm 0.40) \times 10^{13} \exp(-5200 \pm 100/RT)$ $cm^3\ mol^{-1}\ sec^{-1}$ for the H + CH_3OH and D + CH_3OH reactions, respectively. Unfortunately, as explained above, we do not have available mass spectrometric data on these reactions to help in determining the stoichiometric factors involved. That subsequent reactions are indeed involved in this system is apparent in view of the higher preexponential factor obtained in the D + CH_3OH reaction compared with the H + CH_3OH system. By analogy with the proposed mechanism for the DME reaction, the following mechanism is suggested for the methanol reaction

$$H + CH_3OH \longrightarrow H_2 + CH_2OH \qquad (8)$$

$$H + CH_2OH \longrightarrow CH_3 + OH \qquad (9)$$

Under the esr conditions of $[CH_3OH] \gg H_2$, the likely fate of the OH radical would be abstraction from CH_3OH to form another CH_2OH radical. Thus, in principle, one might initiate a chain reaction leading to the consumption of many H atoms each time reaction 8 occurs. If this were the case, the preexponential factor obtained in this present study would be much too high. However, since the *A* factor we obtain is in the more or less normal range for a H atom abstraction reaction, we feel that subsequent consumption of H atoms after the initiation reaction must be limited. Additional support for this idea comes from the fact that the atom decay plots, as shown in Figure 1, revealed excellent linearity over substantial changes in the concentration of H atoms. If a chain reaction were operative, one might expect to see upward curvature of the atom decay plots. We did not observe any such upward curvature in any of the runs carried out in these studies.

In the D + CH_3OH reaction mechanism, we must also include the exchange reaction 6, which would occur under our reaction conditions. The net result of this exchange reaction would be the consumption of additional D atoms and thus an apparent preexponential factor higher than the H + CH_3OH reaction, as observed experimentally.

Obviously, in view of these stoichiometric considerations and the lack of available mass spectrometric results on the CH_3OH reactions, we can only recommend a specific rate constant expression for H + CH_3OH based on an assumed stoichiometry for this reaction. If we assume a preexponential factor for the H + CH_3OH reaction of approximately one-half that obtained in the H + DME work (based on there being only one-half as many C–H bonds available), we obtain a preexponential value of 6.5×10^{12} $cm^{13}\ mol^{-1}\ sec^{-1}$. Relative to the experimental value of 1.8×10^{13}, this would indicate the consumption of an additional two H atoms per initiating reaction step. We feel that this is not an unreasonable number in view of our flow conditions and the results obtained in the DME reaction. Nevertheless, as a result of this problem, we are unable to attach error limits to the *A* factor of 6.5×10^{12} $cm^3\ mol^{-1}\ sec^{-1}$.

Comparison of the DME and CH_3OH Reactions and Kinetic Isotope Effects. As stated in the Introduction, one basic objective in this work was to contrast the differences in perturbation effects of the $-OCH_3$ and $-OH$ groups on these reactions. This we hoped to accomplish through the precise measurements of activation energies and kinetic isotope effects. From the results obtained, it is clear that the activation energy for the DME reaction is approximately 700 cal lower than the corresponding CH_3OH reaction. The lower value for the DME reaction, as opposed to the CH_3OH system, parallels the probable difference in C–H bond dissociation energies. For example, Cruickshank and Benson[16] report C–H bond energies of 93.8 ± 1 and 95.1 ± 2 kcal mol^{-1} for DME and CH_3OH, respectively. Thus, it is apparent that the replacement of the methyl group in DME by an H atom and the resultant formation of the highly polar CH_3OH molecule produces relatively little change in the potential energy interactions involved in the formation of the activated complexes in this case of H atom attack.

That the activated complexes formed in the DME and CH_3OH systems must be similar is seen more closely in the comparison of kinetic isotope effects of H and D atoms with these substrates. From the results obtained, it is clear that the activation energy difference in the H and D atom reactions with DME is essentially identical (within experimental error) with the difference measured in the CH_3OH reactions. In the former case, an activation energy difference of 270 cal mol^{-1} was obtained and a value of 240 cal mol^{-1} was obtained in the methanol studies. In making comparisons of the relative reaction rates of H and D atoms with a given substrate, one expects to find a lower activation energy for the D atom reaction. This results from the fact that in this particular comparison the isotope effect arises entirely from differences in the zero point energies in the two activated complexes $H\cdots H\cdots C{-}X$ and $D\cdots H\cdots C{-}X$. In view of the heavier mass of the D atoms, the vibrational frequencies would be somewhat lower in the D atom activated complex and this complex would have a lower zero point energy than the corresponding complex involved in the H atom reaction. Thus, one predicts a lower activation energy for the D atom reaction and this agrees with the experimental results in both the DME and CH_3OH reactions. However, of considerably more significance is the fact that the activation energy difference between H and D atoms is the same for these two molecules. On this basis, one can conclude that the zero point energy

TABLE IV: Experimental Results Obtained in the Esr Study of the H + CH_3OH Reaction

T, °K	p, Torr	v, cm/sec	$10^{10}[CH_3OH]$, mol/cm^3	$[CH_3OH]/[H_2]$	k,[a] cc/mol sec
298	1.60	1193	8.72	2.76	3.46×10^9
	3.29	585	17.8	2.90	2.29
	2.38	271	27.1	1.55	2.40
	2.35	270	9.94	0.57	1.38
	2.32	276	17.6	1.02	2.20
					k_{av} 2.35×10^9
343	1.54	1221	8.37	2.38	8.32×10^9
	1.90	1001	10.2	2.25	7.28
	2.50	768	13.5	2.42	6.45
	3.29	589	17.8	2.72	5.54
	4.30	457	22.9	2.95	5.45
					k_{av} 6.51×10^9
391	1.60	1295	8.73	2.41	1.18×10^{10}
	2.09	993	10.5	2.22	1.35
	3.11	673	14.4	2.04	1.39
	1.68	577	16.5	2.21	1.37
	1.69	576	4.36	0.58	1.10
					k_{av} 1.28×10^{10}
491	2.12	1258	3.42	1.20	7.72×10^{10}
	2.13	1262	6.68	2.35	7.62
	1.78	1523	4.83	2.05	8.16
	1.78	1530	3.05	1.30	8.68
	2.50	1102	4.23	1.30	6.68
					k_{av} 7.77×10^{10}
575	1.75	1760	5.81	3.26	1.70×10^{11}
	1.69	1831	1.47	0.86	2.47
	1.80	1739	4.12	2.29	2.00
	2.22	1417	1.90	0.86	1.48
					k_{av} 1.91×10^{11}

[a] The specific rate coefficients are uncorrected for any reaction stoichiometry.

TABLE V: Experimental Results Obtained in the Esr Study of the D + CH_3OH Reaction

T, °K	p, Torr	v, cm/sec	$10^{10}[CH_3OH]$, mol/cc	$[CH_3OH]/[D_2]$	k,[a] cc/mol sec
298	1.72	943	8.00	1.65	4.37×10^9
	1.90	472	16.0	2.90	4.78
	1.90	470	10.5	1.08	4.03
	2.29	390	12.7	1.22	3.49
					k_{av} 4.17×10^9
343	1.59	1155	9.00	1.87	8.66×10^9
	2.45	757	14.5	1.97	9.60
	2.82	417	26.7	2.50	11.70
					k_{av} 9.99×10^9
391	1.59	1319	7.28	1.39	2.29×10^{10}
	2.12	971	9.79	1.38	2.53
	2.12	978	5.87	0.83	2.18
	2.50	839	6.63	0.81	2.09
	2.50	845	10.50	1.28	2.54
					k_{av} 2.33×10^{10}
491	1.59	1591	4.96	1.05	10.5×10^{10}
	1.60	1581	1.59	0.53	9.60
	1.99	1271	1.97	0.63	9.61
	1.99	1269	1.97	0.63	9.50
	2.01	1292	6.05	1.89	14.7
	2.06	1264	3.55	1.09	11.4
					k_{av} 10.9×10^{10}
575	1.76	1725	5.20	2.0	2.84×10^{11}
	1.72	1773	1.51	0.6	2.09
	1.72	1791	3.00	1.2	3.31
	2.82	1895	2.56	0.9	2.71
	1.99	1509	1.78	0.7	2.64
					k_{av} 2.72×10^{11}

[a] The specific rate coefficients are uncorrected for reaction stoichiometry.

differences between these two sets of activated complexes must be the same. Thus, we can assume that the force constants involved in these reaction complexes are similar and, from this, we conclude that the activated complexes formed in the H and D atom reactions with DME and CH_3OH involve essentially the same extent of bond formation and bond breakage in each case. This is a strong indication that a negligible effect on reaction dynamics (as de-

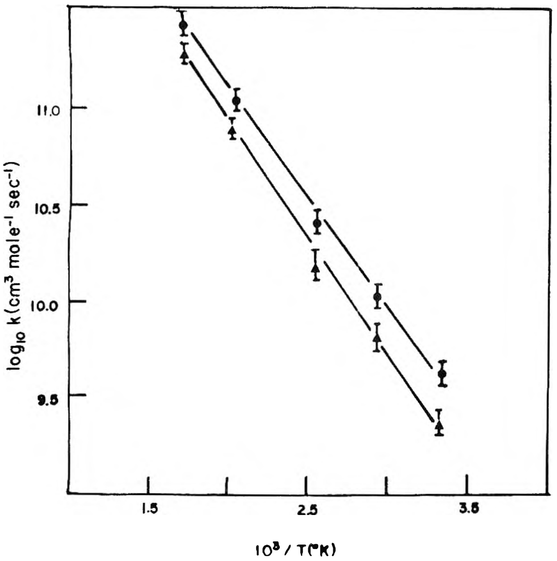

Figure 3. Arrhenius plot of the data obtained in kinetic studies with CH_3OH; (●) esr results from the D + CH_3OH reaction; (▲) esr results from the H + CH_3OH reaction. The data plotted in this figure are uncorrected for any reaction stoichiometry.

fined with respect to the geometry and properties of the activated complexes) is noted in going from DME to methanol in this case of attack by hydrogen atoms.

Comparison with Other Reactions. We feel it is of interest to compare, briefly, the results from the present studies with other kinetic data, some of which had been reported previously from our laboratory. Of particular interest are the results obtained in the reactions of H and D atoms with CH_4 using the same technique as employed in the present work.[12] The kinetic isotope effect observed in the methane reactions was larger than that obtained in the present study with an activation energy difference of 500 cal mol^{-1} observed in comparing H and D atom reactions with CH_4. The larger isotope effect in the methane reactions is in accord with theoretical predictions. In the case of the H + CH_4 reaction, one has a nearly thermoneutral reaction and, thus, one that leads to the formation of a reasonably symmetrical activated complex, as defined with respect to the extent of bond breakage and bond formation in the transition state. In such a case, one can visualize the H atom being transferred as remaining relatively motionless during the symmetrical stretching vibration. Since the major contributor to the zero point energy difference is this symmetrical stretching vibration, one then obtains a maximal effect of the mass difference in comparing the H and D atom reaction rates. In the reactions with DME and CH_3OH we have two exothermic processes ($\Delta H \sim -10$ kcal/mol). In these reactions the activated complexes are established earlier along the reaction coordinate, that is, when the bond order for the new H ··· H bond being formed is less than the bond order of the C–H bond being broken. Under this condition one anticipates a somewhat smaller difference in vibrational frequencies between H and D atom complexes than observed in the CH_4 reactions and this is borne out in the experimental results obtained in this work.

The preexponential factor obtained in the H + DME reaction of 1.3×10^{13} cm^3 mol^{-1} sec^{-1} is significantly lower than the value of 6.25×10^{13} cm^3 mol^{-1} sec^{-1} obtained in the H + CH_4 studies.[8] Calculated on a basis of per primary C–H bond this difference would, of course, become somewhat larger. In terms of a simple collision theory approach this difference represents a lower reaction cross section for the DME reaction than for the CH_4 reaction. Or, alternatively, one could invoke a larger steric factor in the case of the DME reaction. In terms of the geometry of the reactants there appears to be no obvious reason why a significantly different steric factor would be required in contrasting these two reactions. It would be valuable, at this point, to have available other bimolecular reaction rate data for comparison. The obvious reaction of H + C_2H_6 is not particularly useful in this respect in that the preexponential factors reported vary over a fairly wide range.[10] However, the majority of the reported values lie in the range of 1×10^{14} cm^3 mol^{-1} sec^{-1} and, as such, we might again infer that the preexponential factor for the DME reaction is lower than anticipated.

Finally, it seems worthy noting that in similar studies on $O(^3P)$ atom reactions with DME and CH_3OH carried out in our laboratories[17] that, although the activation energies for DME and CH_3OH observed were approximately the same being 2.85 and 2.28 kcal mol^{-1}, respectively, the methanol activation energy is lower than that obtained for DME. This is the reverse of the situation observed in the present study of the H (and D) atom reactions with these same compounds. The inversion of these activation energy differences appears to be real, as it is outside the error limits we have obtained in these studies. The reactions of $O(^3P)$ atoms have been discussed in terms of their being electrophilic in nature whereas the H atom reactions are normally taken to be neutral free-radical type processes. If these ideas are accurate, the comparison of activation energy differences might then indicate a higher electron density on the CH_3 group in CH_3OH as compared to DME, resulting in a somewhat greater reactivity of methanol toward oxygen atom attack as revealed by the lower activation energy. As more kinetic data become available on other comparable systems involving $O(^3P)$ and H atom reactions, it should be of interest to determine if any generalization can be made along these lines with respect to the nature of the relative potential energy interactions involved in establishing the activated complexes in such reactions.

Acknowledgment. The authors are very pleased to acknowledge support of this work by the National Science Foundation, under Grant No. GP-38648X. We wish also to thank Richard Bonanno and Gerald Hollinden for assistance in this work.

References and Notes

(1) P. Kim, R. J. Bonanno, J. H. Lee, and R. B. Timmons, *J. Chem. Phys.*, **59**, 4593 (1973).
(2) A. A. Westenberg and N. de Haas, *J. Chem. Phys.*, **46**, 490 (1967).
(3) A. A. Westenberg and N. de Haas, *J. Chem. Phys.*, **50**, 707 (1969).
(4) R. J. Bonanno, P. Kim, J. H. Lee, and R. B. Timmons, *J. Chem. Phys.*, **57**, 1377 (1972).
(5) L. F. Phillips and H. I. Schiff, *J. Chem. Phys.*, **37**, 1233 (1962).
(6) M. F. R. Mulcahy and R. H. Smith, *J. Chem. Phys.*, **54**, 5215 (1971).
(7) A. A. Westenberg and N. de Haas, *J. Chem. Phys.*, **43**, 1550 (1965).
(8) M. J. Kurylo and R. B. Timmons, *J. Chem. Phys.*, **50**, 5076 (1969).
(9) P. B. Davies, B. A. Thrush, and A. F. Tuck, *Trans. Faraday Soc.*, **66**, 886 (1970).
(10) A. F. Trotman-Dickenson and G. S. Milne, *Nat. Stand. Ref. Data Ser., Nat. Bur. Stand.*, **No. 9** (1967).
(11) A. A. Westenberg and N. de Haas, *J. Chem. Phys.*, **58**, 4061 (1973).
(12) M. J. Kurylo, G. A. Hollinden, and R. B. Timmons, *J. Chem. Phys.*, **52**, 1773 (1970).
(13) H. S. Johnston, "Gas Phase Reaction Rate Theory," The Ronald Press, New York, N.Y. 1966.
(14) A. A. Westenberg and N. de Haas, *J. Chem. Phys.*, **47**, 1393 (1967).
(15) D. M. Mitchell and D. J. Le Roy, *J. Chem. Phys.*, **58**, 3449 (1973).
(16) F. R. Cruickshank and S. W. Benson, *Int. J. Chem. Kinet.*, **1**, 381 (1969).
(17) H. F. LeFevre, J. F. Meagher, and R. B. Timmons, *Int. J. Chem. Kinet.*, **4**, 103 (1972).

Comparison of General-Acid-Catalyzed Ethyl Vinyl Ether Hydrolysis in 80% Dimethyl Sulfoxide with that in Water[1a]

Robert Eliason*[1b] and Maurice M. Kreevoy

Chemical Dynamics Laboratory, University of Minnesota, Minneapolis, Minnesota 55455 *(Received June 26, 1974)*

Publication costs assisted by the National Science Foundation

The acid-catalyzed hydrolysis of ethyl vinyl ether in 80% DMSO–20% water, by weight, has been investigated. The Brφnsted catalysis law for a series of five monobasic carboxylic acids is compared with the Brφnsted relation previously obtained in water. The present Brφnsted plot appears to show some curvature; however, the paucity of points and the limited pK_{HA} range do not allow this to be uniquely established. The results strongly suggest there is no real change in mechanism upon changing the solvent from pure water to aqueous DMSO.

In many mechanistic studies it is convenient to compare results obtained in water with those from mixed aqueous–organic solvents. This study was undertaken to see how valid such comparisons are by studying a system, already carefully studied in water, in 80% dimethyl sulfoxide (DMSO)–20% water, by weight.

The hydrolysis of ethyl vinyl ether in aqueous solutions has been shown to be general-acid-catalyzed and a Brφnsted α is known.[2] The reaction has also been studied in DMSO–water mixtures using HCl as the catalyst.[3] The present paper reports the results of the hydrolysis of ethyl vinyl ether in 80% DMSO using a series of carboxylic acids as catalysts.

Experimental Section

DMSO (Aldrich Chemical Co.) and the water used for all solutions were purified as previously described.[4] All the carboxylic acids were purified by distillation under vacuum. Ethyl vinyl ether was purified as described before.[2] Potassium trifluoromethane sulfonate was prepared by the method of Gramstad and Hazeldine[5] (mp 250–252°;[6] lit. mp 230°).

Aqueous buffer solutions of the carboxylic acids were prepared in the usual way.[7] A weighed amount of the aqueous buffer solution was added to a known weight of DMSO giving solutions with a buffer ratio 1:1, an ionic strength, μ, of 0.1 *M* and a solvent composition of 80% DMSO–20% water, by weight. Differing buffer concentrations were prepared by dilution of the parent buffer solution, maintaining the ionic strength at 0.1 *M* by addition of 0.1 *M* potassium trifluoromethane sulfonate in 80% DMSO–20% water. Perchloric acid solutions in the solvent mixture were prepared by adding the acid first to water, then adding this solution to the DMSO. Adding perchloric acid directly to the DMSO–water solution resulted in a violent reaction producing a blue flash.

Acid dissociation constants for trifluoroacetic, dichloroacetic, and cyanoacetic acids were measured in 80% DMSO–20% water by the methods of Kolthoff and Chantooni.[8] All emf measurements were made on a Radiometer (Copenhagen) pH meter using a Radiometer G202 B standard glass electrode. The cell was maintained at ambient temperature (25 ± 2°) by air conditioning. In 80% DMSO a response of 56 mV/pH unit was found using $HClO_4$ solutions, acetic acid buffers, *p*-chlorophenol buffer, and 2,4,6-trimethylphenol buffer covering 13 pH units. The pK_{HA}'s of the organic acids have been determined independently by Baughman and Kreevoy.[4]

Kinetic measurements were made by the usual spectrophotometric techniques in a thermostated cell, 25.0 ± 0.2°. For very slow reactions the reaction mixtures were kept in a thermostated water bath. Aliquots were periodically withdrawn, and optical density measurements made. It was inconvenient to follow the slow reactions to completion; thus, an "artificial" infinity point for each experiment was prepared by adding a known amount of 1 *M* $HClO_4$ solution to an equivalent amount of reaction mixture. The infinity points were corrected for the dilutions.

Results

The pK_{HA} values for trifluoroacetic acid, dichloroacetic acid, and cyanoacetic acid at $\mu = 0.1$ *M* in 80% DMSO were determined to be 1.16 ± 0.13, 3.48 ± 0.02, and 4.92 ± 0.01, respectively. These values were obtained from measurements on five buffer concentrations varied from 0.02 to 0.1 *M*. The errors cited are average deviations from the mean. For dichloroacetic acid Baughman and Kreevoy[4] obtained an infinite dilution value of 3.87, and Ballash, *et al.*,[9] obtained 3.12 at $\mu = 0.2$ *M*.

A plot of pK_{HA} (80% DMSO) against pK_{HA} (water) for dichloroacetic, chloroacetic, and acetic acids from the data of Baughman and Kreevoy[4] was linear.[10a] The present dichloroacetic and cyanoacetic acid pK_{HA}'s (80% DMSO) were both displaced from the Baughman–Kreevoy line by about 0.4 unit. It was assumed that chloroacetic and formic acid would have pK_{HA}'s for $\mu = 0.1$ *M* similarly displaced. The calculated pK_{HA} (80% DMSO) for chloroacetic acid is 5.38 and for formic acid 6.42.

General-acid catalytic coefficients, k_{HA}, were obtained from the slopes of plots of $(k_I - k_H[H^+])$ against [HA] in buffered solutions of constant ionic strength and nearly constant $[H^+]$. The method has previously been described.[11] A least-squares criterion was used to evaluate the slopes, k_{HA}, in each case forcing the line thru the origin. These plots for chloroacetic and formic acid were quite scattered, and the slopes are near the maximum one would reasonably draw. The scatter was probably due to the small percentage of reaction (<20%) that was followed and also to the curvature of these plots at high HA concentration. This curvature has been previously observed in 80%

TABLE I: Catalytic Coefficients and Acid Dissociation Constants in 80% DMSO–20% H_2O at 25°

Acid	k_{HA}, M^{-1} sec^{-1a}	K_{HA}, M
CF_3COOH	$(6.35 \pm 0.02) \times 10^{-3}$	$(6.99 \pm 1.06) \times 10^{-2b}$
$Cl_2CHCOOH$	$(5.65 \pm 0.10) \times 10^{-3}$	$(3.28 \pm 0.23) \times 10^{-1b}$
$CNCH_2COOH$	$(1.09 \pm 0.03) \times 10^{-4}$	$(1.20 \pm 0.04) \times 10^{-3b}$
$ClCH_2COOH$	$(5.15 \pm 0.71) \times 10^{-5}$	4.17×10^{-6c}
HCOOH	$(7.63 \pm 0.05) \times 10^{-6}$	3.80×10^{-7c}
H^+	$(5.67 \pm 0.13) \times 10^{-2}$	21.4^d

[a] The reported uncertainties are 50% confidence limits. [b] This work at $\mu = 0.1M$. The uncertainties are 50% confidence limits. [c] Calculated (see Result section). [d] Corrected for total moles of solvent.

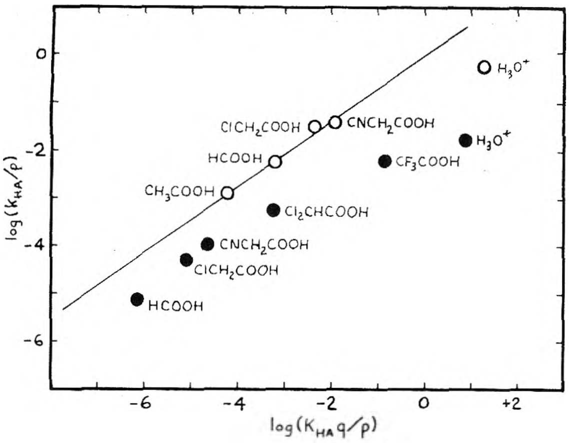

Figure 1. Brϕnsted plot for hydrolysis of ethyl vinyl ether. Open circles are for a solvent of pure water. Closed circles are for 80% DMSO–20% H_2O solvent. The solid line represents a Brϕnsted slope of 0.69.

DMSO–20% water for the hydrolysis of diphenyldiazomethane.[12] Table I gives the catalytic coefficients, their 50% confidence limits, and the dissociation constants, K_{HA}.

The hydronium ion catalytic coefficient, k_H, defined as $k_1/[H^+]$, was determined from 13 measurements at an ionic strength of 0.1 M in $HClO_4$ to be $(5.67 \pm 0.11) \times 10^{-2}$. The error quoted is the 50% confidence limit of the mean.

Discussion

Figure 1 compares the present results with those previously obtained in water.[2,13] All the catalytic coefficients have been reduced in 80% DMSO. However, the relation among the rate constants is not much changed. The diminution in the catalytic power of H^+ for A–SE2 reactions has been reported previously.[3,14] It has been suggested[15] that only acids of similar structural and charge type should be compared. In going from one solvent system to another it may be safe only to compare the same acids. The Brϕnsted slope defined by formic, chloroacetic, and cyanoacetic acids in 80% DMSO is greater (~0.78) than the Brϕnsted slope defined by those acids in H_2O (~0.71). If this difference is real, then it could be attributed to a solvent effect on either the Marcus theory[16] term λ or the term $\Delta F_R^{0\prime}$ or both. From the data presented it is not possible to isolate the effect to a single term nor to postulate the magnitude of the effect on the individual terms.

The Brϕnsted plot for carboxylic acids in 80% DMSO appears to show some curvature. Due to the uncertainty in the k_{HA} and K_{HA} values for formic and chloroacetic acids, the small number of points, and the limited range of pK_{HA}'s, it cannot be unequivocably established that the curvature is real. However, it is reasonable compared to other recent observations.[17] The curvature is not visible in water, but the accessible range of pK_{HA}'s is smaller.

The results shown in Figure 1 suggest that the deviation of the H^+ point from Brϕnsted curves for oxygen acids, which has been frequently commented on,[10b] may be due, in large part, to the curvature of these plots which has not been generally recognized.

These results strongly suggest that no qualitative or substantial quantitative change in the mechanism of acid catalysis occurs on changing the solvent from pure water to aqueous DMSO. This is unlike recent observations[18,19] that changes in solvent lead to quantitative and qualitative changes in mechanism.

References and Notes

(1) (a) This work was supported, in part, by the National Science Foundation through Grant No. GP-31360X. (b) Address correspondence to Southwest State College, Marshall, Minn. 56258.
(2) M. M. Kreevoy and R. Eliason, *J. Phys. Chem.*, **72**, 1313 (1968).
(3) M. M. Kreevoy and J. M. Williams, Jr., *J. Amer. Chem. Soc.* **90**, 6809 (1968).
(4) E. H. Baughman and M. M. Kreevoy, *J. Phys. Chem.*, **78**, 421 (1974).
(5) T. Gramstad and R. N. Hazeldine, *J. Chem. Soc.*, 173 (1956).
(6) Repeated crystallization did not change this melting point. The freezing point of the melt (fp 252–250°) was identical with the melting point.
(7) I. M. Kolthoff and E. B. Sandell, "Textbook of Quantitative Inorganic Analysis," Macmillan, New York, N.Y., 1952.
(8) I. M. Kolthoff and M. K. Chantooni, Jr., *J. Amer. Chem. Soc.*, **87**, 4428 (1965).
(9) N. M. Ballash, E. B. Robertson, and M. D. Sokolowski, *Trans. Faraday Soc.*, **66**, 2622 (1970).
(10) R. P. Bell, "The Proton in Chemistry," Cornell University Press, Ithaca, N.Y. 1973; (a) Chapter IV, (b) Chapter X.
(11) M. M. Kreevoy, T. S. Straub, W. V. Kayser, and J. L. Melquist, *J. Amer. Chem. Soc.*, **89**, 1201 (1967).
(12) A. I. Hassid, Ph.D. Thesis, University of Minnesota, 1974.
(13) R. W. Eliason, Ph.D. Thesis, University of Minnesota, 1968.
(14) A. Kankaanperä and M. Merilahti, *Acta Chem. Scand.*, **26**, 685 (1972).
(15) A. J. Kresge and Y. Chiang, *J. Amer. Chem. Soc.*, **95**, 803 (1973).
(16) R. A. Marcus, *J. Phys. Chem.*, **72**, 891 (1968).
(17) M. M. Kreevoy and S.-W. Oh, *J. Amer. Chem. Soc.*, **95**, 4805 (1973).
(18) E. F. Caldin and S. Mateo, *Chem. Commun.*, 854 (1973).
(19) E. F. Caldin and H. P. Bennetto, *J. Solution Chem.*, **2**, 217 (1973).

Pulse Radiolysis Study of Aqueous Hydrogen Cyanide and Cyanide Solutions[1a]

D. Behar[1b]

Radiation Research Laboratories and Center for Special Studies, Mellon Institute of Science, Carnegie-Mellon University, Pittsburgh, Pennsylvania 15213 *(Received May 13, 1974)*

Publication costs assisted by the Carnegie-Mellon University and the U. S. Atomic Energy Commission

The pulse radiolysis of N_2O saturated solutions of HCN and CN^- has been studied in the pH region 3.7–14. Spectra of three different species were identified. In acid and neutral solutions OH adds to the HCN triple bond and forms the HC(OH)=$\dot{N}$ radical with λ_{max} 240 nm and ϵ_{240} 550 M^{-1} cm^{-1}. This radical disappears according to a second-order rate law with $2k = 1.5 \times 10^9$ M^{-1} sec^{-1}. At pH 10.6 OH adds to CN^- with a rate of $k(OH + CN^-) = 7.1 \times 10^9$ M^{-1} sec^{-1} to form HO$\dot{C}$=N$^-$. This adduct protonates and rearranges to the formamide radical $\dot{C}ONH_2$ with λ_{max} <225 nm and ϵ_{225} 1400 M^{-1} cm^{-1}. The second-order rate constant for disappearance of the $\dot{C}ONH_2$ radical is $2k = 6.2 \times 10^9$ M^{-1} sec^{-1}. At pH 14, O^- reacts with CN^- with a rate constant of $k(O^- + CN^-) = 2.6 \times 10^8$ M^{-1} sec^{-1}. The adduct rearranges in the same way as at lower pH to produce $(\dot{C}ONH)^-$ with λ_{max} 245 nm and ϵ_{245} 2200 M^{-1} cm^{-1}. The $(\dot{C}ONH)^-$ decays in a second-order rate $2k = 2.2 \times 10^9$ M^{-1} sec^{-1}. The formamide radical is in acid–base equilibrium with pK ($\dot{C}ONH_2 \rightleftharpoons \dot{C}ONH^- + H^+$) = 12.25.

Introduction

The nature of the radicals produced in the radiolysis of the halides[2-7] and some pseudo halides[8-10] have been extensively investigated. The halides as well as SCN^-, SH^-, and SeH^- produce X_2^- radical ions from reactions with OH. In some cases indirect evidence for the production of intermediate species XOH^- as precursors to X_2^- was found.[5-7,10] With thiocyanate, the spectrum and the decay kinetics of the $SCNOH^-$ intermediate were observed.[8] The lifetime of $SCNOH^-$ depends on SCN^- concentration in such a way that the higher the SCN^- concentration the shorter the lifetime of the intermediate. In a recent publication by Ogura, *et al.*,[11] on the steady-state radiolysis of HCN and CN^- in aqueous solutions it has been deduced from the behavior of the halides and SCN^- that $\dot{C}N$ is formed by the reaction

$$OH + CN^- \longrightarrow \dot{C}N + OH^- \qquad (1)$$

followed by

$$\dot{C}N + CN^- \longrightarrow (\dot{C}N)_2^- \qquad (2)$$

This assumption was examined by us recently using steady-state esr techniques.[12] We could find no evidence for the formation of $\dot{C}N$ or $(\dot{C}N)_2^-$ radicals but we found that the reaction of OH with CN^- leads to the production of the formamide radical.

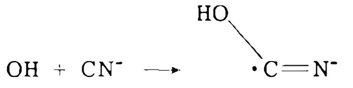

$$OH + CN^- \longrightarrow HO\dot{C}{=}N^- \qquad (3)$$

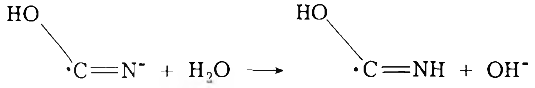

$$HO\dot{C}{=}N^- + H_2O \longrightarrow HO\dot{C}{=}NH + OH^- \qquad (4)$$

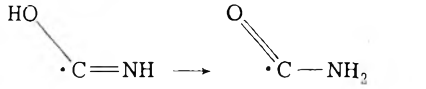

$$HO\dot{C}{=}NH \longrightarrow O{=}\dot{C}{-}NH_2 \qquad (5)$$

The same radical was produced by OH attack on formamide and similar radical yields were obtained. We concluded[12] that the main path of reaction of the OH radicals with CN^- is addition to the carbon–nitrogen triple bond as given in reaction 3, rather than an electron transfer reaction as suggested by Ogura, *et al.*[11] With HCN the OH radical also adds to the triple bond but the radical formed does not rearrange as in the case of CN^-.

$$OH + HCN \longrightarrow H(OH)C\dot{N} \qquad (6)$$

From changes in the esr spectrum of the radical produced in reaction 6 we concluded that this radical has a pK of ~5.

$$H(OH)C\dot{N} \rightleftharpoons H(O^-)C\dot{N} + H^+ \qquad (7)$$

In the present work we tried to identify the absorption spectra of the various species produced in the pulse radiolysis of HCN and CN^-, and to measure their formation and decay kinetics. The identity of the species was compared to those found by esr.[12] Since the time resolution of the present pulse experiments is shorter than that of the esr experiments by about three orders of magnitude, one might expect different intermediate species in the short time scale. Of specific interest would be the identification of the species and kinetics of the rearrangement given in reaction 5. As will be shown below, the rearrangement is too fast to be observed in the microsecond time scale.

Experimental Section

KCN, KOH, Na_2HPO_4, NaH_2PO_4, and $HClO_4$ were all Baker Analyzed reagents. Solutions were prepared with doubly distilled water and all were bubbled with Baker nitrous oxide for at least 0.5 hr. When HCN solutions were desired the water was deoxygenated by bubbling N_2O before addition of the KCN. After addition of the KCN and adjusting the pH with the phosphate buffers the rate of gas flow was restricted to prevent removal of the HCN.

Samples were irradiated in a fused silica cell 2 cm long with the light passing through the cell once. Although in some cases it was desirable to increase the absorption of the intermediates, no attempt has been made to increase the light path, because the amount of stray light severely increased at short wavelengths even with the use of only one multiplication of the path. Optical densities were corrected for stray light for λ <240 nm. In no case was the correction more than 12%. The optical arrangement has been described elsewhere.[13] Pulses of 2.8-MeV electrons of 0.5–2-μsec duration from a Van de Graaff generator were used. The electron beam current in the irradiation pulse was monitored by a secondary emission chamber[14] connected to an integration circuit as described by Bansal and Fessenden.[15] Absorbed doses were in the range of 1–5 krads.

Results and Discussion

Rates of Reactions of Hydroxyl Radicals with CN^-. The reactions of CN^- with OH and O^- were measured in N_2O saturated solutions at pH 10.6 and 14, respectively. Kraljic and Trumbore[16] have previously measured the rate constant of the OH radical with "cyanide" at pH 9. In their measurement the system was poorly defined because the pH was too close to the pK of HCN where HCN and CN^- coexist in comparable concentrations (pK = 9.3[17]). Because the extinction coefficient of the radical produced by the OH attack on CN^- is relatively small (see the spectrum below) derivation of the rate constant from formation curves was not satisfactory. We used the competition method taking the reaction of OH with SCN^- as a standard. The rate of reaction of CN^- with OH was measured at pH 10.6 (borate buffer) by following the absorption of $(SCN)_2^-$ at 480 nm as a function of $(CN^-)/(SCN^-)$. At this pH the system is well defined because most of the cyanide is ionized and most of the hydroxyl radicals are un-ionized. The expression describing the competition between reaction 3 and the reaction of OH with SCN^- is

$$\frac{D_0}{D} = \frac{k_3(CN^-)}{k_{SCN^-}(SCN^-)} + 1$$

where D_0 is the maximum optical density of $(SCN)_2^-$ in the absence of CN^-, D is the maximum optical density of $(SCN)_2^-$ when CN^- is present, and k_{SCN^-} is the rate constant of the overall reaction between OH and SCN^-. A plot of D_0/D as a function of $(CN^-)/(SCN^-)$ is given in Figure 1. Values of D_0 and D were normalized to a common pulse current. From the slope of Figure 1 the ratio k_3/k_{SCN^-} = 0.69 is obtained. To determine k_3, k_{SCN^-} should be known. There is some controversy in the literature concerning the value of k_{SCN^-}. Willson, *et al.*,[18] have pointed out that the high value published by Baxendale, *et al.*,[9] for k_{SCN^-} leads in all examined cases to significantly higher rate constants than the values obtained by other methods. Taking $k_{SCN^-} = 1.03 \times 10^{10}\ M^{-1}\ sec^{-1}$ as suggested by Willson, *et al.*,[18] one arrives at $k_3 = 7.1 \times 10^9\ M^{-1}\ sec^{-1}$. This value is higher by about a factor of 2 from the previous value measured by Kraljic and Trumbore.[16] (They used for standardization the rate constant of the oxidation reaction of ferrocyanide by OH radical $k_{OH + Fe(CN)_6^{4-}} = 1 \times 10^{10}\ M^{-1}\ sec^{-1}$ in accordance with the determination by Willson, *et al.*,[18] and therefore comparison of the rate constant is appropriate.) The difference in the values obtained by us and by Kraljic and Trumbore[16] might originate from differences in pH. In their work more than 60% of the "cyanide" is present as HCN while in the present work only ~5% of the solute is in the acid form. This result would imply a smaller rate constant for the reaction of OH with HCN. No attempt was made to measure the rate constants of OH with HCN, because of the difficulties arising on determining the HCN concentration at pH values below the pK of HCN.

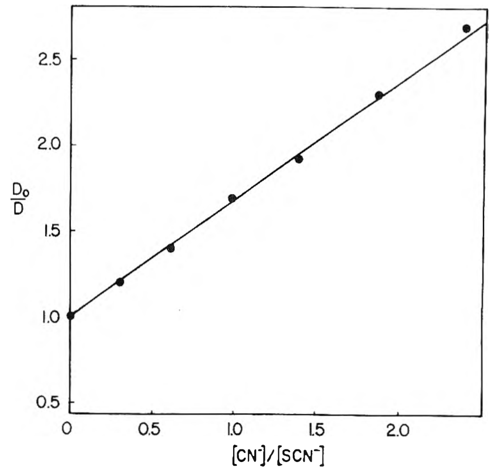

Figure 1. Competition of thiocyanate and cyanide for the hydroxyl radical: $(SCN^-) = 10^{-3}$ M, pH 10.6 (borate buffer), N_2O saturated, absorption of $(SCN)_2^-$ was followed at 480 nm.

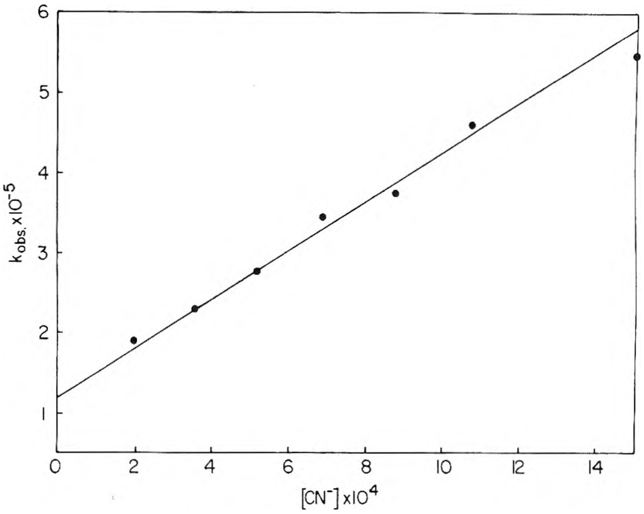

Figure 2. The dependence of the pseudo-first-order rate constant of the reaction of O^- with CN^- on (CN^-), at 1 M KOH, N_2O saturated solutions.

The radical produced from the reaction of O^- with CN^- absorbs relatively strongly in the uv region and therefore formation curves could be measured directly at 250 nm. On pulse radiolysis of KCN solutions at 1 M KOH, exponential growth curves were obtained from which pseudo-first-order rate constants k_{obsd} were calculated. A plot of k_{obsd} as a function of (CN^-) is given in Figure 2. From the slope $k_{O^- + CN^-} = 3.0 \times 10^8\ M^{-1}\ sec^{-1}$ was calculated. This value should be corrected for the contribution of OH reaction. Even at pH 14, where the un-ionized OH radicals are only 0.6% of the total hydroxyl radicals, the contribution of reaction 3 is not negligible. With pK_{OH} = 11.8[19] the corrected rate constant would reduce to $k_{O^- + CN^-} = 2.6 \times 10^8$ $M^{-1}\ sec^{-1}$. It is assumed that the radicals produced at pH 10.6 and 14 are essentially the same species except for their ionization state. This assumption was confirmed in experiments with nitromethane as a trapping agent.[12] It was shown there[12] that the esr spectrum observed in strongly basic solution is the same as that at lower pH except for the absence of one proton splitting. It is concluded that the radical ion $O{=}\dot{C}{-}NH^-$ is formed in the highly alkaline solutions in a similar mechanism described above for the formation of $O{=}\dot{C}{-}NH_2$, and most probably is in resonance with $^-O{-}\dot{C}{=}NH$. In both pH regions (slightly and highly alkaline) the first step is OH or O^- addition to the cyanide triple bond, followed by lactim–lactam rearrangement to produce the formamide radical. In none of the experiments

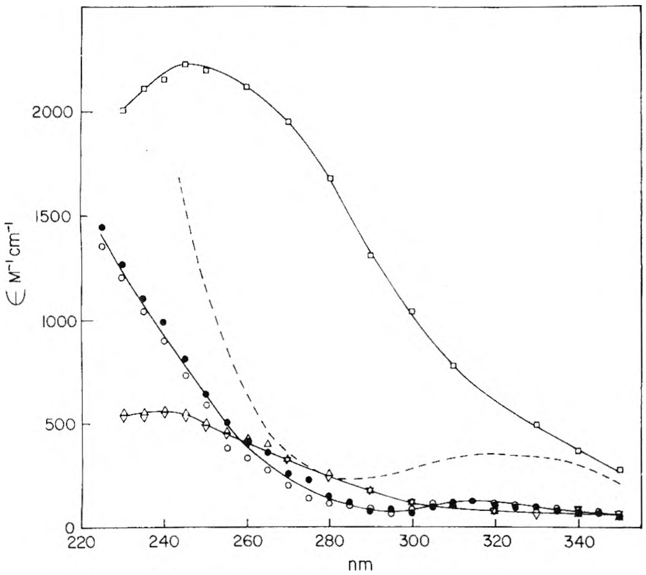

Figure 3. Spectra of species in N_2O saturated solution produce in pulse radiolysis of HCN, CN^-, and $HCONH_2$ at different pH's: △, 3 m*M* HCN, pH 7.0; ▽, 3 m*M* HCN, pH 3.7; ●, 5 m*M* KCN, pH 10.6; ○, 5 m*M* $HCONH_2$, neutral; □, 1 m*M* KCN in 1 *M* KOH. The dotted line is the spectrum obtained by Hayon, *et al.*,[21] from neutral formamide solution. Extinction coefficients were calculated using the thiocyanate as a relative dosimeter taking[9] $\epsilon^{max}{}_{(SCN)_2^-} = 7600\ M^{-1}\ cm^{-1}$.

could either spectral or kinetic evidence for the existence of the precursors of the formamide radical be found, reflecting the short lifetime of the initially produced form of the OH adduct.

Spectra of Radicals. The spectra of the radicals produced in the pulse radiolysis of N_2O saturated solutions of HCN and CN^- at different pH's are given in Figure 3. For the evaluation of the extinction coefficients it was assumed that all radicals in the N_2O saturated solutions were produced with a yield equal to $G_e + G_{OH}$. Extinction coefficients were determined by comparing absorptions of the radical to that of the thiocyanate radical, taking[9] $\epsilon^{max}{}_{(SCN)_2^-} = 7600\ M^{-1}\ cm^{-1}$ and $G_{(SCN)_2^-} = G_e + G_{OH}$.

Below pH 9.3 where HCN is present, OH adds to the triple bond to form $HC(OH)\dot{N}$ radicals. The esr spectrum of this radical has been observed previously[12] and a p*K* of ~5 was estimated for the dissociation of the hydroxyl proton (reaction 7). The optical spectra of the radicals produced in HCN solutions at pH 3.7 and 7 were found to be identical within the experimental accuracy (triangles in Figure 3), with a maximum absorption at ~240 nm, and ϵ_{max} of 550 $M^{-1}\ cm^{-1}$. The assignment of the optical spectrum at pH 3.7 and 7.0 to the $HC(OH)\dot{N}$ radicals, as detected by esr,[12] might not necessarily be correct since the time resolution of the esr experiment was of the order of 500 μsec and the optical spectra were detected at a few microseconds after the pulse. The possibility of hydrogen abstraction to form CN radical instead of OH adduct should be considered. If this is the case then CN radicals could be scavenged by nitromethane at the pH region 9–10 where HCN is still present and nitromethane reacts as a scavenger. No evidence for the formation of the adduct $CNCH_2\dot{N}O_2^-$ was found using esr techniques. (A radical believed to be ·CN was produced on allowing $\cdot SO_4^-$ to react with cyanide and was scavenged by nitromethane at the pH region 9–10.[20]) This argument and the spectral considerations (see below) lead us to assume that the spectrum given in Figure 3 at pH 3.7 and 7.0 belong to the OH adducts $HC(OH)\dot{N}$ and possibly to $HC(O^-)\dot{N}$. Interestingly enough, Ogura, *et al.*,[11] found a pH dependence of *G*(−HCN) in the steady-state radiolysis of HCN. *G*(−HCN) changes from 2.8 at pH ≤3.5 to 5.8 at pH ≥6. It seems likely that the acid–base equilibrium of $HC(OH)\dot{N}$ causes this dependence of *G*(−HCN) on the pH.

It should be mentioned that the absorption spectrum of the radical formed from the reaction of H with HCN in the N_2O saturated solutions was neglected. Therefore, some uncertainty exists concerning the spectrum of the OH adduct to HCN. But if the absorption of $H_2C\dot{N}$ is not much different than that of $HC(OH)\dot{N}$ then the uncertainty in the spectrum would not exceed 10% since $G_{HC(OH)N}/G_{H_2CN} \simeq 10$.

At pH 10.6 (N_2O saturated) where most of the cyanide is ionized, a different spectrum than that discussed above was obtained. As seen in Figure 3 (circles) a weak maximum is observed in the region of 320 nm but no further maximum was found down to 225 nm. It is believed that the reaction of OH with CN^- produces $\dot{C}ONH_2$ radicals as given in reactions 3–5. For comparison the spectrum of the radicals produced from reaction of OH with formamide was also measured and is given in Figure 3 (open circles). It is evident that the same spectrum is obtained confirming our previous results that the same radicals are produced under attack of OH on either CN^- or $HCONH_2$.[12] The spectrum obtained by Hayon, *et al.*,[21] in pulse radiolysis of N_2O saturated solutions of formamide is also given in Figure 3 (broken line). The extinction coefficients given by them[21] are higher than those measured in the present work by about a factor of 2. In their work[21] they claim that OH can abstract hydrogen at two positions.

$$HCONH_2 + OH \longrightarrow HCO\dot{N}H + H_2O \qquad (8)$$

$$HCONH_2 + OH \longrightarrow \dot{C}ONH_2 + H_2O \qquad (9)$$

The absorption below 250 nm was attributed to the radical with the free electron on the nitrogen while the absorption at 320 nm was assumed to be due to the $\dot{C}ONH_2$ radical.[21] According to our experiments the same two bands at 320 nm and below 250 nm were obtained by reactions of OH with either formamide or cyanide. Since there is little doubt as to the identification of the radicals produced in the CN^- solutions assigning them to $\dot{C}ONH_2$, and since the same spectrum is obtained with formamide, we believe that the absorption below 250 nm belongs also to $\dot{C}ONH_2$ and that $HCO\dot{N}H$ is not formed as a major product from reaction of OH with formamide. In their work[21] it is not clear how the extinction coefficient of $\dot{C}ONH_2$ was calculated since the relative distribution of OH between reactions 8 and 9 was not known to them, and therefore the concentration of each radical was not known. If they had assumed production of one radical only, as we did, their extinction coefficient should be corrected downward. Supposing that they took 50% of the OH radicals reacting through reaction 9, then the correction would be by a factor of 2 and the two sets of results would be identical.

The possibility of an electron transfer reaction (reaction 1) as suggested by Ogura, *et al.*,[11] should be considered on the basis of the spectral findings. If such a reaction takes place it would probably lead to the formation of $(CN)_2^-$ according to reaction 2. $(CN)_2^-$ was previously produced by allowing e_{aq}^- to react with $(CN)_2$ and the absorption spectrum shows[22] maximum absorption at 290 nm with ϵ_{max}

TABLE I: Second-Order Rate Constants of the Radicals Produced in the Radiolysis of N_2O Saturated Solutions of HCN, CN$^-$, and $HCONH_2$ at Different pH's

Solute	pH	Radical	$2k$, M^{-1} sec^{-1}
HCN	3.7	$HC(OH)\dot{N}$	1.5×10^9
HCN	7.0	$HC(O^-)\dot{N}$[b]	1.3×10^9
CN$^-$	10–11	$\dot{C}ONH_2$	6.2×10^9
$HCONH_2$[a]	7	$\dot{C}ONH_2$	5.5×10^9
CN$^-$	13.8	$\dot{C}ONH^-$	2.2×10^9

[a] Hayon, *et al.*,[21] measured the same decay assuming the absorption belongs to $HCO\dot{N}H$ at ~245 nm and obtained $2k \sim 1.10.^{10}$ If an ϵ_{245} of 800 is taken according to the present work a rate constant of $\sim 5 \times 10^9$ M^{-1} sec^{-1} would be obtained, in very good agreement with our value. [b] No evidence was found in this work for the existence of the ionized form.

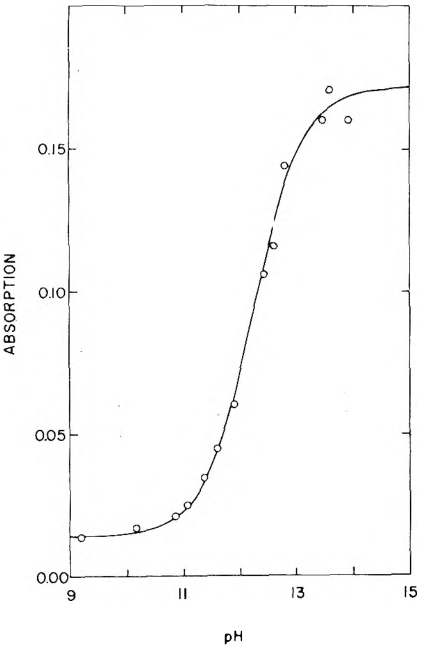

Figure 4. The effect of pH on the absorption of the formamide radical at 260 nm, obtained by pulse radiolysis of 2 mM KCN solution saturated with N_2O. The curve is calculated for pK = 12.25 of the reaction $\dot{C}ONH_2 \rightleftarrows \dot{C}ONH^- + H^+$.

2100 M^{-1} cm^{-1}. The spectrum measured by us at pH 10.7 on allowing OH to react with CN$^-$ does not show any absorption at 290 nm, and therefore rules out the electron transfer reaction.

In the very alkaline pH region the absorption spectrum obtained from reaction of O$^-$ with CN$^-$ is significantly different from that obtained at pH 10.6 (see Figure 3). In this case a well-defined maximum at 245 nm was obtained with ϵ_{max} 2200 M^{-1} cm^{-1}. This spectrum is attributed to $(NH\dot{C}O)^-$ which is in acid–base equilibrium with $NH_2\dot{C}O$.

$$NH_2\dot{C}O + OH^- \rightleftarrows (NH\dot{C}O)^- + H_2O \qquad (10)$$

The big difference in the extinction coefficients between $NH_2\dot{C}O$ and $(HN\dot{C}O)^-$ at 260 nm enabled determination of the pK of this radical. In Figure 4 the initial absorption of the radical is plotted as a function of pH. Each point is the average of four measurements and all values were normalized to a common dose. The solid line is a calculated line assuming extinction coefficients of 180 and 2150 M^{-1} cm^{-1} at 260 nm for $NH_2\dot{C}O$ and $(NH\dot{C}O)^-$, respectively, and pK = 12.25.

Decay Kinetics of the Radicals. All radicals mentioned above, which were formed by allowing OH to react with HCN, CN$^-$, and $HCONH_2$ disappeared to stable products by second-order rate laws. The decay rate constants at different pH's are summarized in Table I. The rates were measured at 250 nm, and the extinction coefficients were taken from the spectra in Figure 3. In all cases the radicals decay to absorbing products. The OH adduct formed by allowing OH to react with HCN is presented in the table as the ionized and the un-ionized forms. It should be emphasized that in this work no evidence was found for this dissociation since the absorption spectra and the second-order decay rate constants at pH 3.7 and 7 were identical within the experimental accuracy.

The radical formed from CN$^-$ has the same decay rate constant as that formed from $HCONH_2$ confirming our previous conclusion[12] that the same radical is formed from CN$^-$ and $HCONH_2$ and which is different from the radical formed from HCN.

Conclusions

CN$^-$ ions react with OH radicals in an addition reaction and not by electron transfer. Contrary to the halides and some pseudo halides where X_2^- is formed, CN$^-$ does not form $(CN)_2^-$ in its reaction with OH. The radical formed by OH addition to CN$^-$ is identical with that formed by hydrogen abstraction from formamide. The abstraction found with the formamide was of the hydrogen on the carbon only, no evidence for abstraction of the hydrogen on the nitrogen was found. The precursor to $\dot{C}ONH_2$ obtained by reaction of OH with CN$^-$ (reactions 3 and 4) could not be observed in the μsec time scale.

Although esr evidence was found[12] for the acid–base equilibrium of the radical $H(OH)C{=}\dot{N} \rightleftarrows H(O^-)C{=}N + H^+$ no kinetic or spectral evidence for this equilibrium could be found. On the other hand different spectra and decay rates were found for the acid and base forms of the formamide radical $\dot{C}ONH_2 \rightleftarrows (CONH)^- + H^+$ and a pK = 12.25 was determined.

References and Notes

(1) (a) Supported in part by the U. S. Atomic Energy Commission. (b) Address correspondence to the Israel Atomic Energy Commission, Soreq Nuclear Research Centre, Yavne, Israel.
(2) M. Anbar and J. K. Thomas, *J. Phys. Chem.*, **68**, 3829 (1964).
(3) B. Cercek, M. Ebert, C. W. Gilbert, and A. J. Swallow, "Pulse Radiolysis," Academic Press, New York, N.Y., 1965, p 83.
(4) J. K. Thomas, *Trans. Faraday Soc.*, **61**, 702 (1965).
(5) M. S. Matheson, W. A. Mulac, J. L. Weeks, and J. Rabani, *J. Phys. Chem.*, **70**, 2092 (1966).
(6) D. Zehavi and J. Rabani, *J. Phys. Chem.*, **76**, 312 (1972).
(7) D. Behar, *J. Phys. Chem.*, **76**, 1815 (1972).
(8) D. Behar, P. L. T. Bevan, and G. Scholes, *J. Phys. Chem.*, **76**, 1537 (1972).
(9) J. H. Baxendale, P. L. T. Bevan, and D. A. Stott, *Trans. Faraday Soc.*, **64**, 2389 (1968).
(10) W. Warmann, G. Meissner, and A. Henglein, *Z. Naturforsch. B*, **22**, 273 (1967).
(11) H. Ogura, T. Fujimura, S. Murozono, K. Hirano, and M. Kondo, *J. Nucl. Sci. Technol.*, **9**, 339 (1972).
(12) D. Behar and R. W. Fessenden, *J. Phys. Chem.*, **76**, 3945 (1972).
(13) L. K. Patterson and K. M. Bansal, *J. Phys. Chem.*, **76**, 2392 (1972).
(14) C. J. Karzmark, *Rev. Sci. Instrum.*, **35**, 1646 (1964).
(15) K. M. Bansal and R. W. Fessenden, *J. Chem. Phys.*, **59**, 1760 (1973).
(16) I. Kraljic and C. N. Trumbore, *J. Amer. Chem. Soc.*, **87**, 2547 (1965).
(17) "Handbook of Chemistry and Physics," 42nd ed, The Chemical Rubber Publishing Co., Cleveland, Ohio, 1960–1961.
(18) R. L. Willson, C. L. Greenstock, G. E. Adams, R. Wageman, and L. M. Dorfman, *Int. J. Radiat. Phys. Chem.*, **3**, 211 (1971).
(19) J. L. Weeks and J. Rabani, *J. Phys. Chem.*, **70**, 2100 (1966).
(20) O. P. Chawla and R. W. Fessenden, to be submitted for publication.
(21) E. Hayon, T. Ibat N. Lichtin, and M. Simic, *J. Amer. Chem. Soc.*, **92**, 3898 (1970).
(22) I. G. Draganic, Z. D. Draganic, and R. A. Holroyd, *J. Phys. Chem.*, **75**, 608 (1971).

Thermal Decomposition of Three Crystalline Modifications of Anhydrous Copper(II) Formate

Andrew Knox Galwey,* David M. Jamieson,

Chemistry Department, The Queen's University of Belfast, Belfast BT9 5AG, Northern Ireland

and Michael Ewart Brown

Chemistry Department, Rhodes University, Grahamstown, South Africa *(Received January 17, 1974; Revised Manuscript Received September 12, 1974)*

Comparative measurements have been made of the thermal decompositions of the three crystalline modifications of copper(II) formate. Curves of fractional decomposition with time were sigmoid shaped and the significant differences in behavior observed have been tentatively ascribed to variations in the crystal lattices and sizes and shapes of reactant particles. Decomposition was accompanied by sublimation of copper metal but such volatility was reduced and the reaction rate was accelerated by pelleting the reactant crystallites. From examination of electron micrographs it was concluded that salt crystals underwent disintegration during decomposition and the appearance of the product particles suggested that sintering had occurred. There is evidence that the reaction involved the formation of an unstable volatile intermediate, probably copper(I) formate, and a detailed reaction scheme is proposed.

Introduction

The kinetics of the thermal decomposition of metal carboxylates may be influenced by the method of reactant preparation and the conditions under which the constituent water of crystallization is removed. Such pretreatment determines particle sizes, surface textures, and, in some instances, the crystal lattices of the reactant particles and, in consequence, influences the development and advance of the reaction interface during a subsequent decomposition reaction which proceeds by a mechanism involving the nucleation and growth of a product phase. While the importance of such effects has long been accepted, there have been few quantitative investigations of the effect of reactant structure upon the rate of salt breakdown. It was considered appropriate, therefore, to make comparative kinetic and microscopic studies of the thermal decompositions of the three crystallographic modifications[1] of anhydrous copper(II) formate. The chemical compositions of these three reactants (and probably also the products) are identical, though the lattices, habits, and defect structures of the reactant phases are different. Unlike nickel formate,[2] the copper salt does retain a lattice on dehydration.[1] The structures of the hydrates and of the anhydrous preparation are known. The tetrahydrate[3] consists of infinite polymeric-like layers of copper and formate ions with anti–anti bridging of copper ions by the formate ions. There is unlikely to be significant modification of these layers during dehydration.[4,5] The dihydrate[6] consists of three-dimensional chains of copper ions bridged by formate ions in an anti–syn and anti–anti arrangement, while the anhydrous preparation[7] has a dimer structure of copper ions with anti–syn bridging by formate ions. Although the detailed structures of the dehydrated salts are not known, their X-ray powder diffraction patterns are distinctly different.[1]

It is, of course, possible that the decompositions of all three anhydrous solids may, however, proceed through an identical rate-determining step, if decomposition involves the catalytic breakdown[8] of an ion, or molecule, chemisorbed at the surface of a product metal particle. These three compounds, therefore, should constitute an appropriate system for direct measurement of the influence of structure on reactivity.

In a previous study of the decompositions of copper(II) formate, Schuffenecker, *et al.*,[9] concluded that reaction proceeded through a branching chain mechanism with the possible intermediate formation of copper(I) formate. Erofeev and Kravchuk[10] reported that there was a progressive change in the composition of the product gases ($H_2 + CO_2$) during the early stages of reaction, and also that[5] the activation energies for decomposition of two of the crystalline modifications of salt were slightly different. The kinetics and mechanism of dehydration of copper(II) formate tetrahydrate have been studied in detail,[4] and the enthalpies of formation of four copper(II) formates have been reported.[11]

Experimental Section

Salt Preparation and Analyses. A single batch of each of the three crystal modifications was prepared by methods based on those described by Martin, *et al.*[1,12] All water of crystallization was then removed from the hydrates to give the following "anhydrous" preparations.

Anhydrous Copper(II) Formate Tetrahydrate (ACFT). Basic copper carbonate was added slowly to a slight excess of dilute (20%) formic acid and the solution was filtered. The blue crystals which subsequently separated were briefly washed with water and dehydrated for 150 min at 373 K under vacuum ($\sim 10^{-5}$ Torr).

Anhydrous Copper(II) Formate Dihydrate (ACFD). Basic copper carbonate was added to concentrated (90%) formic acid until neutralization was almost complete. This solution was filtered into a large excess of ether and the light blue precipitate which separated was filtered and dehydrated for 120 min at 373 K under vacuum ($\sim 10^{-5}$ Torr).

Anhydrous Copper(II) Formate (ACF). A small quantity of basic copper carbonate was added to excess concentrated (90%) formic acid and the blue-green solution was filtered. The crystals which separated on boiling the filtrate for several hours were dried.

TABLE I: Analytical Data for Composition of Reactant Samples

	ACFT	ACFD	ACF	Theor $(HCO_2)_2Cu$
%C[a]	15.3	15.1	15.4	15.6
%H[a]	1.31	1.51	1.27	1.31
%Cu[b]	41.5	41.3	41.8	41.4

[a] Microchemical combustion analysis. [b] Atomic absorption analysis.

Reactant samples were stored in a desiccator before use. X-Ray powder diffraction patterns obtained from all three preparations were in good agreement with data reported by Martin and Waterman.[1] Chemical analyses of the salts are given in Table I.

Kinetic Measurements. Two techniques[13] were used to study the kinetics of the decomposition under isothermal (±1 K) conditions. During *accumulatory* runs the pressure of gaseous products evolved in a constant volume system was measured at time intervals. The system was initially evacuated for 2 hr at 10^{-5} Torr and a 193 K trap was maintained between the heated reactant sample and the McLeod pressure gauge. During *differential* runs the volatile products were withdrawn from the reaction vessel at known times for analysis by gas–solid chromatography.

Electron Microscopy. Replicas of the surface of samples of reactants, products, and reactant, partially decomposed to a known extent, were prepared by a two-stage carbon replication technique,[13] shadowed with gold and palladium at $\cot^{-1} 2$ and photographed using an Akashi TRS-80 transmission microscope.

Results

Decomposition Products. The following observations apply equally to all three reactants. The major gaseous product was carbon dioxide. This was identified by gas chromatography and estimated from pressure measurements, in a known volume, using 80 and 193 K traps, as 1.9 ± 0.1 mol of CO_2 (mol of salt decomposed)$^{-1}$. No carbon monoxide was detected and the gas not condensed at 80 K was hydrogen in a yield of 0.8 ± 0.1 mol of H_2 (mol of salt decomposed)$^{-1}$. These observations confirm[14] that the overall decomposition may be satisfactorily represented as

$$(HCO_2)_2Cu \longrightarrow Cu + H_2 + 2CO_2$$

Decomposition under accumulatory conditions was accompanied by sublimation of up to 25% of the constituent copper. Attempts to identify the volatile intermediate by mass spectrometric measurements were unsuccessful. This is ascribed to the rapid rate of decomposition of the volatile species, since copper was deposited on the vessel walls only in the immediate vicinity of the heated reactant sample.

Decomposition Kinetics. Typical fractional decomposition (α)–time curves for the isothermal decomposition of all three microcrystalline reactant preparations were sigmoid with relatively short induction and acceleratory periods. Representative data for the reaction of ACF under accumulatory conditions at various temperatures are shown in Figure 1. Plots for the decomposition of the three different salts at the same temperature are compared in Figure 2. The shapes of the α–time curves and also the rates of reactions are significantly different. The acceleratory period of the decompositions was found to obey the power law

$$\alpha^{1/n} = k(t - t_0) \qquad (1)$$

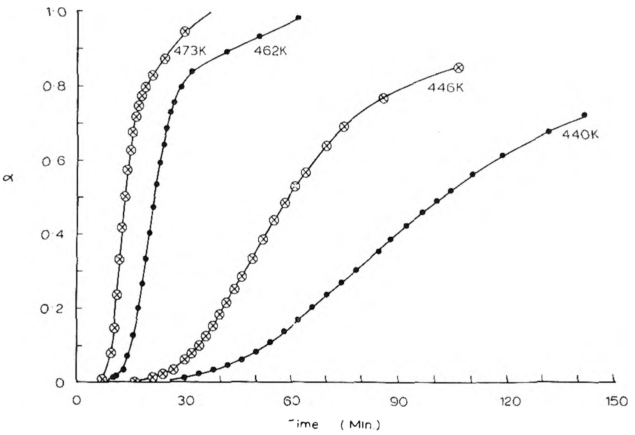

Figure 1. Typical α–time curves for the isothermal decomposition of ACF at four different temperatures. Behavior was somewhat irreproducible $\alpha > 0.8$.

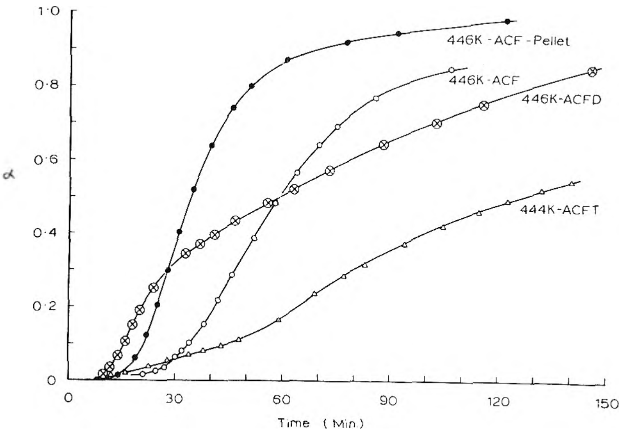

Figure 2. Comparable α–time plots for the thermal decomposition reactions of the three crystalline modifications of copper(II) formate at 445 ± 1 K. The increase in reaction rate which resulted from pelleting is shown for ACF.

In the latter stages of reaction, data fitted the equation

$$1 - (1 - \alpha)^{1/n} = k'(t - t_0') \qquad (2)$$

Equation 2 is the contracting area formula when $n = 2$ and the contracting volume formula when $n = 3$. t_0 is the induction period, including the "warm-up" time, and t_0' is the time at which the contracting envelope is established. The principal kinetic observations for the decomposition of the three salts under accumulatory conditions (with a 193 K trap) are summarized in Table II.

ACFT. The rate of decomposition of ACFT decreased appreciably at $\alpha \sim 0.25$ (see Figure 2) and no single equation which provided a kinetic description of the whole reaction could be found. During the acceleratory period, α–time data fitted eq 1 with $n = 2$, for $0.01 < \alpha < 0.25$ and subsequently eq 2 was obeyed, again with $n = 2$.

ACFD. The kinetic analysis of the reaction of ACFD was similarily considered in two parts, again because of the appreciable reduction in reaction rate at $\alpha \sim 0.3$ (Figure 2). For this solid, eq 1, with $n = 3$, held for $0.02 < \alpha < 0.13$; the rate of reaction was almost constant $0.13 < \alpha < 0.20$ and no satisfactory kinetic obedience was found for the interval $0.20 < \alpha < 0.49$. In the latter stages of the decomposition eq 2 with $n = 3$ applied and the activation energy was increased by about 30 kJ mol^{-1} (Table II).

TABLE II: Summary of Principal Kinetic Data for the Decomposition Reactions of Three Different Crystal Forms of Anhydrous Copper(II) Formate

	Salt	Value of n (± 0.1)	Range of α obeyed	Activation energy, E, ± 10 kJ mol^{-1}	Temp interval, K
Acceleratory period (eq 1)	ACFT	2.0	0.01–0.25	115	432–506
	ACFD	3.0	0.01–0.13	115	446–477
	ACF	3.0	0.02–0.35	120	440–485
Deceleratory period (eq 2)	ACFT	2.0	0.25–0.90	115	432–506
	ACFD	3.0	0.49–0.95	146	446–477
	ACF	3.0	0.30–0.75	132	440–485

ACF. Unlike the other two solids, there was no decrease in reaction rate for ACF at $\alpha \sim 0.3$ (Figure 1) but in the final stages ($\alpha > 0.8$) there was somewhat irreproducible behavior, including a period of almost constant reaction rate. Kinetic behavior over the greater part of reaction was satisfactorily expressed by eq 1 and 2, both with $n = 3$.

The kinetics of hydrogen formation with all three salts, decomposed under accumulatory conditions with an 80 K trap, were identical within experimental accuracy, with the above observations for total gas ($H_2 + CO_2$) evolution. In contrast, the evolution of carbon dioxide, as studied in the differential apparatus, showed appreciable differences from the characteristic behavior under accumulatory conditions. For ACFT the decomposition under differential conditions was more rapid (by a factor of 1.4), and the α–time plot was almost linear for $0.1 < \alpha < 0.5$, but the activation energy remained unchanged. The differential decomposition of ACFD was closely comparable with its behavior under accumulatory conditions, until the later stages ($\alpha > 0.8$) when there was an appreciable enhanced rate of carbon dioxide evolution. Throughout the differential decomposition of ACF the rate of gas formation was reduced (by a factor of 0.5) in comparison with the accumulatory reaction.

Effect of Pelleting. The initial rates of decomposition, under accumulatory conditions, of fragments of pellets formed by compression (20 MN m^{-2} for 5 min) of reactant preparations were always greater than those for the untreated powder samples (Figure 2). Pelleting also markedly reduced the quantity of copper sublimed. This increase in reaction rate was greatest for the decomposition of ACFT (by a factor of 6) but neither the shape of the α–time curve nor the activation energy was appreciably changed. Incorporation of platinum metal in a pellet exerted no detectable influence on reaction rate; a similar (negative) result has been observed for nickel formate.[15] Pelleting increased the rate of reaction of ACFD (by a factor of 1.5). The shape of the α–time plot was changed, the decrease in rate at $\alpha \sim 0.25$ was absent but the reaction became deceleratory for $\alpha > 0.5$ and the rate diminished subsequently to a value comparable with that of the uncompressed material. Pelleting of ACF increased the reaction rate (by a factor of 2) for $0.2 < \alpha < 0.7$ (Figure 2) but after $\alpha \sim 0.8$ the deceleratory process was comparable with that of the uncompacted reactant.

Successive interruptions of the decomposition of ACFD under accumulatory conditions, with transfer of the partially decomposed material to a clean sample tube, showed, by the repeated formation of a copper mirror, that decomposition was accompanied by sublimation to at least $\alpha = 0.5$. Admission of carbon dioxide, at 0.14 Torr, to the reaction vessel prior to the commencement of a decomposition exerted no detectable influence on the subsequent kinetic behavior. Two accumulatory runs on ACFD at 458 K were interrupted at $\alpha = 0.1$ and at 0.25, and the partially decomposed salt was exposed to water vapor. On recommencing decomposition there was a further induction period, comparable with the initial process, and the rate of the continuing decomposition was similar to that following the decrease in the reaction rate at $\alpha = 0.3$.

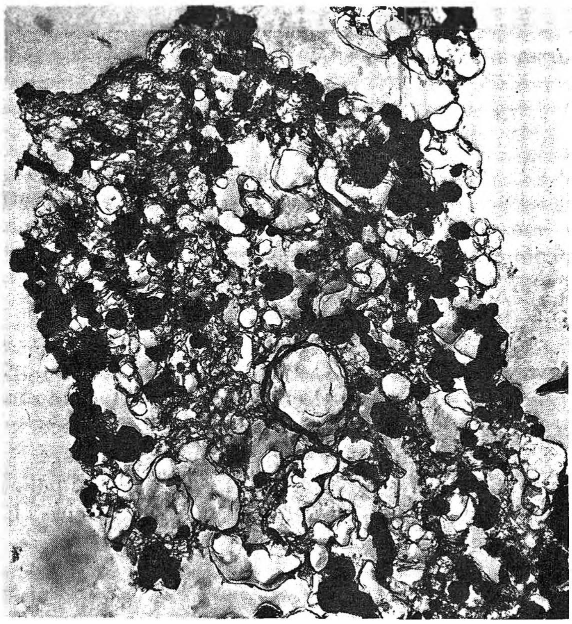

Figure 3. Typical electron micrograph of the residue from the completed decomposition of ACF, showing the important features of the structure of the product phase (X 21,300).

Electron Microscopy. The three anhydrous copper formate preparations ($\alpha = 0.00$) exhibited some variation in sizes and shapes of crystallites and these materials did not tend to adhere to the replica. Surfaces were approximately planar but included irregularities such as step edges, which were sometimes parallel, and a small concentration of surface cracks and pits. The relative absence of acute angular boundary features suggested that surfaces were developed during preparation from solution and that no extensive disintegration occurred during dehydration, handling, and storage.

The textures of the solid products from the completed decomposition ($\alpha = 1.00$) of all three reactants were closely comparable. The residual particles in each case consisted of smaller crystallites aggregated into assemblages of about the size of the original reactant crystals. The sizes of the approximately spherical constituents of such assemblages showed considerable variation, from <10 nm to >10 μm, but there was a marked preponderance of approximate

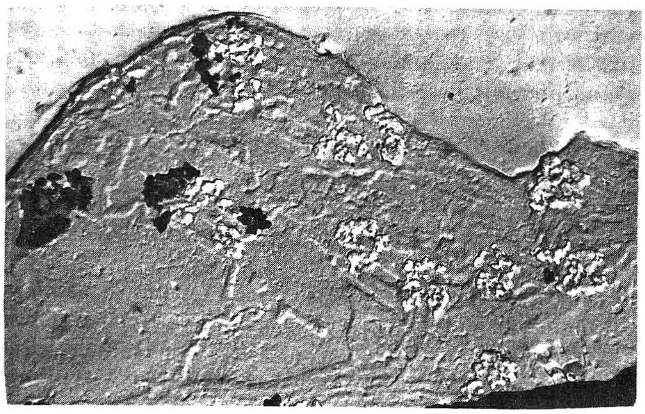

Figure 4. Pits and (probably) particles of product at the surfaces of crystals of partially decomposed (α = 0.12) ACFD (X 14,200).

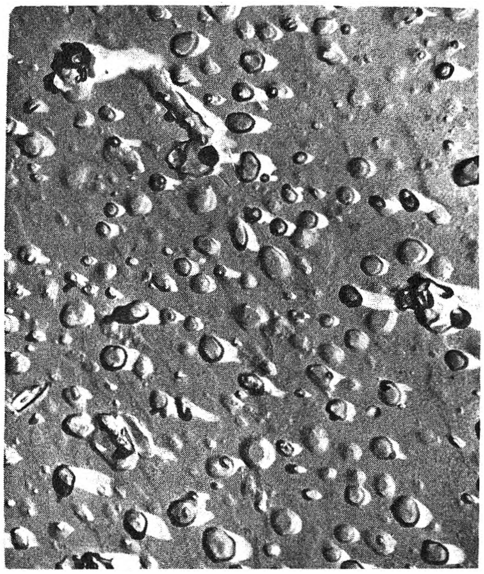

Figure 5. Pitting (~200 nm diameter) of the surface of partially decomposed (α = 0.18) ACF. There was no evidence of superficial product particle formation (X 35,500).

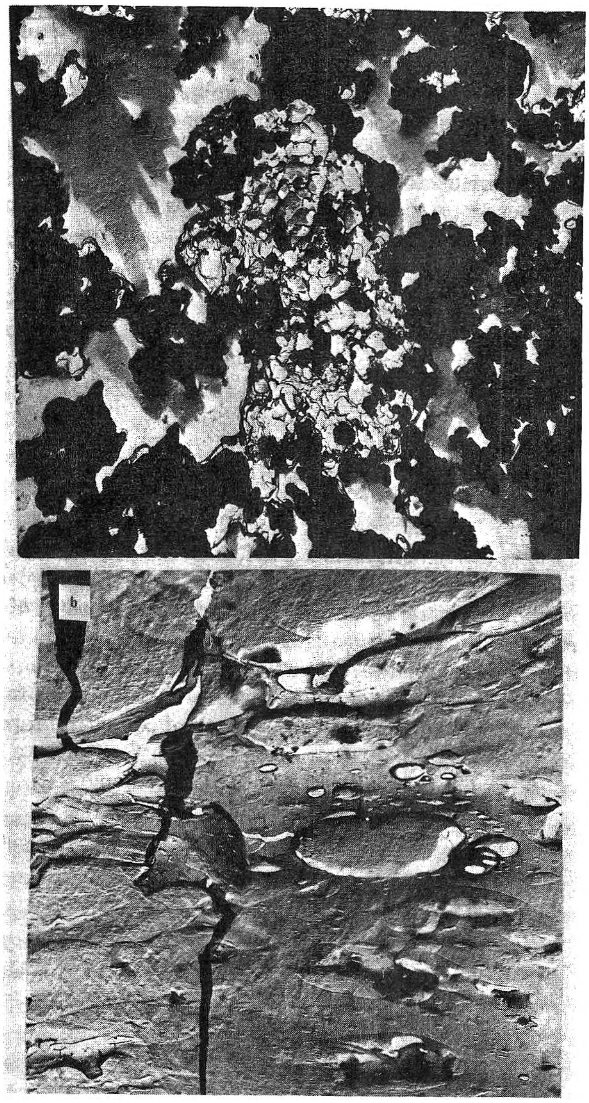

Figure 6. Typical surface features of different fragments from a single pellet of ACFD, following decomposition to α = 0.39 (a, X 14,200) during the initial rapid rate of reaction and α = 0.66 (b, X 14,200) after the reaction became deceleratory.

spheres of diameters ~30 nm, ~0.3 μm, and ~3 μm. The surfaces of larger particles often included rounded protuberances, such as could be expected to arise during coalescence, intergrowth, or sintering of groups of smaller constituents. Most of these features, recorded during examination of some 50 photographs, are seen in the electron micrograph of the residue from ACF, Figure 3. Particles of product did tend to adhere to the replica.

Surface textures of the three reactants showed some individual characteristic changes during the course of the decomposition.

ACFT. No distinctive textural changes occurred during this reaction but textural variations from specimen to specimen increased the difficulties of interpretation. Initially (α = 0.02, 0.05, and 0.21) there was some pitting (with pits ~100 nm diameter) and parallel surface cracking but there was no evidence that any product formation occurred on crystal surfaces. At α = 0.41 fragments of material tended to adhere to the replica and there was some crystal disintegration. For $\alpha > 0.5$ extensive product formation on many crystallite surfaces became apparent.

ACFD. At α = 0.03 the surface texture was indistinguishable from that of reactant and this included surface pits (of ~200 nm diameter) disposed in approximately circular groups (~2 μm diameter). At α = 0.12 particles which adhered to the replica were present in such pits (Figure 4). This is interpreted as evidence of surface nucleation. From critical examination of these photographs it was concluded that such surface reaction can represent only a small proportion of the decomposition which had occurred. At α = 0.3 the surfaces of some crystallites were indistinguishable from the product texture, others were apparently not changed at all, and yet others contained regions with both characteristic appearances.

ACF. At α = 0.08 there were numerous pits (of 20–100 nm in diameter and spaced at 0.4–1 μm intervals) on the surfaces. These pits were occasionally aligned to form a surface crack. At α = 0.18 (Figure 5) the diameter of the pits had increased, typically to ~200 nm, but there was no evidence of superficial product formation. At α = 0.57 many surfaces retained this pitted appearance while others were indistinguishable from product. A similar description is applicable to reactant decomposed to $\alpha = 0.77$, although the proportion of product present was relatively greater.

ACFD Pellet. The surface of a partially decomposed pellet (at $\alpha = 0.39$, which is toward completion of the initial relatively rapid period of reaction) was coherent, there was no evidence of disintegration or product formation (Figure 6a). The surface of a different fragment of the same pellet decomposed further ($\alpha = 0.66$, which is after the point at which the reaction became deceleratory) had disintegrated and much of the surface had the appearance of the residual product (Figure 6b).

Discussion

Many features of the kinetic behavior described above are characteristic of those solid-phase decompositions which proceed through the nucleation and growth of particles of a solid phase. The α–time plots are sigmoid shaped, and eq 1 and 2 are obeyed, although there were decreases in the rate of decomposition of ACFT at $\alpha \sim 0.25$ and of ACFD at $\alpha \sim 0.3$ and the behavior of ACF $\alpha > 0.8$ was less straightforward. The nucleation and growth model does not, however, represent a complete description of the changes occurring, since there was evidence of concurrent sublimation and sintering of the product metal. Accordingly, to account for these and other observations we propose that the mechanism of decomposition of copper(II) formate may be described by the interlinked pattern of rate processes diagrammatically represented by Scheme I.

Scheme I: Mechanism for Thermal Decomposition of Copper(II) Formate

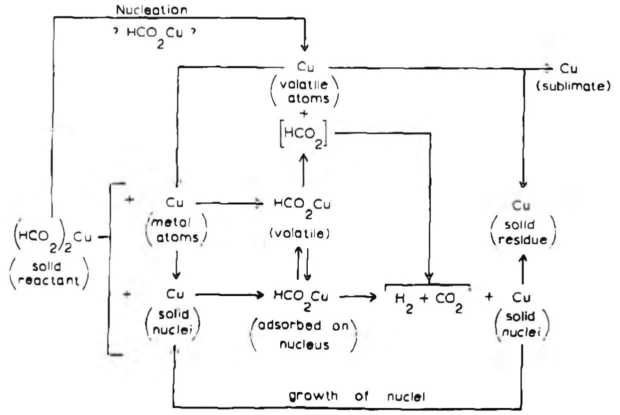

Central in this reaction mechanism is the formation of a volatile, unstable intermediate, tentatively identified as copper(I) formate[16] (see below). This may decompose (i) in the gas phase to yield copper sublimate, (ii) catalytically on metallic copper with consequent growth of nuclei (or, perhaps, sublimate), or (iii) at or near the salt surface, where the copper evolved may react to yield more volatile intermediate[9]

$$(HCO_2)_2Cu\,(\text{solid}) + Cu\,(\text{adsorbed}) \longrightarrow 2HCO_2Cu\,(\text{volatile})$$

While this reaction iii may predominate at external surfaces, some at least of the copper derived from decomposition at confined spaces within the reactant (internal pores and cracks) undoubtedly undergoes coalescence to form metal nuclei which grow by reaction ii above.

The participation of the unstable volatile reaction intermediate explains the observed variations in kinetic behavior which result from alteration of such variables as reactant structure, reactant pretreatment (*e.g.*, pelleting), extent of reaction (α), and decomposition under accumulatory or differential conditions. Such alterations in the experimental system may change the relative proportions of reactions which proceed through the different routes indicated by the scheme and consequently modify the overall kinetics.

Interpretation of these kinetic results must include due consideration of the microscopic observations. There is strong evidence from the electron micrographs that for $\alpha < 0.3$ there was no development of particles of product phase at the surfaces of the original crystallites. In the only possible exception (ACFD, Figure 4), the particles detected represented only a small proportion of the reaction and these did not appreciably increase in size or in number with increase in α. The only significant change in the textures of crystallite surfaces at low α was etch pit formation; this will be discussed below. Further decomposition resulted in disintegration of the crystallites with the appearance of relatively large rounded product particles. The sizes of many such product particles indicate their development through a growth process and the irregularity of the shapes and sizes strongly suggests that many of the particles were formed by coalescence of smaller spheres of product. We conclude, therefore, that reaction commenced at internal surfaces and that metallic nuclei, so generated, grew through catalytic decomposition of the volatile intermediate. Growth of these internal nuclei eventually caused disintegration of crystallite surfaces. When copper was deposited at points of contact of two such nuclei a sintered appearance was produced. Melting of the metal does not occur at the decomposition temperature, but the mobility of the copper arises from that of the intermediate assumed. Nickel formate also yielded spherical particles of metal on decomposition[15] but there was no indication of a volatile intermediate and sintering was less extensive.

On this model it is envisaged that during the initial stages of reaction much of the volatile intermediate is retained in the immediate vicinity of the internal nuclei. Accordingly, decomposition is autocatalytic and the α–time plot is acceleratory. As the decomposition proceeds the crystallites disintegrate, and allow the volatile intermediate to diffuse from the crystallite interior and to decompose on external surfaces or to yield sublimate. The consequent reduction in the effective concentration of the autocatalytic intermediate results in a decrease in the reaction rate. The observed variations in kinetic behavior are very satisfactorily explained by this model. The reduction in the slopes of the α–time curves for ACFT and for ACFD at $\alpha \sim 0.3$ (Figure 2) occurs during the onset of surface disintegration. This was confirmed by examination of the electron micrographs, and the reduction may thus be ascribed to loss of the unstable intermediate from the reaction sites. Breakdown of the crystal surfaces of ACF occurred at larger values of α and became more and more marked between $0.57 < \alpha < 0.77$. Consequently the autocatalytic behavior persisted relatively longer, but there was clear evidence of distortion of the sigmoid curve for $\alpha > 0.7$ and irreproducibility during the final stages of reaction is attributed to crystallite disintegration.

Pelleting of reactant reduced the external surface area of the solid and the observed increase in reaction rate is (again) ascribed to the relative immobility of the volatile species, within voids of the pellet, as shown by the reduced quantity of sublimate. This initially increased rate of reaction subsequently returned toward values characteristic of decomposition of uncompressed salt once the pellet had broken down and the crystallite surfaces had disintegrated (Figure 6a and b).

The kinetic observations summarized in Table II are consistent with the above mechanism. For $\alpha < 0.3$ the autocatalytic reactions were satisfactorily described by the power law. The value of $n = 3$ observed during the decompositions of ACFD and ACF is interpreted as the rapid completion of the initial nucleation process followed by three-dimensional growth, through the erosion of approximately spherical volumes within reactant crystallites. The behavior of ACFT presents an interesting contrast. The value of $n = 2$ indicates that growth is predominantly a two-dimensional process, possibly through the development of disk-like voids, such a process is appropriate within the lattice of this solid which possesses a laminar structure.[3] The activation energies measured for the earlier part of the decomposition ($\alpha < 0.3$) of all three salts were virtually identical (115–120 kJ mol^{-1}) and thus independent of lattice structure. A similar result was obtained by Erofeev and Kravchuk[5] for ACFT and ACF under similar conditions over the same temperature range. Their kinetic analyses were based on application of the Avrami–Erofeev equation

$$[-\ln(1-\alpha)]^{1/n} = k''(t - t_0'') \qquad (3)$$

over as wide a range of α as possible, with values of n of from 3 to 5. Their reported activation energies were 99 and 91 kJ mol^{-1} for ACFT and ACF, respectively. The unambiguous identification of the energy barrier with a particular rate limiting step is difficult, but possible reactions include the interaction of copper with the salt to yield the volatile intermediate and the decomposition of this intermediate.

The establishment of detailed reaction models for the deceleratory process ($\alpha > 0.3$) was more difficult. The contracting area model for the ACFT decomposition (eq 2, $n = 2$) was not directly supported by the electron micrographs, as features attributable to the decomposition reaction could not be unambiguously identified. The indications were that this relatively slow reaction (see Figure 2) proceeded by the continued development of initial nuclei. Obedience of the decomposition of ACFD to the contracting volume model (eq 2, $n = 3$) is supported by the electron micrographs. The relatively high activation energy is ascribed to a temperature dependent change in the extent of participation of the volatile intermediate in the autocatalytic process. (The influence of temperature dependent variations of the concentrations of reaction intermediates on the activation energies of catalytic reactions has been discussed elsewhere[17].) Kinetic analyses of the decomposition of ACF beyond $\alpha \sim 0.3$ were not satisfactory, due to uncertainty in the yield which corresponded to completion of the sigmoid curve, and irreproducibility when $\alpha > 0.8$. The evidence was that the initial reaction continued up to $\alpha \sim 0.8$ accompanied by progressive disintegration of increasing numbers of particles.

The original goals of this research were not directly achieved because of the complex kinetic behavior. The kinetic analyses above do, however, show distinct differences in the behavior of the various preparations of anhydrous copper(II) formate (Figure 2 and Table II). Although reaction was not exclusively confined to a salt–product interface but involved at least one volatile intermediate, it must be presumed, with additional evidence from electron microscopy and pelleting studies, that these differences in kinetic behavior arise from the influences of variations in particle sizes,[5] shapes, porosity, and distribution of imperfections.

The volatile reaction intermediate(s) could not be positively characterized in the present work, due to the rapid rate of decomposition in the gas phase. It is concluded (with previous workers[9,18]), however, that the most probable identity of such a species is copper(I) formate, since it has been shown that this carboxylate is very unstable thermally, and that an acceptable mass spectrum is very difficult to obtain.[16] These characteristics are also those of the intermediate postulated in Scheme I for the decomposition of copper(II) formate. Moreover, there were indications that the same volatile species may also participate in the copper-catalyzed decomposition of formic acid, since experiments[19] have shown that this reaction may be accompanied by volatilization of metal. This observation is significant here since copper(II) formate may yield formic acid during pyrolysis.[9] Yields of formic acid in the present work were, however, always <10% and we conclude that this intermediate, if produced in appreciable amounts, must undergo catalytic breakdown on the copper metal product. This is an alternative reaction pathway which could be incorporated in Scheme I. It was not possible, however, to make meaningful calculations of the rate of breakdown of such acid on the copper metal due to the scatter of reported kinetic data.[20]

The pitting of external surfaces during reaction (particularly ACF, Figure 5), without the concurrent formation of product particles, is evidence for the occurrence of the surface disproportionation step included in Scheme I. Metal atoms may be present on the reactant surface as the result of a nucleation step, or be deposited as sublimate, following the decomposition of a volatile intermediate which has escaped, together with the products, from the internal cavities formed during decomposition. Metal deposited on the surface reacts with the salt at preferred surface sites and etch pits are formed. Similarly, subsurface reaction may commence at specific regions of distorted lattice.

The present study extends the previous work by Schuffenecker, *et al.*,[9] and Erofeev and Kravchuk[5] to include a wider range of reactants and by the application of electron microscopy to the study of these solids. We suggest that the autocatalytic properties of the unstable intermediate, discussed in Scheme I, offer a more comprehensive and generally applicable explanation of decomposition, sublimation, and sintering processes than the chain-branching model.[9]

Acknowledgments. We thank Mr. R. Reed and Mr. T. Conway for their able assistance in obtaining and interpreting the electron micrographs. M.E.B. thanks the Leverhulme Trust for a Visiting Fellowship and the South African Council for Scientific and Industrial Research for financial support. D.M.J. thanks the Ministry of Education for Northern Ireland for a Postgraduate Studentship.

References and Notes

(1) R. L. Martin and H. Waterman, *J. Chem. Soc.*, 1359 (1959).
(2) B. R. Wheeler and A. K. Galwey, *J. Chem. Soc., Faraday Trans. 1*, **70**, 661 (1974).
(3) R. Kiriyama, H. Ibamoto, and K. Matsuo, *Acta Crystallogr.*, **7**, 482 (1954).
(4) P. M. Fichte and T. B. Flanagan, *Trans. Faraday Soc.*, **67**, 1467 (1971).
(5) B. V. Erofeev and L. S. Kravchuk, *Kinet. Catal.*, **10**, 533 (1969).

(6) M. Bukowska-Strzyzewska, *Acta Crystallogr.*, **19**, 357 (1965).
(7) G. A. Barclay and C. H. L. Kennard, *J. Chem. Soc.*, **3289** (1961).
(8) G. C. Bond, "Catalysis by Metals," Academic Press, London, 1962.
(9) R. Schuffenecker, Y. Trambouze, and M. Prettre, *Ann. Chim.* (*Paris*), **7**, 127, 133 (1962).
(10) B. V. Erofeev and L. S. Kravchuk, *Dokl. Akad. Nauk Beloruss., SSR*, **11**, 516 (1967).
(11) N. I. Ostanni, L. A. Zharkova, and B. V. Erofeev, *Zh. Fiz. Khim.*, **44**, 1427 (1970).
(12) R. L. Martin and A. Whitley, *J. Chem. Soc.*, 1394 (1958).
(13) M. J. McGinn, B. R. Wheeler, and A. K. Galwey, *Trans. Faraday Soc.*, **67**, 1480 (1971).
(14) R. Schuffenecker, Thesis, University of Lyon, 1962.
(15) A. K. Galwey, M. J. McGinn, and M. E. Brown, "Reactivity of Solids," Chapman and Hall, London, 1972, p 431.
(16) D. A. Edwards and R. Richards, *Inorg. Nucl. Chem. Lett.*, **8**, 783 (1972).
(17) M. C. Wilson and A. K. Galwey, *Nature* (*London*), **243**, 402 (1973).
(18) A. Keller and F. Korosy, *Nature* (*London*), **162**, 580 (1948).
(19) D. M. Jamieson and A. K. Galwey, *J. Catal.*, **34**, 156 (1974).
(20) Reference 8, p 420.

The Copper|Copper Oxide|Carbonate Electrode at 350° in Fused Potassium Nitrate–Sodium Nitrate[1]

A. G. Keenan* and Carlos G. Fernandez

Department of Chemistry, University of Miami, Coral Gables, Florida 33124

(Received June 18, 1974)

Publication costs assisted by the University of Miami

A Cu|CuO electrode in KNO_3–$NaNO_3$ melts at 350° has been found to respond reversibly to the electroactive species O_2, CO_2, and CO_3^{2-} according to the equation $CuO + CO_3^{2-} \rightleftharpoons Cu + CO_2 + O_2 + 2e$. Standard potentials with respect to a silver electrode are reported for pure and mixed solvents. If CO_3^{2-} is the only active species of interest, the electrode system can be used exposed to the ambient atmosphere which provides the necessary equilibrium concentrations of O_2 and CO_2.

Introduction

Alkali metal carbonates have played an important role in the chemistry of molten salts.[2,3] Due to their basic characteristics, they have been employed in neutralization reactions[4] and in potentiometric[5] and voltammetric[6] studies in molten nitrates. In the present work the electroactive species, the Nernst equation for the electrode reaction and the standard potential have been determined for the copper|copper oxide electrode in pure and mixed potassium and sodium nitrate melts containing carbonate.

Experimental Section

Reagent grade chemicals were used throughout. The KNO_3 and $NaNO_3$ were dried *in vacuo* at 130° for 24 hr, then stored at 110°. K_2CO_3 and Na_2CO_3 were dried at 110° for 24 hr prior to use. $AgNO_3$ was kept in a desiccator containing silica gel. The gases CO_2, O_2, and N_2 were of high purity grade and were dried by passing through silica gel. A 99.8% copper wire, 22 gauge, and a 99.9% silver wire, 18 gauge, were used as electrode materials.

The potentiometric measurements were made in a 100-ml three-neck Pyrex flask. When KNO_3 or $NaNO_3$ was used as the solvent, 125.0 g of the salt was used. When equimolar KNO_3–$NaNO_3$ was the solvent, 56.66 g of $NaNO_3$ and 67.46 g of KNO_3 were mixed together. The flask containing the solvent was placed in a constant temperature molten salt bath[7] at 350°. The solvent, upon melting, was purged with dry N_2 for several hours to ensure dryness. The temperature of the bath was regulated by a Bayley Model 253 controller to ±0.1° and measured with a calibrated iron–constantan thermocouple. The indicating copper|copper oxide electrode was prepared by placing a section of copper wire, which was coiled at one end, into approximately 50 g of KNO_3 at 350° for 24 hr. A black film of CuO formed on the electrode surface.[8] The reference electrode consisted of a silver wire dipping into a 2.4 wt % solution of $AgNO_3$ in the molten solvent. The reference electrode was contained in a 10-mm glass sealing tube whose end was a Pyrex frit of medium porosity. This frit separated the two electrode compartments. It was flamed and partially sealed to reduce diffusion. The electrodes were positioned in the side necks of the flask.

The emf of the cell was measured to within 0.1 mV by the use of a Leeds and Northrup Type K-3 potentiometer in combination with a Keithley Model 601 electrometer as null detector. This model has an input impedance of 10^{14} ohm on the millivolt range. The emf was followed for several hours until a series of readings showed only random fluctuations of about 1 mV and no net drift. The last five or six readings were then averaged. Micropolarization tests, consisting of momentarily short circuiting the cell and observing the potential rise back to its equilibrium value, confirmed reversibility of the electrodes. Potentials were corrected for asymmetry of the frits.

The melts were saturated with mixtures of N_2, O_2, and CO_2 of known composition. The N_2 flow was adjusted to give a constant total flow rate in all runs while the proportions of O_2 and CO_2 were varied. The gas mixtures were prepared by passing the individual gases from cylinders through SiO_2 towers and calibrated flowmeters into a mixing chamber and then through the melt at atmospheric pressure. The exiting gas formed an atmosphere over the surface of the melt. Glass wool packed into the necks of the

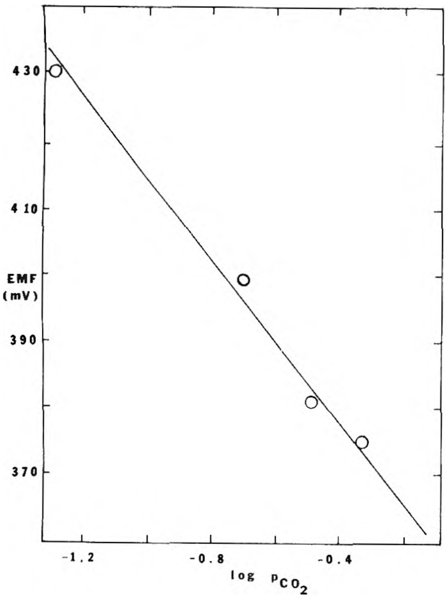

Figure 1. Plot of emf of Cu|CuO electrode against logarithm of CO_2 pressure in atm in KNO_3 at 350°.

electrode vessel prevented back diffusion of laboratory air. After several hours of saturation, a slow stream of the gas mixture was continued over the top of the melt throughout the emf readings. In some experiments, water vapor was introduced into compressed air by passing the air through a saturated KNO_3 solution at room temperature. Runs were also made in which the melt was allowed to equilibrate with the ambient laboratory atmosphere after being purged with dry nitrogen.

Results

It has already been shown[9] that, under the conditions of this research, carbonate ion is stable and does not undergo dissociation or decomposition in molten KNO_3 or $NaNO_3$ at 350°.

Preliminary experiments showed that the Cu|CuO electrode was sensitive not only to CO_3^{2-} but also to O_2 and CO_2 from the atmosphere. A systematic study of the emf dependence on the concentrations of these electroactive species was therefore carried out as already described. Some 40 measurements were made in all, divided into nine series in each of which two of the concentrations were held constant while the third was varied over its experimentally feasible range. The ranges were as follows: O_2, 0.17 to 0.80 atm; CO_2, 0.05 to 0.55 atm; CO_3^{2-} 2.5×10^{-3} to 11×10^{-3} *m*. Typical graphs are shown in Figures 1-3 plotted according to the Nernst equation. The Cu|CuO electrode was anodic with respect to the silver. Straight lines were fitted to the nine series of data using a standard least-squares computer program. The average value of *n* in the Nernst slope $2.3RT/nF$ was found to be 2.08 ± 0.13.

It is clear that the data fit a Nernst equation of the form

$$E = E^{0\prime}_{\mathrm{Cu|CuO}} - \frac{2.303RT}{2F}\log\frac{p_{CO_2}p_{O_2}}{[CO_3^{2-}]} \qquad (1)$$

where $E^{0\prime}$ is taken with respect to the 2.4 wt % silver|silver ion reference electrode and includes the Henry's law constants for the solubilities of O_2 and CO_2. As is usual in this area, partial pressures in atmospheres and molalities have been used for activities. The equation for the electrode reaction is therefore

$$CuO + CO_3^{2-} \longrightarrow Cu + CO_2 + O_2 + 2e^- \qquad (2)$$

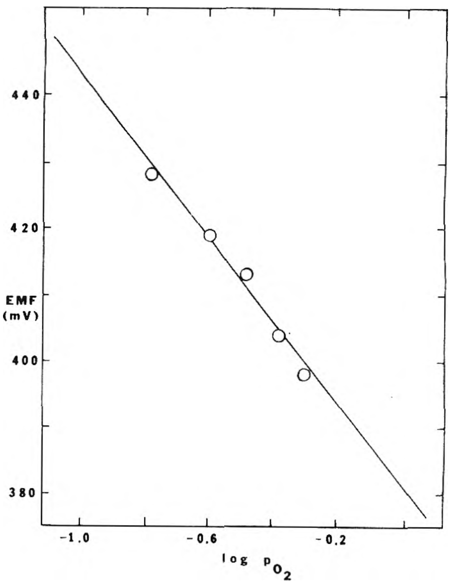

Figure 2. Plot of emf of Cu|CuO electrode against logarithm of O_2 pressure in atm in KNO_3 at 350°.

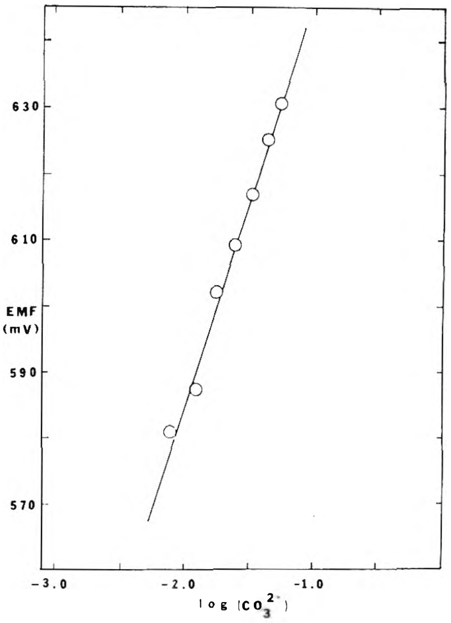

Figure 3. Plot of emf of Cu|CuO electrode against logarithm of CO_3^{2-} concentration in molal units in KNO_3 at 350°.

The average value of $E^{0\prime}$ from all the data points was 489.7 ± 7.2 mV.

When the partial pressure of CO_2 exceeded about 0.6 atm, the emf data were no longer reproducible and the Nernst plots curved upward indicating *n* values as high as 16. The solvent in the Cu|CuO electrode compartment gradually turned blue at the highest CO_2 pressures.

While the above data were obtained using carefully prepared atmospheres, it was also observed that the nitrate melts equilibrated rapidly (*ca.* 30 min) with the ambient laboratory atmosphere after purging with N_2 to dryness. Stable, reproducible values of the emf were obtained over intervals of several months, which depended only on the CO_3^{2-} concentration. Purging the melt with air passed through saturated aqueous KNO_3 solution had no effect on the subsequent steady emf value.

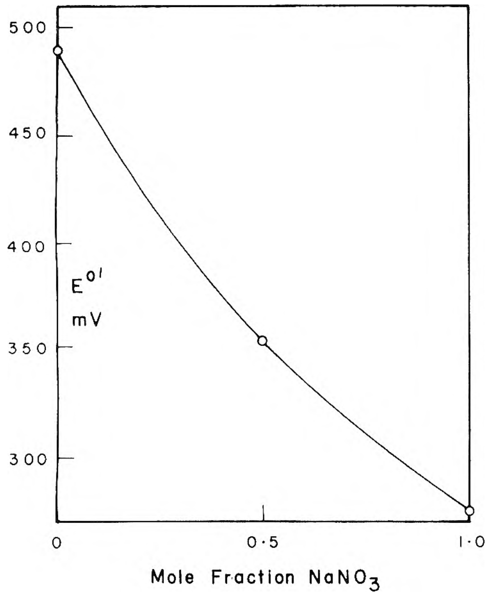

Figure 4. Plot of relative standard potential of Cu|CuO electrode at 350° in KNO_3-$NaNO_3$ melts containing CO_3^{2-} against mole fraction of $NaNO_3$.

Several series of runs, involving 20 data points, were made in which the melt was exposed to laboratory air and the CO_3^{2-} concentration varied. Least-square lines, similar to Figure 3, gave an average value of 2.04 ± 0.11 for the n factor in the Nernst slope. Substituting the known values of $E^{0'}$ and of the oxygen content of air into eq 1 gave a value of 1.33×10^{-3} atm for the pressure of CO_2. This is within the expected range for recirculated laboratory air. Thus the Cu|CuO electrode can also be used in a routine manner in carbonate containing nitrate melts without the elaboration of preparing an accurately known $CO_2|O_2$ atmosphere.

The experiments in an equimolar KNO_3-$NaNO_3$ melt and in pure $NaNO_3$ were done in equilibrium with air and by varying the CO_3^{2-} concentration. The average value of the Nernst n factor was found to be 1.95 ± 0.05. Using the partial pressures of O_2 and of CO_2 which were found to apply in KNO_3 the $E^{0'}$ values were found to be 353.7 ± 1.2 mV in KNO_3-$NaNO_3$ and 275.6 ± 3.9 mV in $NaNO_3$. Figure 4 shows a graph of the relative standard potentials *plotted* against the mole fraction of $NaNO_3$.

Discussion

Shams El Din and Gerges[8] reported the use of a copper|copper oxide electrode in the potentiometric titration of $K_2Cr_2O_7$ with Na_2O_2 in molten KNO_3 at 350°. This electrode was defined as an electrode of the second kind since it responded reversibly to changes in the activity of oxide ion produced from the thermal decomposition of Na_2O_2. While it is not stated in the report, the atmosphere over the melt probably was room air. Conte and Cassadio[10] in their study on the anodic polarization of a copper electrode in equimolar $NaNO_3$-KNO_3 at 250° proposed that passivation of the electrode occurred at the oxidation potential of oxide ion by the oxidation of Cu_2O to CuO. At 300°, the oxide on the copper electrode was CuO. There are no other reports on the use of copper electrodes in molten nitrates.

The present results show that the Cu|CuO electrode is a stable reproducible system responsive to CO_3^{2-}, O_2, and CO_2 in fused solvent mixtures ranging from pure KNO_3 to pure $NaNO_3$. If CO_3^{2-} is the only electroactive species of interest, the cell may be used open to the atmosphere using an $E^{0'}$ value appropriate to the particular ambient atmosphere present. Variations in atmospheric humidity have no effect. The electrode reaction throughout the range of solvents is given by eq 2 with the corresponding Nernst expression eq 1.

The relative standard potential, $E^{0'}$ in eq 1, varies with the solvent as shown in Figure 4. Kust[11] reported a similar variation for the Pt|O_2 electrode in KNO_3-$NaNO_3$ mixtures at 360° and attributed it to the different solvating powers of the cations. Duke and Schlegel[12] observed that both the equilibrium and rate constants for the reaction of $Cr_2O_7^{2-}$ with BrO_3^- varied with the cation ratio in KNO_3-$NaNO_3$ mixtures. Shams El Din,[13] *et al.*, attributed the observed variation in the K_{sp} of Ag_2O in KNO_3-$NaNO_3$ mixtures to a difference in the acidic character of the cations. In the present case, since $E^{0'}$ contains the Henry's law constants for the solubilities of O_2 and CO_2, changes in these constants with solvents may be responsible for the observed variations in $E^{0'}$. No data are available to check this.

The erratic results at high CO_2 pressures are undoubtedly due to dissolution of copper as some form of carbonato complex. A spectrophotometric study of this complex is currently underway. Shams El Din and Gerges[8] reported that their Cu|CuO electrode was attacked by acids such as $NaPO_3$ and NaH_2PO_4 with copper going into solution. A similar observation has been reported by Delarue in molten chlorides.[14]

It was found in the present work that the Cu|CuO|CO_3^{2-} electrode system in nitrates could also be set up by using oxalate as a source of carbonate. It has already been shown[9] that oxalate reacts according to the equation

$$C_2O_4^{2-} + NO_3^- \longrightarrow CO_3^{2-} + CO_2 + NO_2^- \qquad (3)$$

The CO_2 equilibrates rapidly with the ambient pressure and the NO_3^- has no effect on the electrode potential. In most cases the use of oxalate, however, would have no advantage over the direct addition of carbonate.

References and Notes

(1) This work comprises part of the Ph.D. dissertation (May 1974) of C.G.F. and was supported by the Office of Naval Research, Material Sciences Division, Power Program.

(2) (a) G. J. Janz and F. Saegusa, *Electrochim. Acta*, **7**, 393 (1962); (b) *J. Electrochem. Soc.*, **108**, 663 (1961).

(3) (a) R. N. Kust, *Inorg. Chem.*, **3**, 1035 (1964); (b) *J. Phys. Chem.*, **69**, 3662 (1965).

(4) (a) A. M. Shams El Din and A. A. El Hosary, *J. Electroanal. Chem.*, **16**, 551 (1969); (b) A. M. Shams El Din, H. D. Taki El Din, and A. A. El Hosary, *Electrochim. Acta*, **13**, 407 (1968); (c) J. D. Van Norman and R. A. Osteryoung, *Anal. Chem.*, **32**, 398 (1960).

(5) (a) M. Fredericks and R. B. Temple, *Aust. J. Chem.*, **25**, 2319 (1972); *Inorg. Chem.*, **11**, 962 (1972); (b) M. Fredericks, R. B. Temple, and G. W. Thicket, *J. Electroanal. Chem.*, **38**, App. 5 (1972).

(6) P. G. Zambonin, *Anal. Chem.*, **44**, 763 (1972).

(7) A. G. Keenan, K. Notz, and F. L. Wilcox, *J. Phys. Chem.*, **72**, 1085 (1968).

(8) A. M. Shams El Din and A. A. A. Gerges, *Electrochim. Acta*, **9**, 613 (1964).

(9) A. G. Keenan, C. G. Fernandez, and T. R. Williamson, *J. Electrochem. Soc.*, **121**, 885 (1974).

(10) (a) A. Conte and S. Cassadio, *Ric. Sci.*, **36**, 433 (1966); (b) A. Conte, *Electrochim. Acta*, **11**, 1579 (1966).

(11) R. N. Kust, *J. Electrochem. Soc.*, **116**, 1137 (1969).

(12) F. R. Duke and J. Schlegel, *J. Phys. Chem.*, **67**, 2487 (1963).

(13) A. M. Shams El Din, T. Gouda, and A. A. El Hosary, *J. Electroanal. Chem.*, **17**, 137 (1968).

(14) G. Delarue, *Chim. Anal. (Paris)*, **44**, 91 (1962).

Dependence of the Glass Transition Temperature on Heating and Cooling Rate

Cornelius T. Moynihan,* Allan J. Easteal, James Wilder,

Vitreous State Laboratory, Chemical Engineering and Materials Science Department,
The Catholic University of America, Washington, D.C. 20064

and Joseph Tucker

Department of Chemistry, Purdue University, Lafayette, Indiana 47907 *(Received June 26, 1974)*

Publication costs assisted by the Air Force Office of Scientific Research and the Advanced Research Projects Agency

It is shown that under certain conditions the dependence of the glass transition temperature T_g on heating or cooling rate $|q|$ is given to a high degree of approximation by $d \ln|q|/dT_g = \Delta h^*/RT_r^2$ or alternatively by $d \ln|q|/d(1/T_g) = -\Delta h^*/R$, where T_r is a temperature in the middle of the transition range and Δh^* is the activation enthalpy for the relaxation times controlling the structural enthalpy or volume relaxation. The conditions necessary for the validity of these relations are that the structural relaxation be describable by a temperature-independent distribution of relaxation times and that the glass be cooled from a starting temperature well above the transition region and subsequently reheated at the same rate starting from a temperature well below the transition region. Experimental measurements of T_g *vs.* $|q|$ are presented for As_2Se_3, B_2O_3, potassium silicate, and borosilicate crown glasses. Δh^* is found to be equal within experimental error to the activation enthalpy for the shear viscosity.

Introduction

Changes in macroscopic properties of liquids, such as the enthalpy or the volume, induced by isobaric changes in temperature are of two types.[1] The first type may be termed a solid- or glass-like response and on ordinary experimental time scales occurs instantaneously. The second type of response arises from changes in the structure or configuration of the liquid. The time scale on which this structural response occurs is highly temperature dependent and at sufficiently low temperatures becomes so long that a rapid temperature change can "freeze in" the liquid structure. It is this last process that is ordinarily understood to be involved in the formation of a glass from a supercooled liquid.

In Figure 1 are shown schematic plots of enthalpy H and heat capacity C_p for isobaric cooling and subsequent reheating at a constant rate of a glass-forming liquid.[2] The temperature range during cooling in which the rate of structural relaxation in the liquid starts to become sufficiently slow that the H–T and C_p–T curves depart from the equilibrium liquid curves is the beginning of the glass transition or transformation region. The temperature range in which the structural relaxation becomes so slow that it effectively ceases on the experimental time scale marks the end of the transition region and the beginning of glass-like behavior. Irrespective of the direction of temperature change, the direction of the structural relaxation process is always toward equilibrium. Consequently on reheating the glass the H–T and C_p–T curves follow paths different from those for the prior cooling, as shown in Figure 1 and explained previously by a number of workers.[3–5]

The glass transition temperature, T_g, is defined as some characteristic temperature on the H–T or C_p–T curve in the transition region during heating or cooling at a constant rate, for example, the temperature of intersection of the extrapolated liquid and glass H–T curves during cooling, the extrapolated temperature of onset of rapid increase of the C_p–T curve during heating, or the temperature of inflection in the region of rapid rise of the C_p–T curve during heating. Because the "break" in the C_p–T curve is more pronounced during heating than during cooling and probably because constant heating rate experiments are easier to realize than constant cooling rate experiments, the majority of investigators in the past have reported T_g values determined from heating curves.

Experimentally, it is found[3,5–14] that T_g shows a dependence on the heating or cooling rate, higher values of T_g being observed for faster heating or cooling rates, as shown in Figure 1. The reason for this is not difficult to see if one notes that isobaric heating or cooling at a constant rate is the limit as $\Delta T \to 0$ of a series of instantaneous, small temperature changes ΔT, each of which is following by an isothermal hold of time duration

$$\Delta t = \Delta T/q \tag{1}$$

where q is the heating or cooling rate

$$q = dT/dt = \Delta T/\Delta t \tag{2}$$

We may define at any stage of the process a relaxation time τ by the equation

$$(\partial H/\partial t)_T = -(H - H_e)/\tau \tag{3}$$

where $(H - H_e)$ is the departure of the enthalpy H from the equilibrium liquid value, H_e, at the temperature of interest. τ decreases with increasing temperature. The three temperature regions of Figure 1 then correspond roughly to the conditions

$$\text{liquid} \qquad \Delta t >> \tau \tag{4a}$$

$$\text{transition region} \qquad \Delta t \sim \tau \tag{4b}$$

$$\text{glass} \qquad \Delta t << \tau \tag{4c}$$

From eq 1 it is evident that if the heating or cooling rate q is increased in magnitude, then the relaxation time τ must be correspondingly smaller for eq 4b to hold, and the transition region is shifted to a higher temperature.

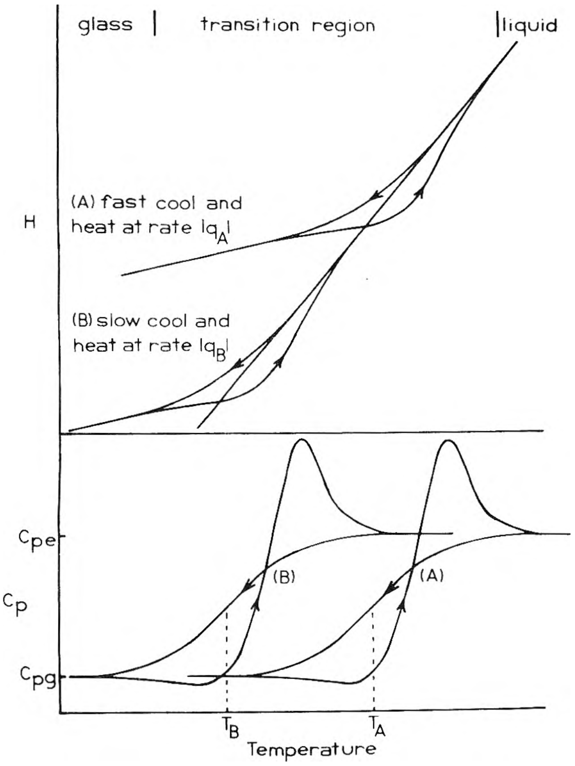

Figure 1. Enthalpy and heat capacity *vs.* temperature plots for a glass cooled and then reheated through the transition region at different rates. Temperatures T_A and T_B are a pair of corresponding temperatures in eq 15.

From the above discussion it is also evident that the dependence of T_g on heating or cooling rate q yields information on the temperature dependence of the kinetic parameter τ. The essential features of a treatment which can relate the dependence of T_g on q to the temperature dependence of τ for T_g's determined from cooling curves were presented some years ago by Ritland.[6] More recently McMillan[8] and Rasmussen and MacKenzie[12] attempted to obtain this information from the T_g's determined from heating curves. However, it was pointed out in a communication from this laboratory[15] that the temperature dependence of τ assessed from heating curve T_g's depends on the thermal history received by the glasses during the prior cool through the transition region and is apt to differ from the true temperature dependence. It is the purpose of the present paper to consider the conditions under which the temperature dependence of τ can be assessed correctly from the dependence of T_g on either heating or cooling rate and to present experimental evidence in support of our conclusions.

Dependence of T_g on Heating or Cooling Rate

We begin with a set of assumptions about the kinetic and thermodynamic parameters controlling the evolution of the enthalpy during the structural relaxation process.

(1) Following an instantaneous, isobaric change in temperature from an initial equilibrium state, the system exhibits at time zero an enthalpy H_0, but in time the enthalpy relaxes isothermally to a new equilibrium value, H_e, at the new temperature. We assume that this isothermal relaxation may be described as a sum of n independent processes[16,17]

$$(\partial H/\partial t)_T = \sum_{i=1}^{n} (\partial H_i/\partial t)_T \qquad (5)$$

H_i may be thought of as the enthalpy associated with some order parameter[3,16,17] which changes during the structural relaxation; there are n distinct order parameters labeled $1, 2, \ldots i, \ldots n$. It should be noted, however, that eq 5 is strictly phenomenological and that there need exist no one-to-one correspondence between the order parameters which give an adequate description of the macroscopic process and the elementary or microscopic processes actually taking place on a molecular level. The rate of isothermal change of H_i is given by a time and temperature dependent relaxation time, τ_i

$$(\partial H_i/\partial t)_T = -(H_i - H_{ei})/\tau_i \qquad (6)$$

Combination of eq 5 and 6 and integration gives for isothermal relaxation

$$H = H_e + (H_0 - H_e)\sum_{i=1}^{n} g_i \exp\left(-\int_0^t dt'/\tau_i\right) \qquad (7)$$

where g_i is a weighting coefficient for each order parameter i

$$g_i = (H_{0i} - H_{ei})/(H_0 - H_e)$$

and is subject to the normalization condition $\Sigma_{i=1}^{n} g_i = 1$.

(2) The difference between the equilibrium liquid and glass heat capacities, $(C_{pe} - C_{pg})$ (see Figure 1), is assumed to be constant over the experimental range of T_g. As shown below experimentally, the variation in T_g produced by changes in q of, *e.g.*, a factor of 10^2, is comparatively small, and over this range this assumption is valid to a high degree of approximation for most glasses.

(3) At constant pressure the dependence of relaxation time τ_i on temperature and structure is assumed to be of the form

$$\tau_i = a_i \exp(-bT) \exp[-c(H - H_e)] \qquad (8)$$

b and c are constants and the relaxation times differ only in their preexponential terms a_i. Equation 8, along with eq 5–7, corresponds to a condition frequently designated as "thermorheologically simple behavior" or as a "temperature independent distribution of relaxation times."

The relaxation time expression of Sharanov and Vol'kenshtein[9] is identical with that of eq 8, as is the relaxation time expression of Tool[18]

$$\tau_i = a_i \exp(-b'T) \exp(-c'T_f)$$

where b' and c' are constants, if one notes that the fictive temperature T_f is defined by

$$H - H_e = (C_{pe} - C_{pg})(T_f - T)$$

The relaxation time expression of Narayanaswamy[17]

$$\tau_i = a_i'' \exp(x\Delta h^*/RT) \exp[(1 - x)\Delta h^*/RT_f]$$

where a_i'', Δh^*, and x $(0 \leq x \leq 1)$ are constants, is also of the form of eq 8 in any region centered at a temperature T_r in which $1/T$ and $1/T_f$ may be approximated by the first two terms in their Taylor's series expansions about T_r

$$1/T \approx 1/T_r - (T - T_r)/T_r^2 \qquad (9)$$

and similarly for $1/T_f$. An activation enthalpy, Δh^*, may be defined which expresses the temperature dependences of the logarithms of the relaxation times of eq 8 both for constant departure from equilibrium (constant $(H - H_e)$ or constant $(T_f - T)$) and for the linear regime where $(H - H_e)$ is so small that the second exponential in eq 8 differs negligibly from unity

$$\left[\frac{\partial}{\partial T}(\ln \tau_i)\right]_{(H-H_e)} = \frac{d}{dT}\left(\lim_{H \to H_e} \ln \tau_i\right) = -b = -\Delta h^*/RT^2 \approx -\Delta h^*/RT_r^2 \qquad (10)$$

where R is the ideal gas constant. The approximation in eq 10 is valid in a temperature region around T_r where eq 9 is valid.

We now note that under isobaric conditions the enthalpy is a function of temperature and time[9]

$$H = H(T, t)$$

and

$$\frac{dH}{dT} = \left(\frac{\partial H}{\partial T}\right)_t + \left(\frac{\partial H}{\partial t}\right)_T\left(\frac{dt}{dT}\right) \tag{11}$$

dH/dT is the total observed heat capacity, C_p. $(\partial H/\partial T)_t$ is the heat capacity observed when the temperature is changed instantaneously (t is constant, so that the system has no time to undergo structural relaxation) and hence is the glass heat capacity, C_{pg}. Making these notation changes and substituting for the other terms from eq 2, 5, and 6, eq 11 becomes on rearrangement

$$(C_p - C_{pg}) = -\sum_{i=1}^{n}\frac{(H_i - H_{ei})}{q\tau_i} = \mp\sum_{i=1}^{n}\frac{(H_i - H_{ei})}{|q|\tau_i} \tag{12}$$

In the last expression of eq 12 the minus sign applies for heating (q is positive) and the plus sign for cooling (q is negative).

Let us consider first the case in which the structural enthalpy relaxation (eq 5–7) is controlled by a single order parameter and hence by a single relaxation time τ of the form of eq 8. Substituting for τ in eq 12 and noting that $|q|$ may be written $\exp(\ln|q|)$ we get

$$(C_p - C_{pg}) = \mp\left[\frac{H - H_e}{a\exp[-c(H - H_e)]}\right]\exp(-\ln|q| + bT) \tag{13}$$

From eq 13 and Figure 1 it is evident that for two heat capacity curves, A and B, produced during cooling at respective rates $|q_A|$ and $|q_B|$ the condition will hold that

$$(C_p - C_{pg})_A\big|_{T_A} = (C_p - C_{pg})_B\big|_{T_B} \tag{14}$$

at all pairs of corresponding temperatures T_A and T_B chosen according to the criterion

$$-\ln|q_A| + bT_A = -\ln|q_B| + bT_B \tag{15}$$

provided that the condition

$$(H - H_e)_A\big|_{T_A} = (H - H_e)_B\big|_{T_B} \tag{16}$$

is also satisfied. Since C_p determines the rate at which the enthalpy changes during the rate cool, it is further evident that eq 16 will be valid for all pairs of corresponding temperatures, T_A and T_B, if it can be satisfied for any one pair, T_A' and T_B'. Let us choose T_A' and T_B' in the range above the transition region where the enthalpy and heat capacity curves A and B of Figure 1 follow the equilibrium liquid H–T and C_p–T curves. If we return to the picture of a constant cooling rate corresponding to a series of small instantaneous temperature jumps ΔT followed by isothermal holds of duration $\Delta t = \Delta T/q$, then immediately following the jumps which bring us respectively to temperatures T_A' and T_B' we have

$$(H - H_e)_A\big|_{T_A'} = (H - H_e)_B\big|_{T_B'} = -(C_{pe} - C_{pg})\Delta T$$

since just prior to the jumps the system was in equilibrium and $(H - H_e)$ was zero. From this it follows that eq 14–16 become experimentally self-fulfilling for heat capacity cooling curves which commence at any temperature well above the transition region. (These arguments are presented in greater detail in Ritland's paper.[6])

If after cooling at a rate of magnitude $|q|$ one reverses the direction of temperature change and reheats the glass at the same rate, eq 13 will also describe the subsequent evolution of $(C_p - C_{pg})$ on reheating if one switches from the plus sign to the minus sign in eq 13 at the temperature at which the reheating commences. Further, eq 14–16 will continue to apply to a pair of heat capacity heating curves such as A and B in Figure 1 if the direction of temperature change is reversed at a pair of respective corresponding temperatures T_A'' and T_B'' chosen according to eq 15. Suppose that these two temperatures T_A'' and T_B'' are chosen to lie below the transition region. Since below the transition region no structural relaxation takes place and the heating and cooling heat capacity curves superimpose, one could cool through temperatures T_A'' or T_B'' at respective rates $|q_A|$ or $|q_B|$ to any arbitrary lower temperature and return to them *via* reheating at the same rates without altering the glass structure Consequently, for eq 14–16 to be valid for heating curves it is necessary only that the direction of temperature change be reversed somewhere below the transition region.

The derivation of eq 13–16 is easily extended to the case for which more than one order parameter and associated relaxation time τ_i are required to account for the structural relaxation. If the assumptions listed previously allow for an adequate description of the structural relaxation, then associated with each order parameter will be a corresponding relaxational heat capacity of the form of eq 13

$$(C_{pi} - C_{pgi}) = \mp\left[\frac{H_i - H_{ei}}{a_i\exp[-c(H - H_e)]}\right]\exp(-\ln|q| + bT) \tag{17}$$

The total relaxational heat capacity at any temperature is merely the sum of these

$$(C_p - C_{pg}) = \sum_{i=1}^{n}(C_{pi} - C_{pgi}) \tag{18}$$

Equations 14–16 apply to each of the individual $(C_{pi} - C_{pgi})$ and hence apply also to their sum.

To complete our derivation of the dependence of T_g on $|q|$, we need only note that for a given heating or cooling rate T_g is *defined* as the temperature at which some particular value of the relaxational heat capacity, $(C_p - C_{pg})$, is observed. Consequently, we may rewrite eq 15 as

$$-\ln|q_A| + bT_{gA} = -\ln|q_B| + bT_{gB}$$

so that we have, using eq 10

$$\frac{d\ln|q|}{dT_g} = b \approx \Delta h^*/RT_r^2 \tag{19}$$

where T_r is now some temperature in the middle of the transition region. Alternatively, using eq 9 to relate to T_g to T_r, we may write eq 19 in the form

$$d\ln|q|/d(1/T_g) \approx -\Delta h^*/R \tag{20}$$

In addition to the assumptions made in eq 5–9, it should be recalled that eq 19 and 20 are valid only for T_g's measured from heat capacity cooling curves in which the cooling was started well above the transition region or from heat capacity heating curves obtained by reheating the glass from a temperature well below the transition region after it has been previously cooled through the transition region at a rate $|q|$ equal to the heating rate.

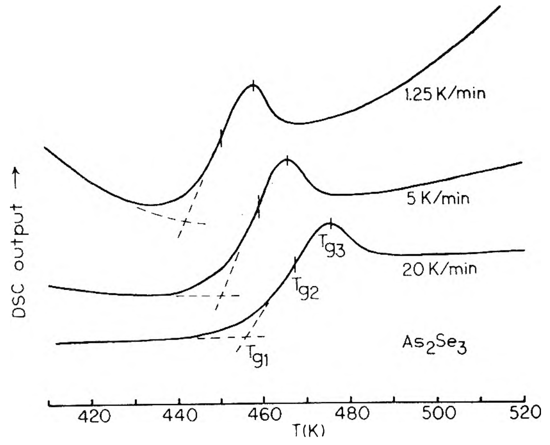

Figure 2. Differential scanning calorimeter traces for heating of As_2Se_3 glass through the transition region at various rates after cooling the glass through the transition region at the same respective rates.

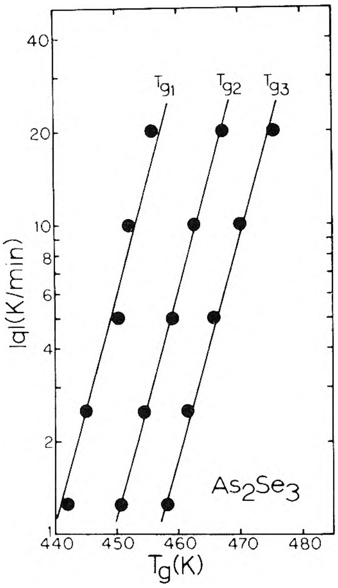

Figure 3. Log $|q|$ *vs.* T_g plots for As_2Se_3 glass. Slopes of lines were calculated from eq 19 using $\Delta h^* = 70$ kcal/mol and $T_r = 460$ K.

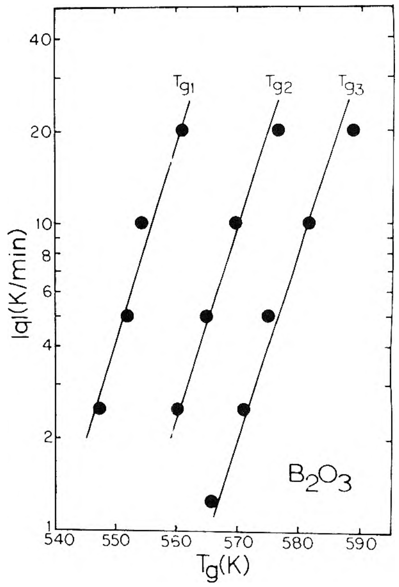

Figure 4. Log $|q|$ *vs.* T_g plots for B_2O_3 glass. Slopes of lines were calculated from eq 19 using $\Delta h^* = 92$ kcal/mol and $T_r = 570$ K.

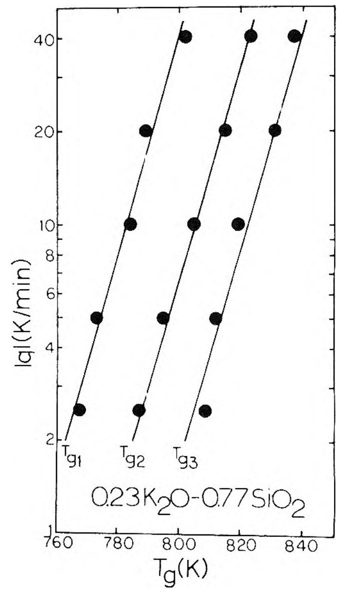

Figure 5. Log $|q|$ *vs.* T_g plots for 23 mol % K_2O–77 mol % SiO_2 glass. Slopes of lines were calculated from eq 19 using $\Delta h^* = 101$ kcal/mol and $T_r = 800$ K.

Experimental Results and Discussion

To test eq 19 and 20 we have carried out measurements of T_g *vs.* $|q|$ for three glasses: As_2Se_3, B_2O_3, and 23 mol % K_2O–77 mol % SiO_2. The T_g measurements were performed on a Perkin-Elmer DSC-2 differential scanning calorimeter, whose output is proportional to the heat capacity, as a function of heating rate after first cooling the glasses through the transition region at a rate equal to the heating rate. For each glass a temperature calibration was performed at each heating rate using an appropriate melting point standard. Excessive baseline curvature and loss of instrument sensitivity limited the heating rates investigated to 1.25 or 2.5 K/min on the low side; temperature gradients in the sample which prevented accurate temperature determinations limited the heating rates to 20 or 40 K/min on the high side.

A typical set of DSC outputs for different heating rates is shown for As_2Se_3 glass in Figure 2. T_g was determined for three characteristic points on each curve as shown in Figure 2: the extrapolated onset of the heat capacity break (designated T_{g1}), the inflection point in the rapidly rising part of the heat capacity curve (designated T_{g2}), and the heat capacity maximum (designated T_{g3}).

In Figures 3–5 are shown semilogarithmic plots of heating rate $|q|$ *vs.* T_{g1}, T_{g2}, and T_{g3} for the three glasses. As expected from eq 19 if the assumptions of eq 5–9 are valid, the three plots for each glass are linear and parallel within the scatter of the data.

It is generally accepted that the molecular motions involved in the structural relaxation are roughly of the same sort as those involved in viscous flow. A number of studies[3,16,17,19,20] of isothermal volume or enthalpy relaxation of glasses in the transition region have shown that the activation enthalpy Δh^* for the volume or enthalpy relaxation is generally the same within experimental error as the activation enthalpy for the shear viscosity, η_s. The shear viscosities of each of the three glasses of Figures 3–5 exhibit Ar-

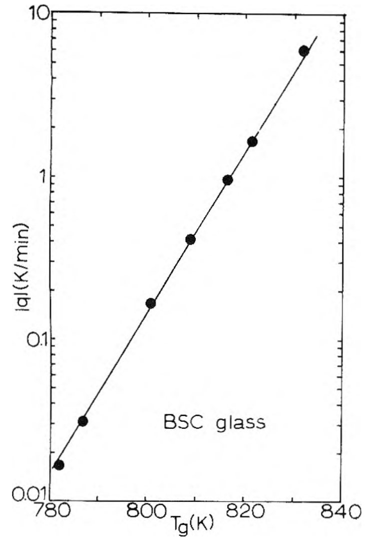

Figure 6. Log $|q|$ *vs.* T_g for borosilicate crown glass. Slope of line was calculated from eq 19 using $\Delta h^* = 147$ kcal/mol and $T_r = 805$ K.

rhenius behavior (constant Δh^*) in the glass transition region ($\eta_s = 10^9$ to 10^{14} P). The lines shown in Figures 3–5 were drawn with slopes calculated from eq 19 using Δh^* values for the shear viscosities in the transition region: 70 kcal/mol for As_2Se_3,[21-23] 92 kcal/mol for B_2O_3,[24,25] and 101 kcal/mol for $0.23K_2O–0.77SiO_2$ glass.[26] Within the scatter of the data the calculated slopes agree with the experimental slopes of the log $|q|$ *vs.* T_g plots, showing that for the present examples the activation enthalpy controlling the enthalpy structural relaxation is essentially the same as the activation enthalpy for viscous flow.

As a final illustration of the good agreement between Δh^* values for shear viscosity and those assessed from the dependence of T_g on $|q|$, we show in Figure 6 a plot of log $|q|$ *vs.* T_g for a borosilicate crown glass using the data of Ritland[6] and covering some 2.5 orders of magnitude in $|q|$. Here T_g was taken to be the extrapolated point of intersection of the equilibrium liquid and glass density *vs.* temperature curves for cooling at various rates. The line through the data was drawn with a slope calculated from the shear viscosity Δh^* value of 147 kcal/mol obtained from Macedo and Napolitano's high-precision viscosity measurements[24] in the transition region of a glass sample from the same blank. The agreement between the experimental and calculated slopes in Figure 6 is very good.

Acknowledgments. The authors wish to thank Professor P. B. Macedo for numerous helpful discussions, Professor C. A. Angell for his assistance with the part of this study carried out at Purdue University, and Dr. J. S. Berkes for providing viscosity data on As_2Se_3 in advance of publication. This research was supported by contracts from the Air Force Office of Scientific Research and from the Advanced Research Projects Agency.

References and Notes

(1) T. A. Litovitz and C. M. Davis, "Physical Acoustics," Vol. IIA, W. P. Mason, Ed., Academic Press, New York, N.Y., 1965, pp 281–349.
(2) In this paper we shall discuss the glass transition in terms of the dependent macroscopic properties enthalpy and heat capacity. The discussion, equations, and conclusions apply equally well to other properties such as volume, index of refraction, or logarithm of the electrical conductivity or shear viscosity and their corresponding temperature derivatives.
(3) R. O. Davies and G. O. Jones, *Advan. Phys.*, **2,** 370 (1953); *Proc. Roy. Soc., Ser. A*, **217,** 26 (1953).
(4) M. V. Vol'kenshtein and O. B. Ptitsyn, *Sov. Phys.-Tech. Phys.*, **1,** 2138 (1957).
(5) S. M. Wolpert, A. Weitz, and B. Wunderlich, *J. Polym. Sci., Part A-2*, **9,** 1887 (1971).
(6) H. N. Ritland, *J. Amer. Ceram. Soc.*, **37,** 370 (1954).
(7) B. Wunderlich, D. M. Bodily, and M. H. Kaplan, *J. Appl. Phys.*, **35,** 95 (1964).
(8) J. A. McMillan, *J. Chem. Phys.*, **42,** 3497 (1965).
(9) Yu. A. Sharanov and M. V. Vol'kenshtein, *Sov. Phys.-Solid State*, **6,** 992 (1964); "The Structure of Glasses," Vol. 6, E. A. Porai-Koshits, Ed., Consultants Bureau, New York, N.Y. 1966, pp 62–66.
(10) N. Onodera, H. Suga, and S. Seki, *J. Non-Cryst. Solids*, **1,** 331 (1969).
(11) U. E. Schnaus, C. T. Moynihan, R. W. Gammon, and P. B. Macedo, *Phys. Chem. Glasses*, **11,** 213 (1970).
(12) D. H. Rasmussen and A. P. MacKenzie, *J. Phys. Chem.*, **75,** 967 (1971).
(13) H. Rotger, "Amorphous Materials," R. W. Douglas and B. Ellis, Ed., Wiley-Interscience, New York, N.Y., 1972, pp 125–132.
(14) S. E. B. Petrie, *J. Polym. Sci., Part A-2*, **10,** 1255 (1972).
(15) C. T. Moynihan and P. B. Macedo, *J. Phys. Chem.*, **75,** 3379 (1971).
(16) P. B. Macedo and A. Napolitano, *J. Res. Nat. Bur. Stand., Sect. A*, **71,** 231 (1967).
(17) O. S. Narayanaswamy, *J. Amer. Ceram. Soc.*, **54,** 491 (1971).
(18) A. Q. Tool, *J. Amer. Ceram. Soc.*, **29,** 240 (1946).
(19) A. Napolitano and P. B. Macedo, *J. Res. Nat. Bur. Stand., Sect. A*, **72,** 425 (1968).
(20) L. Boesch, A. Napolitano, and P. B. Macedo, *J. Amer. Ceram. Soc.*, **53,** 148 (1970).
(21) M. Kunugi, R. Ota, and M. Suzuki, *Zairyo*, **19,** 145 (1970).
(22) N. L. Laberge, Ph.D. Thesis, Catholic University of America, 1973.
(23) J. S. Berkes, paper presented at 73rd Annual Meeting of the American Ceramic Society, Chicago, Ill., April 26, 1971.
(24) P. B. Macedo and A. Napolitano, *J. Chem. Phys.*, **49,** 1887 (1968).
(25) T. J. M. Visser and J. M. Stevels, *J. Non-Cryst. Solids*, **7,** 376 (1972).
(26) J. P. Poole, *J. Amer. Ceram. Soc.*, **32,** 230 (1949).

The Four Electron (or Hole) Noncubic Ligand Field Spectrum. I. Tetragonal Energy Levels

Jayarama R. Perumareddi

Department of Chemistry, Florida Atlantic University, Boca Raton, Florida 33432 *(Received April 26, 1974; Revised Manuscript Received September 18, 1974)*

Tetragonal energy matrices were constructed for d^4 and d^6 electronic configurations with full configuration interaction in the limit of zero spin–orbit perturbation in a strong field scheme in which cubic orientation was maintained. The necessary matrix elements were obtained with the explicit use of the symmetry adapted wave functions. Applications of the energy levels to optical spectra and magnetic cross overs of d^4 and d^6 tetragonal systems were discussed.

Introduction

Although there has been a great surge of activity in recent years in the development of semiempirical and semiquantitative molecular orbital approximations for transition-metal compounds, it is well known that they can do no better than the complete symmetry based parametric ligand field approximation if the study is limited to the molecular electronic energy levels resulting from the d orbitals of the transition-metal ion.[1] Despite this fact, progress in deriving and employing complete ligand field energy levels for the interpretation of the electronic spectra of transition-metal systems of symmetry lower than cubic has not been rapid. This is understandable because when the symmetry is lowered from cubic, the number of ligand field parameters increases and the interpretation of the electronic energy levels becomes somewhat difficult particularly if the expected splittings of all the cubic bands concomitant with the noncubic symmetry are not realized in the experimental spectra. However, our recent work[2] showed that it is still possible to make a definitive study of the electronic spectra of trigonal and tetragonal (or quadrate) systems in the case of $d^{3,7}$ and $d^{2,8}$ electronic configurations with the ligand field energy levels if full configuration interaction and spin–orbit perturbation are included. The ligand field and electron correlation parameters obtained by such a study can be successfully employed in understanding covalency in complexes and σ and π antibonding characteristics of ligands.[3]

We are currently carrying out similar studies on $d^{4,6}$ noncubic systems. We present in this report the derivation of energy levels in tetragonal ligand fields with full configuration interaction but neglecting spin–orbit perturbation. Extensions of the theory to trigonal and other noncubic ligand fields and applications to experimental electronic spectra will be presented in the future reports. The reason for first carrying out the calculations in the limit of zero spin–orbit perturbation is explained below.

The cobalt(III) ion perhaps is the most prolific in forming six-coordinate octahedral complexes among all transition-metal ions. Many of the octahedral cobalt(III) complexes are also substituted resulting in tetragonal and trigonal symmetry. The tetragonally and trigonally substituted octahedral Co(III) systems do show the expected splittings of cubic bands.[4] Our immediate interest is in the thorough interpretation of these spectra. With the exception of a few complexes (halides and perhaps some mixed halides) all are of magnetically low spin, which means that the ground state is a spin singlet. The spin-allowed bands in the spectra of these systems are thus singlet–singlet transitions. The spin-singlet levels do *not* split up under spin–orbit perturbation. Spin–orbit interaction can only have second-order effects through configurational interaction with the same symmetry levels arising from spin–triplet and spin–quintet levels. This is the reason why we derived the energy levels first in the limit of zero spin–orbit perturbation. Spin–orbit interaction becomes more important in the analysis of the intercombination bands and may become important in the interpretation of the spectra of high-spin cobalt(III) and iron(II), and of both high-spin and low-spin manganese(III) compounds. It is definitely necessary to include spin–orbit perturbation in the study of any of the corresponding 4d and 5d transition-metal systems.

Theory

We chose to develop the theory in strong field representation, maintaining cubic orientation. Energy levels derived in strong field method more closely approximate to the actual experimental situtations, and cubic disposition is needed because the systems under consideration are only slightly deviated from cubic symmetry. This means that the axial component of the ligand field is added as a minor perturbation to the strong field cubic energy levels. Thus, the energy levels of this report are applicable to the study of the substituted octahedral and five coordinate square pyramidal complexes (D_{4h} and C_{4v} symmetries) and slightly distorted cubic (octahedral, tetrahedral, and cubic) systems. Cubic parentage loses its significance if the distortion is large or in the limit of square planar geometry and hence energy levels derived in a representation which diagonalizes the total ligand field characterize systems of this type more closely. Derivation of energy levels in such a scheme had been carried out by Otsuka in the limit of zero spin–orbit perturbation.[5]

As pointed above, the zero order functions for carrying out tetragonal perturbation are the symmetry adapted strong field four-electron wave functions in cubic symmetry. These functions can be made symmetry adapted relative to quadrate symmetry by the decomposition that A_1^C, $E_a^C \rightarrow A_1^Q$; A_2^C, $E_b^C \rightarrow B_1^Q$; $T_{1a}^C \rightarrow A_2^Q$; $T_{2a}^C \rightarrow B_2^Q$; and

$T_{1b,c}{}^{C}$, $T_{2b,c}{}^{C} \rightarrow E_{a,b}{}^{Q}$. The procedure for constructing the cubic functions using parent functions of three, one, and two electrons has been described by Sugano, Tanabe, and Kamimura,[6,7] hence will not be detailed here. It is important to note that in order to utilize the matrix elements of Coulomb interaction given by these authors, it is necessary to maintain the phases prescribed by them for the base functions. The derived wave functions are listed in the Appendix.[8] We have used the notation that $(xy) = \zeta$, $(zx) = \eta$, $(yz) = \xi$, $(z^2) = \theta$, and $(x^2 - y^2) = \epsilon$. Only one component of the doubly degenerate E^Q representation is included in this listing for the spin singlets and spin triplets. The unlisted component in these cases can be obtained by the $C_3(z')$ symmetry operation.[2c] The $C_3(z')$ symmetry operation cyclically permutes ζ, η, and ξ, and mixes θ and ϵ as follows: $C_3(z')\theta = -(1/2)\theta - (\sqrt{3}/2)\epsilon$; and $C_3(z')\epsilon = -(1/2)\epsilon + (\sqrt{3}/2)\theta$. The wave functions of d^6 electronic configuration can be promptly derived from the d^4 functions by considering the four electrons as holes.

The ligand field perturbation has been carried out with the set of Dq, Dt, and Ds parameters.[2a] In this scheme of parameters, Dq retains exactly the same definition as in the cubic case while Dt and Ds parameters describe the addend axial component of the ligand field. Although these parameters are defined on the basis of tetragonal ligand field potential, they can still be treated as symmetry based parameters as shown previously.[2,3] It should be noted that in an alternate scheme of generalized symmetry parameters which can be developed by insisting that the center of gravity be maintained among the split tetragonal levels, the definition of Dq cannot be same as in the cubic case.[5] With our set of ligand field parameters, the nonzero one-electron matrix elements in strong field representation become $\langle\epsilon|\epsilon\rangle = 6Dq - 2Ds + Dt$, $\langle\theta|\theta\rangle = 6Dq + 2Ds + 6Dt$, $\langle\zeta|\zeta\rangle = -4Dq - 2Ds + Dt$, and $\langle\eta|\eta\rangle = \langle\xi|\xi\rangle = -4Dq + Ds - 4Dt$. The resulting energy matrices including coulombic repulsion matrix elements are given in Table I.[8] We have also calculated the matrix elements of the Coulomb interaction directly using the wave functions of the Appendix and verified those of Sugano, Tanabe, and Kamimura.[6a,9] The corresponding energy matrices of d^6 electronic configuration can be obtained by simply reversing the sign of Dq, Dt, and Ds parameters and adding a constant $(9A - 14B + 7C)$ term to all diagonal elements of the given matrices. The common $[n(n-1)/2]A$, where n is of d^n, *i.e.*, $6A$ for d^4 has been omitted in the diagonal elements of the matrices of Table I.

Results

Let us consider spin-allowed transitions in the tetragonally distorted or substituted octahedral systems. In the case of high-spin d^4, all are of quintet–quintet transitions. The energies of quintet levels, including configuration interaction, are simply the one-electron energies with signs of Dq, Dt, and Ds reversed since high-spin d^4 is equivalent to one hole in the d orbitals. Ground state can be $^5B_1$ or $^5A_1$ depending upon whether $(4Ds + 5Dt)$ is negative or positive. (See also Figure 1.) The other two excited states are $^5B_2$ and ^5E. Thus, three spin-allowed transitions are expected.[10,11] In the case of low-spin d^4 systems, the spin-allowed transitions are of triplet–triplet type. The ground state can be either the $^3A_2$ or ^3E component of $^3T_1{}^C(t_2{}^4)$ depending upon whether $(3Ds - 5Dt)$ is positive or negative. Thus, the condition for magnetic cross over which is simple in the case of octahedral systems (namely, change in ground state from high spin to low spin takes place if $10Dq > (6B + 5C)$) becomes complicated in the corresponding tetragonal systems, because of the alternate possibility for the ground state for both high-spin and low-spin complexes.[12] If $^5A_1$ is the ground state of high-spin system, magnetic cross over takes place to $^3A_2$ if $10Dq > (6B + 5C)$ or to ^3E if $(10Dq - 3Ds + 5Dt) > (6B + 5C)$. On the other hand, if $^5B_1$ is the ground state of spin-free system, magnetic cross over takes place to $^3A_2$ if $(10Dq + 4Ds + 5Dt) > (6B + 5C)$ or to ^3E if $(10Dq + Ds + 10Dt) > (6B + 5C)$. Low-spin d^4 systems will have a number of triplet excited levels arising from $(t_2{}^3e)$ configuration resulting in a number of spin-allowed triplet–triplet transitions the positions of which are greatly affected by configuration interaction. This situation is expected in the case of cubic systems also.[13]

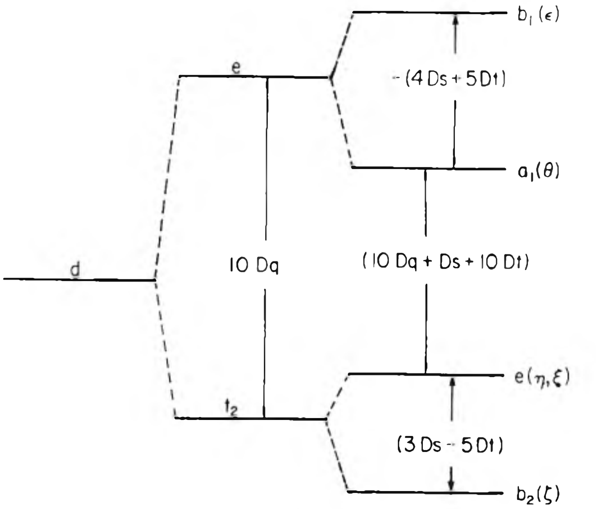

Figure 1. Tetragonal splittings of one-electron cubic t_2 and e levels.

High-spin d^6 complexes are similar to the high-spin d^4 systems in that once again the spin-allowed transitions are among the quintet levels. The energy levels here are reversed and the ground state is either $^5B_2$ or ^5E depending upon whether $(3Ds - 5Dt)$ is positive or negative. (See also Figure 1.) The other two excited states are $^5A_1$ and $^5B_1$. Thus, once again three spin-allowed transitions are expected.[11] The energies of these quintets are just the one-electron energies, including configuration interaction. Singlet, $^1A_1{}^Q[^1A_1{}^C(t_2{}^6)]$, is the ground state in the case of low-spin d^6. The magnetic cross over in octahedral systems takes place when $20Dq > (5B + 8C)$. The condition for magnetic cross over when the ligand field is tetragonal[12] depends on whether $^5B_2$ or ^5E is the ground state in spin-free system. If $^5B_2$ is the ground state, cross over occurs when $(20Dq - 2Ds + 15Dt) > (5B + 8C)$. Change in ground state from ^5E to $^1A_1$ takes place if $(20Dq + Ds + 10Dt) > (5B + 8C)$. Although there are a number of singlet excited states for spin-allowed transitions to occur in low-spin d^6, usually, only the singlets arising from the first excited $(t_2{}^5e)$ configuration are uncovered in the spectra of Co(III) complexes. This configuration in octahedral symmetry gives rise to two spin singlets, $^1T_1$ and $^1T_2$, which are expected to split in tetragonal systems into $^1A_2$, ^1E and $^1B_2$, ^1E, respectively. The magnitude of these splittings, neglecting configuration interaction,[14] are $(^1A_2 - {}^1E) = -35Dt/4$ and $(^1B_2 - {}^1E) = (6Ds - 5Dt/4)$. As noted before, these splittings are exactly same as for the similar splitting of the two lowest energy quartets, $^4T_2$ and $^4T_1$, of d^3 configuration. Not only are the splittings same, but the actual differences between the en-

TABLE I:

d^4 Quadrate Energy Matrices

$^5A_1^Q\{^5E_a^C[t_2^3(^4A_2)e]\} = -21B - 6Dq - 2Ds - 6Dt$

$^5B_1^Q\{^5E_b^C[t_2^3(^4A_2)e]\} = -21B - 6Dq + 2Ds - Dt$

$^5B_2^Q\{^5T_{2a}^C[t_2^2(^3T_1)e^2(^3A_2)]\} = -21B + 4Dq + 2Ds - Dt$

$^5E_{a,b}^Q\{^5T_{2b,c}^C[t_2^2(^3T_1)e^2(^3A_2)]\} = -21B + 4Dq - Ds + 4Dt$

$^3A_1^Q$

$^3A_1^C[t_2^3(^2E)e]$	$^3E_a^C[t_2^3(^4A_2)e]$	$^3E_a^C[t_2^3(^2E)e]$	$^3E_a^C[t_2^2(^1E)e^2(^3A_2)]$
$-12B + 4C - 6Dq - 7Dt/2$	0	$-(4Ds + 5Dt)/2$	0
	$-13B + 4C - 6Dq - 2Ds - 6Dt$	$-4B$	0
		$-10B + 4C - 6Dq - 7Dt/2$	$-3\sqrt{2}B$
			$-11B + 4C + 4Dq + 2Ds - Dt$

$^3A_2^Q$

$^3T_{1a}^C(t_2^4)$	$^3T_{1a}^C[t_2^3(^2T_1)e]$	$^3T_{1a}^C[t_2^3(^2T_2)e]$	$^3T_{1a}^C[t_2^2(^3T_1)e^2(^1A_1)]$	$^3T_{1a}^C[t_2^2(^3T_1)e^2(^1E)]$	$^3T_{1a}^C[t_2^2(^1T_2)e^2(^3A_2)]$	$^3T_{1a}^C(t_2e^3)$
$-15B + 5C - 16Dq - 2Ds - 6Dt$	$\sqrt{6}B$	$3\sqrt{2}B$	$-\sqrt{2}(2B + C)$	$2\sqrt{2}B$	0	0
	$-11B + 4C - 6Dq + 2Ds - Dt$	$5\sqrt{3}B$	$\sqrt{3}B$	$-\sqrt{3}B$	$3B$	$\sqrt{6}B$
		$-3B + 6C - 6Dq - 2Ds - 6Dt$	$-3B$	$-3B$	$5\sqrt{3}B$	$\sqrt{2}(B + C)$
			$-B + 6C + 4Dq + 2Ds - Dt$	$-10B - (4Ds + 5Dt)$	0	$3\sqrt{2}B$
				$-9B + 4C + 4Dq + 2Ds - Dt$	$-2\sqrt{3}B$	$-3\sqrt{2}B$
					$-11B + 4C + 4Dq + 2Ds - Dt$	$\sqrt{6}B$
						$-16B + 5C + 14Dq + 14Dt$

$^3B_1^Q$

$^3A_2^C[t_2^3(^2E)e]$	$^3A_2^C[t_2^2(^1A_1)e^2(^3A_2)]$	$^3E_b^C[t_2^3(^4A_2)e]$	$^3E_b^C[t_2^3(^2E)e]$	$^3E_b^C[t_2^2(^1E)e^2(^3A_2)]$
$-8B + 4C - 6Dq - 7Dt/2$	$-12B$	0	$-(4Ds + 5Dt)/2$	0
	$-2B + 7C + 4Dq + 7Dt/3$	0	0	$2\sqrt{2}(3Ds - 5Dt)/3$
		$-13B + 4C - 6Dq + 2Ds - Dt$	$-4B$	0
			$-10B + 4C - 6Dq - 7Dt/2$	$-3\sqrt{2}B$
				$-11B + 4C + 4Dq - 2Ds + 17Dt/3$

$^1B_2^Q$

$^1T_{2a}^C(t_2^4)$	$^1T_{2a}^C[t_2^3(^2T_1)e]$	$^1T_{2a}^C[t_2^3(^2T_2)e]$	$^1T_{2a}^C[t_2^2(^3T_1)e^2(^3A_2)]$	$^1T_{2a}^C[t_2^2(^1T_2)e^2(^1E)]$	$^1T_{2a}^C[t_2^2(^1T_2)e^2(^1A_1)]$	$^1T_{2a}^C(t_2e^3)$
$-9B + 7C - 16Dq - 2Ds - 6Dt$	$-3\sqrt{2}B$	$5\sqrt{6}B$	0	$2\sqrt{2}B$	$-\sqrt{2}(2B + C)$	0
	$-9B + 6C - 6Dq - 2Ds - 6Dt$	$-5\sqrt{3}B$	$3B$	$-3B$	$-3B$	$-\sqrt{6}B$
		$3B + 8C - 6Dq + 2Ds - Dt$	$-3\sqrt{3}B$	$5\sqrt{3}B$	$-5\sqrt{3}B$	$\sqrt{2}(3B + C)$
			$-9B + 6C + 4Dq + 2Ds - Dt$	$-6B$	0	$-3\sqrt{6}B$
				$-3B + 6C + 4Dq + 2Ds - Dt$	$-10B - (4Ds + 5Dt)$	$\sqrt{6}B$
					$5B + 8C + 4Dq + 2Ds - Dt$	$\sqrt{6}B$
						$7C + 14Dq - 4Ds + 9Dt$

$^1E^Q$

$^1T_1^C[t_2^3(^2T_1)e]$	$^1T_1^C[t_2^3(^2T_2)e]$	$^1T_1^C[t_2^2(^1T_2)e^2(^1E)]$	$^1T_1^C(t_2e^3)$	$^1T_2^C(t_2^4)$	$^1T_2^C[t_2^3(^2T_1)e]$	$^1T_2^C[t_2^3(^2T_2)e]$	$^1T_2^C[t_2^2(^3T_1)e^2(^3A_2)]$	$^1T_2^C[t_2^2(^1T_2)e^2(^1E)]$	$^1T_2^C[t_2^2(^1T_2)e^2(^1A_1)]$	$^1T_2^C(t_2e^3)$
$-3B + 6C - 6Dq - Ds - 19Dt/4$	$5\sqrt{3}B$	$3B$	$\sqrt{6}B$	0	$\sqrt{3}(4Ds + 5Dt)/4$	$-(3Ds - 5Dt)$	0	0	0	0
	$-3B + 8C - 6Dq + Ds - 9Dt/4$	$-5\sqrt{3}B$	$\sqrt{2}(B + C)$	0	$(3Ds - 5Dt)$	$-\sqrt{3}(4Ds + 5Dt)/4$	0	0	0	0
		$-3B + 6C + 4Dq - Ds + 4Dt$	$-\sqrt{6}B$	0	0	0	0	0	$-\sqrt{3}(4Ds + 5Dt)/2$	0
			$-16B + 7C + 14Dq + 21Dt/4$	0	0	0	0	0	0	$\sqrt{3}(4Ds + 5Dt)/4$
				$-9B + 7C - 16Dq + Ds - 11Dt$	$-3\sqrt{2}B$	$5\sqrt{6}B$	0	$2\sqrt{2}B$	$-\sqrt{2}(2B + C)$	0
					$-9B + 6C - 6Dq + Ds - 9Dt/4$	$-5\sqrt{3}B$	$3B$	$-3B$	$-3B$	$-\sqrt{6}B$
						$3B + 8C - 6Dq - Ds - 19Dt/4$	$-3\sqrt{3}B$	$5\sqrt{3}B$	$-5\sqrt{3}B$	$\sqrt{2}(3B + C)$
							$-9B + 6C + 4Dq - Ds + 4Dt$	$-6B$	0	$-3\sqrt{6}B$
								$-3B + 6C + 4Dq - Ds + 4Dt$	$-10B + (4Ds + 5Dt)/2$	$\sqrt{6}B$
									$5B + 8C + 4Dq - Ds + 4Dt$	$\sqrt{6}B$
										$7C + 14Dq + 2Ds + 31Dt/4$

$^1A_1^Q$

$^1A_1^C(t_2^4)$	$^1A_1^C[t_2^3(^2E)e]$	$^1A_1^C[t_2^2(^1A_1)e^2(^1A_1)]$	$^1A_1^C[t_2^2(^1E)e^2(^1E)]$	$^1A_1^C(e^4)$	$^1E_a^C(t_2^4)$	$^1E_a^C[t_2^3(^2E)e]$	$^1E_a^C[t_2^2(^1E)e^2(^1A_1)]$	$^1E_a^C[t_2^2(^1A_1)e^2(^1E)]$	$^1E_a^C[t_2^2(^1E)e^2(^1E)]$
$10C - 16Dq - 28Dt/3$	$-12\sqrt{2}B$	$2\sqrt{2}(2B + C)$	$2\sqrt{2}B$	0	$2\sqrt{2}(3Ds - 5Dt)/3$	0	0	0	0
	$6C - 6Dq - 7Dt/2$	$-12B$	$-6B$	0	0	$-(4Ds + 5Dt)/2$	0	0	0
		$14B + 11C + 4Dq + 7Dt/3$	$20B$	$\sqrt{6}(2B + C)$	0	0	$-2\sqrt{2}(3Ds - 5Dt)/3$	$-(4Ds + 5Dt)$	0
			$-3B + 6C + 4Dq + 7Dt/3$	$2\sqrt{6}B$	0	0	$-(4Ds + 5Dt)/\sqrt{2}$	$-2(3Ds - 5Dt)/3$	$2(3Ds - 5Dt)/3$
				$-16B + 8C + 24Dq + 14Dt$	0	0	0	0	0
					$-9B + 7C - 16Dq + 2Ds - 38Dt/3$	$-6B$	$-\sqrt{2}(2B + C)$	$2B$	$4B$
						$-6B + 6C - 6Dq - 7Dt/2$	$-3\sqrt{2}B$	$-12B$	0
							$5B + 8C + 4Dq - 2Ds + 17Dt/3$	$10\sqrt{2}B$	$-10\sqrt{2}B + (4Ds + 5Dt)/\sqrt{2}$
								$6B + 9C + 4Dq + 7Dt/3$	$2(3Ds - 5Dt)/3$
									$-3B + 6C + 4Dq + 7Dt/3$

${}^3E^Q$

${}^3T_1^C(t_2^4)$	${}^3T_1^C[t_2^3({}^2T_1)e]$	${}^3T_1^C[t_2^3({}^2T_2)e]$	${}^3T_1^C[t_2^2({}^3T_1)e^2({}^1A_1)]$	${}^3T_1^C[t_2^2({}^3T_1)e^2({}^1E)]$	${}^3T_1^C[t_2^2({}^1T_2)e^2({}^3A_2)]$
$-15B + 5C - 16Dq + Ds - 11Dt$	$\sqrt{6}B$	$3\sqrt{2}B$	$-\sqrt{2}(2B + C)$	$2\sqrt{2}B$	0
	$-11B + 4C - 6Dq - Ds - 19Dt/4$	$5\sqrt{3}B$	$\sqrt{3}B$	$-\sqrt{3}B$	$3B$
		$-3B + 6C - 6Dq + Ds - 9Dt/4$	$-3B$	$-3B$	$5\sqrt{3}B$
			$-B + 6C + 4Dq - Ds + 4Dt$	$-10B + (4Ds + 5Dt)/2$	0
				$-9B + 4C + 4Dq - Ds + 4Dt$	$-2\sqrt{3}B$
					$-11B + 4C + 4Dq - Ds + 4Dt$

${}^3T_1^C(t_2e^3)$	${}^3T_2^C[t_2^3({}^2T_1)e]$	${}^3T_2^C[t_2^3({}^2T_2)e]$	${}^3T_2^C[t_2^2({}^3T_1)e^2({}^3A_2)]$	${}^3T_2^C[t_2^2({}^3T_1)e^2({}^1E)]$	${}^3T_2^C(t_2e^3)$
0	0	0	0	0	0
$\sqrt{6}B$	$\sqrt{3}(4Ds + 5Dt)/4$	$-(3Ds - 5Dt)$	0	0	0
$\sqrt{2}(B + C)$	$(3Ds - 5Dt)$	$-\sqrt{3}(4Ds + 5Dt)/4$	0	0	0
$3\sqrt{2}B$	0	0	0	$\sqrt{3}(4Ds + 5Dt)/2$	0
$-3\sqrt{2}B$	0	0	0	0	0
$\sqrt{6}B$	0	0	0	0	0
$-16B + 5C + 14Dq + 21Dt/4$	0	0	0	0	$\sqrt{3}(4Ds + 5Dt)/4$
	$-9B + 4C - 6Dq + Ds - 9Dt/4$	$-5\sqrt{3}B$	$\sqrt{6}B$	$\sqrt{3}B$	$-\sqrt{6}B$
		$-5B + 6C - 6Dq - Ds - 19Dt/4$	$-3\sqrt{2}B$	$3B$	$\sqrt{2}(3B + C)$
			$-13B + 4C + 4Dq - Ds + 4Dt$	$-2\sqrt{2}B$	$-6B$
				$-9B + 4C + 4Dq - Ds + 4Dt$	$3\sqrt{2}B$
					$-8B + 5C + 14Dq + 2Ds + 31Dt/4$

${}^3B_2^Q$

${}^3T_{2a}^C[t_2^3({}^2T_1)e]$	${}^3T_{2a}^C[t_2^3({}^2T_2)e]$	${}^3T_{2a}^C[t_2^2({}^3T_1)e^2({}^3A_2)]$
$-9B + 4C - 6Dq - 2Ds - 6Dt$	$-5\sqrt{3}B$	$\sqrt{6}B$
	$-5B + 6C - 6Dq + 2Ds - Dt$	$-3\sqrt{2}B$
		$-13B + 4C + 4Dq + 2Ds - Dt$

${}^3T_{2a}^C[t_2^2({}^3T_1)e^2({}^1E)]$	${}^3T_{2a}^C(t_2e^3)$
$\sqrt{3}B$	$-\sqrt{6}B$
$3B$	$\sqrt{2}(3B + C)$
$-2\sqrt{2}B$	$-6B$
$-9B + 4C + 4Dq + 2Ds - Dt$	$3\sqrt{2}B$
	$-8B + 5C + 14Dq - 4Ds + 9Dt$

${}^1B_1^Q$

${}^1A_2^C[t_2^3({}^2E)e]$	${}^1A_2^C[t_2^2({}^1E)e^2({}^1E)]$	${}^1E_b^C(t_2^4)$	${}^1E_b^C[t_2^3({}^2E)e]$
$-12B + 6C - 6Dq - 7Dt/2$	$6B$	0	$-(4Ds + 5Dt)/2$
	$-3B + 6C + 4Dq + 7Dt/3$	0	0
		$-9B + 7C - 16Dq - 2Ds - 6Dt$	$-6B$
			$-6B + 6C - 6Dq - 7Dt/2$

${}^1E_b^C[t_2^2({}^1E)e^2({}^1A_1)]$	${}^1E_b^C[t_2^2({}^1A_1)e^2({}^1E)]$	${}^1E_b^C[t_2^2({}^1E)e^2({}^1E)]$
0	0	0
$(4Ds + 5Dt)/\sqrt{2}$	$-2(3Ds - 5Dt)/3$	$-2(3Ds - 5Dt)/3$
$-\sqrt{2}(2B + C)$	$2B$	$4B$
$-3\sqrt{2}B$	$-12B$	0
$5B + 8C + 4Dq + 2Ds - Dt$	$10\sqrt{2}B$	$-10\sqrt{2}B - (4Ds + 5Dt)/\sqrt{2}$
	$6B + 9C + 4Dq + 7Dt/3$	$-2(3Ds - 5Dt)/3$
		$-3B + 6C + 4Dq + 7Dt/3$

${}^1A_2^Q$

${}^1T_{1a}^C[t_2^3({}^2T_1)e]$	${}^1T_{1a}^C[t_2^3({}^2T_2)e]$	${}^1T_{1a}^C[t_2^2({}^1T_2)e^2({}^1E)]$	${}^1T_{1a}^C(t_2e^3)$
$-3B + 6C - 6Dq + 2Ds - Dt$	$5\sqrt{3}B$	$3B$	$\sqrt{6}B$
	$-3B + 8C - 6Dq - 2Ds - 6Dt$	$-5\sqrt{3}B$	$\sqrt{2}(B + C)$
		$-3B + 6C + 4Dq + 2Ds - Dt$	$-\sqrt{6}B$
			$-16B + 7C + 14Dq + 14Dt$

ergy of a cubic band and each of its tetragonal components are same in d^3 and d^6 systems. This means that the spectral fitting procedure[2a,b,3] used in the case of d^3 tetragonal systems applies to d^6 tetragonal systems also. It is interesting to note that the two lowest energy spin-forbidden transitions, ${}^3T_1$ and ${}^3T_2$ of $t_2{}^5e$, in d^6 systems are also predicted to give rise to the same amount of tetragonal splittings. Thus, the energy differences, $({}^3A_2 - {}^3E)$ and $({}^3B_2 - {}^3E)$, respectively, are given by $-35Dt/4$ and $(6Ds - 5Dt/4)$, excluding configuration interaction.

Finally, applications to distorted tetrahedral systems are similar. Thus, the conclusions arrived at in the case of high-spin octahedral d^4 and d^6 systems apply equally to tetrahedral d^6 and d^4, respectively. The actual parameters, of course, will differ.

Supplementary and Miniprint Material Available. An Appendix containing quadrate wave functions will appear following these pages in the microfilm edition of this volume of the journal. Photocopies of the supplementary material and full-sized photocopies of the miniprint material (Table I) from this paper only or microfiche (105 × 148 mm, 24× reduction, negatives) containing all of the supplementary material for the papers in this issue may be obtained from the Journals Department, American Chemical Society, 1155 16th St., N.W., Washington, D. C. 20036. Remit check or money order for \$4.00 for photocopy or \$2.00 for microfiche, referring to code number JPC-74-2678.

References and Notes

(1) J. P. Dahl and C. J. Ballhausen, *Advan. Quantum. Chem.*, **4,** 170 (1968).

(2) (a) J. R. Perumareddi, *J. Phys. Chem.*, **71,** 3144, 3155 (1967); (b) J. R. Perumareddi, *Coord. Chem. Pev.*, **4,** 73 (1969); (c) J. R. Perumareddi, *J. Phys. Chem.*, **76,** 3401 (1972); (d) *Z. Naturforsch. A*, **27,** 1820 (1972); (e) J. S. Merriam and J. R. Perumareddi, Abstracts, Inorganic Division, presented at the 166th National Meeting of the American Chemical Society, Chicago, Ill., Aug 26–31, 1973; to be submitted for publication.

(3) (a) R. K. Lowry, Jr., and J. R. Perumareddi, *J. Phys. Chem.*, **74,** 1371 (1970); (b) L. Dubicki and R. L. Martin, *Aust. J. Chem.*, **22,** 839 (1969); (c) L. Dubicki and P. Day, *Inorg. Chem.*, **10,** 2043 (1971); (d) R. L. Klein, Jr., N. C. Miller, and J. R. Perumareddi, *Inorg. Chim. Acta*, **7,** 685 (1973).

(4) N. S. Hush and R. J. M. Hobbs, "Progress in Inorganic Chemistry," Vol. 10, F. A. Cotton, Ed., Interscience, New York, N.Y., 1968.

(5) (a) J. Otsuka, *J. Phys. Soc. Jap.*, **21,** 596 (1966); [errata, *ibid.*, **21,** 1229 (1966).] Otsuka's *X, Y, Z* parameters are related to our *Dq, Dt,* and *Ds* parameters by the expressions: $X = 10Dq + 35Dt/6$, $Y = -2Ds - 5Dt/2$, and $Z = 2Ds - 10Dt/3$; *cf.* (b) J. R. Perumareddi, *Phys. Stat. Solidi. B*, **59,** K127 (1973).

(6) (a) S. Sugano, Y. Tanabe, and H. Kamimura, "Multiplets of Transition-Metal Ions in Crystals," Academic Press, New York, N.Y., 1970; (b) see also, J. S. Griffith, "The Theory of Transition-Metal Ions," Cambridge University Press, New York, N.Y., 1961.

(7) A knowledge of the cubic two- and three-electron wave functions facilitates the process of building four-electron functions. The complete set of two- and three-electron cubic functions can be found in ref 2a–c and also in ref 6a. References 2a and b contain two misprints. In the notation of the present paper the ${}^2B_1^Q$ of ${}^2A_{2g}{}^C[t_{2g}{}^2({}^1E_g)e_g]$ should be $(1/\sqrt{2})\{(1/\sqrt{6})[-2|\zeta\bar{\zeta}\epsilon| + |\eta\bar{\eta}\epsilon| + |\xi\bar{\xi}\epsilon|] - (1/\sqrt{2})[|\eta\bar{\eta}\theta| - |\xi\bar{\xi}\theta|]\}$, and ${}^2E_b{}^Q$ of ${}^2T_{1g}{}^C[t_{2g}e_g{}^2({}^1E_g)]$ should be $(1/\sqrt{2})\{(1/2)[|\xi\theta\bar{\epsilon}| - |\xi\bar{\theta}\epsilon|] + (\sqrt{3}/2)[|\xi\epsilon\bar{\epsilon}| - |\xi\theta\bar{\theta}|]\}$. The two-electron functions given in ref 2c are spin adapted also. The required functions in coordinate space only are obvious. It should also be noted that the phases of base functions of ref 2 differ from those of ref 6.

(8) See paragraph at end of text regarding supplementary material.

(9) We noted a misprint in the $^3T_2$ electrostatic matrix of Sugano, Tanabe, and Kamimura (ref 6a). The $\langle t_2^3(^2T_1)e\,^3T_2\|t_2e^3\,^3T_2\rangle$ matrix element should be $-\sqrt{6}B$. It is correctly listed in an earlier paper of Tanabe and Sugano, *J. Phys. Soc. Jap.*, **9**, 753 (1954).

(10) E. W. Baker and J. R. Perumareddi, *Z. Naturforsch. B*, **25**, 912 (1970).

(11) Actually, if the tetragonal component of the ligand field is small, the one spin-allowed band of the parent octahedral complex is expected to split into two components and an additional spin-allowed band from the splitting of the octahedral ground state is expected to appear in the infrared region of the electronic spectrum.

(12) (a) The conditions for magnetic cross over given in this section are excluding configurational interaction effects. The exact conditions in all the cases will be affected by an amount of energy equal to the configuration interaction energy experienced by the low-spin state. (b) The following discussion on change in the ground states assumes that the axial component of the tetragonal ligand field is small. If the axial ligand field is large, it is possible for a singlet to become the ground state for d^4 systems and similarly for a triplet to become the ground state for d^6 systems (*cf.* Figure 1).

(13) J. R. Perumareddi and A. D. Liehr, Abstracts, Symposium on Molecular Structure and Spectroscopy, Ohio State University, Columbus, Ohio, June 1964.

(14) (a) These splittings using diagonal elements only were first derived and employed in the analysis of the spectra of tetragonal Co(III) complexes by W. Moffitt and C.J. Ballhausen, *J. Inorg. Nucl. Chem.*, **3**, 178 (1956). (b) Based on these diagonal elements and including configuration interaction qualitatively, a further attempt at interpreting the tetragonal band splittings in Co(III) complexes was made by R. A. D. Wentworth and T. S. Piper, *Inorg. Chem.*, **4**, 709 (1965). (c) The semiempirical molecular orbital treatment of these same systems was given by H. Yamatera, *Bull. Chem. Soc. Jap.*, **31**, 95 (1958).

Approximate Molecular Orbital Study of Organic Positron and Positronium Complexes

W. J. Madia, J. C. Schug, A. L. Nichols, and H. J. Ache*

Department of Chemistry, Virginia Polytechnic Institute and State University, Blacksburg, Virginia 24061 *(Received June 19, 1974)*

A study has been made to determine the possibility for the existence of positron and positronium complexes with a selected number of organic molecules. The CNDO/2 approximation is used for all electronic integrals and for electron–positron Coulomb integrals. The core Hamiltonian matrix elements for the positron were estimated by combining the Wolfsberg–Helmholtz and Cusachs–Cusachs approximations. This approach shows that the positron should become bound to the molecules; using the same criteria the formation of stable positronium complexes is more improbable. The calculated binding energies are strongly dependent on the value of the Wolfsberg–Helmholtz proportionality constant for positrons.

Introduction

Experimental observations on the rates of two-photon positron (e^+) annihilation and on the attendant angular correlation curves for the γ photons have led a number of investigators to postulate the existence of stable positron complexes with atoms, ions, and molecules.[1-7] Theoretical calculations of the stability of e^+ complexes with atoms and atomic ions, and of the positron lifetimes in these complexes, have generally been rewarding.[3,8-11] The most extensive theoretical work in this area has been done by Schrader and coworkers: a 1970 paper[12] provides a general nonrelativistic self-consistent-field theory of one-positron, many-electron systems and explains the approximations involved in most of the earlier work; a more recent paper describes a variational treatment of e^+H^- which incorporates interparticle coordinates in the wave function.[11] The most accurate result of Navin, Schrader, and Lebeda[11] indicates that e^+H^- is 0.794 eV more stable than separated positronium and hydrogen atoms. This means that the positron binding energy (positron affinity) of the hydride ion is of the order of 6.8 eV. Earlier calculations indicated positron affinities of the order of 2 eV for Cl^- and alkali atoms.[3,9]

This paper is concerned with the existence of e^+ complexes with relatively large organic compounds. For large compounds, containing many electrons, a variational treatment similar to that[11] for e^+H^- is presently intractable, and it is necessary to retreat to some form of the self-consistent-field theory.[12] We take the natural approach of employing the Born–Oppenheimer separation and the Hartree–Fock approximation. The former implies that we treat the nuclei as fixed point charges, and the latter, that we treat the positron on an equal basis with the electrons, calculating only average coulombic interactions between all light particles. In general this approach should give reasonable results. The necessary corrections for more accurate calculations will arise from short-range interparticle potentials, and should be amenable to treatment by an extension of Sinanoglu's theory of purely electronic correlation effects.[13] The positron–electron correlation effects are expected to be extremely important in the prediction of e^+ annihilation rates, so we have not tried to calculate these; we are concerned here only with the stability of the e^+ complexes.

We make use of the approximate all-valence-electron self-consistent-field theory developed by Pople and coworkers,[14] the so-called CNDO/2 approximation. We seek positronic and electronic molecular orbitals and express both as linear combinations of the same set of Slater-type atomic orbitals.[14,15] This has the advantage of providing a basis for estimating the necessary integrals over positron coordinates without a great deal of computation. For all electronic matrix elements, the CNDO/2 approximations and the parametrization suggested by Pople and Beveridge were retained. The positronic matrix elements of the core Hamiltonian were estimated by comparison with the corresponding electronic integrals. The latter were approximately decomposed into kinetic and potential energy parts using the virial theorem. A sign change of the potential part provided the approximation for the one-center positron matrix elements. For the two-center core matrix elements, these considerations were combined with the Wolfsberg–Helmholtz approximation[16] and the formulation given by Cusachs and Cusachs.[17] All Coulomb integrals were evaluated using the CNDO/2 approximations, but accounting of course for the positive charge of the positron. It is recognized that these procedures only provide first approximations. In particular, the virial theorem is not strictly applicable to the electronic integrals involving Slater-type orbitals, and the Slater-type orbitals provide improper cusp behavior for the positron wave functions. Such shortcomings will have to be remedied in future work.

This paper deals primarily with e^+ complexes with closed shell molecules. By making use also of the lowest unoccupied electronic molecular orbital, we obtain a first approximation for the binding energies of e^+ complexes with molecular anions. (These are alternatively referred to as positronium–molecule complexes.) Our general conclusions are that *both types* of complexes, e^+M and e^+M^-, are probably stable, and therefore future, more accurate, work is certainly warranted.

Hartree–Fock Theory

The total Hamiltonian, in atomic units, for a one-positron $2n$- electron system is given by

$$\mathcal{H} = \sum_{\mu} h_{\mu}^{\text{core}(-)} + \sum_{\mu<\nu} g_{\mu\nu} + h_p^{\text{core}(+)} + \sum_{\mu} g_{\mu p} \qquad (1)$$

where (using atomic units)

$$h_{\mu}^{\text{core}(-)} = -\nabla_{\mu}^2/2 - \sum_{\alpha} Z_{\alpha}/r_{\mu\alpha}$$

$$h_p^{\text{core}(+)} = -\nabla_p^2/2 + \sum_{\alpha} Z_{\alpha}/r_{p\alpha}$$

$$g_{\mu\nu} = r_{\mu\nu}^{-1}$$

$$g_{\mu p} = -r_{\mu p}^{-1}$$

The subscripts μ and ν are used to indicate electron terms, p indicates positron terms, and α refers to nuclei. The superscripts $(-)$ and $(+)$ will be used with electron and positron terms, respectively, for clarity. The core Hamiltonian terms include the kinetic energies and coulombic interactions with all nuclei of the molecule. For a system containing $2n$ electrons, and one positron, the wave function is

$$\psi = \psi_p(p)[(2n)!]^{-1/2}\det|\psi_1(1)\psi_2(2)\ldots\psi_{2n}(2n)| \qquad (2)$$

where each function, ψ_i, is a product of a molecular orbital, ϕ_i, and a spin wave function, either α or β. The positron spin is arbitrary. Since we are dealing with a closed-shell electronic system, each occupied electronic orbital occurs twice, being associated once with spin function α and once with β. We make the usual assumptions of orthonormality

$$\langle\phi_p|\phi_p\rangle = 1;\ \langle\phi_i|\phi_j\rangle = \delta_{ij} \qquad (3)$$

The energy expectation value is

$$E = \langle\psi|H|\psi\rangle = \langle\psi|\sum_{\mu}^{2n} h_{\mu}^{\text{core}(-)}|\psi\rangle + \langle\psi|\sum_{\mu<\nu}^{2n} g_{\mu\nu}|\psi\rangle + \langle\psi|h_p^{\text{core}(+)}|\psi\rangle + \langle\psi|\sum_{\mu}^{2n} g_{\mu p}|\psi\rangle \qquad (4)$$

Using the fact that the electronic part of ψ consists of n doubly occupied orbitals, this can be written in terms of summations over those molecular orbitals

$$E = 2\sum_{i}^{n} H_{ii}^{(-)} + 2\sum_{i<j}^{n}(2J_{ij}^{(-)} - K_{ij}^{(-)}) + H_{pp}^{(+)} + 2\sum_{i}^{n} J_{pi}^{(+-)} \qquad (5)$$

Here, $H_{pp}^{(+)}$ and $J_{pi}^{(+-)}$ are respectively the positron–core and positron–electron contributions

$$H_{pp}^{(+)} = \langle\phi_p|h_p^{\text{core}(+)}|\phi_p\rangle \qquad (6)$$

$$J_{pi}^{(+-)} = -\langle\phi_p(p)\phi_i(i)|r_{ip}^{-1}|\phi_p(p)\phi_i(i)\rangle \qquad (7)$$

and $H_{ii}^{(-)}$, $J_{ij}^{(-)}$, and $K_{ij}^{(-)}$ are the purely electronic core interactions, Coulomb and exchange integrals involving the molecular orbitals indicated by the subscripts. The molecular orbitals are expanded as linear combinations of the atomic valence-shell orbitals $\{\chi_{\mu}\}$

$$\phi_i = \sum_{\mu}^{m}\chi_{\mu}C_{\mu i} \qquad \phi_p = \sum_{\mu}^{m}\chi_{\mu}C_{\mu p} \qquad (8)$$

If we introduce charge-density and bond-order matrices for both electrons and the positron

$$P_{\mu\nu}^{(-)} = 2\sum_{i}^{n} C_{\mu i}^{*}C_{\nu i} \qquad P_{\mu\nu}^{(+)} = C_{\mu p}^{*}C_{\nu p} \qquad (9)$$

the energy can be written in terms of integrals over atomic orbitals

$$E = \sum_{\mu,\nu}^{m} P_{\mu\nu}^{(-)}H_{\mu\nu}^{(-)} + (1/2)\sum_{\mu,\nu,\lambda,\sigma}^{m} P_{\mu\nu}^{(-)}P_{\lambda\sigma}^{(-)}[\langle\chi_{\mu}(1)\chi_{\lambda}(2)|r_{12}^{-1}|\chi_{\nu}(1)\chi_{\sigma}(2)\rangle - (1/2)\langle\chi_{\mu}(1)\chi_{\lambda}(2)|r_{12}^{-1}|\chi_{\sigma}(1)\chi_{\nu}(2)\rangle] + \sum_{\mu,\nu}^{m} P_{\mu\nu}^{(+)}H_{\mu\nu}^{(+)} - \sum_{\mu,\nu,\lambda,\sigma}^{m} P_{\nu\sigma}^{(-)}P_{\nu\lambda}^{(+)}\langle\chi_{\mu}(p)\chi_{\nu}(1)|r_{1p}^{-1}|\chi_{\lambda}(p)\chi_{\sigma}(1)\rangle \qquad (10)$$

Again, the first two terms are identical with those arising in the simple closed shell electronic case,[14] and the latter two are caused by the positron

$$H_{\mu\nu}^{(+)} = \langle\chi_{\mu}(p)|h_p^{\text{core}(+)}|\chi_{\nu}(p)\rangle \qquad (11)$$

Minimizing the energy with respect to variations in the electronic and positronic orbitals leads to two sets of Hartree–Fock equations

$$\begin{aligned} F^{(-)}\phi_i &= \epsilon_i\phi_i \\ F^{(+)}\phi_p &= \epsilon_p\phi_p \end{aligned} \qquad (12)$$

where the electron and positron Fock operators are defined as

$$F^{(-)} = h^{\text{core}(-)} + \sum_{j}(2J_j^{(-)} - K_j^{(-)}) + J_p^{(+-)} \qquad (13)$$

and

$$F^{(+)} = h^{\text{core}(+)} + 2\sum_{j} J_j^{(+-)}$$

J_j and K_j are the usual electronic Coulomb and exchange operators associated with the jth molecular orbital; $J_p^{(+-)}$ is the positronic Coulomb operator

$$J_p^{(+-)}(\mathbf{r}_i) = -\int\phi_p^{*}(\mathbf{r}_p)[1/r_{ip}]\phi_p(\mathbf{r}_p)\,d\tau_p$$

and $J_j^{(+-)}$ is the operator providing the Coulomb potential seen by a positron due to an electron in the jth orbital

$$J_j^{(+-)}(\mathbf{r}_p) = -\int \phi_j^*(\mathbf{r}_i)[1/r_{ip}]\phi_j(\mathbf{r}_i)\, d\tau_i$$

For computational purposes, it is convenient to express the energy as

$$E = (1/2)\sum_{\mu,\nu} P_{\mu\nu}^{(-)}(H_{\mu\nu}^{(-)} + F_{\mu\nu}^{(-)}) + (1/2)\sum_{\mu,\nu} P_{\mu\nu}^{(+)}(H_{\mu\nu}^{(+)} + F_{\mu\nu}^{(+)}) \quad (14)$$

where all matrix elements are in the basis set of atomic orbitals. It should also be noted that in forming the wave function (2) from the self-consistent solutions to eq 12 we consistently employ the Aufbau principle. That is, the $2n$ electrons are put into the n lowest lying electronic orbitals, and the positron is assumed to occupy the positron orbital of lowest orbital energy, ϵ_p.

Approximations and Parametrization

By using the zero-differential overlap approximation, the multicentered interaction integrals are simplified so that

$$\langle\chi_\mu\chi_\nu|r_{12}^{-1}|\chi_\lambda\chi_\alpha\rangle = \langle\chi_\mu\chi_\nu|r_{12}^{-1}|\chi_\mu\chi_\nu\rangle\delta_{\mu\lambda}\delta_{\nu\alpha} = \gamma_{\mu\nu}\delta_{\mu\lambda}\delta_{\nu\alpha} \quad (15)$$

and the Fock matrix elements become

$$F_{\mu\mu}^{(+)} = H_{\mu\mu}^{(+)} - \sum_\lambda P_{\lambda\lambda}^{(-)}\gamma_{\mu\lambda}$$

$$F_{\mu\nu}^{(+)} = H_{\mu\nu}^{(+)} \quad (\mu \neq \nu)$$

$$F_{\mu\mu}^{(-)} = H_{\mu\mu}^{(-)} - (1/2)P_{\mu\mu}^{(-)}\gamma_{\mu\mu} + \sum_\lambda P_{\lambda\lambda}^{(-)}\gamma_{\mu\lambda} - \sum_\lambda P_{\lambda\lambda}^{(+)}\gamma_{\mu\lambda} \quad (16)$$

$$F_{\mu\nu}^{(-)} = H_{\mu\nu}^{(-)} - (1/2)P_{\mu\nu}^{(-)}\gamma_{\mu\nu} \quad (\mu \neq \nu)$$

One of the CNDO approximations is to reduce Coulomb integrals to one per atom pair, *i.e.*, $\gamma_{\mu\nu} = \gamma_{AB}$, where χ_μ is located on atom A and χ_ν on atom B.

It should be noted that the electron Fock matrix contains a contribution of the form, $-P_{\mu\nu}^{(-)}\gamma_{\mu\nu}/2$ and that this term is absent in the corresponding $F_{\mu\nu}^{(+)}$. This exchange term arises from the two-electron repulsions; since our system contains only one positron, this term does not appear in the positron matrix.

Equations 12 can now be solved by iterative techniques and the electron and positron wave functions can be obtained in which the electronic orbitals have been altered by the presence of the positron, and the positron orbital has been altered by the electrons.

The diagonal positron core matrix elements are approximated as

$$H_{\mu\mu}^{(+)} = U_{\mu\mu}^{(+)} + \sum_{B\neq A} Z_B\gamma_{AB} \quad (\chi_\mu \text{ on atom A}) \quad (17)$$

$U_{\mu\mu}^{(+)}$ is an atomic term containing the kinetic energy and potential energy of the positron in the field of the Ath core; the second term describes the positron interactions with the other atomic cores.

The CNDO/2 parameterization as described by Pople and Beveridge[15] is used for all electron terms. However, for the positron no data such as ionization potentials and positron affinities are available. In order to parametrize the positron Fock terms we relate them to the corresponding electronic integrals as follows. For kinetic energy (T) and potential energy (V) matrix elements

$$T_{\mu\nu}^{(+)} = T_{\mu\nu}^{(-)} \quad \text{and} \quad V_{\mu\nu}^{(+)} = -V_{\mu\nu}^{(-)} \quad (18)$$

so that

$$U_{\mu\mu}^{(+)} = T_{\mu\mu}^{(+)} + V_{\mu\mu}^{(+)} = T_{\mu\mu}^{(-)} - V_{\mu\mu}^{(-)} \quad (19)$$

Applying the virial theorem

$$T_{\mu\mu}^{(-)} = -(1/2)V_{\mu\mu}^{(-)} = -U_{\mu\mu}^{(-)} \quad (20)$$

we see that

$$U_{\mu\mu}^{(+)} = -3U_{\mu\mu}^{(-)} \quad (21)$$

Treatment of the off-diagonal core terms is not as direct. Because of the empirical nature of the bonding parameters, $\beta_{AB}^{0(-)}$, used by Pople and Beveridge, no direct conversion to $\beta_{AB}^{0(+)}$ was found. Therefore, we decided to combine the Wolfsberg–Helmholtz approximation[16] with the ideas of Cusachs and Cusachs.[17] For the electronic core Hamiltonian matrix, we have

$$H_{\mu\nu}^{(-)} = T_{\mu\nu}^{(-)} + V_{\mu\nu}^{(-)} \quad (22a)$$

$$\cong k^{(-)}S_{\mu\nu}(H_{\mu\mu}^{(-)} + H_{\nu\nu}^{(-)})/2 \quad (22b)$$

$$\cong S_{\mu\nu}(2 - |S_{\mu\nu}|)(H_{\mu\mu}^{(-)} + H_{\nu\nu}^{(-)})/2 \quad (22c)$$

The analogous expressions for the positron are

$$H_{\mu\nu}^{(+)} = T_{\mu\nu}^{(+)} + V_{\mu\nu}^{(+)} \quad (23a)$$

$$\cong k^{(+)}S_{\mu\nu}(H_{\mu\mu}^{(+)} + H_{\nu\nu}^{(+)})/2 \quad (23b)$$

The terms in eq 23a are now treated by the method of Cusachs and Cusachs

$$T_{\mu\nu}^{(+)} \cong S_{\mu\nu}|S_{\mu\nu}|(T_{\mu\mu}^{(+)} + T_{\nu\nu}^{(+)})/2$$

$$V_{\mu\nu}^{(+)} \cong S_{\mu\nu}(V_{\mu\mu}^{(+)} + V_{\nu\nu}^{(+)})/2$$

and substituting eq 18 into the analog of eq 19 yields

$$H_{\mu\mu}^{(+)} = (3/2)V_{\mu\mu}^{(+)} = 3T_{\mu\mu}^{(+)}$$

This gives directly

$$H_{\mu\nu}^{(+)} \cong (1/3)S_{\mu\nu}(2 + |S_{\mu\nu}|)(H_{\mu\mu}^{(+)} + H_{\nu\nu}^{(+)})/2 \quad (23c)$$

Values typically used[18] for the Wolfsberg–Helmholtz $k^{(-)}$ in eq 22b range from 1.75 to 2.0, and comparison with eq 22c shows that this corresponds to a range of $|S_{\mu\nu}|$ between 0 and 0.25. When these values are employed in eq 23c and the result equated to eq 23b, it appears that $k^{(+)}$ should be in the range ⅔ to ¾.

Our computer program was developed by modifying the CNDO program listed by Pople and Beveridge.[15] Along with the other approximations already described, we employed eq 23b for $H_{\mu\nu}^{(+)}$ and varied $k^{(+)}$ over the indicated range.

Results

Using this formalism, we have studied the stability of positron complexes of benzene and a number of substituted benzene derivatives. In the process of carrying out the iterations to self-consistency, two slight problems arose. A number of calculations, especially with the larger values of $k^{(+)}$, oscillated rather than converging directly to an energy minimum. The oscillations were successfully eliminated by taking the modified density matrices and averaging the new calculated matrices with the old ones on each iteration. Also, for some of the symmetric molecules, the symmetry

TABLE I: Positron and Positronium Binding Energies (au)[c]

	$k^{(+)} = {}^2/_3$				$k^{(+)} = {}^3/_4$			
Compound	$-\epsilon_p$	BE (e^+)	e^+ site[a]	BE (Ps)	$-\epsilon_p$	BE (e^+)	e^+ site[a]	BE (Ps)
Benzene	0.0082	0.0031	C–H	−0.2197	+0.2840	+0.2831	C–H	+0.0597
Toluene	0.1877	0.1427	α-C–H	−0.0608	+0.4717	+0.4270	α-C–H	+0.2225
Fluorobenzene	0.2083	0.1030	*p*-C–H	−0.0809[b]	+0.4426	+0.3451	*p*-C–H	+0.1582[b]
Aniline	0.3375	0.2736	N–H	+0.1184[b]	+0.6528	+0.5890	N–H	+0.4339[b]
Benzonitrile	0.0780	0.0371	*m*-C–H	−0.1726	+0.3671	+0.3194	C≡N	+0.1573
Benzaldehyde	0.2256	0.1234	Carbonyl C–H	−0.0002	+0.4686	+0.3757	Carbonyl C–H	+0.2533
Nitrobenzene	0.0608	0.0200	*m*-C–H	−0.1512	+0.4268	+0.3250	*p*-C–H	+0.1740
p-Benzoquinone	0.0213	0.0131	C–H	−0.0232	+0.3137	+0.3084	C–H	+0.2802

[a] Greater than 90% of the e^+ charge density occurs here. [b] LUMO of the positronium complex is a σ orbital; in all other cases it is a π orbital. [c] 1 au = 27.21 eV = 627.71 kcal/mol.

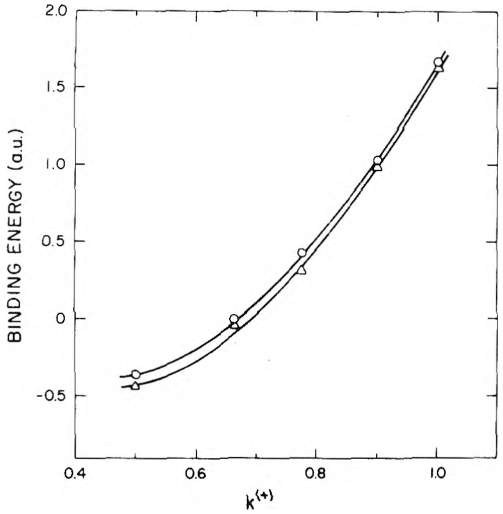

Figure 1. Variation in positron binding energy of nitrobenzene with $k^{(+)}$. Koopman's theorem estimate (O) and change in energy directly calculated using eq 14 (Δ) for complex.

TABLE II: Calculated Total Charge Densities for Aniline and Positron–Aniline Complex ($k^{(+)} = {}^3/_4$)

Atom	Charge density in molecule	Charge density in complex	
		Electron	Positron
N	5.214	5.342	0.194
H_N	0.939	1.041	0.399
C_{subst}	3.770	3.789	0.002
C_{ortho}	4.010	3.971	0.001
H_{ortho}	1.057	1.032	0.001
C_{meta}	3.912	3.897	0.000
H_{meta}	1.066	1.014	0.000
C_{para}	3.982	3.942	0.000
H_{para}	1.064	1.016	0.000

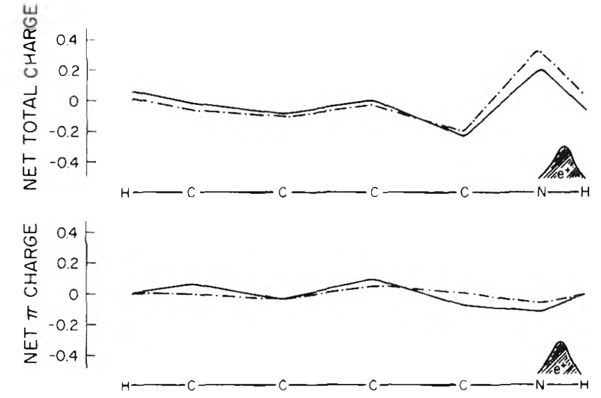

Figure 2. Profiles of electronic total charge and π charge for aniline, before (–) and after (– · –) positron addition. The position of the highest positron density (not to scale) is indicated in the N–H bond.

was lost during the iteration process. We believe that this resulted from round-off errors in the positron density matrix, where the elements are generally quite small. To eliminate the need for symmetry projection, we restricted our solutions to the symmetric cases by symmetrizing the molecular orbitals at each iteration.

The important results are listed in Table I for the two limiting values of $k^{(+)}$ mentioned previously. All calculations indicated that the positron should be bound by these molecules. Two approximations for the positron binding energies are given: ($-\epsilon_p$) is the negative of the positron orbital energy, and provides a Koopmans' theorem[19] estimate; the other entry (BE) was a direct calculation of the binding energy as the difference between the total energy of the neutral molecule and that of the positron–molecule complex. The two estimates are fairly comparable to one another, but the former is always of greater magnitude than the latter. The calculated positron binding energy depends critically on the value used for $k^{(+)}$. This is illustrated graphically in Figure 1, which shows the two estimates of the positron affinity of nitrobenzene as a function of $k^{(+)}$. Corresponding to this, the number of bound positronium orbitals also increased with $k^{(+)}$. For the majority of the complexes, we found one or two bound orbitals for $k^{(+)} = {}^2/_3$, and six to eight for $k^{(+)} = {}^3/_4$.

Also indicated in Table I are the locations of maximum positron density found for the several complexes. The positron was always found to be essentially localized in a single bond (or in equivalent bonds when this was required by symmetry). The position at which the positron was found varies widely through the series of molecules, and for some cases the positron's location was seen to change as $k^{(+)}$ was varied. We have not been able so far to reconcile these findings consistently with chemical intuition. For example, if the complex formation is considered to be an example of electrophilic attack, one might expect the positron to locate in the meta position of nitrobenzene. This was observed for $k^{(+)} = {}^2/_3$, but when $k^{(+)}$ was taken as ${}^3/_4$, the positron moved to the para position. Similar shifts were observed for benzonitrile, but for the larger $k^{(+)}$ the positron localized on the cyanide group. A number of additional points could be made, but at the present level of approximation extended discussion is probably not justified.

It is of some interest to note that the positron was always found to be most stable in a σ rather than a π molecular orbital. This is in fact expected if one looks at the positron's Fock matrix elements. In our approximations, all diagonal elements, $F_{\mu\mu}^{(+)}$, are positive, but the minimum values always occur for the hydrogen 1s orbitals. This situation could easily be expected to change if different approximations are employed.

Addition of the positron to a molecule is of course expected to cause some shifting of electronic charge density. As a typical case, we list in Table II the calculated total atomic charge densities for the aniline molecule and its positron complex. The atomic charge density is obtained by summing the diagonal elements of the electronic charge-density and bond-order matrix (see eq 9) over all the valence orbitals for each atom. The same data are shown graphically in slightly different form in Figure 2. This shows profiles of net π charge and net total charge before and after positron addition. The net total charge is the difference between the calculated charge density and the atomic core charge. The net π charge is the π-orbital density minus one. The figure is intended to show electron buildup at the various atoms; the numbers between the atoms are not meaningful. In all cases, the electron density is enhanced in the vicinity of the positron, as expected from the mutual attraction. The largest changes seen in the electron density upon positron addition were about 0.1 e, and most changes were appreciably less.

The positron densities listed in Table II illustrate the high degree of localization found for the positron as indicated earlier. In this case, more than 99% of the total positron density is located in the NH_2 group.

It is possible to estimate positronium binding energies for the molecules considered. This is done by considering the following cycle of processes, in which M denotes a neutral molecule, and Ps indicates the positronium atom (e^+e^-)

$$\begin{tikzcd}
\mathrm{Ps} + \mathrm{M} \arrow[r, "-\mathrm{BE}\ (\mathrm{Ps})"] \arrow[d, "6.8\ \mathrm{eV} ="', "0.25\ \mathrm{au}"] & \mathrm{PsM} \\
e^+ + e^- + \mathrm{M} \arrow[r, "-\mathrm{BE}\ (e^+)"'] & e^+\mathrm{M} + e^- \arrow[u, "-", "\mathrm{EA}\ (e^+\mathrm{M})"']
\end{tikzcd}$$

Thus, the positronium binding energy is approximately

$$\mathrm{BE}\ (\mathrm{Ps}) = \mathrm{BE}\ (e^+) + \mathrm{EA}\ (e^+\mathrm{M}) - 0.25\ \mathrm{au} \quad (24)$$

Here, BE (e^+) is the molecular positron affinity discussed earlier, EA (e^+M) is the electron affinity of the positron–molecule complex, obtained by Koopmans theorem from the orbital energy of the first unoccupied electronic orbital in the complex, and the last term is the dissociation energy of the ground state of the hydrogen-like positronium atom.[20] The values obtained from eq 24 are listed in Table I for each molecule.

These calculations do not unambiguously show whether these molecules form stable positronium complexes. For all but aniline, the PsM complex was found to be unstable with respect to dissociation to Ps + M when $k^{(+)} = 2/3$. But with $k^{(+)} = 3/4$, all positronium–molecule complexes were found to be stable. The fact that our calculated positronium binding energies range from small negative to small positive values is actually gratifying because recent experimental studies suggest[21,22] that the heats of complexation are negative and of the order of several kcal/mole.

Acknowledgment. This work was supported in part by the U. S. Atomic Energy Commission.

References and Notes

(1) V. I. Goldanskii, *At. Energy Rev.*, 6(**1**), 3 (1968).

(2) S. J. Tao and J. H. Green, *J. Chem. Soc. A*, 408 (1968).

(3) L. Simons, *Phys. Rev.*, **90**, 165 (1953).

(4) R. E. Green and R. E. Bell, *Can. J. Phys.*, **35**, 398 (1957).

(5) H. J. Horstman, *J. Inorg. Nucl. Chem.*, **27**, 1191 (1965).

(6) For general references see the following monographs and review article (a) J. Green and J. Lee, "Positronium Chemistry," Academic Press, New York, N.Y., 1964; (b) J. O. McGervey in "Positronium Annihilation," A. T. Stewart and L. O. Roellig, Ed., Academic Press, New York, N.Y., 1967; (c) H. J. Ache, *Angew. Chem., Int. Ed. Engl.*, **11**, 179 (1972).

(7) S. Y. Chuang and B. G. Hogg, *Can. J. Phys.*, **45**, 3895 (1967); S. Y. Chuang, W. H. Holt, and B. G. Hogg, *ibid.*, **46**, 2309 (1968).

(8) V. I. Goldanskii, A. V. Ivanova, and E. P. Prokopyev, *Zh. Eksp. Teor. Fiz.*, **47**, 659 (1964); A. V. Ivanova and E. P. Prokopyev, *ibid.*, **48**, 1155 (1965).

(9) Din Van Huang, *Zh. Eksp. Teor. Fiz.*, **49**, 630 (1965).

(10) C. F. Lebeda and D. M. Schrader, *Phys. Rev.*, **178**, 24 (1964).

(11) (a) P. B. Navin, D. M. Schrader, and C. F. Lebeda, *Appl. Phys.*, **3**, 159 (1974); (b) *Phys. Rev. A*, **9**, 2248 (1974).

(12) D. M. Schrader, *Phys. Rev. A*, **1**, 1070 (1970).

(13) O. Sinanoglu, *Proc. Nat. Acad. Sci. U.S.*, **47**, 1217 (1961).

(14) J. A. Pople, D. P. Santry, and G. A. Segal, *J. Chem. Phys.*, **43**, S129 (1965); J. A. Pople and G. A. Segal, *ibid.*, **43**, S136 (1965).

(15) J. A. Pople and D. L. Beveridge, "Approximate Molecular Orbital Theory," McGraw-Hill, New York, N.Y., 1970.

(16) M. Wolfsberg and L. Helmholtz, *J. Chem. Phys.*, **20**, 837 (1952).

(17) L. C. Cusachs and B. B. Cusachs, *J. Phys. Chem.*, **71**, 1060 (1967).

(18) S. P. McGlynn, L. G. Vanquickenborne, M. Kinoshita, and D. G. Carroll, "Introduction to Applied Quantum Chemistry," Holt, Rinehart, and Winston, New York, N.Y., 1972.

(19) T. Koopmans, *Physica*, **1**, 104 (1933).

(20) H. A. Bethe and E. E. Salpeter, "Quantum Mechanics of One- and Two-Electron Atoms," Springer-Verlag, Berlin, 1951.

(21) V. I. Goldanskii and V. P. Shantarovich, *Appl. Phys.*, **3**, 335 (1974).

(22) S. J. Tao, T. M. Kelly, S. Y. Chuang, and J. M. Wilkenfeld, *Appl. Phys.*, **3**, 31 (1974).

Conductance Behavior of Some Ammonium and Partially Substituted Ammonium Tetraphenylborates in 3-Methyl-2-oxazolidone and 3-*tert*-Butyl-2-oxazolidone at 25°

Barbara J. Barker and Paul G. Sears*

Department of Chemistry, University of Kentucky, Lexington, Kentucky 40506 *(Received May 24, 1974)*

Publication costs assisted by the University of Kentucky

Equivalent conductances of ammonium and mono-, di-, and triethylammonium tetraphenylborates in 3-methyl-2-oxazolidone and 3-*tert*-butyl-2-oxazolidone have been determined over broad concentration ranges (4–218 × 10^{-4} M) at 25°. For each salt, data from two independent sets of measurements were combined and evaluated by the Fernández-Prini expanded forms of the Pitts and Fuoss–Hsia equations. Analyses of data by these equations yielded the same values for the limiting equivalent conductances of the salts and further indicated that all of the salts, excepting the completely dissociated diethylammonium tetraphenylborates, were very slightly associated in the two 3-alkyl-2-oxazolidones. Values of limiting ionic equivalent conductances, estimated using the tri(isoamyl)butylammonium tetraphenylborate method, interestingly reveal for both solvents that the diethylammonium ion has the highest λ_0^+ value. The absence of a definite trend in the λ_0^+ values for the ammonium through tetraethylammonium series in each of the two 3-alkyl-2-oxazolidones indicates specific ion–solvent interactions in these systems.

Introduction

Recently several 3-substituted 2-oxazolidones, including 3-*tert*-butyl-2-oxazolidone (3*t*Bu2Ox) and 3-methyl-2-oxazolidone (3Me2Ox), were found to have very promising potential as new electrolytic solvents.[1] Since electrolytic conductance measurements are one of the most accurate techniques for determination of ion–solvent interactions in solution, an initial investigation of the conductance behavior of a series of electrolytes in 3*t*Bu2Ox and 3Me2Ox was undertaken. Partially substituted ammonium salts were chosen for study since there have been relatively few conductance investigations[2–6] of these types of electrolytes.

Experimental Section

The synthesis and purification of 3*t*Bu2Ox and 3Me2Ox have been described previously.[1] The procedure and apparatus used in the present investigation also have been described in detail.[7] The easily prepared and very soluble tetraphenylborate salts of ammonium, ethylammonium, diethylammonium, and triethylammonium were prepared by mixing aqueous equimolar solutions of sodium tetraphenylborate (Baker Analyzed Reagent) and ammonium bromide (Baker Analyzed Reagent), ethylamine hydrobromide, diethylamine hydrochloride, and triethylamine hydrobromide (all Eastman chemicals), respectively. The precipitates were recrystallized from acetone–ether mixtures. Conductivity water, obtained by passing laboratory distilled water through IWT (Illinois Water Treatment Co.) ion-exchange resin, was used in the salt preparations. All salts were ground finely and dried *in vacuo* prior to use.

Results and Discussion

All data were evaluated with computer programs[8] written in Fortran IV for an IBM 360/65 computer system. All electrolyte solution concentrations and conductances appear in the microfilm edition of this volume of the journal.[9] For each salt two independent sets of measurements were made and the data from both sets were combined and evaluated by the Fernández-Prini expanded forms[10] of the Pitts[11] and Fuoss–Hsia[12] equations. Neglecting any viscosity corrections in the data evaluation, the expanded Pitts and Fuoss–Hsia equations are expressed as

$$\Lambda = \Lambda_0 - S(C\gamma)^{1/2} + EC\gamma \log C\gamma + J_1C\gamma - J_2(C\gamma)^{3/2} - K_AC\gamma f^2\Lambda \quad (1)$$

in which $S = \alpha\Lambda_0 + \beta$, $E = E_1\Lambda_0 - E_2$, $J_1 = \sigma_1\Lambda_0 + \sigma_2$, and $J_2 = \sigma_3\Lambda_0 + \sigma_4$. In these equations all symbols have their usual meanings. For the data analysis a range of d values was selected[13] and values of Λ_0, K_A, and d corresponding to a minimum standard deviation, $\sigma\Lambda$, were chosen as the best fit set of parameters for the system. Initial Λ_0 values used in the expanded equations were those obtained from the evaluation of data by the Fuoss–Onsager equation for unassociated electrolytes.[14] Conductance parameters were calculated each 0.5 Å throughout the range of d values 2.0–20.0 Å. The conductance parameters obtained from the expanded Pitts and Fuoss–Hsia equations are listed in Table I; the equivalent conductances of the ammonium and partially substituted ammonium ions are presented in Table II.

The absence of a definite trend in the limiting equivalent conductances within the ammonium through tetraethylammonium ion series in 3*t*Bu2Ox and 3Me2Ox indicates specific ion–solvent interactions in these systems. Interestingly in both solvents, as in N-methylacetamide,[4] nitromethane,[5] and ethanolamine,[6] the diethylammonium ion has the highest λ_0^+ value in the series. As Table I reveals, whereas most salts are determined to be very slightly associated electrolytes in the 2-oxazolidones, the diethylammonium salt is an unassociated electrolyte in 3*t*Bu2Ox and 3Me2Ox. Also of interest is the observation that in 3*t*Bu2Ox larger values of d and K_A are obtained from the expanded Fuoss–Hsia equation than from the expanded Pitts equation; in 3Me2Ox the reverse trend is observed. Both expanded equations yield the same values for the electrolyte limiting equivalent conductances. The expanded equations appear to provide a complete description of

TABLE I: Conductance Parameters from Expanded Pitts and Fuoss–Hsia Equations for Partially Substituted Ammonium Salts in 2-Oxazolidones at 25°

		Expanded Pitts evaluation				Expanded Fuoss–Hsia evaluation			
Salt	10^4C[a]	d	$\sigma\Lambda$	Λ_0	K_A	$\mathring{d}$	$\sigma\Lambda$	Λ_0	K_A
			3*t*Bu2Ox[b]						
NH_4BPh_4	11.86–133.3 (13)	7.5	0.019	7.92	1.3	8.5	0.019	7.92	2.1
$EtNH_3BPh_4$	6.582–169.4 (19)	4.0	0.014	8.55	0.3	6.0	0.014	8.55	1.6
$Et_2NH_2BPh_4$	15.97–143.2 (13)	11.5	0.031	9.70		12.0	0.031	9.70	
Et_3NHBPh_4	4.002–218.2 (20)	6.0	0.027	9.28	1.8	7.5	0.027	9.28	2.8
			3Me2Ox[b]						
$EtNH_3BPh_4$	5.791–104.1 (15)	13.0	0.024	20.47	0.5	12.5	0.025	20.47	
$Et_2NH_2BPh_4$	12.50–68.95 (16)	16.5	0.015	22.66	0.3	14.5	0.016	22.66	
Et_3NHBPh_4	5.322–85.93 (15)	13.0	0.024	21.83	1.9	12.0	0.024	21.83	1.2

[a] The number in parentheses indicates the number of data points included in the analysis. [b] Density, viscosity, and dielectric constant are as follows: 3*t*Bu2Ox 1.0501 g/ml, 0.05628 P, 57.6; 3Me2Ox 1.1702 g/ml, 0.02450 P, 77.5 (ref 1).

TABLE II: Ionic Limiting Equivalent Conductances in 2-Oxazolidones at 25° [a–e]

Cation	λ_0^+(3*t*Bu2Ox)	λ_0^+(3Me2Ox)
NH_4^+	4.52	12.07[e]
$EtNH_3^+$	5.15	11.93
$Et_2NH_2^+$	6.30	14.12
Et_3NH^+	5.88	13.29
Et_4N^+	6.09[d]	13.71[e]

[a] Based on Λ_0 values from the expanded Pitts and Fuoss–Hsia equations. [b] Determined with $TABBPh_4$ as a reference electrolyte. $\lambda_0(BPh_4^-)$ = 3.40 in 3*t*Bu2Ox[15] and $\lambda_0(BPh_4^-)$ = 8.54 in 3Me2Ox.[7] [c] $EtNH_3^+$ = ethylammonium, $Et_2NH_2^+$ = diethylammonium, Et_3NH^+ = triethylammonium, Et_4N^+ = tetraethylammonium, TAB^+ = tri(isoamyl)butylammonium, BPh_4^- = tetraphenylborate. [d] Reference 15. [e] Reference 7.

the behavior of partially substituted ammonium salts in the 2-oxazolidones. Application of the recently expanded conductance equations to data for other partially substituted ammonium salt–nonaqueous solvent systems should be of interest in future investigations.

Acknowledgments. This work was supported in part by Project Themis Grant DAA B07-69-C-0366. The authors also express their appreciation to Drs. J. E. Prue and A. D. Pethybridge of the University, Reading, England, who kindly provided the computer program used for the analysis of data by the expanded Pitts and Fuoss–Hsia equations, and to Dr. J. F. Casteel of the University of Kentucky for his advice and assistance.

Supplementary Material Available. Conductance data for the salts studied in 3*t*Bu2Ox and 3Me2Ox will appear following these pages in the microfilm edition of this volume of the journal. Photocopies of the supplementary material from this paper only or microfiche (105 × 148 mm, 24× reduction, negatives) containing all of the supplementary material for the papers in this issue may be obtained from the Journals Department, American Chemical Society, 1155 16th St., N.W., Washington, D. C. 20036. Remit check or money order for $3.00 for photocopy or $2.00 for microfiche, referring to code number JPC-74-2687.

References and Notes

(1) H. L. Huffman, Jr., and P. G. Sears, *J. Solution Chem.*, **1**, 187 (1972).

(2) (a) B. M. Lowe and H. M. Rendall, *J. Chem. Soc., Faraday Trans. 1*, **68**, 2191 (1972); (b) B. M. Lowe, N. A. MacGilp, and J. M. Prichard, *J. Chem. Eng. Data*, **18**, 220 (1973).

(3) (a) M. M. Davis, *Nat. Bur. Stand.* (*U. S.*), Monogr., **No. 105** (Aug 1968); (b) G. J. Janz and R. P. T. Tomkins, Ed., "Nonaqueous Electrolytes Handbook," Vol. I, Academic Press, New York, N.Y., 1972; (c) R. D. Singh, *Bull. Chem. Soc. Jap.*, **46**, 14 (1973).

(4) L. R. Dawson, E. D. Wilhoit, and P. G. Sears, *J. Amer. Chem. Soc.*, **78**, 1569 (1956).

(5) P. Walden and E. J. Birr, *Z. Phys. Chem.*, **A163**, 263 (1933).

(6) H. T. Briscoe and T. P. Dirkse, *J. Phys. Chem.*, **44**, 388 (1940).

(7) H. L. Huffman, Jr., Ph.D. Dissertation, University of Kentucky, 1972.

(8) The computer program for analysis of data by the expanded Pitts and Fuoss–Hsia equations kindly was provided by Drs. J. E. Prue and A. D. Pethybridge of the University, Reading, England.

(9) See paragraph at end of text regarding supplementary material.

(10) (a) R. Fernández-Prini and J. E. Prue, *Z. Phys. Chem.* (*Leipzig*), **228**, 373 (1965); (b) R. Fernández-Prini, *Trans. Faraday Soc.*, **65**, 3311 (1969).

(11) (a) E. Pitts, *Proc. Roy. Soc., Ser. A*, **217**, 43 (1953); (b) E. Pitts, B. E. Tabor, and J. Daly, *Trans. Faraday Soc.*, **65**, 849 (1969).

(12) (a) R. M. Fuoss and K.-L. Hsia, *Proc. Nat. Acad. Sci. U. S.*, **57**, 1550 (1967); (b) K.-L. Hsia and R. M. Fuoss, *J. Amer. Chem. Soc.*, **90**, 3055 (1968).

(13) (a) E. M. Hanna, A. D. Pethybridge, and J. E. Prue, *Electrochim. Acta*, **16**, 677 (1971); (b) E. M. Hanna, A. D. Pethybridge, and J. E. Prue, *J. Phys. Chem.*, **75**, 291 (1971); (c) W. C. Duer, R. A. Robinson, and R. G. Bates, *J. Chem. Soc., Faraday Trans. 1*, **68**, 716 (1972).

(14) (a) R. M. Fuoss and L. Onsager, *J. Phys. Chem.*, **61**, 668 (1957); (b) R. M. Fuoss and F. Accascina, "Electrolytic Conductance," Interscience, New York, N.Y., 1959.

(15) B. J. Barker, H. L. Huffman, Jr., and P. G. Sears, *J. Phys. Chem.*, **78**, 2689 (1974).

Conductance Behavior of Tetraalkylammonium Salts in 3-*tert*-Butyl-2-oxazolidone at 25° [1]

Barbara J. Barker, Hugh L. Huffman, Jr., and Paul G. Sears*

Department of Chemistry, University of Kentucky, Lexington, Kentucky 40506 *(Received May 24, 1974)*

Publication costs assisted by the University of Kentucky

Conductance measurements for a series of tetraalkylammonium salts in 3-*tert*-butyl-2-oxazolidone (3*t*Bu20x), a recently synthesized nonaqueous solvent of exceptionally high purity, were made over a relatively wide concentration range ($2-200 \times 10^{-4}$ *M*) at 25°. All conductance data were evaluated by the Fuoss–Onsager equations for associated and unassociated electrolytes and by the expanded Pitts and Fuoss–Hsia equations. From the Fuoss–Onsager data analysis, which yielded unrealistically small ion size parameters, all of the tetramethyl- through tetrahexylammonium tetraphenylborates, perchlorates, bromides, nitrates, and picrates were found to be unassociated electrolytes in 3*t*Bu2Ox. From the expanded Pitts and Fuoss–Hsia equations with values of the ion size parameter ranging from 3 to 9 Å, small association constants ranging from 0.4 to 9.2 M^{-1} were obtained for these electrolytes. Association within the salt series decreased in the order nitrates > bromides > perchlorates > tetraphenylborates. The same values of the electrolyte limiting equivalent conductance were obtained from the two expanded equations; however, these Λ_0 values were slightly smaller than the values obtained from the Fuoss–Onsager equations. Ionic limiting equivalent conductances were obtained by using triisoamylbutylammonium tetraphenylborate as a reference electrolyte. Generally, the limiting equivalent conductances of the tetraalkylammonium ions decreased as the crystallographic radii of these ions increased; but surprisingly, the λ_0^+ value of the tetraethylammonium ion was higher than that of the tetramethylammonium ion in 3*t*Bu2Ox.

Introduction

Frequent use of nonaqueous solvents as media for chemical reactions has created an increasing interest in the properties of electrolytes in solution. Electrolyte behavior in solution can be determined directly from fundamental electrochemical investigations. Measurement of electrolyte conductance is one of the most accurate techniques for determination of ion–solvent interactions in solution.

The Fuoss–Onsager equations[2] have been used extensively for the evaluation of conductance data; however, these equations often yield unrealistically small ion size parameters. This shortcoming has led to considerable interest in the analysis of conductance data by the relatively recent Fernández-Prini expanded forms[3] of the Pitts[4] and Fuoss–Hsia[5] equations.

Recently 3-*tert*-butyl-2-oxazolidone (3*t*Bu2Ox), a new nonaqueous solvent of very low specific conductance ($3-8 \times 10^{-9}$ ohm^{-1} cm^{-1}), moderate dielectric constant (57.6), and relatively high viscosity (5.63 cP), was found to have promising potential as a new electrolytic solvent.[6] Since tetralkylammonium salts are very soluble in many nonaqueous solvents and also form systematic series containing cations of relatively large crystallographic size and low charge density, these electrolytes often serve as theoretical models in solution chemistry. Therefore, an initial investigation of the conductance behavior of a series of tetraalkylammonium salts in 3*t*Bu2Ox was undertaken.

Experimental Section

The synthesis and purification of 3-*tert*-butyl-2-oxazolidone have been described previously.[6] Recrystallization of the salts and the apparatus also have been described previously.[7] Aqueous potassium chloride solutions ranging in concentration from 6.0×10^{-5} to 6.0×10^{-3} *M* were used in the determination of the cell constants. The constants, 0.7402 ± 0.0011 and 0.3181 ± 0.0005 cm^{-1}, were calculated from the conductance equation of Lind, Zwolenik, and Fuoss.[8] Procedures used in the present study have been described in detail.[7,9]

Results and Discussion

All conductance data were evaluated by the Fuoss–Onsager equations[2] for unassociated and associated electrolytes and by the expanded equations[3] of Pitts[4] and Fuoss–Hsia.[5] All data were evaluated with computer programs[10] written in Fortran IV for an IBM 360/65 computer system. Values of the density, viscosity, and dielectric constant of 3-*tert*-butyl-2-oxazolidone at 25° which were used in all calculations were 1.0501 g/ml, 0.05628 P, and 57.6, respectively.[6] All electrolyte solution concentrations and conductances appear in the microfilm edition of this volume of the journal.[11]

The Fuoss–Onsager method of evaluation yielded values of Λ_0, K_A, and a_J from the equation

$$\Lambda = \Lambda_0 - S(C\gamma)^{1/2} + EC\gamma \log C\gamma + JC\gamma - K_A C\gamma f^2 \Lambda \quad (1)$$

in which $S = \alpha\Lambda_0 + \beta$, $E = E_1\Lambda_0 - E_2$, and $J = \sigma_1\Lambda_0 + \sigma_2$. In these equations all symbols have their usual meaning. The physical properties of 3*t*Bu2Ox at 25° lead to values of 0.3645, 11.19, 1.337, and 6.010 for the coefficients α, β, E_1, and E_2, respectively. The coefficients σ_1 and σ_2 are functions of both the solvent physical properties and the ion size parameter. For unassociated electrolytes $\gamma = 1$ and $K_A = 0$; for associated electrolytes $\gamma < 1$ and $K_A > 0$. As in numerous other conductance studies, the viscosity term $F\Lambda_0$ was omitted in the present Fuoss–Onsager data evaluation.

TABLE I: Fuoss–Onsager Conductance Parameters for Tetraalkylammonium Salts in 3-*tert*-Butyl-2-oxazolidone at 25°

Salt	$10^9\kappa_0$[a]	10^4C[b]	$\sigma\Lambda$	Λ_0	a_J
Me_4NBPh_4	0.71	5.464–78.61 (8)	0.003	9.25 ± 0.012	4.2 ± 0.22
	1.6	88.13–202.6 (7)	0.004	9.21 ± 0.021	2.9 ± 0.14
		5.464–202.6 (15)	0.009	9.34 ± 0.023	2.2 ± 0.17
Me_4NPi	5.6	5.216–95.90 (6)	0.004	12.29 ± 0.011	2.9 ± 0.13
	4.9	49.67–163.8 (6)	0.004	12.43 ± 0.014	2.3 ± 0.09
		5.216–163.8 (12)	0.009	12.32 ± 0.025	2.9 ± 0.18
Et_4NClO_4	3.5	9.964–91.04 (6)	0.006	15.07 ± 0.022	2.5 ± 0.22
	8.2	21.76–179.6 (6)	0.004	15.16 ± 0.015	1.9 ± 0.07
		9.964–179.6 (12)	0.005	15.12 ± 0.012	2.1 ± 0.06
Et_4NNO_3	5.6	13.09–128.0 (9)	0.004	15.94 ± 0.012	0.8 ± 0.05
Pr_4NBPh_4	8.8	16.65–88.40 (7)	0.002	8.12 ± 0.008	3.4 ± 0.14
Pr_4NClO_4	6.7	6.436–101.1 (7)	0.002	13.74 ± 0.006	2.0 ± 0.06
Pr_4NBr	3.5	13.30–99.80 (7)	0.003	13.20 ± 0.011	0.6 ± 0.06
	8.2	21.28–181.5 (7)	0.006	13.20 ± 0.020	0.5 ± 0.05
		13.30–181.5 (14)	0.004	13.20 ± 0.009	0.5 ± 0.03
Bu_4NBPh_4	12.0	56.59–165.3 (7)	0.002	7.50 ± 0.009	2.8 ± 0.08
Bu_4NClO_4	3.5	15.13–78.60 (5)	0.004	13.08 ± 0.014	2.1 ± 0.17
	8.2	63.45–162.1 (5)	0.004	13.13 ± 0.016	1.9 ± 0.09
		15.13–162.1 (10)	0.004	13.09 ± 0.011	2.1 ± 0.08
Bu_4NBr	3.5	10.52–142.1 (11)	0.003	12.54 ± 0.010	0.9 ± 0.05
Bu_4NNO_3	5.8	17.82–206.2 (8)	0.002	13.92 ± 0.006	1.1 ± 0.02
Pen_4NClO_4	3.5	2.287–60.38 (7)	0.004	12.71 ± 0.015	2.7 ± 0.25
	8.2	9.923–122.4 (7)	0.005	12.76 ± 0.018	2.3 ± 0.15
		2.287–122.4 (14)	0.005	12.73 ± 0.012	2.6 ± 0.12
Pen_4NBr	8.2	2.875–151.1 (8)	0.008	12.29 ± 0.018	0.5 ± 0.06
Hex_4NBr	3.5	6.668–59.49 (5)	0.001	11.87 ± 0.002	1.5 ± 0.03
	8.2	19.91–103.0 (5)	0.005	11.84 ± 0.018	1.3 ± 0.15
		6.668–103.0 (10)	0.007	11.89 ± 0.018	1.0 ± 0.14
$TABBPh_4$	5.6	2.773–82.08 (8)	0.002	6.84 ± 0.006	4.6 ± 0.12
	6.6	9.535–176.4 (8)	0.017	6.88 ± 0.005	3.4 ± 0.16
		2.773–176.4 (16)	0.004	6.88 ± 0.010	3.4 ± 0.11

[a] *Solvent specific conductance.* [b] *The number in parentheses indicates the number of data points.*

Including viscosity corrections in conductance data analyses leads to unchanged Λ_0 values and essentially unchanged K_A and a_J values. Initial Λ_0 values used in the Fuoss–Onsager equations were those obtained from the Shedlovsky Λ_0' *vs.* C method of analysis.[12] For all salts the use of data weighted by C or $C\gamma$ led to a smaller standard deviation $\sigma\Lambda$ for individual conductance values than did unweighted data. Evaluation of data for all salts as associated electrolytes led to negative association constants and to degrees of dissociation greater than unity. Therefore, from the Fuoss–Onsager evaluation all salts were considered to *be unassociated electrolytes.*

The conductance parameters obtained from the Fuoss–Onsager evaluation of data for all salts are presented in Table I. For some salts two independent sets of measurements were made and the data from each set were evaluated by the Fuoss–Onsager method. For these salts the two sets of measurements then were combined and treated as one set of data. Included in Table I are the electrolyte limiting equivalent conductances obtained after combining these data sets.

As Table I reveals, exceedingly small values of "the contact distance" a_J were obtained for the salts in 3*t*Bu2Ox. These values, which are physically meaningless, indicated the need for additional methods of data evaluation. Currently, the Fernández-Prini expanded forms of the Pitts and Fuoss–Hsia equations are of interest in the evaluation of conductance data. In these expanded equations an additional concentration term is included and the ion size parameter is defined as "a distance of closest approach." Neglecting any viscosity corrections in the data evaluation, the expanded Pitts and Fuoss–Hsia equations are expressed as

$$\Lambda = \Lambda_0 - S(C\gamma)^{1/2} + EC\gamma \log C\gamma + J_1C\gamma - J_2(C\gamma)^{3/2} - K_AC\gamma f^2\Lambda \quad (2)$$

The coefficients S and E are defined as in eq 1; the coefficients J_1 and J_2, which are functions of the solvent physical properties and the ion size parameter, have different values in the Pitts and the Fuoss–Hsia equations.[3-5]

In the expanded Pitts and Fuoss–Hsia analyses of data several procedures exist for the determination of conductance parameters. A value of d, the distance of closest approach of the ions, can be assigned[13] and corresponding values of Λ_0 and K_A can be calculated or a range of d values can be selected[14] and values of Λ_0, K_A, and d corresponding to the minimum standard deviation, $\sigma\Lambda$, can be chosen as the best fit set of parameters for the system.

This latter procedure was used in the present investigation. Initial values of Λ_0 used in the expanded equations were the Fuoss–Onsager Λ_0 values obtained after combining the data sets (Table I). All experimental equivalent conductance data[11] relating to concentrations in the range of 2–200 × 10^{-4} M were used in the expanded Pitts and Fuoss–Hsia analyses. This approach appeared reasonable since conductance data for comparable or broader concentration ranges have been analyzed in terms of the same expanded equations by other investigators.[3,14] As previously discussed,[5,15] the expanded Pitts and Fuoss–Hsia methods of analysis require data from relatively wide concentration ranges, such as those used in the present study.

Conductance parameters were calculated at each 0.5 Å throughout the range of d values 2.0–20.0 Å. Typical Pitts and Fuoss–Hsia plots are presented in Figures 1 and 2. As these figures indicate the association constants are a function of the d values. The best fit d values (and correspond-

TABLE II: Expanded Pitts and Expanded Fuoss–Hsia Conductance Parameters for Tetraalkylammonium Salts in 3-*tert*-Butyl-2-oxazolidone at 25°

Salt	Pitts evaluation				Fuoss–Hsia evaluation			
	d	$\sigma\Lambda$	Λ_0	K_A	d	$\sigma\Lambda$	Λ_0	K_A
Me_4NBPh_4	6.5	0.040	9.27	2.80	8.0	0.040	9.27	3.80
Me_4NPi	6.0	0.033	12.25	1.47	7.5	0.033	12.26	2.54
Et_4NClO_4	6.0	0.021	15.05	2.73	8.0	0.021	15.05	3.87
Et_4NNO_3	7.5	0.014	15.93	6.48	9.0	0.014	15.94	7.51
Pr_4NBPh_4	6.0	0.006	8.10	1.87	7.5	0.006	8.10	2.83
Pr_4NClO_4	6.0	0.008	13.72	3.78	8.0	0.008	13.72	4.94
Pr_4NBr	7.0	0.013	13.21	7.81	9.0	0.013	13.20	8.76
Bu_4NBPh_4	3.0	0.006	7.48	0.44	3.5	0.006	7.48	0.28
Bu_4NClO_4	3.0	0.013	13.08	1.90	5.5	0.013	13.09	3.54
Bu_4NBr	2.5	0.009	12.58	4.84	5.0	0.009	12.58	6.55
Bu_4NNO_3[a]	5.7	0.002	13.91	5.49	7.7	0.002	13.92	6.65
Pen_4NClO_4	7.0	0.020	12.68	2.64	9.0	0.020	12.67	3.69
Pen_4NBr[a]	7.0	0.025	12.30	8.24	9.0	0.025	12.30	9.24
Hex_4NBr	8.5	0.020	11.86	6.50	10.0	0.020	11.86	7.32
$TABBPh_4$	7.0	0.007	6.81	0.63	8.0	0.007	6.81	1.40

[a] See text for discussion.

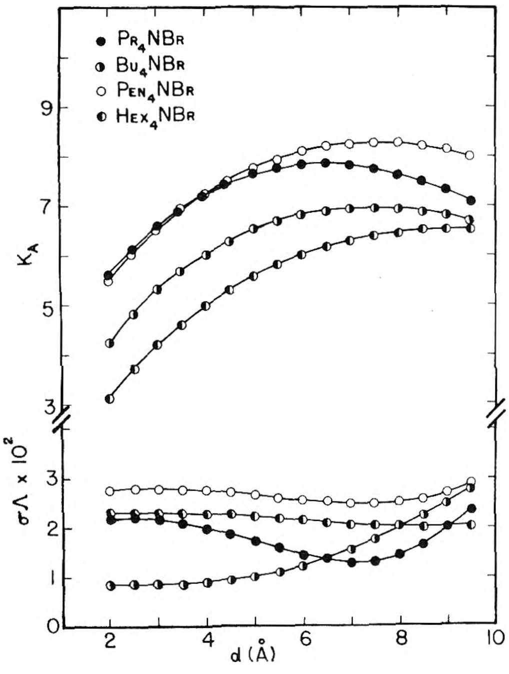

Figure 1. Plots of the expanded Pitts equation for tetraalkylammonium bromides in 3-*tert*-butyl-2-oxazolidone.

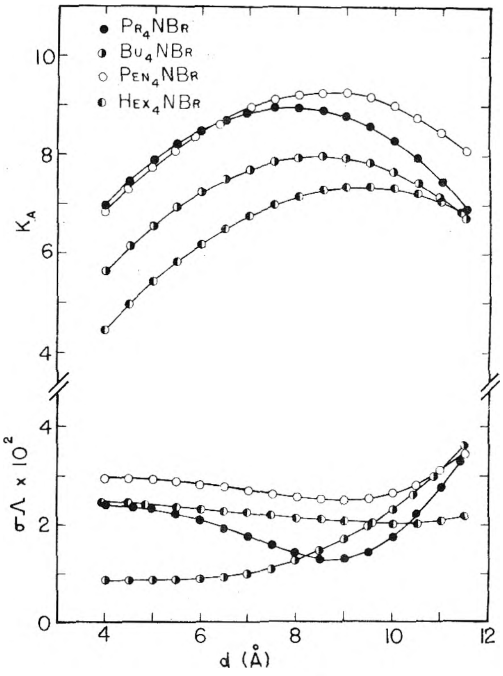

Figure 2. Plots of the expanded Fuoss–Hsia equation for tetraalkylammonium bromides in 3-*tert*-butyl-2-oxazolidone.

ing Λ_0 and K_A values) are dependent on the concentration range included in the data analysis. For example, evaluation of data for Et_4NClO_4 in 3*t*Bu2Ox within the concentration range 9.964–179.6 × 10^{-4} *M* produced the results listed in Table II. Narrowing the concentration range to upper limits of 152.8, 91.04, and 66.60 × 10^{-4} *M* resulted in best fit *d* values of 6.0, 10.5, and 18.0 Å, respectively, in the Pitts evaluation of data and to best fit values of 8.0, 11.5, and 16.0 Å, respectively, in the Fuoss–Hsia data evaluation.

As Figures 1 and 2 indicate and as previously observed,[14] the values of $\sigma\Lambda$ often remain essentially constant over a relatively wide range of *d* values. Therefore, any set of parameters within this minimum $\sigma\Lambda$ range may be considered as an "acceptable" set of values.[14] The conductance parameters presented in Table II correspond to the minimum $\sigma\Lambda$ evaluated to four significant figures. Very sharp minima in the $\sigma\Lambda$ *vs.* *d* plots were obtained for only one electrolyte, tetrabutylammonium nitrate, in 3*t*Bu2Ox. For this salt the data were evaluated in 0.1-Å intervals.

For example, in the expanded Pitts analysis of data for Pen_4NBr (Figure 1) $\sigma\Lambda$ values of 0.02513, 0.02490, 0.02492, and 0.02524, correspond to *d* values of 6.5, 7.0, 7.5, and 8.0 Å, respectively. In the expanded Fuoss–Hsia analysis for this salt (Figure 2) $\sigma\Lambda$ values of 0.02510, 0.02498, and 0.02535 correspond to *d* values of 8.5, 9.0, and 9.5 Å, respectively. Therefore, conductance parameters for Pen_4NBr in Table II are listed at $d = 7.0$ in the Pitts evaluation and at $d = 9.0$ in the Fuoss–Hsia evaluation. For Bu_4NNO_3, $\sigma\Lambda$ values of 0.00530, 0.00227, and 0.00282 corresponded to *d* values of 5.0, 5.5, and 6.0 Å, respectively, in the Pitts analysis; in the Fuoss–Hsia analysis $\sigma\Lambda$ values of 0.00621, 0.00241, and 0.00347 corresponded to *d* values of 7.0, 7.5, and 8.0, respectively. Reevaluation of the data at 0.1-Å intervals within these ranges yielded a minimum $\sigma\Lambda$

TABLE III: Ionic Limiting Equivalent Conductances in 3-*tert*-Butyl-2-oxazolidone at 25°[a–c]

Cation	λ_0^+	Anion	λ_0^-
Me_4N^+	5.87	NO_3^-	9.84
Et_4N^+	6.09	ClO_4^-	8.96
Pr_4N^+	4.74	Br^-	8.49
Bu_4N^+	4.10	Pi^-	6.39
Pen_4N^+	3.76	BPh_4^-	3.40
Hex_4N^+	3.37		
TAB^+	3.40		

[a] Based on Λ_0 values from the expanded Pitts and Fuoss–Hsia evaluation of data. [b] Determined with $TABBPh_4$ as a reference electrolyte. [c] Me = methyl, Et = ethyl, Pr = *n*-propyl, Bu = *n*-butyl, Pen = *n*-pentyl, Hex = *n*-hexyl, Pi = picrate.

of 0.00164 at $d = 5.7$ in the Pitts evaluation and a minimum $\sigma\Lambda$ of 0.00163 at $d = 7.7$ in the Fuoss–Hsia analysis.

With the exception of the tetrabutylammonium salts in 3*t*Bu2Ox, both expanded equations gave best fit parameters at contact distances greater than the Bjerrum critical distance q which is 4.86 Å for 3*t*Bu2Ox at 25°. Figures 1 and 2 and Table II indicate that larger association constants and contact distances for tetraalkylammonium salts in 3*t*Bu2Ox are obtained from the expanded Fuoss–Hsia equation than from the expanded Pitts equation. These same observations have been made for other electrolyte systems.[3b,14a]

As expected and as Table II indicates, electrolyte association decreases in the order $NO_3^- > Br^- > ClO_4^- > BPh_4^-$. Both expanded equations yielded the same values of the electrolyte limiting equivalent conductance. Generally, these Λ_0 values were, at most, 0.07 unit less than the average Λ_0 values obtained from the Fuoss–Onsager equations.

Ionic limiting equivalent conductances often are obtained indirectly by using triisoamylbutylammonium tetraphenylborate ($TABBPh_4$) as a reference electrolyte. Values of $\lambda_0^{\pm}$ are obtained by assuming that the limiting equivalent conductance of the triisoamylbutylammonium ion, shown to be equal to that of the tetraphenylborate ion in methanol,[16] is the same as that of the tetraphenylborate ion in other nonaqueous solvents. Evaluation of the validity of using any reference electrolyte in a nonaqueous solvent requires a direct measurement of transference numbers in that solvent. However, since the purpose of the present investigation is the determination of relative solvation effects within a tetraalkylammonium salt series, the set of ionic limiting equivalent conductances, which is presented in Table III, was obtained by assuming $\lambda_0(TAB^+) = \lambda_0(BPh_4^-)$ in 3*t*Bu2Ox. Addition of cationic and anionic limiting equivalent conductances which reproduces most salt limiting equivalent conductances in Table II within 0.3% indicates the reliability of the data. Another indication of the precision of the measurements can be obtained from the differences $\Lambda_0(R_4NNO_3) - \Lambda_0(R_4NClO_4)$, $\Lambda_0(R_4NClO_4)$, $- \Lambda_0(R_4NBPh_4)$, and $\Lambda_0(R_4NBr) - \Lambda_0(R_4NBPh_4)$. These values and their ranges are 0.86 ± 0.03, 5.61 ± 0.01, and 5.10 ± 0.00, respectively.

Generally, as expected, the limiting equivalent conductances of the tetraalkylammonium ions decrease as the crystallographic radii of these ions increase. The limiting equivalent conductance of the Et_4N^+ ion, however, is higher than that of the Me_4N^+ ion in 3*t*Bu2Ox. This anomalous behavior of the tetraethylammonium ion has been observed in conductance studies of tetraalkylammonium salts in other nonaqueous solvents, such as 1-propanol,[17] 2-propanol,[18] and 1-butanol.[19] Of interest in the solvent 3*t*Bu2Ox is the order of decreasing λ_0^+ values within the series $Bu_4N^+ > Pen_4N^+ > TAB^+$. In another derivative of 2-oxazolidone, 3-methyl-2-oxazolidone (3Me2Ox),[7] values of λ_0^+ decrease in the order $Bu_4N^+ > TAB^+ > Pen_4N^+$. Also in 3Me2Ox, as in several other heterocyclic aprotic solvents, such as ethylene carbonate[20] and propylene carbonate,[21] the limiting equivalent conductance of the bromide ion is greater than that of the perchlorate ion. However, in 3*t*Bu2Ox $\lambda_0(ClO_4^-) > \lambda_0(Br^-)$. These reversals in the order of ionic limiting equivalent conductances in 3*t*Bu2Ox may be attributed to specific ion–solvent interactions in this medium.

A more complete description of electrolyte behavior in 3-*tert*-butyl-2-oxazolidone has been provided by the expanded Pitts and Fuoss–Hsia equations than by the Fuoss–Onsager equations. The promising potential of 3*t*Bu2Ox as an electrolytic solvent has been verified in the present study.

Acknowledgments. This work was supported in part by Project Themis Grant DAA B07-69-C-0366. The authors also express their appreciation to Drs. J. E. Prue and A. D. Pethybridge of the University, Reading, England, who kindly provided the computer program used for the analysis of data by the expanded Pitts and Fuoss–Hsia equations, and to Dr. J. F. Casteel of the University of Kentucky for his advice and assistance.

Supplementary Material Available. Conductance data for the salts studied in 3-*tert*-butyl-2-oxozolidone will appear following these pages in the microfilm edition of this volume of the journal. Photocopies of the supplementary material from this paper only or microfiche (105 × 148 mm, 24× reduction, negatives) containing all of the supplementary material for the papers in this issue may be obtained from the Journals Department, American Chemical Society, 1155 16th St., N.W., Washington, D.C. 20036. Remit check or money order for $3.00 for photocopy or $2.00 for microfiche, referring to code number JPC-74-2689.

References and Notes

(1) This study was presented, in part, at the Fifth Central Regional Meeting of the American Chemical Society, Cleveland, Ohio, May 1973.

(2) (a) R. M. Fuoss and L. Onsager, *J. Phys. Chem.*, **61**, 668 (1957); (b) R. M. Fuoss and F. Accascina, "Electrolytic Conductance," Interscience, New York, N.Y., 1959.

(3) (a) R. Fernàndez-Prini and J. E. Prue, *Z. Phys. Chem. (Leipzig)*, **228**, 373 (1965); (b) R. Fernàndez-Prini, *Trans. Faraday Soc.*, **65**, 3311 (1969).

(4) (a) E. Pitts, *Proc. Roy. Soc., Ser. A*, **217**, 43 (1953); (b) E. Pitts, B. E. Tabor, and J. Daly, *Trans. Faraday Soc.*, **65**, 849 (1969).

(5) (a) R. M. Fuoss and K.-L. Hsia, *Proc. Nat. Acad. Sci. U. S.*, **57**, 1550 (1967); (b) K.-L. Hsia and R. M. Fuoss, *J. Amer. Chem. Soc.*, **90**, 3055 (1968).

(6) H. L. Huffman, Jr., and P. G. Sears, *J. Solution Chem.*, **1**, 187 (1972).

(7) H. L. Huffman, Jr., Ph.D. Dissertation, University of Kentucky, 1972.

(8) J. E. Lind, Jr., J. J. Zwolenik, and R. M. Fuoss, *J. Amer. Chem. Soc.*, **81**, 1557 (1959).

(9) B. J. Barker and J. A. Caruso, *J. Amer. Chem. Soc.*, **93**, 1341 (1971).

(10) Kay program: (a) R. L. Kay, *J. Amer. Chem. Soc.*, **82**, 2099 (1960); (b) J. L. Hawes and R. L. Kay, *J. Phys. Chem.*, **69**, 2420 (1965). Pethybridge program: The computer program for analysis of data by the expanded Pitts and Fuoss–Hsia equations kindly was provided by Drs. J. E. Prue and A. D. Pethybridge.

(11) See paragraph at end of text regarding supplementary material.

(12) (a) T. Shedlovsky, *J. Franklin Inst.*, **225**, 739 (1938); (b) R. M. Fuoss and T. Shedlovsky, *J. Amer. Chem. Soc.*, **71**, 1496 (1949).

(13) (a) B. M. Lowe and H. M. Rendall, *J. Chem. Soc., Faraday Trans. 1*, **68**, 2191 (1972); (b) B. M. Lowe, N. A. MacGilp, and J. M. Prichard, *J.*

Chem. Eng. Data, **18**, 220 (1973); (c) R. Fernández-Prini, *Trans. Faraday Soc.*, **64**, 2146 (1968); (d) C. DeRossi, B. Sesta, M. Battistini, and S. Petrucci, *J. Amer. Chem. Soc.*, **94**, 2961 (1972).
(14) (a) E. M. Hanna, A. D. Pethybridge, and J. E. Prue, *Electrochim. Acta*, **16**, 677 (1971); (b) E. M. Hanna, A. D. Pethybridge, and J. E. Prue, *J. Phys. Chem.*, **75**, 291 (1971); (c) W. C. Duer, R. A. Robinson, and R. G. Bates, *J. Chem. Soc., Faraday Trans. 1*, **68**, 716 (1972).
(15) J. Barthel, J.-C. Justice, and R. Wachter, *Z. Phys. Chem. (Frankfurt am Main)*, **84**, 100 (1973).
(16) M. A. Coplan and R. M. Fuoss, *J. Phys. Chem.*, 68, 1177 (1964).
(17) D. F. Evans and P. Gardam, *J. Phys. Chem.*, **72**, 3281 (1968).
(18) M. A. Matesich, J. A. Nadas, and D. F. Evans, *J. Phys. Chem.*, **74**, 4568 (1970).
(19) D. F. Evans and P. Gardam, *J. Phys. Chem.*, **73**, 158 (1969).
(20) R. F. Kempa and W. H. Lee, *J. Chem. Soc.*, 100 (1961).
(21) (a) L. M. Mukherjee and D. P. Boden, *J. Phys. Chem.*, **73**, 3965 (1969); (b) L. M. Mukherjee, D. P. Boden, and R. Lindauer, *ibid.*, **74**, 1942 (1970).

Heats of Transport of Gases. III. Thermoosmosis of Ternary Gaseous Mixtures

R. P. Rastogi* and A. P. Rai

Department of Chemistry, University of Gorakhpur, Gorakhpur (U.P.), India

(Received August 2, 1973; Revised Manuscript Received July 12, 1974)

Thermoosmosis of ternary mixtures of oxygen, ethylene, and carbon dioxide has been investigated. The thermoosmotic pressure, ΔP, and heat of transport, Q^*, for various values of temperature difference, ΔT, are reported. It is found that $Q^* = \Sigma c_i [Q_i^*]^0$, in agreement with earlier studies on binary mixtures, where c_i is the mass fraction and $[Q_i^*]^0$ is the heat of transport of pure component i.

Introduction

Recently Rastogi and coworkers[1-3] reported the thermoosmotic pressures of oxygen, ethylene, carbon dioxide, nitrogen, hydrogen sulfide, and mixtures of oxygen and carbon dioxide across unglazed porcelain. Linear phenomenological equations obtained on the basis of thermodynamics of irreversible processes were shown to be applicable within the range of investigation. The heats of transport of the mixtures were found to vary linearly with concentration. However, it is difficult to say whether this would also be true for ternary mixtures since no data have been available up to now.

In the present paper thermoosmosis of ternary mixtures of oxygen, ethylene, and carbon dioxide have been studied, and heats of transport of mixtures have been estimated using thermodynamics of irreversible processes.

Theoretical

We consider two compartments, filled with a multicomponent mixture, separated by a membrane having pores whose diameters are small enough to avoid purely viscous flow. The two compartments are kept at two different temperatures T_1 and T_2. Following the methods of nonequilibrium thermodynamics,[4] the rate of entropy production can be written as

$$\sigma = J_u X_u + \sum_{k=1}^{n} J_k X_k \qquad (1)$$

where J_u and J_k are the energy flow and mass flow of the kth component, respectively. The corresponding forces are given by

$$X_u = -\Delta(1/T) = \Delta T/T_m^2 \qquad (2)$$

$$X_k = -(\Delta\mu_k/T_m) + (\mu_k \Delta T/T_m^2) \qquad (3)$$

where ΔT and $\Delta\mu_k$ denote the difference in temperature and chemical potential, respectively, on the two sides of the membrane. T_m is the mean temperature, given by $(T_1T_2)^{1/2}$. Equation 3 can be written explicitly by using the equation

$$\Delta\mu_k = v_k \Delta P - s_k \Delta T + \sum_{i=1}^{n-1} \left(\frac{\partial \mu_k}{\partial c_i}\right)_{T,P,c_j} \Delta c_i \qquad (4)$$

where the c_j's are the quantities of the type c_i excluding c_i itself. c_i is the arithmatic mean[5] of the mass fraction of component i in the two compartments. v_k and s_k are the partial specific volume and partial specific entropy of component k.

For a multicomponent system, the linear phenomenological equations are given by

$$J_i = \sum_{k=1}^{n} L_{ik} X_k + L_{iu} X_u \qquad (6)$$

$$J_u = \sum_{k=1}^{n} L_{uk} X_k + L_{uu} X_u \qquad (7)$$

where L is the phenomenological coefficient. We define the energy of transfer U_k^* as follows

$$L_{iu} = \sum_{k=1}^{n} L_{ik} U_k^* \qquad (8)$$

so that

$$J_i = \sum_{k=1}^{n} L_{ik}[X_k + U_k^* X_u] \qquad (9)$$

From eq 2, 3, and 9, we obtain

$$J_i = \sum_{k=1}^{n} L_{ik}\left[v_k\Delta P/T_m + \sum_{i=1}^{n-1}\left(\frac{\partial \mu_k}{\partial c_i}\right)_{T,P,c_j}\frac{\Delta c_i}{T_m} + Q_k^*\Delta T/T_m^{\,2}\right] \tag{10}$$

Equation 10 represents the general equation for flow. In the case of a steady state such that the flow of matter is zero, we have

$$v_k\Delta P/T_m + \sum_{i=1}^{n-1}\left(\frac{\partial \mu_k}{\partial c_i}\right)_{T,P,c_j}\frac{\Delta c_i}{T_m} + Q_k^*\Delta T/T_m^{\,2} = 0 \tag{11}$$

For a three component system, we will have the following relations in the steady state

$$v_1\Delta P + \left(\frac{\partial \mu_1}{\partial c_1}\right)_{T,P,c_j}\Delta c_1 + \frac{Q_1^*\Delta T}{T_m} = 0 \tag{12}$$

$$v_2\Delta P + \left(\frac{\partial \mu_2}{\partial c_2}\right)_{T,P,c_j}\Delta c_2 + \frac{Q_2^*\Delta T}{T_m} = 0 \tag{13}$$

$$v_3\Delta P + \left(\frac{\partial \mu_3}{\partial c_3}\right)_{T,P,c_j}\Delta c_3 + \frac{Q_3^*\Delta T}{T_m} = 0 \tag{14}$$

According to the Gibbs–Duhem relation

$$c_1\Delta\mu_1 + c_2\Delta\mu_2 + c_3\Delta\mu_3 = 0 \tag{15}$$

Now multiplying eq 12, 13, and 14 by c_1, c_2, and c_3 respectively, and adding, we obtain

$$(c_1v_1 + c_2v_2 + c_3v_3)\Delta P + \left[c_1\left(\frac{\partial \mu_1}{\partial c_1}\right)_{T,P,c_j}\Delta c_1 + c_2\left(\frac{\partial \mu_2}{\partial c_2}\right)_{T,P,c_j}\Delta c_2 + c_3\left(\frac{\partial \mu_3}{\partial c_3}\right)_{T,P,c_j}\Delta c_3\right] + (c_1Q_1^* + c_2Q_2^* + c_3Q_3^*)\Delta T/T_m = 0 \tag{16}$$

Using eq 15 and 16 we obtain

$$(\Delta P/\Delta T)_{J_1=J_2=J_3=0} = -Q^*/vT_m \tag{17}$$

for $Q^* = c_1Q_1^* + c_2Q_2^* + c_3Q_3^*$ and $v = c_1v_1 + c_2v_2 + c_3v_3$. Since v is a linear function of T_m, a straight line should be obtained by plotting ΔP against $\Delta T/T_m^{\,2}$, provided Q^* is independent of the mean temperature.

When ΔT is large, eq 17 would be transformed as

$$(\Delta P/\Delta T)_{J_1=J_2=J_3=0} = -Q^*T_m/vT_1T_2 \tag{18}$$

Equation 18 would also be valid when $c_2 = 0$ and $c_3 = 0$. On solving eq 12–14 for Δc_1 and Δc_2 and keeping ΔT fixed, we obtain

$$\frac{\Delta c_1}{\Delta T} = \left[\left(\frac{\partial \mu_3}{\partial c_3}\right)_{T,P,c_j}(v_1Q_2^* - v_2Q_1^*) + \left(\frac{\partial \mu_2}{\partial c_2}\right)_{T,P,c_j}(v_1Q_3^* - v_3Q_1^*)\right]\Big/\left[v_1\left(\frac{\partial \mu_2}{\partial c_2}\right)_{T,P,c_j}\times\left(\frac{\partial \mu_3}{\partial c_3}\right)_{T,P,c_j} + v_2\left(\frac{\partial \mu_1}{\partial c_1}\right)_{T,P,c_j}\left(\frac{\partial \mu_3}{\partial c_3}\right)_{T,P,c_j} + v_3\left(\frac{\partial \mu_1}{\partial c_1}\right)_{T,P,c_j}\left(\frac{\partial \mu_2}{\partial c_2}\right)_{T,P,c_j}\right]\frac{1}{T} \tag{19}$$

$$\frac{\Delta c_2}{\Delta T} = \left[\left(\frac{\partial \mu_3}{\partial c_3}\right)_{T,P,c_j}(v_2Q_1^* - v_1Q_2^*) + \left(\frac{\partial \mu_1}{\partial c_1}\right)_{T,P,c_j}(v_2Q_3^* - v_3Q_2^*)\right]\Big/\left[v_1\left(\frac{\partial \mu_2}{\partial c_2}\right)_{T,P,c_j}\times\left(\frac{\partial \mu_3}{\partial c_3}\right)_{T,P,c_j} + v_2\left(\frac{\partial \mu_1}{\partial c_1}\right)_{T,P,c_j}\left(\frac{\partial \mu_3}{\partial c_3}\right)_{T,P,c_j} + v_3\left(\frac{\partial \mu_1}{\partial c_1}\right)_{T,P,c_j}\left(\frac{\partial \mu_2}{\partial c_2}\right)_{T,P,c_j}\right]\frac{1}{T} \tag{20}$$

In deriving the above equations the condition $c_1 + c_2 + c_3 = 1$ has been used.

TABLE I: Heats of Transport of Pure Component

	Heats of transport $[Q_i^*]^0$, cal/g		
P, cm	Oxygen	Ethylene	Carbon dioxide
5.4	−1.15 ± 0.01	−1.04 ± 0.01	−0.78 ± 0.03
9.3	−0.83 ± 0.05	−0.82 ± 0.02	−0.42 ± 0.01
11.0	−0.67 ± 0.04	−0.61 ± 0.02	−0.45 ± 0.02
17.7	−0.44 ± 0.04	−0.43 ± 0.02	−0.27 ± 0.01

TABLE II: Heat of Transport of Ternary Mixtures[a]

Mass fraction			Q^*, cal/g	
Oxygen	Ethylene	Carbon dioxide	Exptl	Using eq 21
0.601	0.223	0.176	−0.97 ± 0.01	−1.06 ± 0.1
0.480	0.250	0.270	−0.86 ± 0.02	−1.02 ± 0.1
0.324	0.254	0.422	−0.80 ± 0.02	−0.97 ± 0.08
0.092	0.188	0.720	−0.70 ± 0.02	−0.86 ± 0.08
0.085	0.050	0.865	−0.65 ± 0.02	−0.83 ± 0.08

[a] Pressure = 5.4 cm, mean temperature = 59°.

TABLE III: Heat of Transport of Ternary Mixtures[a]

Mass fraction			Q^*, cal/g	
Oxygen	Ethylene	Carbon dioxide	Exptl	Using eq 21
0.669	0.111	0.220	−0.68 ± 0.03	−0.74 ± 0.05
0.617	0.189	0.194	−0.72 ± 0.05	−0.75 ± 0.05
0.337	0.185	0.478	−0.66 ± 0.02	−0.63 ± 0.04
0.180	0.149	0.671	−0.57 ± 0.01	−0.56 ± 0.04

[a] Pressure = 9.2 cm, mean temperature = 50°.

TABLE IV: Heat of Transport of Ternary Mixtures[a]

Mass fraction			Q^*, cal/g	
Oxygen	Ethylene	Carbon dioxide	Exptl	Using eq 21
0.689	0.107	0.204	−0.62 ± 0.02	−0.64 ± 0.04
0.608	0.152	0.240	−0.61 ± 0.01	−0.63 ± 0.04
0.475	0.146	0.379	−0.58 ± 0.01	−0.59 ± 0.04
0.343	0.186	0.471	−0.56 ± 0.01	−0.56 ± 0.04

[a] Pressure = 11.0 cm, mean temperature = 50°.

Experimental and Results

Thermoosmotic pressures for gaseous mixtures of different composition were measured using the experimental procedure described previously.[1,2] The gases were introduced successively and their partial pressure noted, which gave the mass fraction of each component. The thermoosmotic pressure ΔP and the corresponding ΔT were measured for different mean temperatures at a fixed pressure. The measurements were repeated for different pressures. Q^* was calculated using eq 18 knowing the experimental values of ΔP, ΔT, and T_m. The means of several values of Q^* calculated for different mean temperatures are recorded in the Tables I–V. We shall call this Q^* the experimental Q^*. The uncertainty in Q^* due to uncertainty in ΔP and ΔT would not exceed ±0.05 cal/g. The experimental Q^* values for different mean temperatures at a fixed pressure do not deviate more than ±0.05 cal/g from the mean

TABLE V: Heat of Transport of Ternary Mixtures[a]

Mass fraction			Q^*, cal/g	
Oxygen	Ethylene	Carbon dioxide	Exptl	Using eq 21
0.738	0.110	0.152	−0.42 ± 0.02	−0.42 ± 0.03
0.622	0.168	0.210	−0.40 ± 0.01	−0.41 ± 0.03
0.572	0.175	0.253	−0.39 ± 0.01	−0.40 ± 0.03
0.365	0.203	0.432	−0.37 ± 0.01	−0.37 ± 0.03

[a] Pressure = 17.7 cm, mean temperature = 49°. Experimental data show that eq 21 is satisfied within experimental error although Knudsen conditions do not obtain. This shows that the three components migrate independently of each other as was found in the case of binary mixtures. The dusty gas model theory of Mason[7,8] predicts eq 21 only for Knudsen gases. The deviation from Knudsen conditions in the present case may affect Q^* values to such an extent that it may not be possible to detect the deviations from eq 21 at the present level of experimental accuracy or else the dusty gas model may be a poor approximation. More work is needed to settle this point.

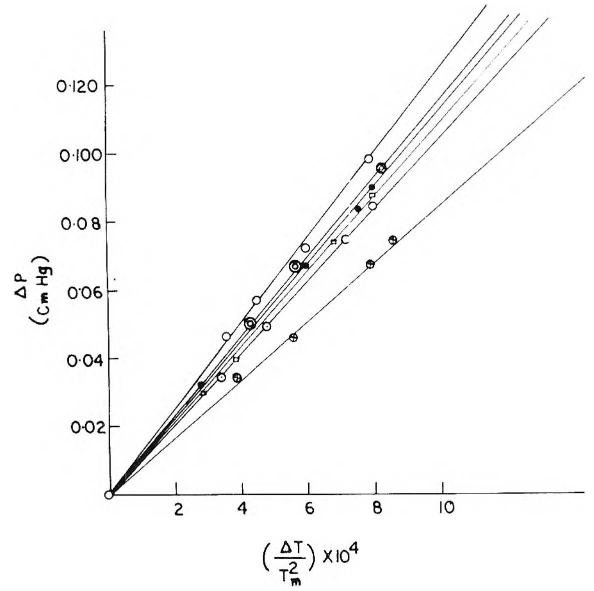

Figure 1. Thermoosmotic pressure of ternary gaseous mixtures: (○) oxygen; (◎) ethylene; (⊗) carbon dioxide; (●) ternary mixture containing oxygen, ethylene, and carbon dioxide: $C_{O_2} = 0.617$, $C_{C_2H_4} = 0.189$, $C_{CO_2} = 0.194$; (□) $C_{O_2} = 0.337$, $C_{C_2H_4} = 0.185$, $C_{CO_2} = 0.478$; (⊙) $C_{O_2} = 0.180$, $C_{C_2H_4} = 0.149$, $C_{CO_2} = 0.671$.

Q^* recorded in Tables I–V and therefore are within experimental error. This shows that Q^* is independent of temperature. This is further confirmed by the fact that when ΔP is plotted against $\Delta T/T_m^2$, a straight line is obtained (Figure 1).

Discussion

Results recorded in Tables I–V show that the data satisfy eq 18. It is known that for a Knudsen gas, $[Q_i^*]^0 = -RT/2M$. The experimental values of $[Q_i^*]^0$ for oxygen, ethylene, and carbon dioxide recorded in Table I do not agree with this expression showing thereby that the present case does not conform to Knudsen behavior. The observed pressure dependence of the heat of transport supports this conclusion. The values of the heat of transport for a ternary mixture Q^* are recorded in Tables II–V along with the values of Q^* calculated from the relation

$$Q^* = \sum c_i[Q_i^*]^0 \qquad (21)$$

where $[Q_i^*]^0$ is the heat of transport of pure component i. The experimental and theoretical values of Q^* for mixtures recorded in columns 4 and 5 of Tables II–V are in agreement within experimental error. The uncertainty in the calculated value of Q^* in Table II was larger because of the low partial pressures used.

Acknowledgment. The authors are thankful to the Indian Council of Scientific and Industrial Research for supporting the investigation and to Shri M. L. Yadava for very fruitful discussions.

References and Notes

(1) R. P. Rastogi, K. Singh, and H. P. Singh, *J. Phys. Chem.*, **73**, 2798 (1969).
(2) R. P. Rastogi and H. P. Singh, *J. Phys. Chem.*, **74**, 1946 (1970).
(3) R. P. Rastogi, P. C. Shukla, and B. Yadava, *Biochim. Biophys. Acta*, 249 (1971).
(4) S. R. de Groot, "Thermodynamics of Irreversible Processes," North-Holland Publishing Co., Amsterdam, 1952.
(5) It has been suggested[6] that for transformation from a local formulation to a finite difference formulation, the mean concentration

$$c_i = \tfrac{1}{2}(c_i^A + c_i^B)$$

or

$$c_i = (c_i^B - c_i^A)/\ln(c_i^B/c_i^A) \qquad (5)$$

where A and B refer to the two sides of the membrane. In the present paper the former type of average has been taken for computing the local concentration since the linear phenomenological relation which makes use of it is valid over a wider range.
(6) E. A. Mason, R. P. Wendt, and E. H. Bresler, *J. Chem. Soc., Faraday Trans. 2*, **68**, 1938 (1972).
(7) A. P. Malinauskas and E. A. Mason, *Trans. Faraday Soc.*, **67**, 2243 (1971).
(8) E. A. Mason, R. B. Evans, III, and G. M. Watson, *J. Chem. Phys.*, **38**, 1808 (1963); R. E. Jerkins and E. A. Mason, *Phys. Fluids*, **13**, 2478 (1970).

COMMUNICATIONS TO THE EDITOR

On the Carcinogenicity of Bis(chloromethyl) Ether and Chloromethyl Methyl Ether

Publication costs assisted by Polaroid Corporation

Sir: Recently a paper dealing with the hydrolysis of bis-(chloromethyl) ether (bis-CME) appeared in this journal.[1] Although we find the chemistry described in this paper to be a contribution to science, we are deeply concerned over the introductory paragraph of this article. References are given documenting the cancer-causing properties of bis-CME. It is also stated that bis-CME is an impurity contained in the commonly used chloromethylating agent, chloromethyl methyl ether (CMME). Thus the inference is that CMME is only to be feared if bis-CME is present as an impurity.

We wish to point out that current regulations of the Occupational Safety and Health Administration (OSHA) list both CMME as well as bis-CME as carcinogens and very strict precautions are required when dealing with both of these compounds. The regulations state that although there is confusion in some of the testing due to the presence of bis-CME in CMME, nonetheless purified CMME has also been shown to have carcinogenic potential in animals.[2]

We thus feel that this latter reference and regulation should also have been given in the introductory paragraph of the paper.

References and Notes

(1) J. C. Tow, L. B. Westover, and L. F. Sonnabend, *J. Phys. Chem.*, **78**, 1096 (1974).
(2) *Fed. Regist.*, **39**, 3757 (1974).

Chemical Research Laboratories
Polaroid Corporation
Cambridge, Massachusetts 02139

Lloyd D. Taylor*
Myron S. Simon

Received July 17, 1974

Scavenging of Electrons in 3-Methylpentane Glass at 77 K

Sir: When molecules which can react with electrons to form stable negative ions are present in an organic matrix during irradiation, they scavenge the electrons in competition with physical trapping and neutralization.

It has been found that after irradiation of such a system, the concentration of trapped electrons, e_t^-, decreases and that of negative ions increases.[1-5] Transfer of e_t^- to biphenyl, Bph, in γ-irradiated 3-methylpentane (3MP) glass, for example, has been observed using spectrophotometric[1-3] and pulse radiolysis[4,5] techniques. We report here experiments which provide new information concerning these phenomena.

Deaerated 3MP glass containing 1 m*M* Bph was γ-irradiated to 8×10^{21} eV $l.^{-1}$ at 77 K. The concentrations of e_t^- (at 1550 nm) and biphenyl anions, Bph^- (at 408 nm), were measured at 77 K, using a Beckman DK-2A *spectrophotometer*. The measurements were done either by repetitive scanning of the complete spectrum of the sample from 2700 to 360 nm (case I) or at 30-min intervals (case II). The results of these experiments for Bph^- are shown in Figure 1a. In case I, growth of Bph^- absorption is observed whereas in case II the Bph^- concentration remains practically unchanged. When the irradiated sample is kept in the dark for 30 min in a 77 K cell compartment and then again subjected to illumination for 30 min by a spectrophotometric lamp set at 1000 nm, the growth of Bph^- is again observed. No appreciable influence of such treatment on electron decay in pure 3MP glass has been observed. The results of the above experiments strongly suggest that after irradiation Bph reacts mainly with photobleached electrons. If so, the bleaching effect should be particularly im-

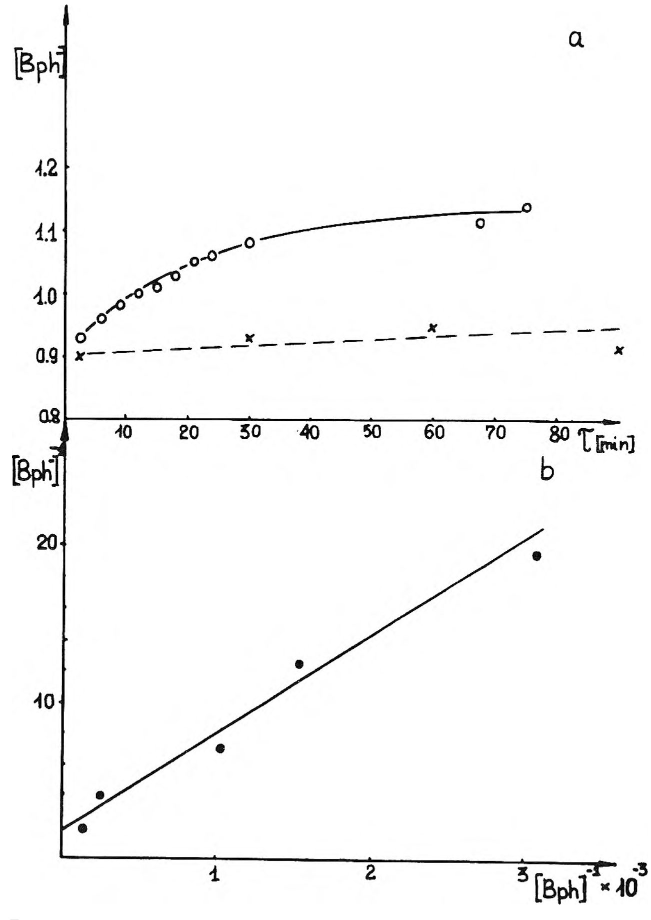

Figure 1. (a) The dependence of Bph^- concentration on time after γ-irradiation of 3MP glass containing 1 m*M* Bph, 5-mm cell: (O) repetitive scanning of the complete spectrum (case I); (X) spectrophotometric analysis performed every 30 min (case II). (b) $[Bph^-]^{-1}$ as a function of $[Bph]^{-1}$ in 3MP glass at 77 K: the pulse radiolysis experiments, 5-mm cell, 4-nm monochromator bandwidth.

portant in pulse radiolysis experiments at 77 K, since the intensity of analyzing light in these measurements is very high compared with that used in standard spectrophotometry.

In our pulse radiolysis experiments we have used a 13-MeV linear accelerator, type LAE-139 (USSR made). The degassed samples were positioned in a special shielded dewar (with Spectrosil windows) filled with liquid nitrogen. The dose in a single 2.5-μsec pulse was ~35 Krads. An EMI 9558Q photomultiplier in conjunction with a 556 Tektronix oscilloscope has been used as detection equipment.[6] In order to minimize the possibility of optical bleaching by the 450-W Xe lamp, the appropriate blue filter (maximum at 420 nm and 80 nm-half-bandwidth) and 1-cm cell filled with water were placed between the lamp and the sample cell. The above combination allowed us to observe the Bph^- absorption at 405 nm whereas the ir light did not reach the sample. Additionally, the neutralizing filters have been used to decrease the intensity of analyzing light.

Using such precautions we have observed no growth of Bph^- absorption at 405 nm for 3MP glass containing ~1 and ~3.9 mM Bph, in the time range from 10^{-5} to 5 sec.

The linear dependence of the reciprocal of Bph^- absorption, taken at 10 μsec after the pulse, against the reciprocal of Bph concentration (Figure 1b) seems to support our conclusion that Bph reacts mainly with mobile or photodetrapped electrons. Taking into account the slope of this dependence (Figure 1b) we are able to calculate the ratio of the rate constants of electron trapping (k_t) and scavenging by Bph (k_s); $k_t/k_s = 3.5 \times 10^{-3}$. The results of our experiments indicate that some of the previously reported data on trapped electron scavenging may be essentially affected by electron bleaching under the influence of analyzing light and in fact cannot be referred to trapped electron reactions.

References and Notes

(1) W. H. Hamill in "Radical Ions," E. T. Kaiser and L. Kevan, Ed., Wiley, New York, N.Y., 1968, Chapter 9.
(2) J. R. Miller, *J. Chem. Phys.*, **56**, 5173 (1972).
(3) J. Kroh and J. Mayer, *Int. J. Radiat. Phys. Chem.*, in press.
(4) J. T. Richards and J. K. Thomas, *J. Chem. Phys.*, **53**, 218 (1970).
(5) N. V. Klassen, H. A. Gillis, and G. G. Teather, *J. Phys. Chem.*, **76**, 3847 (1972).
(6) Z. Zimek Ph.D. Thesis, Institute of Nuclear Research, Warsaw, 1974.

The Institute of Radiation Technics
Technical University
Lodz, Poland
J. Kroh*
J. Mayer
E. Wojciechowska

Department of Radiation Chemistry
Institute of Nuclear Research
Warsaw, Poland
J. Grodkowski

Received May 15, 1974

ADDITIONS AND CORRECTIONS

1964, Volume 68

R. M. Wallace and S. M. Katz: A Method for the Determination of Rank in the Analysis of Absorption Spectra of Multicomponent Systems.

Page 3891. The third term in eq 2 should read

$$S_{i1}{}^{2}\left(\frac{A_{1j}}{A_{11}}\right)^{2} \text{ instead of } S_{i1}{}^{2}\left(\frac{A_{ij}}{A_{11}}\right)^{2}$$

We wish to thank Laszlo Bodoni for bringing this error to our attention.—Richard M. Wallace

1973, Volume 77

J. A. Ghormley, R. L. Ellsworth, and C. J. Hochanadel: Reaction of Excited Oxygen Atoms with Nitrous Oxide. Rate Constants for Reaction of Ozone with Nitric Oxide and with Nitrogen Dioxide.

Page 1345. In the right-hand column, line 15, the correct expression for k_6 is $k_6 = 2.303$ slope/(2$[O_3]_0$ − $[NO_2]_0$), giving the value $k_6 = 1.9 \pm 0.3 \times 10^4\ M^{-1}\ \text{sec}^{-1}$. We thank Earl D. Morris, Jr., of the Ford Motor Company for calling the error to our attention.—C. J. Hochanadel

Kazuo Kikuchi and Koshiro Yoshioka: Electric Birefringence of Potassium Polystyrenesulfonate in Aqueous Solution as a Function of Molecular Weight, Concentration, and Field Strength.

Page 2106. In the right-hand column, the sentence below eq 30 (line 2) should read as follows: "Equation 30 is the same as the expression for the saturated induced dipole moment."—Koshiro Yoshioka

Anders Lund and Larry Kevan: Free Radical Formation in Hydrocarbon Crystals by γ Irradiation. Anisotropic Hyperfine Couplings in $CH_3\dot{C}H(CH_2)_{33}CH_3$ and Relative Radical Yields in Single Crystal Hexatriacontane.

Page 2180. We have found that the crystal provided to us in this work was n-$C_{20}H_{42}$ instead of n-$C_{36}H_{74}$. We have confirmed this by its melting point. Fortunately, the even alkanes crystalize in a similar way (see ref 5 in paper), so the epr analysis and conclusions are unchanged except for the length of the radicals studied.

Kenneth S. Pitzer and Guillermo Mayorga: Thermodynamics of Electrolytes. II. Activity and Osmotic Coefficients for Strong Electrolytes with One or Both Ions Univalent.

Page 2301. In Table III the parameters for the tetraalkylammonium chlorides and bromides (but not the fluorides or iodides) should be increased as follows: for $\beta^{(0)}$, +0.0281$_5$; for $\beta^{(1)}$, +0.0542; for C^{ϕ}, +0.00211. For $(Et)_4NI$ corrected constants are $\beta^{(0)} = -0.179$, $\beta^{(1)} = -0.571$, and $C^{\phi} = 0.0412$.

Page 2303. Sign errors should be corrected by reversing the sign of E in eq 12, the signs of the last two terms in eq 13, and the sign preceding $2m$ in eq 15.—Kenneth S. Pitzer

1974, Volume 78

John D. Petersen and Peter C. Ford: Photochemistry of Rhodium(III) Complexes. Ligand Field Excitation of Hexaamminerhodium(III) and Characteristics of Nonradiative Deactivation Paths.

Page 1146. The caption for Figure 1, "Spectrum of $Ru(NH_3)_6{}^{3+}$ . . . ," should read "Spectrum of $Rh(NH_3)_6{}^{3+}$ . . . ."—Peter C. Ford

AUTHOR INDEX to Volume 78, 1974

Note: In this Author Index, titles of papers are listed after the name of each author of the paper. Multiple authorship is not indicated. Complete authorship may be ascertained by consulting the original paper.

Ache, H. J. Approximate molecular orbital study of organic positron and positronium complexes. 2683
Ache, H. J. Stereochemistry of the decay-induced gas-phase halogen exchange in diastereomeric 2,3-dichlorobutanes. 1043
Ache, H. J. Reactivity of aromatic compounds toward positronium atoms. 1881
Acrivos, J. V. Insertion compounds of transition element disulfides. 2399
Adam, W. Mechanism of direct and rubrene enhanced chemiluminescence during α-peroxylactone decarboxylation. 2559
Adams, W. A. High-pressure laser raman spectroscopic investigation of aqueous magnesium sulfate solutions. 246
Ahluwalia, J. C. Temperature dependence of limiting heat capacities of dissolution of tetrabutylphosphonium bromide, tetraphenylphosphonium bromide, and tetraphenylarsonium chloride in water and hydrophobic hydration. 738
Ahumada, J. J. Chemical kinetic effects of walls on active species. Results for hydrogen atoms. 465
Aksay, I. A. Wetting under chemical equilibrium and nonequilibrium conditions. 1178
Alcacer, L. Electrically conducting metal dithiolate-perylene complexes. 215
Alchalel, A. Role of the triplet state in the photoisomerization of retinal isomers. 336
Alegria, A. E. Equilibrium studies by electron spin resonance. VIII. Use of time averaged coupling constants to determine free ion-ion pair equilibrium constants. 1771
Alexander, A. G. Photolysis of hydrogen sulfide in the presence of dimethylsilane. 203
Allaert, J. Disproportionation and recombination of cyclopentyl radicals. 462
Allen, A. O. Chemical reaction rates of quasi free electrons in nonpolar liquids. 796
Alvord, H. Chemiluminescent reactions of disulfur monoxide. 1248
Amey, R. L. Apparent quadrupole moments of carbon monoxide and nitrogen and their librational motion in the liquid state. 1968
Ander, P. Self-diffusion coefficients for chloride ion in aqueous solutions of sodium polyacrylate containing sodium chloride. 1756
Andermann, G. Chlorine Kβ x-ray emission spectra of several solid organic chlorine compounds. 2592
Anderson, C. W. Programmed temperature dehydration studies of octacalcium phosphate. 1631
Anderson, H. L. Heats of mixing and heats of dilution of tetrapropylammonium chloride. Temperature dependence. 77
Anderson, J. E. Membrane-water partition coefficients of ions. Calculated effects of membrane thickness. 2259
Anderson, K. P. Complex solubility of silver iodide in ethanol-water, methanol-water, acetone-water, and dioxane-water mixtures. 2244
Angell, C. A. Heat capacities and fusion entropies of the tetrahydrates of calcium nitrate, cadmium nitrate, and magnesium acetate. Concordance of calorimetric and relaxational ideal glass transition temperatures. 278
Aniansson, E. A. G. Kinetics of step-wise micelle association. 1024
Anpo, M. Photochemistry in the adsorbed layer. I. Photolyses of alkyl ketones in the presence of nitric oxide. 2442
Anpo, M. Photochemistry in the adsorbed layer. II. Energy transfer in the adsorbed layer. 2446
Arai, S. Low-temperature pulse radiolysis. I. Negative ions of halogenated compounds. 519
Arai, S. Low-temperature pulse radiolysis. II. Time-dependent spectra of anions of aromatic ketones. 1473
Arshadi, M. R. High-pressure mass spectrometry. V. Thermodynamics of solvation reactions. NH_4^+-NH_3. 1482
Arvis, M. Isothermal flash photolysis of hydrazine. 1356
Ash, S. K. Metachromasia of basic dyes induced by mercuric chloride. II. 536
Asmus, K. D. Formation of positive ions in the reaction of disulfides with hydroxyl radicals in aqueous solution. 282
Atkinson, G. Ultrasonic absorption in aqueous solutions of calcium acetate and other bivalent metal acetates. 1913
Atkinson, R. Absolute rate constants for the reaction of O(^{3}P) atoms with selected alkanes, alkenes, and aromatics as determined by a modulation technique. 1780
Avila, M. J. Photolysis of diazo-n-propane. Route for the photochemical activation of propylene. 1348
Babiak, S. Solvent effects on the fluorescence lifetime of 2-aminopyridine. 201
Baer, S. Stable intermediates in kinetic models of catalase action. 1919
Baker-Blocker, A. Chemiluminescent reactions of disulfur monoxide. 1248
Balcerski, J. S. Time-dependent Hartree calculations of the sequence dependence of DNA hypochromism. 444
Baleiko, M. O. Diffusion and thermal diffusion in binary dense gas mixtures of loaded spheres and rough spheres. 1564
Bales, B. L. Electron paramagnetic resonance and electron-nuclear double resonance line shape studies of trapped electrons in γ-irradiated deuterium-substituted 10 M sodium hydroxide alkaline ice glass. 221
Bales, S. E. Ion association between naphtho[b]cyclobutene radical anion and alkali metal ions. 723
Balzani, V. Intersystem crossing efficiency in the hexacyanochromate(III) ion. 541
Balzani, V. Dynamic and static quenching of the tris(2,2'-dipyridyl)ruthenium(II) phosphorescence by anionic coordination compounds in various solvents. 1374
Bandmann, H. Radiation chemistry of ethers. V. Solvated electrons from excited (λ 185 nm) p-dioxane. 2181
Bansal, K. M. Pulse radiolytic polarography. Competitive oxidation and reduction of hydroxycyclohexadienyl radicals at the mercury drop electrode in aqueous solutions. 160
Barcza, L. Heteroconjugation of inorganic anions in nonaqueous solvents. II. Perchlorate complexes of some organic hydroxy compounds. 168
Bard, A. J. Simultaneous electrochemical-electron spin resonance measurements. II. Kinetic measurments using constant current pulse. 290
Bard, A. J. Simultaneous electrochemical-electron spin resonance measurements. III. Determination of rate constants for second-order radical anion dimerization. 295
Barkatt, A. Yields of radiation products in sodium metaphosphate glasses. 752
Barker, B. J. Conductance behavior of some ammonium and partially substituted ammonium tetraphenylborates in 3-methyl-2-oxazolidone and 3-tert-butyl-2-oxazolidone at 25°. 2687
Barker, B. J. Conductance behavior of tetraalkyammonium salts in 3-tert-butyl-2-oxazolidone at 25°. 2689
Barker, J. R. Intramolecular vibrational energy relaxation. Decomposition of a series of chemically activated fluoroalkyl cyclopropanes. 2535
Barnes, J. A. Spectra and structure of boron-nitrogen compounds. II. Infrared and Raman spectra of trimethylamine-borane. 1503
Barthomeuf, D. Crystal structure of a dealuminated Y-type zeolite. 1550
Bartle, K. D. Proton magnetic resonance study of molecular interactions in solutions of fluoranthene in carbon tetrachloride and cyclohexane. 1330
Bartocci, C. Wavelength dependence of nitropentaamminecobalt(III) photochemistry. Charge transfer and ligand field excited-state behavior. 572
Bartocci, C. Mechanism of photosubstitution reactions of square-planar platinum(II) complexes. II. Effect of the leaving ligand on the photosubstitution mechanism of diethylenetriamineplatinum(II) complexes. 2349
Barzaghi, M. Geometry and electronic structure of nitrostyrene molecules and anions. 49
Bascom, W. D. Mechanism of the hydrolysis of triethylethoxysilane at the silica-carbon tetrachloride interface. Reply to comments. 758
Bass, A. M. Rate constants for reactions of methylene with carbon monoxide, oxygen, nitric oxide, and acetylene. 1344
Bauer, S. H. Relative cis-trans isomerization rates. Another test of the energy randomization hypothesis. 770
Bauer, S. H. Thermochemical state of gaseous electron diffraction samples. 2380
Bauer, S. H. Reinvestigation of the structure of perfluoroethane by electron diffraction. 2389
Baughman, E. H. Determination of acidity in 80% dimethyl sulfoxide-20% water. 421
Baur, M. E. Dielectric properties of liquid sulfur in the ring-chain transition region 1670
Beaumont, R. Crystal structure of a dealuminated Y-type zeolite. 1550
Beebe, R. A. Programmed temperature dehydration studies of octacalcium phosphate. 1631
Behar, D. Electron spin resonance study of the radiolysis of aqueous solutions of cyanate ion. 1074
Behar, D. Pulse radiolysis study of aqueous hydrogen cyanide and cyanide solutions. 2660
Bell, A. Growth mechanism of hydrous chromium(III) oxide spherical particles of narrow size distribution. 2621
Ben-Naim, A. Effects of solutes on the strength of hydrophobic interaction and its temperature dependence. 170
Ben-Naim, A. Solvophobic interaction. 175
Bennett, S. L. High-temperature vaporization of ternary systems. I. Mass spectrometry of oxygen-rich vanadium-tungsten-oxygen species. 266
Bent D. V. Laser flash photolysis of substituted stilbenes in solution. 446
Bent D. V. Evidence for the triplet route in the photochemical trans → cis isomerization of nitrostilbenes in solution. 451
Ben Taarit, Y. Temperature dependence of hyperfine coupling for copper complexes in sodium Y zeolite. 531
Bente, H. B. Inelastic scattering of vibrationally excited potassium bromide by polyatomic partners. 2438
Bergmann, E. Isotherm for mobile physiscrption of noble gases. 405
Bernardi, F. Theoretical interpretation of the rotational barrier in benzophenone ketyl. 2144
Bernas, A. Electron capture in γ-irradiated methylcyclohexane glass. 867
Bernhard, W. A. Electron spin resonance study of γ-irradiated silver diethyl phosphate. 958

Bernier, P. Investigation of the hydrophobic interaction between tert-butyl alcohol and paramagnetic solutes in aqueous solutions by proton nuclear magnetic resonance relaxation. 851
Bertrand, C. Ions in ammonia flames. 2320
Bertrand, C. Photolysis of 2-methyl-1-butene at photon energies below and above the ionization energy. 98
Beruto, D. Transition state theory for vaporization and condensation. 1298
Beveridge, D. L. Statistical thermodynamic consideration of solvent effects on conformational stability. Supermolecule-continuum model. 2064
Beverly, G. D. Hot hydrogen atom-hydrocarbon reactions. Dependence of yields on structure and energy. 559
Bhatia, K. Radiation chemical studies on systems related to ascorbic acid. Radiolysis of aqueous solutions of α-bromotetronic acid. 1063
Bhatia, K. Oxidation of hydroxycyclohexadienyl radical by metal ions. 2335
Bibler, N. E. Curium-244 α radiolysis of nitric acid. Oxygen production from direct radiolysis of nitrate ions. 211
Bigelow, R. W. Photoconductivity of trinitrofluorenone in tetrahydrofuran. 1395
Bills, J. L. Singlet-triplet separation in helium. 1334
Bina, M. J. The $a^3\Pi_{0^+} \rightarrow X^1\Sigma^+$ system of bromine chloride. 1833
Blander, M. Phase diagrams of reciprocal molten salt systems. Calculations of liquid-liquid miscibility gaps. 1091
Blander, M. Lithium-lithium hydride system. 1933
Blokhra, R. L. Nonequilibrium thermodynamic studies of electrokinetic effects. V. Onsager's reciprocity relations. 2302
Blyholder, G. Hydrocarbon surface species on cobalt. 618
Bobik, M. Mixtures of trifluoroacetic acid with acetic acid and carbon tetrachloride 1709
Boettcher, J. W. Calorimetric and spectrophotometric comparison of adducts of phenol and deuteriophenol. 429
Bogsanyi, D. Physical properties and electrochemical stability of the thio solvents dimethylthioformamide and hexamethylphosphorothioic triamide. 1018
Bolletta, F. Dynamic and static quenching of the tris(2,2'-dipyridyl)ruthenium(II) phosphorescence by anionic coordination compounds in various solvents. 1374
Bolton, P. H. Anaerobic chemiluminescent reaction of aryl Grignard reagents with aryl peroxides. 1896
Bone, L. I. Ion-molecule reactions in methanol and hydrogen sulfide. 2527
Bone, L. I. Reactions of nitrogen oxide (NO^+) ion with methanol. 501
Bonifacic, M. Formation of positive ions in the reaction of disulfides with hydroxyl radicals in aqueous solution. 282
Bonneau, R. Laser flash photolytic study of mercury(II) iodide in aqueous solution. 1698
Bonner, O. D. Hydrogen bonding of water in organic solvents. 1. 1723
Bonner, O. D. Hydrogen bonding of water in organic solvents. II. Change of water structure with composition. 1727
Bos, A. Matrix isolation infrared study of the reaction between germanium vapor and molecular oxygen. Characterization and mechanism of formation of moleclar germanium dioxide and ozone. 1763
Bose, R. A. Electrical relaxation in a glass-forming molten salt. 639
Bowen, D. E. Ultrasound propagation in binary mixtures of dimethyl sulfoxide and water. 2611
Boyd, D. Simultaneous electrochemical-electron spin resonance measurements. III. Determination of rate constants for second-order radical anion dimerization. 295
Boyd, D. B. Sequence and shape of the molecular orbitals of the disulfide hydrogen persulfide. 1554
Boyd, D. B. Electronic structures of cephalosporins and penicillins. III. EH [extended Hueckel] and CNDO/2D electron density maps of 7-amino-3-cephem. 2604
Boyd, G. E. Mobility of organic cations in cross-linked polyelectrolyte gels. Measurements of the self-diffusion of tetramethylammonium ion. 735
Boyd, G. E. Thermodynamic calculations of equilibrium constants for ion-exchange reactions between unequally charged cations in polyelectrolyte gels. 1110
Brabson, G. D. The $a^3\Pi_{0^+} \rightarrow X^1\Sigma^+$ system of bromine chloride. 1833
Brand, J. C. D. Singlet-triplet intersystem coupling in formaldehyde. 2270
Brandon, J. R. Solvated electrons in alcohol-alkane and alcohol-amine solutions. 792
Breslauer, K. J. Thermodynamics of transfer of molecules and groups from nonpolar to aqueous environments. I. Method. Butyric acid at 25°. 2363
Brocklehurst, B. Triplet formation in ion recombination in spurs. Comment. 309
Brookes, B. I. Effect of silylation upon the hydrogenating activity of supported platinum catalysts. 875
Brown, M. E. Thermal decomposition of three crystalline modifications of anhydrous copper(II) formate. 2664
Brown, R. G. Mechanisms of electronic energy transfer in the gas phase. 2407
Bruno, G. V. Analysis of inertial effects on electron spin resonance spectra in the slow tumbling region. 935
Bruylants, A. Charge-transfer complexes in organic chemistry. XI. Effect of acceptors on the properties of charge-transfer complexes formed by cyclic anhydrides. 980
Buckfelder, J. Potential function model of weak and strong hydrogen bonds. 1415
Bunton, C. A. Micellar effects on the ionization of carboxylic acids and interactions between quaternary ammonium ions and aromatic compounds. 1490
Burggraf, L. W. Pulse radiolysis of liquid n-pentane and n-pentane-oxygen solutions. Rate constants and activation energies for second-order decay of pentyl and pentylperoxy radicals. 508
Burrows, H. D. Optical spectra and reactivities of radical anions of 4-nitrobenzyl compounds produced by pulse radiolysis of acetonitrile solutions. 112
Burwell, R. L. Jr. Effect of silylation upon the hydrogenating activity of supported platinum catalysts. 875
Bush, C. A. Theoretical treatment of the circular dichroism of N-acetyl amino sugars. 1829
Butler, E. A. Complex solubility of silver iodide in ethanol-water, methanol-water, acetone-water, and dioxane-water mixtures. 2244
Butler, S. M. Determination of the equivalence point of the nitrogen + nitric oxide titration reaction by electrical conduction. 1120
Cabani, S. Volumetric properties of aqueous solutions of organic compounds. III. Aliphatic secondary alcohols. cyclic alcohols, primary, secondary, and tertiary amines. 1030
Cady, S. S. Aromatic radical cation formation on the intracrystal surfaces of transition metal layer lattice silicates. 994
Campano, D. D. Generation of radicals in the charge-transfer photochemistry of coordination complexes of colbalt(III) in aqueous solution. 686
Carassiti, V. Mechanism of photosubstitution reactions of square-planar platinum(II) complexes. II. Effect of the leaving ligand on the photosubstitution mechanism of diethylenetriamineplatinum(II) complexes. 2349
Carlson, K. D. Reinvestigation of the symmetric stretching mode of matrix-isolated dialuminum monoxide. 236
Carmichael, H. Radiolysis of 1,1-difluoroethane. 2183
Carruthers, L. M. Intermolecular potentials from crystal data. III. Determination of empirical potentials and application to the packing configurations and lattice energies in crystals of hydrocarbons, carboxylic acids, amines, and amides. 1595
Carruthers, L. M. Intermolecular potentials from crystal data. IV. Application of empirical potentials to the packing configurations and lattice energies in crystals of amino acids. 1621
Carter, W. P. Behavior of collisional efficiencies in external activation systems. 612
Carter, W. P. L. Homoallylic isomerization of 1-penten-4-yl and the critical energy for methyl + 1,3-butadiene. 1245
Carter, W. P. L. Ring opening of chemically activated cyclopentyl and methylcyclobutyl radicals. 1573
Carter, W. P. L. Analysis of external activation systems with multiple isomerizations and decompositions. 1579
Carter, W. P. L. Reactions of chemically activated pentenyl radicals. Kinetic parameters of 1,4 hydrogen shifts and the cis-trans isomerization of homoallylic radicals. 2201
Casey, G. J. Jr. Potential function model of weak and strong hydrogen bonds. 1415
Cassel, R. B. Heats of mixing aqueous electrolytes. XI. Charge-asymmetric limiting law at low concentrations. Barium chloride with sodium chloride and sodium sulfate with sodium chloride. 1924
Cassel, R. B. Interactions of aqueous electrolytes with nonelectrolytes. Enthalpy of dilution of urea and tert-butyl alcohol in salt solutions. 2460
Cassel, R. B. Heat of mixing aqueous nonelectrolytes at constant molality. Sucrose, urea, and glycine. 2465
Castelli, F. Absolute quantum yields of ${}^2E_g \rightarrow {}^4A_{2g}$ luminescence in potassium hexacyano(cobaltate, chromate) powders. 2122
Cate, R. L. 2537-Ang mercury-sensitized photochemical decomposition of perfluorocyclobutane. 2071
Cavanaugh, J. R. Nuclear magnetic resonance studies of frozen aqueous solutions. 807
Cercek, B. Solvent participation in electron transfer reactions. 285
Chachaty, C. Electron spin resonance of γ irradiation induced free radicals in polyvinylpyridines. 899
Chambers, J. Q. Effect of water-hydrocarbon interactions on proton mobility. Chronoamperometric diffusion coefficients in aqueous tert-butyl alcohol. 70
Chambers, R. W. Effect of dimer formation on the electronic absorption and emission spectra of ionic dyes. Rhodamines and other common dyes. 380
Chang, S-G. Photolysis of nitric acid vapor. 1
Chang, Y-L. T. Experimental determination and scaled particle theory calculation of the activity coefficients of benzene and cyclohexane in aqueous sodium chloride solutions. 165
Chantooni, M. K. Jr. Transfer activity coefficients of ortho-substituted and non-ortho-substituted benzoates between water, methanol, and polar aprotic solvents. 839
Chao, C-C. Infrared and electron paramagnetic resonance study of some silver-nitric oxide complexes in Y type zeolites. 1174
Chao, K. J. Intramolecular vibrational energy relaxation. Decomposition of a series of chemically activated fluoroalkyl cyclopropanes. 2535
Chatterjee, R. M. High-pressure laser raman spectroscopic investigation of aqueous magnesium sulfate solutions. 246
Chawla, B. Temperature dependence of limiting heat capacities of dissolution of tetrabutylphosphonium bromide, tetraphenylphosphonium bromide, and tetraphenylarsonium chloride in water and hydrophobic hydration. 738
Chen, K. S. Electron spin resonance studies of fluoroalkyl radicals in solutions. I. Structures, conformations, and barriers to hindered internal rotation. 2014
Chen, K. S. Electron spin resonance studies of fluoroalkyl radicals in solution. II. Adducts to fluoroolefins. 2030
Chen, K. S. Electron spin resonance studies of fluoroalkyl radicals in solution. III. Photolysis of perfluoroketones and adduct formation. 2036
Chen, S. H. Surface drag viscosity of bovine serum albumin monolayers. 2266
Chen, S-N. Reactivity of the carbonate radical in aqueous solution. Tryptophan and its derivatives. 2099
Cheng, T. M. H. Ion-molecule reactions in disilane. 1184
Chesnut, D. B. Hyperfine models for piperidine nitroxides. 1410
Chiou, C. C. T. Application of the Polanyi adsorption potential theory to adsorption from solution on activated carbon. V. Adsorption from water of some solids

and their melts, and a comparison of bulk and adsorbate melting points. 622

Choi, Y. S. Hydrogen bonding of water in organic solvents. 1. 1723

Choi, Y. S. Hydrogen bonding of water in organic solvents. II. Change of water structure with composition. 1727

Chou, C. C. Rice-Ramsperger-Kassel-Marcus theory applied to decomposition of hot atom substitution products. Cyclobutane-t and cyclobutane-d_7t. 2309

Christen, H. Monte Carlo model of micelle formation. 1423

Christensen, K. A. Optimal determination of relaxation times of fourier transform nuclear magnetic resonance. Determination of spin-lattice relaxation times in chemically polarized species. 1971

Christian, S. D. Complexes of hydrogen chloride with ethers in carbon tetrachloride and heptane. Effects of induction on the basicity of ethers. 432

Christian, S. D. Calculation of equilibrium constants and extinction coefficients for 1:1 complexes. Comments. 557

Christian, S. D. Hydrogen bonding of phenol in carbon tetrachloride. Use of activity data to evaluate association models. 1443

Christianson, M. Forst fall-off procedures utilizing direct count state densities. 2326

Chuang, S. Y. Positron annihilation in amino acids and proteins. 1261

Chung, Y. J. Methyl radical-methanesulfenate anion pairs formed by dissociative electron capture in γ-irradiated crystalline dimethyl-d_6 sulfoxide at 77°K. 1882

Claes, P. Disproportionation and recombination of cyclopentyl radicals. 462

Clarke, J. H. R. Coordination of cadmium(II) with chloride ions in molten potassium tetrachloroaluminate. Raman spectral study. 595

Claverie, P. Calculation of the interaction energy of one molecule with its whole surrounding. II. Method of calculating electrostatic energy. 1853

Claverie, P. Calculation of the interaction energy of one molecule with its whole surrounding. III. Application to pure polar compounds. 1862

Clearfield, A. Mechanism of ion exchange in crystalline zirconium phosphates. X. Calorimetric determination of heats of sodium(1+) ion-proton exchange. 152

Clearfield, A. Mechanisms of ion exchange in crystalline zirconium phosphates. XI. Variation in unit cell dimensions and sodium ion/hydrogen ion exchange behavior in highly crystalline α-zirconium phosphates. 1150

Clearfield, A. Mechanism of ion exchange in zirconium phosphates. XII. Calorimetric determination of heats of cesium ion-hydrogen ion exchange. 1812

Cocke, D. L. Gaseous phosphorus compounds. X. Mass spectrometric determination of the dissociation energies of arsenic and bismuth monophosphides. 603

Cohen, A. H. Nitrogen-14 and oxygen-17 hyperfine interactions in perturbed nitroxides. 1313

Cohen de Lara, E. Infrared spectra of methane adsorbed on NaA, CaA, and NaX zeolites. 2180

Cole, R. H. Dielectric response by real time analysis of time domain spectroscopy data. 1440

Colen, A. H. Relaxation kinetics of micelle formation. 1676

Collin, G. J. Photolysis of 2-methyl-1-butene at photon energies below and above the ionization energy. 98

Colmenares, C. Infrared spectroscopic studies of the surface bond of carbon dioxide on uranium oxides. 2117

Compton, L. E. Hot hydrogen atom-hydrocarbon reactions. Dependence of yields on structure and energy. 559

Comstock, D. Pulse radiolysis study of thallium(II) in aqueous perchloric acid solutions. 488

Conally, T. G. Heats of mixing and heats of dilution of tetrapropylammonium chloride. Temperature dependence. 77

Concepcion, J. G. Electron spin resonance study of the effect of electron-releasing groups upon the molecular orbitals of substituted cyclooctatetraene anion radicals. 90

Conti, G. Volumetric properties of aqueous solutions of organic compounds. III. Aliphatic secondary alcohols, cyclic alcohols, primary, secondary, and tertiary amines. 1030

Conway, B. E. Orientation behavior of adsorbed pyridine and pyrazine at the mercury-water interface in relation to solution thermodynamic properties. 1226

Cooper, W. External heavy-atom effect on the photoisomerization of cyanine dyes. 16

Cordemans, L. Flash photolysis of potassium tris(oxalato)cobaltate(III). 1361

Cordes, H. F. Thermal decomposition of lithium perchlorate. I. Initiation rate. 773

Cordes, H. F. Thermal decomposition of lithium perchlorate. II. Chloride catalysis. 776

Costantino, L. Cation exchange diffusion experiments. 2292

Cox, B. G. Coordination and ionic solvation. 1731

Craig, A. C. Predicted observable fluorescent lifetimes of several cyanines. 1154

Crescenzi, V. Thermodynamics of polycarboxylate aqueous solutions. I. Dilatometry and calorimetry of protonation and copper(II) binding. 607

Crim, F. F. Inelastic scattering of vibrationally excited potassium bromide by polyatomic partners. 2438

Crippen, G. M. Conformation of N-acetyl-L-alanine-N′-methylamide in 1,2-dichloroethane by circular dichroism and optical rotatory dispersion. 1127

Criss, C. M. Estimation of ionic entropies in various solvents. 1000

Cullen, P. F. Apparent molal volumes of some dilute aqueous rare earth salt solutions at 25°. 1106

Cunningham, J. Reactions involving electron transfer at semiconductor surfaces. V. Reactivity and electron paramagnetic resonance of electron transfer sites on rutile. 870

Curtat, M. Isothermal flash photolysis of hydrazine. 1356

Cvetanovic, R. J. Photolysis of liquid and solid ethylene at 184.9 nm. 1254

Cvetanovic, R. J. Relative rates of the reactions of $O(^1D_2)$ atoms with alkanes and cycloalkanes. 1457

Czapski, G. Hydroperoxyl radical reactions. II. Cupric ions in modulated photolysis. Electron paramagnetic resonance experiments. 779

Czapski, G. Hydroperoxyl radical reactions. III. Pulse-radiolytic study of the reaction of the hydroperoxyl radical with some metal ions. 2330

Danesi, P. R. Electrical liquid membrane potential. Biionic isothermal potential. 2370

Daniel, S. H. Stereochemistry of the decay-induced gas-phase halogen exchange in diastereomeric 2,3-dichlorobutanes. 1043

Danoczy, E. Sequence studies in liquid phase hydrocarbon oxidation. II. Mechanism of the alcohol-ketone transition in the oxidation of ethylbenzene. 828

D'Aprano, A. Dielectric constants of 1-pentanol-water mixtures at 25°. 652

Das Gupta, G. Mechanisms of electronic energy transfer in the gas phase. 2407

Davis, A. R. High-pressure laser raman spectroscopic investigation of aqueous magnesium sulfate solutions. 246

Davis, D. D. Dye laser flash photolysis kinetics study of the reaction of ground-state atomic oxygen with hydrogen peroxide. 463

Davis, D. D. Flash photolysis-resonance fluorescence kinetics study of the reaction sulfur(^3p) + carbonyl sulfide. 1137

Davis, D. D. Stop-flow time-of-flight mass spectrometry kinetics study. Reaction of ozone with nitrogen dioxide and sulfur dioxide. 1775

Davis, H. T. Diffusion and thermal diffusion in binary dense gas mixtures of loaded spheres and rough spheres. 1564

DeArmond, K. Electrochemistry of rhodium-dipyridyl complexes. 727

De Bettignies, B. J. Raman spectroscopic study of binary systems. I. Molecular association in the ammonia hexadeuterobenzene liquid system. 2106

De Boer, J. J. Crystal structure of hydrated thallium-exchanged zeolite X. 2395

Dedhiya, M. G. Mechanism of hydroxyapatite dissolution. Synergistic effects of solution fluoride, strontium, and phosphate. 1273

De Jaegere, S. Flash photolysis of potassium tris(oxalato)cobaltate(III). 1361

DeKock, C. W. Interaction of matrix-isolated nickel fluoride and nickel chloride with carbon monoxide, molecular nitrogen, nitric oxide, and molecular oxygen and of calcium fluoride, chromium(II) fluoride, manganese(II) fluoride, copper(II) fluoride, and zinc(II) fluoride with carbon monoxide in argon matrixes. 134

Delaval, Y. Infrared spectra of methane adsorbed on NaA, CaA, and NaX zeolites. 2180

Delben, F. Thermodynamics of polycarboxylate aqueous solutions. I. Dilatometry and calorimetry of protonation and copper(II) binding. 607

Delben, F. Thermodynamics of polycarboxylate aqueous solutions. II. Dilatometry and calorimetry of nickel and barium binding. 1486

DeMore, W. B. Temperature dependence of the reactions of hydroxy and hydroperoxy radicals with ozone. 1447

De Pena, R. G. Kinetics of particle growth. III. Particle formation in the photolysis of sulfur dioxide-acetylene mixtures. 325

De Pena, R. G. Thermodynamics of the reactions $(NH_3)_n \cdot SO_2(s) \rightarrow nNH_3(g) + SO_2(g)$. 1378

Derouane, E. G. Temperature dependence of hyperfine coupling for copper complexes in sodium Y zeolite. 531

Desnoyers, J. E. Apparent molal volumes, heat capacities, and excess enthalpies of n-alkylamine hydrobromides in water as a function of temperature. 1217

Desrosiers, N. Relation between molal volumes and molal compressibilities from the viewpoint of the scaled-particle theory. Prediction of the apparent molal compressibilities of transfer. 2367

Devillers, C. Isothermal flash photolysis of hydrazine. 1356

De Visser, C. Hydrophobic interactions in mixtures of N,N-dimethylformamide and water. Model calculations and enthalpies of solution. 1719

Devore, D. I. Equivalent conductances of univalent counterions and coions in polyelectrolyte solutions. 1242

Devore, J. A. Thermodynamics of caffeine and the 1-1 caffeine-salicylate complex in water at 25°. 1922

Dhar, H. P. Orientation behavior of adsorbed pyridine and pyrazine at the mercury-water interface in relation to solution thermodynamic properties. 1226

Diggle, J. W. Physical properties and electrochemical stability of the thio solvents dimethylthioformamide and hexamethylphosphorothioic triamide. 1018

Doddapaneni, N. Electrochemical behavior of substituted polycyclic aromatic quinones. 1820

Doddapaneni, N. Electrochemical behavior of cis and trans azobenzenes. 1825

Dodge, M. C. Kinetics of nitric oxide catalyzed decomposition of nitryl chloride and its related nitrogen isotope exchange reactions. 2073

Dodson, R. W. Pulse radiolysis study of thallium(II) in aqueous perchloric acid solutions. 488

Dodson, R. W. Pulse radiolysis studies of chloride complexes of thallium(II). Absorption spectra and stability constants of thallium chloride(1+) ion, thallium dichloride, and thallium trichloride(1−) ion. 892

Dole, M. Second-order diffusion-controlled reaction. Decay of allyl free radicals in irradiated polyethylene. 1798

D'Olieslager, J. Flash photolysis of potassium tris(oxalato)cobaltate(III). 1361

Donnay, R. H. Conformational analysis and electronic structure of para-substituted phenyl vinyl ethers. 440

Dorfman, L. M. Optical absorption spectrum of the solvated electron in some liquid amides and amines. 2631

Dorko, E. A. Ultraviolet spectrum and photophysical properties of trimethylenecyclopropane. 568

Drago, R. S. Calorimetric and spectrophotometric comparison of adducts of phenol and deuteriophenol. 429

Drago, R. S. Extension of models for evaluating solvent transfer enthalpies. 454

Dullien, F. A. L. Diffusivities and viscosities of some binary liquid nonelectrolytes at 25°. 2283

Dunlop, P. J. Isotope effect in diffusion of carbon-14-substituted benzenes in benzene, n-heptane, n-octane, and cyclohexane at 25°. 846

Durig, J. R. Spectra and structure of boron-nitrogen compounds. II. Infrared and Raman spectra of trimethylamine-borane. 1503

Dwyer, M. Stop-flow time-of-flight mass spectrometry kinetics study. Reaction of ozone with nitrogen dioxide and sulfur dioxide. 1775

Easteal, A. J. Dependence of the glass transition temperature on heating and cooling rate. 2673

Eastman, M. P. Ultrasound propagation in binary mixtures of dimethyl sulfoxide and water. 2611

Eberhardt, M. K. Radiation induced homolytic aromatic substitution. II. Hydroxylation and phenylation of benzene. 1795

Eichinger, B. E. Gas-liquid chromatography on polymers. I. Polyisobutylene-hydrocarbons at 25°. 60

Eicke, H. F. Monte-Carlo model of micelle formation. 1423

Eliason, R. Comparison of general-acid-catalyzed ethyl vinyl ether hydrolysis in 80% dimethyl sulfoxide with that in water. 2658

Eliel, E. L. Aspects of the information explosion. 1339

Ellsworth, R. L. Reaction of excited oxygen atoms with nitrous oxide. Rate constants for reaction of ozone with nitric oxide and with nitrogen dioxide (correction). 2698

El Samahy, A. Radiolysis and photolysis of the hydrogen peroxide-p-nitrosodimethylaniline-oxygen system. 888

Emara, M. M. Ultrasonic absorption in aqueous solutions of calcium acetate and other bivalent metal acetates. 1913

Ensor, D. D. Heats of mixing and heats of dilution of tetrapropylammonium chloride. Temperature dependence. 77

Ewing, C. T. Equilibrium vaporization rates and vapor pressures of solid and liquid sodium chloride, potassium chloride, potassium bromide, cesium iodide, and lithium fluoride. 1998

Eyring, E. M. Solvent isotope effects for sulfonephthalein indicator dianion-proton recombination kinetics. 1021

Eyring, E. M. Photophysical efffects of stereoisomersin thiacarbocyanine dyes. 2355

Ezra, F. S. Electron spin resonance study of γ-irradiated silver diethyl phosphate. 958

Fabiani, C. Electrical liquid membrane potential. Biionic isothermal potential. 2370

Failor, R. Radicals formed after electron attachment to 5-halouracils in aqueous glasses. 696

Fair, R. W. Photolysis of hydrogen sulfide in the presence of dimethylsilane. 203

Fanelli, A. J. Kinetics of gas-phase thermal decomposition of tris(difluoroamino)methyl compounds. 2189

Fateley, W. G. Gauche-trans rotational isomerism in ethylamine. Far-infrared spectra of ethylamine-d_2. 803

Fee, D. C. Recoil tritium reactions with cyclohexene and alkenes. Determination of rate parameters. 347

Fee, D. C. Recoil tritium reactions with methylcyclohexene. Test of the assumption of energy randomization prior to unimolecular decomposition. 354

Feher, J. J. Self-association and solvent-association of cholesterol and other 3β-hydroxysteroids in nonpolar media. 250

Fehsenfeld, F. C. Formation of negative ions in nitric oxide and the interaction of nitric oxide with hydride and oxygen(1-) ions from water. Comments. 1445

Feng, D-F. Application of the semicontinuum model to temperature effects on solvated electron spectra and relaxation rates of dipole orientation around an excess electron in liquid alcohols. 393

Fenwick, D. E. Effect of ethanol on hydrophobic interactions. Conductometric study of ion-pair formation by double-long-chain electrolytes. 1759

Ferguson, E. E. Formation of negative ions in nitric oxide and the interaction of nitric oxide with hydride and oxygen(1-) ions from water. Comments. 1445

Ferguson, S. Hyperfine models for piperidine nitroxides. 1410

Fernandez, C. G. Copper/copper oxide/carbonate electrode at 350° in fused potassium nitrate-sodium nitrate. 2670

Fernandez, E. Photolysis of diazo-n-propane. Route for the photochemical activation of propylene. 1348

Fernandez-Prini, R. Ultrasonic absorption in aqueous solutions of calcium acetate and other bivalent metal acetates. 1913

Ferro, D. R. CNDO [complete neglect of differential overlap]/2 study of NH...O hydrogen bonds in ions, zwitterions, and neutral molecules. 970

Fessenden, R. W. Hydroxyl radical reactions with phenols and anilines as studied by electron spin resonance. 523

Fessenden, R. W. Electron spin resonance study of the radiolysis of aqueous solutions of cyanate ion. 1074

Field, F. H. Negative temperature dependence of slow ion-molecule reactions. 1773

Figuera, J. M. Photolysis of diazo-n-propane. Route for the photochemical activation of propylene. 1348

Filby, G. Electron spin resonance spectra of some hydroxycyclohexadienyl radicals derived from aromatic carboxylic acid anions. 1521

Finch, E. D. Acoustical technique for measuring the temperature of maximum density of dilute aqueous solutions. 2305

Findenegg, G. H. Mixtures of trifluoroacetic acid with acetic acid and carbon tetrachloride. 1709

Firestone, R. F. Pulse radiolysis of liquid n-pentane and n-pentane-oxygen solutions. Rate constants and activation energies for second-order decay of pentyl and pentylperoxy radicals. 508

Firestone, R. F. Solvated electrons in alcohol-alkane and alcohol-amine solutions. 792

Firkins, E. Investigation of the hydrophobic interaction between tert-butyl alcohol and paramagnetic solutes in aqueous solutions by proton nuclear magnetic resonance relaxation. 851

Fisk, G. A. Inelastic scattering of vibrationally excited potassium bromide by polyatomic partners. 2438

Flanagan, J. B. Digital simulation of tubular electrode response in stationary and flowing solution. 718

Fleischauer, P. D. Kinetics of the reaction between iron(II) and silver(I) catalyzed by silver nuclei on titanium dioxide surfaces. 2580

Florence, A. T. Bursting of soap films. VI. Effect of surfactant purity. 234

Ford, P. C. Photochemistry of rhodium(III) complexes. Ligand field excitation of hexaamminerhodium(III) and characteristics of nonradiative deactivation paths. 1144

Ford, P. C. Photochemistry of rhodium(III) complexes. Ligand field excitation of hexaamminerhodium(III) and characteristics of nonradiative deactivation paths (correction). 2698

Fornier de Violet, P. Laser flash photolytic study of mercury(II) iodide in aqueous solution. 1698

Forster, L. S. Absolute quantum yields of $^2E_g \to {}^4A_{2g}$ luminescence in potassium hexacyano(cobaltate, chromate) powders 2122

Fortier, J. L. Apparent molal volumes, heat capacities, and excess enthalpies of n-alkylamine hydrobromides in water as a function of temperature. 1217

Foster, K. R. Acoustical technique for measuring the temperature of maximum density of dilute aqueous solutions. 2305

Foster, M. S. Phase diagrams of reciprocal molten salt systems. Calculations of liquid-liquid miscibility gaps. 1091

Frank, J. P. Isotope effect in energy losses for deactivating collisions of tetrafluoromethane with chemically activated fluoroethyl radicals $CH_2{}^{18}FCH_2$ and $CD_2{}^{18}FCD_2$. 850

Freed, J. H. Analysis of inertial effects on electron spin resonance spectra in the slow tumbling region. 935

Freed, J. H. Theory of saturation and double resonance in electron spin resonance spectra. VI. Saturation recovery. 1155

Freed, J. H. Estimating microsecond rotational correlation times from lifetime broadening of nitroxide electron spin resonance spectra near the rigid limit. 1321

Freed, J. H. Interpretation of electron spin resonance spectra of spin labels undergoing very anisotropic rotational reorientation. Comments. 1324

Freeman, C. D. Measurement of proton magnetic resonance line shape analysis of a small barrier to internal rotation in N,N'-di-tert-butylthiourea. 961

Freeman, G. R. Radiolysis of liquid nitrous oxide. 28

Freeman, G. R. Radiolysis of liquid nitrous oxide. Hydrocarbon additives. 32

Freeman, G. R. Radiolysis of liquid hydrocarbon-nitrous oxide solutions. Precursors of nitrogen. 102

Frens, G. Aerodynamic drag on bursting bubbles. 1949

Freund, F. Interaction of molecular hydrogen with magnesium oxide defect surface. 758

Fricke, B. Predicted properties of the superheavy elements. III. Element 115, Eka-bismuth. 1945

Friedman, H. L. Charge-asymmetric mixtures of electrolytes at low ionic strength 1927

Froben, F. W. Electron spin resonance measurement of ammonia condensed at 77°K after reaction with discharge products and after high-frequency discharge. 2047

Frost, R. L. Structure of aqueous solutions. Structure making and structure breaking in solutions of sucrose and urea. 1754

Fuchs, R. Transition state enthalpies of transfer in aqueous dimethyl sulfoxide solutions. Alkaline hydrolysis of ethyl acetate. 1509

Fueki, K. Application of the semicontinuum model to temperature effects on solvated electron spectra and relaxation rates of dipole orientation around an excess electron in liquid alcohols. 393

Fujimoto, H. Molecular orbital study of the addition of singlet methylene to butadiene. 1167

Fujimoto, H. Perturbation of molecules by static fields, orbital overlap, and charge transfer. 1874

Fujiwara, H. Studies of hydrogen bonding in carboxylic acid-dimethyl sulfoxide systems by nuclear magnetic resonance dilution shifts. 1662

Fujiwara, S. Electron spin resonance of palladium(I). IV. Mixed-ligand complexes of palladium(I). 2136

Fukui, K. Behavior of the excess electron in methane. 148

Fuoss, R. M. Derivation of the Justice conductance equation. 1383

Futrell, J. H. High-pressure mass spectrometry. V. Thermodynamics of solvation reactions. NH_4^+-NH_3. 1482

Gagnon, H. Photolysis of 2-methyl-1-butene at photon energies below and above the ionization energy. 98

Gal, D. Sequence studies in liquid phase hydrocarbon oxidation. II. Mechanism of the alcohol-ketone transition in the oxidation of ethylbenzene. 828

Gallaher, K. L. Thermochemical state of gaseous electron diffraction samples. 2380

Gallaher, K. L. Reinvestigation of the structure of perfluoroethane by electron diffraction. 2389

Gallezot, P. Crystal structure of a dealuminated Y-type zeolite. 1550

Gallezot, P. Structure and texture of a crushed sodium-yttrium zeolite. 1959

Galwey, A. K. Thermal decomposition of three crystalline modifications of anhydrous copper(II) formate. 2664

Gamba, A. Geometry and electronic structure of nitrostyrene molecules and anions. 49

Gangwer, T. E. Solid-state study of the potassium nitrosodisulfonate radical. 375

Gardiner, W. C. Jr. Rate constant for carbon monoxide + molecular oxygen = carbon dioxide + atomic oxygen from 1500 to 2500° K. Reevaluation of induction times in the shock-initiated combustion of hydrogen-oxygen-carbon monoxide-argon mixtures. 497

Gardy, E. M. Direct electron spin resonance detection of free radicals produced in electron-irradiated liquid alcohols. 1977

Garland, F. Calculation of equilibrium constants and extinction coefficients for 1:1 complexes. Comments. 557

Garland, F. Relaxation spectra of 6-methylpurine in aqueous solution. 848

Garnett, J. L. Uncoupled representations in hydrogen isotope exchange reactions. 984

Garnier, F. Conformational analysis and electronic structure of para-substituted phenyl vinyl ethers. 440

Gavlas, J. F. Optical absorption spectrum of the solvated electron in some liquid amides and amines. 2631

Gay, I. D. Carbon-13 nuclear magnetic resonance spectroscopy of molecules adsorbed on silica. 38

Gennick, I. Hydrogen bonding. IV. Correlation of infrared spectral properties with C-H···X hydrogen bonding and crystal habit in tetramethylammonium ion salts. 2585

Gerkin, R. E. Electron paramagnetic resonance absorption in oriented phosphorescent 2,3-benzocarbazole and 1,2,3,4-tetrahydroanthracene at magnetic fields below 65 G. 692

Gershinowitz, H. Negative temperature dependence of slow ion-molecule reactions. 1773

Ghai, R. K. Diffusivities and viscosities of some binary liquid nonelectrolytes at 25°. 2283

Ghormley, J. A. Reaction of excited oxygen atoms with nitrous oxide. Rate constants for reaction of ozone with nitric oxide and with nitrogen dioxide (correction). 2698

Giauque, W. F. Entropies of the hydrates of sodium hydroxide. III. Low-temperature heat capacities and heats of fusion of the α and β crystalline forms of sodium hydroxide tetrahydrate. 1701

Gibson, H. W. Effect of structure on the mesomorphic properties of cholesteryl alkanoates. V. Electric field effects on a uniaxial smectic phase of mixtures of cholesteryl alkanoates. 1740

Gieseke, W. Interaction of molecular hydrogen with magnesium oxide defect surface. 758

Gilles, P. W. High-temperature vaporization of ternary systems. I. Mass spectrometry of oxygen-rich vanadium-tungsten-oxygen species. 266

Gillois, M. Isothermal flash photolysis of hydrazine. 1356

Gingerich, K. A. Gaseous phosphorus compounds. X. Mass spectrometric determination of the dissociation energies of arsenic and bismuth monophosphides. 603

Ginley, D. S. Technique for the determination of absolute emission quantum yields of powdered samples. 2229

Giulianelli, J. L. Chemical states of sulfur-35 formed by the ^{35}Cl(n,p)^{35}S process in potassium chloride. 372

Givens, R. S. Photochemistry of 7-ketonorbornane in vapor phase and solution. 2637

Go, M. K. Raman spectra and structure of water from -10 to 90°. 1304

Goldberg, I. B. Simultaneous electrochemical-electron spin resonance measurements. II. Kinetic measurments using constant current pulse. 290

Goldberg, I. B. Simultaneous electrochemical-electron spin resonance measurements. III. Determination of rate constants for second-order radical anion dimerization. 295

Golden, F. M. Theory of ion-complexing effects in ion-exchange column performance. 926

Gopal, R. Cationic transport number of potassium bromide and solvation of ions in dimethyl sulfoxide. 2405

Gordon, M. D. CNDO [complete neglect of differential overlap] and ab initio derived σ-core charges for Pariser-Parr-Pople π-electron calculations on nitroaromatics. 1868

Graetzel, M. Laser photoionization in micellar solutions. Fate of photoelectrons. 2248

Grant, D. M. Optimal determination of relaxation times of fourier transform nuclear magnetic resonance. Determination of spin-lattice relaxation times in chemically polarized species. 1971

Granzow, A. Flash photolysis of aromatic sulfur molecules. Comments. 1441

Gratzel, M. Luminescence decay of hydrophobic molecules solubilized in aqueous micellar systems. Kinetic model. 190

Green, M. E. Noise spectra of ion transport across an anion membrane. 761

Grodkowski, J. Scavenging of electrons in 3-methylpentane glass at 77°K. 2696

Grunwald, E. Effect of ion pairs on the relaxation of ionic atmospheres. 1431

Grunwald, E. Proton exchange of carboxylic acids in 1-octanol. 2339

Grushka, E. Vapor pressure measurements of 4,4'-dimethoxyazoxybenzene. 275

Grushka, E. Molecular structure effect on the diffusion of heptane isomers. 1428

Grushka, E. Extension of the chromatographic broadening method of measuring diffusion coefficients to liquid systems. I. Diffusion coefficients of some alkylbenzenes in chloroform. 2297

Guenther, K. Electron spin resonance spectra of some hydroxycyclohexadienyl radicals derived from aromatic carboxylic acid anions. 1521

Guerra, M. Theoretical interpretation of the rotational barrier in benzophenone ketyl. 2144

Guidry, R. M. Extension of models for evaluating solvent transfer enthalpies. 454

Guillory, W. A. Condensed-phase photochemistry of cyclobutanone. 1461

Gupta, S. K. Formation of negative ions in nitric oxide and the interaction of nitric oxide with hydride and oxygen(1-) ions from water. Reply to comments. 1446

Gutman, D. Extending the use of the atomic oxygen + nitrogen dioxide → nitric oxide + molecular oxygen reaction for measuring low oxygen atom concentrations. 208

Gutman, D. Direct identification of the reactive channels in the reactions of oxygen atoms and hydroxyl radicals with acetylene and methylacetylene. 311

Gutman, D. Determination of branching ratios for the reaction of oxygen atoms with ethylene. 663

Habenschuss, A. Apparent molal volumes of some dilute aqueous rare earth salt solutions at 25°. 1106

Hackett, P. A. Photochemistry of halogenated acetones. I. Spectroscopic studies. 665

Hackett, P. A. Photochemistry of halogenated acetones. II. Rate constant measurements. 671

Hackett, P. A. Photochemistry of halogenated acetones. III. Vibrational relaxation in singlet state. 679

Hackett, P. A. Photochemistry of halogenated acetones. IV. Quenching of the excited states. 682

Hadermann, A. F. High-voltage electroosmosis. Pressure-voltage behavior in the system γ-alumina-2-propanol. 65

Hadley, S. G. The $a^3\Pi_{0^+} \rightarrow X^1\Sigma^+$ system of bromine chloride. 1833

Hagan, C. P. Transition state enthalpies of transfer in aqueous dimethyl sulfoxide solutions. Alkaline hydrolysis of ethyl acetate. 1509

Hagler, A. T. Structure of liquid water. II. Improved statistical thermodynamic treatment and implications of a cluster model. 1531

Hagler, A. T. Vibrational frequencies of water clusters. 1844

Hakala, D. Dual photon effects in nitrogen dioxide photolysis. 1583

Hale, G. M. Infrared optical constants of aqueous solutions of electrolytes. Alkali halides. 238

Hale, G. M. Infrared optical constants of aqueous solutions of electrolytes. Acids and bases. 1405

Hall, P. L. Aromatic radical cation formation on the intracrystal surfaces of transition metal layer lattice silicates. 994

Hamill, W. H. Prompt electron scavenging by benzene in pulse-irradiated alcohols. 504

Hamill, W. H. Characteristic energy loss, luminescence, and luminescence excitation spectra of methane and other alkane solids under low-energy electron impact. 2077

Hamill, W. H. Luminescence probe analysis of ionic states of cyclopentane, cyclohexane, and n-hexane solids under low-energy electron impact. 2081

Hanck, K. Electrochemistry of rhodium-dipyridyl complexes. 727

Hanrahan, R. J. Effects of iodine and other scavengers on the γ radiolysis of liquid perfluorocyclohexane. 360

Hanrahan, R. J. Effect of iodine as a radical scavenger in the γ radiolysis of liquid-phase cyclohexane-perfluorocyclohexane solutions. 366

Hansen, J. R. High-resolution and pulsed nuclear magnetic resonance studies of microemulsions. 256

Hansen, S. L. Thermodynamics of caffeine and the 1-1 caffeine-salicylate complex in water at 25°. 1922

Harmon, K. M. Hydrogen bonding. IV. Correlation of infrared spectral properties with C-H···X hydrogen bonding and crystal habit in tetramethylammonium ion salts. 2585

Harteck, P. Dual photon effects in nitrogen dioxide photolysis. 1583

Hartley, P. J. Coordination of cadmium(II) with chloride ions in molten potassium tetrachloroaluminate. Raman spectral study. 595

Hase, W. L. Rice-Ramsperger-Kassel-Marcus theory applied to decomposition of hot atom substitution products. Cyclobutane-t and cyclobutane-d$_7$t. 2309

Hatada, M. Radiolysis and photolysis of the hydrogen peroxide-p-nitrosodimethylaniline-oxygen system. 888

Hatano, Y. Competitive electron scavenging of nitrous oxide with sulfur hexafluoride, methyl chloride, and carbon dioxide in liquid neopentane. 853

Hatano, Y. Competitive and noncompetitive electron capture of nitrous oxide with sulfur hexafluoride and electron thermalization in the gas-phase radiolysis of xenon. 954

Hatano, Y. Photolysis of liquid cyclohexane at 1634 Ang and the effect of the addition of carbon tetrachloride and sulfur hexafluoride. 1899

Hathaway, E. J. Existence of associated species in lanthanum (III) chloride-potassium chloride melts. 1134

Hawlicka, E. Self-diffusion in liquid binary solutions. 2307

Hayashi, K. Laser photolysis studies on the primary processes of photoinduced ionic polymerizations. 341

Hayon, E. Interaction of hydrated electrons with the peptide linkage. 1193

Hayon, E. Interaction of hydrated electrons with phenylalanine and related compounds. 1790

Hayon, E. Intermediates produced from the one-electron reduction of nitrogen heterocyclic compounds in solution. 2615

Heicklen, J. Kinetics of particle growth. III Particle formation in the photolysis of sulfur dioxide-acetylene mixtures. 325

Heicklen, J. Reaction of hydroperoxyl radicals with nitric oxide and nitrogen peroxide. 653

Heicklen, J. Thermodynamics of the reactions $(NH_3)_n{\cdot}SO_2(s) \rightarrow nNH_3(g) + SO_2(g)$ 1378

Heicklen, J. Reactions of methylperoxy radicals with nitric oxide and nitrogen dioxide. 2417

Helbert, J. Electron paramagnetic resonance and electron-nuclear double resonance line shape studies of trapped electrons in γ-irradiated deuterium-substituted 10 M sodium hydroxide alkaline ice glass. 221

Hemmes, P. Ultrasonic relaxation of aqueous yttrium nitrate. 261

Hemmes, P. Influence of true chemical equilibrium on the viscosity-mobility product of electrolytes. 907

Hen, J. Counterion binding by poly(vinyl sulfonate). *1013*

Hendifar, A. Catalyzed and uncatalyzed dissolution of anhydrous chromic chloride in aqueous solutions. 1993

Hendra, P. J. Laser Raman spectra of species adsorbed on oxide surfaces. II. 300

Hendrix, J. Flash photolysis of potassium tris(oxalato)cobaltate(III). 1361

Henglein, A. Pulse radiolytic polarography. Competitive oxidation and reduction of hydroxycyclohexadienyl radicals at the mercury drop electrode in aqueous solutions. 160

Henglein, A. Pulse radiolytic study of nickel(1+) ion. Nickel-carbon bond formation. 882

Henglein, A. Pulse radiolytic investigations of $OHCH_2O_2$ radicals. 2089

Hentz, R. R. Influence of molecular structure on optical absorption spectra of solvated electrons in alcohols. 514

Hepburn, D. R. Jr. Charge scavenging in γ radiolysis of cyclohexane solutions of carboranes. 788

Herring, F. G. Structural and solvent effects on the rate of reaction between heterocyclic bases and copper(II) bis(diethyldithiocarbamate). 316

Herron, J. T. Rate constants for the reactions of ozone with ethene and propene, from 235.0 to 362.0°K. 2085

Hertz, H. G. Hydrophobic hydration and quadrupolar magnetic relaxation of ionic nuclei. 1002

Higashimura, T. Triplet formation in ion recombination in spurs. Comment. 309

Higashiyama, T. Infrared attenuated total reflection spectra of adsorbed layers at the interface between a germanium electrode and an aqueous solution of sodium laurate. 941

Highsmith, S. Effect of ion pairs on the relaxation of ionic atmospheres. 1431

Highsmith, S. Proton exchange of carboxylic acids in 1-octanol. 2339

Higuchi, W. I. Mechanism of hydroxyapatite dissolution. Synergistic effects of solution fluoride, strontium, and phosphate. 1273

Hinkson, T. C. 2537-Ang mercury-sensitized photochemical decomposition of perfluorocyclobutane. 2071

Hinman, D. D. Theory of molecular association in cholesteric-nematic liquid crystal mixtures. 1206

Hirasawa, R. Simultaneous electrochemical-electron spin resonance measurements. III. Determination of rate constants for second-order radical anion dimerization. 295

Hirokami, S. Photolysis of liquid and solid ethylene at 184.9 nm. 1254

Hisatsune, I. C. Kinetics of nitric oxide catalyzed decomposition of nitryl chloride and its related nitrogen isotope exchange reactions. 2073

Hochanadel, C. J. Reaction of excited oxygen atoms with nitrous oxide. Rate constants for reaction of ozone with nitric oxide and with nitrogen dioxide (correction). 2698

Hoff, E. V. Isothermal compressibility of aqueous sodium chloride, magnesium chloride, sodium sulfate, and magnesium sulfate solutions from 0 to 45° at 1 atm. 1636

Hoffman, B. M. Electron paramagnetic resonance of a nitroxide adsorbed on silica, silica-alumina, alumina, and decationated zeolites. 2110

Hoffman, B. M. Electron paramagnetic resonance of adsorbed nitroxide. 200

Hoffman, B. M. Nitrogen-14 and oxygen-17 hyperfine interactions in perturbed nitroxides. 1313

Hoffman, M. Z. Generation of radicals in the charge-transfer photochemistry of coordination complexes of colbalt(III) in aqueous solution. 686

Hoffman, M. Z. Reactivity of the carbonate radical in aqueous solution. Tryptophan and its derivatives. 2099

Hoffmann, R. Molecular orbital study of the addition of singlet methylene to butadiene. 1167

Hoffmann, R. Perturbation of molecules by static fields, orbital overlap, and charge transfer. 1874

Hoge, C. E. Wetting under chemical equilibrium and nonequilibrium conditions. 1178

Holroyd, R. A. Chemical reaction rates of quasi free electrons in nonpolar liquids. 796

Holroyd, R. A. Solvent and temperature effects in the photoionization of tetramethyl-p-phenylenediamine. 2128

Holtzer, A. Use of the van't Hoff relation in determinations of the enthalpy of micelle formation. 1442

Holtzer, M. F. Use of the van't Hoff relation in determinations of the enthalpy of micelle formation. 1442

Holz, M. Hydrophobic hydration and quadrupolar magnetic relaxation of ionic nuclei. 1002

Hong, K. C. Enthalpies of mixing in liquid alkaline earth fluoride-alkali fluoride mixtures. II. Calcium fluoride with lithium, sodium, and potassium fluorides 1478

Hooper, D. L. Measurement of proton magnetic resonance line shape analysis of a small barrier to internal rotation in N,N'-di-tert-butylthiourea. 961

Hopmann, R. F. W. Chemical relaxation as a mechanistic probe of hydrogen bonding. Thermodynamics and kinetics of lactam isoassociation in nonpolar solvents. 2341

Horsma, D. A. Dielectric properties of liquid sulfur in the ring-chain transition region. 1670

Hoshino, M. Low-temperature pulse radiolysis. II. Time-dependent spectra of anions of aromatic ketones. 1473

Howard, C. J. Formation of negative ions in nitric oxide and the interaction of nitric oxide with hydride and oxygen(1-) ions from water. Comments. 1445

Howell, F. S. Electrical relaxation in a glass-forming molten salt. 639

Huang, J. T. J. Triplet formation in ion recombination in spurs. Reply to comment. 310

Huang, T. Characteristic energy loss, luminescence, and luminescence excitation spectra of methane and other alkane solids under low-energy electron impact. 2077

Huang, T. Luminescence probe analysis of ionic states of cyclopentane, cyclohexane, and n-hexane solids under low-energy electron impact. 2081

Hudgens, B. A. Spectra and structure of boron-nitrogen compounds. II. Infrared and Raman spectra of trimethylamine-borane. 1503

Huffman, H. L. Jr. Conductance behavior of tetraalkyammonium salts in 3-tert-butyl-2-oxazolidone at 25°. 2689

Huie, R. E. Rate constants for the reactions of ozone with ethene and propene, from 235.0 to 362.0°K. 2085

Hunt, J. W. Yield of solvated electrons in the aliphatic alcohols at picosecond times. 2414

Huron, M. J. Calculation of the interaction energy of one molecule with its whole surrounding. II. Method of calculating electrostatic energy. 1853

Huron, M. J. Calculation of the interaction energy of one molecule with its whole surrounding. III. Application to pure polar compounds. 1862

Hutchins, J. E. C. Solvent isotope effects for sulfonephthalein indicator dianion-proton recombination kinetics. 1021

Hutchinson, R. W. Effect of iron impurities on the thermal decomposition of α-lead azide. 478

Ibuki, T. Isomerizaton of chemically activated propenyl radicals. 2543

Ilan, Y. A. Hydroperoxyl radical reactions. III. Pulse-radiolytic study of the reaction of the hydroperoxyl radical with some metal ions. 2330

Ikada, E. New asymmetric dielectric relaxations in two liquid triacetates. 1078

Ikeda, S. X-ray photoelectron spectroscopic study of the reaction of evaporated metal films with chlorine gas. 107

Ikeda, S. Electric and nonelectric interactions of a nonionic-cationic micelle. 1086

Imai, J. Infrared spectra of butylamine adsorbed on silica-alumina. 704

Imamura, M. Kinetic studies of photobleaching of trapped electrons in protiated and deuterated methanol and ethanol glasses at 77°K. 232

Imamura, M. Low-temperature pulse radiolysis. I. Negative ions of halogenated compounds. 519

Imamura, M. Electronic absorption spectra of ion radicals and their molecular orbital interpretation. IV. Anion radicals of aromatic and unsaturated aliphatic carbonyl compounds. 741

Imamura, M. Low-temperature pulse radiolysis. II. Time-dependent spectra of anions of aromatic ketones. 1473

Imelik, B. Structure and texture of a crushed sodium-yttrium zeolite. 1959

Infelta, P. P. Luminescence decay of hydrophobic molecules solubilized in aqueous micellar systems. Kinetic model. 190

Inoue, Y. Radiochemical study of active sites on palladium. Behavior of preadsorbed carbon-14-labeled acetylene and carbon-14-labeled carbon monoxide in acetylene hydrogenation. 583

Ireton, R. C. Transfer of vibrational energy from highly excited butyl radicals. Relative collision diameters of homologous n-perfluoroalkane bath molecules. 1979

Ireton, R. C. Transfer of vibrational energy from highly excited butyl radicals. Structural effects on the magnitudes of relative collision diameters. 1984

Irie, M. Laser photolysis studies on the primary processes of photoinduced ionic polymerizations. 341

Ishimaru, S. Behavior of the excess electron in methane. 148

Ito, K. Competitive electron scavenging of nitrous oxide with sulfur hexafluoride, methyl chloride, and carbon dioxide in liquid neopentane. 853

Iwata, S. Electronic absorption spectra of ion radicals and their molecular orbital interpretation. IV. Anion radicals of aromatic and unsaturated aliphatic carbonyl compounds. 741

Jackson, H. W. Membrane-water partition coefficients of ions. Calculated effects of membrane thickness. 2259

Jackson, J. L. Charge neutrality in electrolytic solutions and the liquid junction potential. 2060

Jadzyn, J. Dielectric polarization of dilute associating solutions. V. Solvation of alcohols in nondipolar solvents. 1203

Jagodzinski, P. Electrical conductance and ultrasonic relaxation for lithium perchlorate in tetrahydrofuran. 917

James, D. W. Angular overlap model description of the electronic and magnetic properties of copper(II) complexes. 1235

James, D. W. Structure of aqueous solutions. Structure making and structure breaking in solutions of sucrose and urea. 1754

Jamieson, D. Thermal decomposition of three crystalline modifications of anhydrous copper(II) formate. 2664

Janata, E. Pulse radiolytic study of nickel(1+) ion. Nickel-carbon bond formation. 882

Janauer, G. E. Cation exchange in mixed solvent media. I. Equilibrium swelling of polystyrenesulfonate resins in dimethyl sulfoxide-water media. 411

Janini, G. M. Measurement and interpretation of activity coefficients for aromatic solutes at infinite dilution in n-octadecane and n-hexadecyl halide solvents. 1644

Jansen, M. L. Conductance measurements of alkali metal trifluoroacetates in propylene carbonate. 1380

Japar, S. M. Rate constants for the reaction of ozone with olefins in the gas phase. 2318

Jeffers, P. Relative cis-trans isomerization rates. Another test of the energy randomization hypothesis. 770

Jeffers, P. M. Shock tube cis-trans isomerization studies. III. 1469

Jha, J. S. Cationic transport number of potassium bromide and solvation of ions in dimethyl sulfoxide. 2405

Joergensen, P. Electronic spectra of aromatic hydrocarbon anions and cations in the CNDO/S [complete neglect of differential overlap using spectroscopically determined parameters] model. 1420

Johnson, D. R. Second-order diffusion-controlled reaction. Decay of allyl free radicals in irradiated polyethylene. 1798

Johnson, G. E. Spectroscopic study of carbazole by photoselection. 1512

Johnson, G. E. Mechanism of fluorescence quenching by acids in poly(N-vinylcarbazole). 2009

Johnston, H. S. Photolysis of nitric acid vapor. 1

Jolicoeur, C. Investigation of the hydrophobic interaction between tert-butyl alcohol and paramagnetic solutes in aqueous solutions by proton nuclear magnetic resonance relaxation. 851

Jonah, C. D. Indirect measurements for the time dependence of the hydrated electron. 2103

Jones, A. A. Effect of urea on magnetic relaxation in aqueous solutions of poly(ethylene oxide). 1528

Jones, A. C. Structure of triiodide ion in solution. Raman evidence for the existence of higher polyiodide species. 2306

Jones, D. W. Proton magnetic resonance study of molecular interactions in solutions of fluoranthene in carbon tetrachloride and cyclohexane. 1330

Joppien, G. R. Decay kinetics of sorbed methyl radicals generated by photodecomposition and radiolysis of methyl halides on silica gel. 1391
Jorne, J. Conductance studies of the alkali metal chlorides in aluminum chloride-propylene carbonate solution. 2521
Jorne, J. Thermodynamics of ion solvation of the alkali metal chlorides in aluminum chloride-propylene carbonate solution. 2576
Jortner, J. Thermal electron transfer reactions in polar solvents. 2148
Jou, F. Y. Optical absorption spectrum of the solvated electron in some liquid amides and amines. 2631
Jung, K. H. Modified semi-ion-pair model for the evaluation of activation energies of four-center reactions of hydrogen halides to olefins. 1035
Kaba, R. A. Electron paramagnetic resonance study of radicals formed from allyl compounds. 117
Kabe, T. Radiochemical study of active sites on palladium. Behavior of preadsorbed carbon-14-labeled acetylene and carbon-14-labeled carbon monoxide in acetylene hydrogenation. 583
Kadoi, H. Electron spin polarization effects in a study of transient hydrogen atoms in acidic ices under electron irradiation. 1336
Kajiwara, T. Effect of dimer formation on the electronic absorption and emission spectra of ionic dyes. Rhodamines and other common dyes. 380
Kamlet, M. J. Band-shape correlations in the electronic absorption spectra of para-(+M)-substituted nitrobenzene derivatives. 494
Kanamaru, F. Role of interlayer cations in the formation of acrylonitrile-montmorillonite complexes. 42
Kanofsky, J. R. Direct identification of the reactive channels in the reactions of oxygen atoms and hydroxyl radicals with acetylene and methylacetylene. 311
Kantrowitz, E. R. Generation of radicals in the charge-transfer photochemistry of coordination complexes of colbalt(III) in aqueous solution. 686
Kaplan, D. Electron paramagnetic resonance of ruthenium(III) halopentaammines in single crystals. 700
Kaplan, M. L. Chemically induced polarization of fluorine-19 nuclei. Fluorinated phenoxyl and anilinyl radicals. 1837
Kasai, P. H. Electron spin resonance study of synthetic cellulose fiber and film. 308
Kashiwagi, H. Optical saturation and quenching effects in the triplet state of Rhodamine 6G at 77°K. 2006
Kato, H. Behavior of the excess electron in methane. 148
Kato, H. Copper complexes as catalysts of the oxidative coupling reaction of phenol derivatives. 811
Katsumura, Y. Electron spin polarization effects in a study of transient hydrogen atoms in acidic ices under electron irradiation. 1336
Katz, S. M. A method for the determination of rank in the analysis of absorption spectra of multicomponent systems (correction). 2698
Kaulgud, M. V. Volumetric and isentropic compressibility behavior of aqueous amine solutions. I. 714
Kawaizumi, F. Partial molal volumes of ions in organic solvents from ultrasonic vibration potential and density measurements. I. Methanol. 627
Kawaizumi, F. Partial molal volumes of irons in organic solvents from ultrasonic vibration potentials and density measurements. II. Ethanol and dimethylformamide. 1099
Kawasaki, M. Emission of imino radicals in the $c^1\pi$ state formed from the photolysis of ammonia, methylamine, and ethylenimine at 123.6 nm. 1784
Kay, W. B. Solubility of mercury in polar gases. 186
Kearns, D. R. Effect of dimer formation on the electronic absorption and emission spectra of ionic dyes. Rhodamines and other common dyes. 380
Kearns, D. R. Role of singlet oxygen in some chemiluminescence and enzyme oxidation reactions. 1681
Kearns, D. R. Anaerobic chemiluminescent reaction of aryl Grignard reagents with aryl peroxides. 1896
Keenan, A. G. Copper/copper oxide/carbonate electrode at 350° in fused potassium nitrate-sodium nitrate. 2670
Keenan, B. M. Complexes of hydrogen chloride with ethers in carbon tetrachloride and heptane. Effects of induction on the basicity of ethers. 432
Keii, T. Electron spin resonance study of the formation of anion radicals over titanium exchanged Y-zeolite. 218
Keil, M. Cyclopentene decomposition in shock waves. 436
Keller, J. H. Three-element reaction coordinates. III. Barrier curvature effects on intramolecular kinetic isotope effects. 544
Keller, O. L. Jr. Predicted properties of the superheavy elements. III. Element 115, Eka-bismuth. 1945
Kelley, R. D. Cross disproportionation of alkyl radicals. 1586
Kelm, M. Pulse radiolytic study of nickel(1+) ion. Nickel-carbon bond formation 882
Kennedy, G. A. Effects of iodine and other scavengers on the γ radiolysis of liquid perfluorocyclohexane. 360
Kennedy, G. A. Effect of iodine as a radical scavenger in the γ radiolysis of liquid-phase cyclohexane-perfluorocyclohexane solutions. 366
Kenney-Wallace, G. A. Influence of molecular structure on optical absorption spectra of solvated electrons in alcohols. 514
Kern, R. D. Exchange of hydrogen bromide and deuterium behind reflected shock waves. 2549
Kestner, N. R. Thermal electron transfer reactions in polar solvents. 2148
Kevan, L. Spin trapping of hydrogen atoms in γ-irradiated liquid alkanes. 91
Kevan, L. Electron paramagnetic resonance and electron-nuclear double resonance line shape studies of trapped electrons in γ-irradiated deuterium-substituted 10 M sodium hydroxide alkaline ice glass. 221
Kevan, L. Application of the semicontinuum model to temperature effects on solvated electron spectra and relaxation rates of dipole orientation around an excess electron in liquid alcohols. 393
Kevan, L. Energy level structure and mobility of excess electrons in γ-irradiated 5 M potassium carbonate aqueous glasses. Effect of ions on trapped and mobile electrons in aqueous glasses. 2454
Kevan, L. Free radical formation in hydrocarbon crystals by γ irradiation. Anisotropic hyperfine couplings in $CH_3CH(CH_2)_{33}CH_3$ and relative radical yields in single crystals hexatriacontane (correction). 2698
Kew, G. Electrochemistry of rhodium-dipyridyl complexes. 727
Kikta, E. J. Jr. Extension of the chromatographic broadening method of measuring diffusion coefficients to liquid systems. I. Diffusion coefficients of some alkylbenzenes in chloroform. 2297
Kikuchi, K. Electric birefringence of potassium polystyrenesulfonate in aqueous solution as a function of molecular weight, concentration, and field strength (correction). 2698
Kilichowski, K. B. Fluorescence quenching of the indole ring system by lanthanide ions. 1953
Kim, K. C. Unimolecular reactions and energy partitioning. Three- and four-centered elimination reactions of chemically activated 1,1,2-trichloroethane-d_0-d_1, and -d_2. 2166
Kim, P. Stop-flow time-of-flight mass spectrometry kinetics study. Reaction of ozone with nitrogen dioxide and sulfur dioxide. 1775
Kim, P. Kinetic isotope effects in the reactions of hydrogen and deuterium atoms with dimethyl ether and methanol. 2650
King, A. D. Jr. Effect of pressure on the surface tension of water. Adsorption of low molecular weight gases on water at 25°. 2262
King, J. W. Solubility measurements of aromatic hydrocarbons and carbon disulfide in liquid sulfur by gas chromatography. 2635
Kint, S. Raman spectra and structure of water from -10 to 90°. 1304
Kira, A. Equilibria between triplet states of aromatic hydrocarbons. 196
Kira, A. Formation of ions and excited states in the pulse radiolysis of benzonitrile. 2094
Kishi, K. X-ray photoelectron spectroscopic study of the reaction of evaporated metal films with chlorine gas. 107
Kispert, L. D. Electron-electron double resonance investigations of irradiated malonic acid-d_4 single crystals. 1839
Kitching, S. C. Structure and reactions of some mercaptans on a nickel surface. 1648
Kittelberger, J. S. Programmed temperature dehydration studies of octacalcium phosphate. 1631
Kiviat, F. E. Surface acidity of modified alumina. Reply to comments. 2070
Klein, G. Theory of ion-complexing effects in ion-exchange column performance. 926
Klein, R. Cross disproportionation of alkyl radicals. 1586
Klemm, R. B. Flash photolysis-resonance fluorescence kinetics study of the reaction sulfur(^3p) + carbonyl sulfide. 1137
Kleppa, O. J. Thermodynamic studies of binary charge unsymmetrical fused salt systems. Cerium(III) chloride-alkali chloride mixtures. 178
Kleppa, O. J. Enthalpies of mixing in liquid alkaline earth fluoride-alkali fluoride mixtures. II. Calcium fluoride with lithium, sodium, and potassium fluorides 1478
Klingen, T. J. Charge scavenging in γ radiolysis of cyclohexane solutions of carboranes. 788
Klopman, G. Electrochemical behavior of substituted polycyclic aromatic quinones 1820
Klopman, G. Electrochemical behavior of cis and trans azobenzenes. 1825
Klug-Roth, D. Pulse radiolytic investigations of $OHCH_2O_2$ radicals. 2089
Knudtson, J. T. Photophysical efffects of stereoisomersin thiacarbocyanine dyes. 2355
Ko, A-N. Transfer of vibrational energy from highly excited butyl radicals. Structural effects on the magnitudes of relative collision diameters. 1984
Kobayashi, Y. Yields of radiation products in sodium metaphosphate glasses. 752
Kochi, J. K. Electron spin resonance studies of fluoroalkyl radicals in solutions. I. Structures, conformations, and barriers to hindered internal rotation. 2014
Kochi, J. K. Electron spin resonance studies of fluoroalkyl radicals in solution. II. Adducts to fluoroolefins. 2030
Kochi, J. K. Electron spin resonance studies of fluoroalkyl radicals in solution. III. Photolysis of perfluoroketones and adduct formation. 2036
Koenig, E. Octahedral d^4, d^6 ligand field spin-orbit energy level diagrams. 56
Kohl, F. J. Identification and dissociation energy of gaseous hafnium mononitride. 273
Kohler, F. Mixtures of trifluoroacetic acid with acetic acid and carbon tetrachloride 1709
Koizumi, M. Role of interlayer cations in the formation of acrylonitrile-montmorillonite complexes. 42
Kolthoff, I. M. Transfer activity coefficients of ortho-substituted and non-ortho-substituted benzoates between water, methanol, and polar aprotic solvents 839
Kordis, J. Gaseous phosphorus compounds. X. Mass spectrometric determination of the dissociation energies of arsenic and bismuth monophosphides. 603
Kosower, E. M. Optical spectra and reactivities of radical anions of 4-nitrobenzyl compounds produced by pulse radiolysis of acetonitrile solutions. 112
Kraljic, I. Radiolysis and photolysis of the hydrogen peroxide-p-nitrosodimethylaniline-oxygen system. 888
Kreevoy, M. M. Determination of acidity in 80% dimethyl sulfoxide-20% water. 421
Kreevoy, M. M. Comparison of general-acid-catalyzed ethyl vinyl ether hydrolysis in 80% dimethyl sulfoxide with that in water. 2658
Kreglewski, A. Intermolecular energy of fluids at the critical temperature and its dependence on the temperature. 1241
Kreglewski, A. Thermodynamic properties of systems with specific interactions

calculated from the hard-sphere equation of state. I. Binary systems with one inert component. 1961
Kremer, M. L. Stable intermediates in kinetic models of catalase action. 1919
Kremer, S. Octahedral d^4, d^6 ligand field spin-orbit energy level diagrams. 56
Krieger, I. M. Bubble solution method for diffusion coefficient measurements. Experimental evaluation. 2516
Krishnan, C. V. Charge-asymmetric mixtures of electrolytes at low ionic strength 1927
Kroh, J. Scavenging of electrons in 3-methylpentane glass at 77°K. 2696
Krusic, P. J. Electron spin resonance studies of fluoroalkyl radicals in solutions. I. Structures, conformations, and barriers to hindered internal rotation. 2014
Krusic, P. J. Electron spin resonance studies of fluoroalkyl radicals in solution. II. Adducts to fluoroolefins. 2030
Krusic, P. J. Electron spin resonance studies of fluoroalkyl radicals in solution. III. Photolysis of perfluoroketones and adduct formation. 2036
Kubokawa, Y. Photochemistry in the adsorbed layer. I. Photolyses of alkyl ketones in the presence of nitric oxide 2442
Kubokawa, Y. Photochemistry in the adsorbed layer. II. Energy transfer in the adsorbed layer. 2446
Kuder, J. E. Electrochemical studies and molecular energy levels in furanquinones 1714
Kullberg, L. Mechanisms of ion exchange in crystalline zirconium phosphates. XI. Variation in unit cell dimensions and sodium ion/hydrogen ion exchange behavior in highly crystalline α-zirconium phosphates. 1150
Kullberg, L. H. Mechanism of ion exchange in crystalline zirconium phosphates. X. Calorimetric determination of heats of sodium(1+) ion-proton exchange 152
Kullberg, L. H. Mechanism of ion exchange in zirconium phosphates. XII. Calorimetric determination of heats of cesium ion-hydrogen ion exchange. 1812
Kung, H. H. Effect of silylation upon the hydrogenating activity of supported platinum catalysts. 875
Kung, R. T. V. Vaporization of reactive salts. 1433
Kuppers, J. R. Partial molal expansibilities from the temperature of maximum density of aqueous solutions. 1041
Kusunoki, I. Sticking coefficient curves expected for multilayer adsorption 748
Lablache-Combier, A. Electron spin resonance of γ irradiation induced free radicals in polyvinylpyridines. 899
Lagowski, J. J. Liquid ammonia solutions. XI. Raman study of the nature of solutions containing alkali and alkaline earth cations. 143
Lagowski, J. J. Liquid ammonia solutions. XII. Raman study of nitrates and thiocyanates. 708
Lam, K. Y. Yield of solvated electrons in the aliphatic alcohols at picosecond times. 2414
Lampe, F. W. Ion-molecule reactions in disilane. 1184
Lampe, F. W. Kinematics of hydride-ion and hydrogen-atom transfer reactions in monosilane. 2195
Lampe, F. W. Ion-Molecule reactions in methylsilane. 2422
Lampe, F. W. Kinematics of hydride transfer reactions in methylsilane. 2429
Lampe, F. W. Ion-molecule reactions in monosilane-ethylene mixtures. 2433
Lampe, F. W. Ion-molecule reactions in monosilane-acetylene mixtures. 2645
Land, E. J. Chemiluminescent reactions after pulse radiolysis of aqueous dye solutions. Absolute yields. 1251
Landreth, R. Thermodynamics of the reactions $(NH_3)_n{\cdot}SO_2(s) \rightarrow nNH_3(g) + SO_2(g)$. 1378
Lane, E. H. Calculation of equilibrium constants and extinction coefficients for 1:1 complexes. Comments. 557
Lang, J. Ultrasonic absorption in aqueous solutions of nucleotides and nucleosides. II. Kinetics of proton exchange in adenosine 5'-monophosphate. 80
Lang, R. P. Molecular complexes of iodine with trioctylphosphine oxide and triethoxyphosphine sulfide. 1657
Lankard, J. R. Role of trifluoromethyl radicals in the photochemical iodine laser. 951
Lanning, J. A. Effect of water-hydrocarbon interactions on proton mobility. Chronoamperometric diffusion coefficients in aqueous tert-butyl alcohol. 70
Larsen, J. W. Enthalpies of binding of organic molecules to cetyltrimethylammonium bromide micelles. 834
Lau, Y. K. Radiolysis of 1,1-difluoroethane 2183
Laufer, A. H. Rate constants for reactions of methylene with carbon monoxide, oxygen, nitric oxide, and acetylene. 1344
Leduc, P. A. Apparent molal volumes, heat capacities, and excess enthalpies of n-alkylamine hydrobromides in water as a function of temperature. 1217
Lee, J. H. Kinetic isotope effects in the reactions of hydrogen and deuterium atoms with dimethyl ether and methanol 2650
Lemley, A. T. Liquid ammonia solutions. XII. Raman study of nitrates and thiocyanates. 708
Lentz, B. R. Structure of liquid water. II. Improved statistical thermodynamic treatment and implications of a cluster model. 1531
Lentz, B. R. Vibrational frequencies of water clusters. 1844
Lentz, D. J. Solvent isotope effects for sulfonephthalein indicator dianion-proton recombination kinetics. 1021
Lepori, L. Volumetric properties of aqueous solutions of organic compounds. III. Aliphatic secondary alcohols, cyclic alcohols, primary, secondary, and tertiary amines. 1030
Lepple, F. K. Isothermal compressibility of aqueous sodium chloride, magnesium chloride, sodium sulfate, and magnesium sulfate solutions from 0 to 45° at 1 atm. 1636
Leung, Y-K. Gas-liquid chromatography on polymers. I. Polyisobutylene-hydrocarbons at 25°. 60
Levanon, H. Hydroperoxyl radical reactions. II. Cupric ions in modulated photolysis. Electron paramagnetic resonance experiments. 779
Levay, B. Effect of surface-active materials in water on ortho-positronium lifetime and its connection to the bubble model. 2526
Lewis, D. K. Cyclopentene decomposition in shock waves. 436
Libby, W. F. Catalyzed and uncatalyzed dissolution of anhydrous chromic chloride in aqueous solutions. 1993
Lilie, J. Pulse radiolytic study of nickel(1+) ion. Nickel-carbon bond formation. 882
Lin, C-T. Mathematical approach for stopped-flow kinetics of fast second-order reactions involving inhomogeneity in the reaction cell. 305
Lin, D. P. Reversible trap to cabanion electron transfer in γ-irradiated hydrocarbon glasses. 1135
Lin, D. P. Radical pairs, electron spin resonance relaxation times, and limiting radical concentrations in γ-irradiated 3-methylpentane glass. 2233
Lin, L-N. Hydrogen bonding of phenol in carbon tetrachloride. Use of activity data to evaluate association models. 1443
Lin, M. C. Chemical lasers produced from $O(^3P)$ atom reactions. IV. Carbon monoxide laser emission from the oxygen atom + cyanogen reaction. 1451
Lin, S-S. High-temperature vaporization of ternary systems. I. Mass spectrometry of oxygen-rich vanadium-tungsten-oxygen species. 266
Lindenbaum, S. Thermodynamic calculations of equilibrium constants for ion-exchange reactions between unequally charged cations in polyelectrolyte gels. 1110
Litan, A. State of the solution-membrane interface during ion transport across an ion-exchange membrane. 1805
Litt, M. H. Cation radical salts of N-methylphenothiazine and its analogs. Synthesis and characterization. 1750
Liu, D. K. K. Solvation of extracted complex metal acids. VII. Improved model. 2572
Liu, D. S. Singlet-triplet intersystem coupling in formaldehyde. 2270
Loader, E. J. Laser Raman spectra of species adsorbed on oxide surfaces. II. 300
Logan, J. Thermal electron transfer reactions in polar solvents. 2148
Logan, S. R. Laser flash photolytic study of mercury(II) iodide in aqueous solution. 1698
Loos, K. R. Structure of triiodide ion in solution. Raman evidence for the existence of higher polyiodide species. 2306
Lozos, G. P. Electron paramagnetic resonance of a nitroxide adsorbed on silica, silica-alumina, alumina, and decationated zeolites. 2110
Lozos, G. P. Electron paramagnetic resonance of adsorbed nitroxide. 200
Luby, P. Statistical theory of polyfunctional polymerization. 1083
Lucas, D. Direct identification of the reactive channels in the reactions of oxygen atoms and hydroxyl radicals with acetylene and methylacetylene. 311
Lucas, M. Relation between molal volumes and molal compressibilities from the viewpoint of the scaled-particle theory. Prediction of the apparent molal compressibilities of transfer. 2367
Lund, A. Free radical formation in hydrocarbon crystals by γ irradiation. Anisotropic hyperfine couplings in $CH_3CH(CH_2)_{33}CH_3$ and relative radical yields in single crystals hexatriacontane (correction). 2698
Lunsford, J. H. Electron paramagnetic resonance study of sulfur dioxide(1-) and tetraoxosulfate(1-) ions on vanadium oxide supported on silica gel. 649
Lunsford, J. H. Infrared and electron paramagnetic resonance study of some silver-nitric oxide complexes in Y type zeolites. 1174
Luria, M. Kinetics of particle growth. III. Particle formation in the photolysis of sulfur dioxide-acetylene mixtures. 325
Luria, M. Natural and experimental fluorescence lifetimes of benzene in various solvents. 1904
Lutz, H. Photolysis of benzene in cyclohexane at 2537 Ang. 1909
Lynch, D. A. Jr. Reinvestigation of the symmetric stretching mode of matrix-isolated dialuminum monoxide. 236
Lyons, P. A. Computer-recorded Gouy interferometric diffusion and the Onsager-Gosting theory. 2050
Lyons, P. A. Electrolyte diffusion in acetonitrile. Harned conductometric technique. 1667
McCormick, D. B. Self-association and solvent-association of cholesterol and other 3β-hydroxysteroids in nonpolar media. 250
McDonald, R. L. Solvation of extracted complex metal acids. VII. Improved model. 2572
Macedo, P. B. Electrical relaxation in a glass-forming molten salt. 639
McGuire, R. F. Intermolecular potentials from crystal data. III. Determination of empirical potentials and application to the packing configurations and lattice energies in crystals of hydrocarbons, carboxylic acids, amines, and amides. 1595
Machulla, H. J. Pressure and phase dependence of the stereochemical course in hot tritium for hydrogen and chlorine-38 for chlorine substitution in meso- and rac-1,2,-dichloro-1,2-difluoroethane. 658
Maciel, G. E. Carbon-13 chemical shifts of the carbonyl carbon. VII. Phenol-acetone system. 124
McLeod, D. Jr. Electron spin resonance study of synthetic cellulose fiber and film. 308
Madeira, S. L. Hydrogen bonding. IV. Correlation of infrared spectral properties with C-H···X hydrogen bonding and crystal habit in tetramethylammonium ion salts. 2585
Madia, W. J. Approximate molecular orbital study of organic positron and positronium complexes. 2683
Madia, W. J. Reactivity of aromatic compounds toward positronium atoms. 1881
Maeda, H. Electric and nonelectric interactions of a nonionic-cationic micelle. 1086

Maestri, M. Dynamic and static quenching of the tris(2,2'-dipyridyl)ruthenium(II) phosphorescence by anionic coordination compounds in various solvents. 1374
Magee, J. L. Triplet formation in ion recombination in spurs. Reply to comment. 310
Magid, L. J. Enthalpies of binding of organic molecules to cetyltrimethylammonium bromide micelles. 834
Maki, A. H. Electrically conducting metal dithiolate-perylene complexes. 215
Malecki, J. Dielectric polarization of dilute associating solutions. V. Solvation of alcohols in nondipolar solvents. 1203
Mallion, R. B. Proton magnetic resonance study of molecular interactions in solutions of fluoranthene in carbon tetrachloride and cyclohexane. 1330
Maltman, K. R. Modified semi-ion-pair model for the evaluation of activation energies of four-center reactions of hydrogen halides to olefins. 1035
Manes, M. Application of the Polanyi adsorption potential theory to adsorption from solution on activated carbon. V. Adsorption from water of some solids and their melts, and a comparison of bulk and adsorbate melting points. 622
Manion, M. L. Chemically induced polarization of fluorine-19 nuclei. Fluorinated phenoxyl and anilinyl radicals. 1837
Manning, G. S. Equivalent conductances of univalent counterions and coions in polyelectrolyte solutions. 1242
Manocha, A. S. Gauche-trans rotational isomerism in ethylamine. Far-infrared spectra of ethylamine-d_2. 803
Mao, S. W. Spin trapping of hydrogen atoms in γ-irradiated liquid alkanes. 91
Marcoux, L. Digital simulation of tubular electrode response in stationary and flowing solution. 718
Margulies, L. Linear dichroism. XI. Determination of the polarization of electronic transitions in coronene and penta- and hexahelicene. 1400
Marketos, D. G. Reaction of the hydrated electron with benzene studied by pulse radiolysis. 1987
Marketou-Mantaka, A. Reaction of the hydrated electron with benzene studied by pulse radiolysis. 1987
Markowitz, S. S. Recoil tritium reactions with cyclohexene and alkenes. Determination of rate parameters. 347
Markowitz, S. S. Recoil tritium reactions with methylcyclohexene. Test of the assumption of energy randomization prior to unimolecular decomposition. 354
Maroni, V. A. Existence of associated species in lanthanum (III) chloride-potassium chloride melts. 1134
Marshall, J. H. Kinetics of the reaction between triplet benzophenone and diphenylamine. Electron spin resonance study. 2225
Marshall, R. C. Angular overlap model description of the electronic and magnetic properties of copper(II) complexes. 1235
Martin, R. B. Invariance of disulfide stretching wave numbers to disulfide dihedral angles. 855
Martin, R. M. Hot hydrogen atom-hydrocarbon reactions. Dependence of yields on structure and energy. 559
Martire, D. E. Measurement and interpretation of activity coefficients for aromatic solutes at infinite dilution in n-octadecane and n-hexadecyl halide solvents. 1644
Mason, R. P. Estimating microsecond rotational correlation times from lifetime broadening of nitroxide electron spin resonance spectra near the rigid limit. 1321
Mason, R. P. Interpretation of electron spin resonance spectra of spin labels undergoing very anisotropic rotational reorientation. Comments. 1324
Massey, M. W. Jr. Dissociation field effect and temperature-jump kinetics of ethanolic and aqueous phenolphthalein. 2450
Massoudi, R. Effect of pressure on the surface tension of water. Adsorption of low molecular weight gases on water at 25°. 2262
Masterton, W. L. Volume change for the formation of magnesium sulfate ion pairs at various temperatures. 1287
Masuhara, H. Laser photolysis studies on the primary processes of photoinduced ionic polymerizations. 341
Mataga, N. Laser photolysis studies on the primary processes of photoinduced ionic polymerizations. 341
Mathieson, J. G. Orientation behavior of adsorbed pyridine and pyrazine at the mercury-water interface in relation to solution thermodynamic properties. 1226
Matijevic, E. Growth mechanism of hydrous chromium(III) oxide spherical particles of narrow size distribution. 2621
Matijevic, E. Titrimetric applications of multiparametric curve fitting. III. Evaluation of the parameters characterizing acidimetric potentiometric titrations of laurate ion. 2626
Matlub, M. H. Oxidation of titanium, tantalum, and niobium films by oxygen and nitrous oxide. 2486
Matsuoka, Y. Diffuse reflectance spectra of metachromatic dyes. Existence of a long wavelength band in solid states. 1040
Matuszewski, B. Photochemistry of 7-ketonorbornane in vapor phase and solution. 2637
Maxwell, I. E. Crystal structure of hydrated thallium-exchanged zeolite X. 2395
Mayer, J. Scavenging of electrons in 3-methylpentane glass at 77°K. 2696
Mayer, T. M. Kinematics of hydride-ion and hydrogen-atom transfer reactions in monosilane. 2195
Mayer, T. M. Ion-Molecule reactions in methylsilane. 2422
Mayer, T. M. Kinematics of hydride transfer reactions in methylsilane. 2429
Mayer, T. M. Ion-molecule reactions in monosilane-ethylene mixtures. 2433
Mayer, T. M. Ion-molecule reactions in monosilane-acetylene mixtures. 2645
Mayorga, G. Thermodynamics of electrolytes. II. Activity and osmotic coefficients for strong electrolytes with one or both ions univalent (correction). 2698
Mazur, Y. Linear dichroism. XI. Determination of the polarization of electronic transitions in coronene and penta- and hexahelicene. 1400
Meagher, J. F. Intramolecular vibrational energy relaxation. Decomposition of a series of chemically activated fluoroalkyl cyclopropanes. 2535
Meagher, J. F. Kinetic isotope effects in the reactions of hydrogen and deuterium atoms with dimethyl ether and methanol 2650
Meakin, P. Electron spin resonance studies of fluoroalkyl radicals in solutions. I. Structures, conformations, and barriers to hindered internal rotation. 2014
Meakin, P. Electron spin resonance studies of fluoroalkyl radicals in solution. III. Photolysis of perfluoroketones and adduct formation. 2036
Meisel, D. Hydroperoxyl radical reactions. II. Cupric ions in modulated photolysis. Electron paramagnetic resonance experiments. 779
Meisel, D. Hydroperoxyl radical reactions. III. Pulse-radiolytic study of the reaction of the hydroperoxyl radical with some metal ions. 2330
Meites, L. Titrimetric applications of multiparametric curve fitting. III. Evaluation of the parameters characterizing acidimetric potentiometric titrations of laurate ion. 2626
Melamud, E. Oxygen-17 anisotropic dipolar interaction in the carbonyl group of semiquinones. 2140
Melton, C. E. Formation of negative ions in nitric oxide and the interaction of nitric oxide with hydride and oxygen(1-) ions from water. Reply to comments. 1446
Menezes-Affonso, S. Self-diffusion coefficients for chloride ion in aqueous solutions of sodium polyacrylate containing sodium chloride. 1756
Menger, F. M. Interfacial and micellar properties of bolaform electrolytes. 1387
Meot-Ner, M. Negative temperature dependence of slow ion-molecule reactions. 1773
Meyer, R. T. Flash photolysis and time-resolved mass spectrometry. III. Termolecular and surface recombinations of ground state iodine atoms. 878
Michael, J. V. Chemical kinetic effects of walls on active species. Results for hydrogen atoms. 465
Michael, J. V. Absolute quenching cross sections of Hg($^3P_1$) with various molecules. 482
Michaud, P. Relative rates of the reactions of O($^1D_2$) atoms with alkanes and cycloalkanes. 1457
Micic, O. I. Solvent participation in electron transfer reactions. 285
Miller, R. L. Electrochemical studies and molecular energy levels in furanquinones 1714
Millero, F. J. Volume change for the formation of magnesium sulfate ion pairs at various temperatures. 1287
Millero, F. J. Isothermal compressibility of aqueous sodium chloride, magnesium chloride, sodium sulfate, and magnesium sulfate solutions from 0 to 45° at 1 atm. 1636
Milstein, R. Relative reaction rate involving thermal fluorine-18 atoms and thermal fluoroethyl radicals with oxygen, nitric oxide, sulfur dioxide, nitrogen, carbon monoxide, and hydrogen iodide. 857
Minch, M. J. Micellar effects on the ionization of carboxylic acids and interactions between quaternary ammonium ions and aromatic compounds. 1490
Minesinger, R. R. Band-shape correlations in the electronic absorption spectra of para-(+M)-substituted nitrobenzene derivatives. 494
Mishra, S. P. Radicals formed during the radiolysis of a range of oxysulfur and oxyphosphorus compounds. 576
Mittal, J. P. Interaction of hydrated electrons with phenylalanine and related compounds. 1790
Miura, M. Diffuse reflectance spectra of metachromatic dyes. Existence of a long wavelength band in solid states. 1040
Miyahara, K. Intermediate oxygen species of homomolecular oxygen exchange and the oxidation of carbon monoxide over zinc oxide under illumination. 2303
Mochida, I. Transition metal ions on molecular sieves. II. Catalytic activities of transition metal ions on molecular sieves for the decomposition of hydrogen peroxide. 1653
Moeckel, H. Formation of positive ions in the reaction of disulfides with hydroxyl radicals in aqueous solution. 282
Moggi, L. Dynamic and static quenching of the tris(2,2'-dipyridyl)ruthenium(II) phosphorescence by anionic coordination compounds in various solvents. 1374
Momany, F. A. Intermolecular potentials from crystal data. III. Determination of empirical potentials and application to the packing configurations and lattice energies in crystals of hydrocarbons, carboxylic acids, amines, and amides. 1595
Momany, F. A. Intermolecular potentials from crystal data. IV. Application of empirical potentials to the packing configurations and lattice energies in crystals of amino acids. 1621
Moorthy, P. N. Intermediates produced from the one-electron reduction of nitrogen heterocyclic compounds in solution. 2615
Moraweck, B. Structure and texture of a crushed sodium-yttrium zeolite. 1959
Morimoto, T. Infrared spectra of butylamine adsorbed on silica-alumina. 704
Morimoto, T. Adsorption anomaly in the system zinc oxide-water. 1116
Morosi, G. Geometry and electronic structure of nitrostyrene molecules and anions. 49
Morris, E. D. Jr. Reaction of the nitrate radical with acetaldehyde and propylene 1337
Morse, D. L. Technique for the determination of absolute emission quantum yields of powdered samples. 2229
Mortland, M. M. Aromatic radical cation formation on the intracrystal surfaces of transition metal layer lattice silicates. 994
Mowery, D. F. Jr. Derivation of rate equations for Fischer glycosidation of D-glucose and estimation of rate constants using a computer. 1918
Moynihan, C. T. Electrical relaxation in a glass-forming molten salt. 639
Moynihan, C. T. Dependence of the glass transition temperature on heating and cooling rate. 2673

Mraw, S. C. Entropies of the hydrates of sodium hydroxide. III. Low-temperature heat capacities and heats of fusion of the α and β crystalline forms of sodium hydroxide tetrahydrate. 1701

Mulac, W. A. Excited state production by nonionic processes in the pulse radiolysis of gaseous systems containing naphthalene. 22

Murata, T. Isomerizaton of chemically activated propenyl radicals. 2543

Myers, G. E. Thermodynamic calculations of equilibrium constants for ion-exchange reactions between unequally charged cations in polyelectrolyte gels. 1110

Mysels, K. J. Bursting of soap films. VI. Effect of surfactant purity. 234

Naegerl, H. Interaction of molecular hydrogen with magnesium oxide defect surface. 758

Nafisi-Movaghar, J. Photolysis of liquid cyclohexane at 1634 Ang and the effect of the addition of carbon tetrachloride and sulfur hexafluoride. 1899

Nagao, M. Infrared spectra of butylamine adsorbed on silica-alumina. 704

Nagao, M. Adsorption anomaly in the system zinc oxide-water. 1116

Nagy, J. B. Charge-transfer complexes in organic chemistry. XI. Effect of acceptors on the properties of charge-transfer complexes formed by cyclic anhydrides. 980

Nagy, O. B. Charge-transfer complexes in organic chemistry. XI. Effect of acceptors on the properties of charge-transfer complexes formed by cyclic anhydrides. 980

Nakamura, M. Electron spin resonance of palladium(I). IV. Mixed-ligand complexes of palladium(I). 2136

Nakanishi, K. Determination of cross-term diffusion coefficients in ternary systems by the capillary cell method. 2281

Nakashima, T. T. Carbon-13 chemical shifts of the carbonyl carbon. VII. Phenol-acetone system. 124

Nancollas, G. H. Growth of calcium phosphate on hydroxyapatite crystals. Effect of supersaturation and ionic medium. 2218

Nandi, P. K. Effects of tetraalkylammonium salts on the activity coefficient of N-acetyl ethyl esters of phenylalanine, norleucine, and norvaline. 1197

Navon, G. Nuclear magnetic resonance studies of the interaction of molecular oxygen with organic compounds. 1747

Navon, G. Electron paramagnetic resonance of ruthenium(III) halopentaammines in single crystals. 700

Neff, L. D. Structure and reactions of some mercaptans on a nickel surface. 1648

Nestor, C. W. Jr. Predicted properties of the superheavy elements. III. Element 115, Eka-bismuth. 1945

Neta, P. Hydroxyl radical reactions with phenols and anilines as studied by electron spin resonance. 523

Neta, P. Substituted pyridinyl radicals in aqueous solutions. Formation, reactivity, and acid-base equilibriums. 2211

Neumer, J. F. CNDO [complete neglect of differential overlap] and ab initio derived σ-core charges for Pariser-Parr-Pople π-electron calculations on nitroaromatics. 1868

Newsome, D. S. Significant structure theory of multilayer physical adsorption. 2600

Nichol, L. W. Difference gel chromatography of kinetically controlled systems. Irreversible polymerization. 460

Nichols, A. L. Approximate molecular orbital study of organic positron and positronium complexes. 2683

Nichols, A. L. Reactivity of aromatic compounds toward positronium atoms. 1881

Nika, G. G. Exchange of hydrogen bromide and deuterium behind reflected shock waves. 2549

Niki, H. Reaction of the nitrate radical with acetaldehyde and propylene. 1337

Niki, H. Rate constants for the reaction of ozone with olefins in the gas phase. 2318

Nilsson, R. Role of singlet oxygen in some chemiluminescence and enzyme oxidation reactions. 1681

Nishikida, K. Methyl radical-methanesulfenate anion pairs formed by dissociative electron capture in γ-irradiated crystalline dimethyl-d_6 sulfoxide at 77°K. 1882

Nitta, K. Polymer concentration dependence of surface electric potential of cylindrical polyelectrolyte in aqueous salt solutions. 1189

Noda, S. Energy level structure and mobility of excess electrons in γ-irradiated 5 M potassium carbonate aqueous glasses. Effect of ions on trapped and mobile electrons in aqueous glasses. 2454

Novick, J. L. Virial theorem decomposition of molecular force fields. 989

Oakenfull, D. G. Effect of ethanol on hydrophobic interactions. Conductometric study of ion-pair formation by double-long-chain electrolytes. 1759

Odom, J. D. Spectra and structure of boron-nitrogen compounds. II. Infrared and Raman spectra of trimethylamine-borane. 1503

Ofran, M. Natural and experimental fluorescence lifetimes of benzene in various solvents. 1904

Ogden, J. S. Matrix isolation infrared study of the reaction between germanium vapor and molecular oxygen. Characterization and mechanism of formation of moleclar germanium dioxide and ozone. 1763

Ogura, H. Prompt electron scavenging by benzene in pulse-irradiated alcohols. 504

Olszyna, K. J. Kinetics of particle growth. III. Particle formation in the photolysis of sulfur dioxide-acetylene mixtures. 325

Ondercin, D. G. Activation parameters for the restricted rotation of the hydroxyl group in the duroquinol cation radical as determined from the electron spin resonance spectra. 130

Ono, Y. Electron spin resonance study of the formation of anion radicals over titanium exchanged Y-zeolite. 218

O'Reilly, D. E. Pressure dependence of viscosity and nuclear relaxation time in water and deuterium oxide. 1674

O'Reilly, D. E. Self-diffusion of solid and liquid sodium. 2275

Oren, Y. State of the solution-membrane interface during ion transport across an ion-exchange membrane. 1805

Orgee, L. Matrix isolation infrared study of the reaction between germanium vapor and molecular oxygen. Characterization and mechanism of formation of moleclar germanium dioxide and ozone. 1763

Oshima, K. Electron spin polarization effects in a study of transient hydrogen atoms in acidic ices under electron irradiation. 1336

Oskarsson, A. Mechanisms of ion exchange in crystalline zirconium phosphates. XI. Variation in unit cell dimensions and sodium ion/hydrogen ion exchange behavior in highly crystalline α-zirconium phosphates. 1150

Osterhoudt, H. W. Transport properties of hydrophilic polymer membranes. Influence of volume fraction polymer and tortuosity on permeability. 408

Ostvold, T. Thermodynamic studies of binary charge unsymmetrical fused salt systems. Calorimetric and electromotive force measurements of liquid lanthanum(III) chloride-alkali chloride mixtures. 181

Ottolenghi, M. Role of the triplet state in the photoisomerization of retinal isomers. 336

Ouchi, K. Electron nuclear double resonance study of 9-arylxanthyl radicals. 2512

Owicki, J. C. Structure, energetics, and dynamics of the water dimer. 2055

Pal, M. K. Metachromasia of basic dyes induced by mercuric chloride. II. 536

Paniccia, F. Redox mechanism in an ionic matrix. IV. Catalytic effects of peroxide and superoxide on the oxidation of nitrite by molecular oxygen in molten alkali nitrates. 1693

Paoletti, S. Thermodynamics of polycarboxylate aqueous solutions. I. Dilatometry and calorimetry of protonation and copper(II) binding. 607

Paoletti, S. Thermodynamics of polycarboxylate aqueous solutions. II. Dilatometry and calorimetry of nickel and barium binding. 1486

Papatheodorou, G. N. Thermodynamic studies of binary charge unsymmetrical fused salt systems. Cerium(III) chloride-alkali chloride mixtures. 178

Papatheodorou, G. N. Thermodynamic studies of binary charge unsymmetrical fused salt systems. Calorimetric and electromotive force measurements of liquid lanthanum(III) chloride-alkali chloride mixtures. 181

Papatheodorou, G. N. Existence of associated species in lanthanum (III) chloride-potassium chloride melts. 1134

Paraskevopoulos, G. Relative rates of the reactions of O($^1D_2$) atoms with alkanes and cycloalkanes. 1457

Parker, A. J. Coordination and ionic solvation. 1731

Pask, J. A. Wetting under chemical equilibrium and nonequilibrium conditions. 1178

Patel, R. C. Relaxation spectra of 6-methylpurine in aqueous solution. 848

Patil, K. J. Volumetric and isentropic compressibility behavior of aqueous amine solutions. I. 714

Patterson, L. K. Substituted pyridinyl radicals in aqueous solutions. Formation, reactivity, and acid-base equilibriums. 2211

Pedulli, G. F. Theoretical interpretation of the rotational barrier in benzophenone ketyl. 2144

Pekary, A. E. Dipole moment and far-infrared studies on the dimethyl sulfoxide-iodine complex. 1744

Peng, T. C. Carbon disulfide dissociation in a thermal cell. 634

Penny, A. L. Reactions involving electron transfer at semiconductor surfaces. V. Reactivity and electron paramagnetic resonance of electron transfer sites on rutile. 870

Peri, J. B. Infrared study of nitric oxide and carbon monoxide adsorbed on chromia/alumina. 588

Persoons, A. P. Field dissociation effect and chemical relaxation in electrolyte solutions of low polarity. 1210

Perumareddi, J. R. Four electron (or hole) noncubic ligand field spectrum. I. Tetragonal energy levels. 2678

Petersen, J. D. Photochemistry of rhodium(III) complexes. Ligand field excitation of hexaamminerhodium(III) and characteristics of nonradiative deactivation paths. 1144

Petersen, J. D. Photochemistry of rhodium(III) complexes. Ligand field excitation of hexaamminerhodium(III) and characteristics of nonradiative deactivation paths (correction). 2698

Petrakis, L. Surface acidity of modified alumina. Reply to comments. 2070

Petrucci, S. Electrical conductance and ultrasonic relaxation for lithium perchlorate in tetrahydrofuran. 917

Pfeiffer, W. F. Bubble solution method for diffusion coefficient measurements. Experimental evaluation. 2516

Pfister, G. Mechanism of fluorescence quenching by acids in poly(N-vinylcarbazole). 2009

Phillips, D. Mechanisms of electronic energy transfer in the gas phase. 2407

Phillips, D. Photophysics of isolated molecules. Disubstituted benzenes. 7

Phillips, D. Photochemistry of halogenated acetones. I. Spectroscopic studies. 665

Phillips, D. Photochemistry of halogenated acetones. II. Rate constant measurements. 671

Phillips, D. Photochemistry of halogenated acetones. III. Vibrational relaxation in singlet state. 679

Phillips, D. Photochemistry of halogenated acetones. IV. Quenching of the excited states. 682

Pichat, P. Infrared and ultraviolet spectra of adsorbed diazines. Their use in acidity determinations. 2376

Pick, M. Pulse radiolysis of cyclopentane in aqueous solutions. 1049

Pickles, C. K. Proton magnetic resonance study of molecular interactions in solutions of fluoranthene in carbon tetrachloride and cyclohexane. 1330

Pierce, R. C. Low-temperature chemical ionization mass spectrometry of methane-hydrogen mixtures. 93

Pikal, M. J. Effect of water-hydrocarbon interactions on proton mobility. Chronoamperometric diffusion coefficients in aqueous tert-butyl alcohol. 70

Pinnavaia, **T. J.** Aromatic radical cation formation on the intracrystal surfaces of transition metal layer lattice silicates. 994

Pitts, **J. N. Jr.** Absolute rate constants for the reaction of $O(^3P)$ atoms with selected alkanes, alkenes, and aromatics as determined by a modulation technique. 1780

Pitzer, **K. S.** Thermodynamics of electrolytes. II. Activity and osmotic coefficients for strong electrolytes with one or both ions univalent (correction). 2698

Plowman, **K. R.** Liquid ammonia solutions. XI. Raman study of the nature of solutions containing alkali and alkaline earth cations. 143

Pochan, **J. M.** Theory of molecular association in cholesteric-nematic liquid crystal mixtures. 1206

Pochan, **J. M.** Effect of structure on the mesomorphic properties of cholesteryl alkanoates. V. Electric field effects on a uniaxial smectic phase of mixtures of cholesteryl alkanoates. 1740

Polak, **M.** Nuclear magnetic resonance studies of the interaction of molecular oxygen with organic compounds. 1747

Pollack, **M. I.** Electron paramagnetic resonance spectra of tetrachloromanganate(II) in molten tetrabutylammonium tetrachlorocadmate. 1957

Pollock, **T. L.** Model calculations of the hydrogen/deuterium kinetic isotope effect in the atomic hydrogen + disilane reaction. 398

Polnaszek, **C. F.** Interpretation of electron spin resonance spectra of spin labels undergoing very anisotropic rotational reorientation. Comments. 1324

Pope, **M. T.** Heteroconjugation of inorganic anions in nonaqueous solvents. II. Perchlorate complexes of some organic hydroxy compounds. 168

Porter, **R. F.** Low-temperature chemical ionization mass spectrometry of methane-hydrogen mixtures. 93

Pott, **G. T.** Studies of compound formation on alkali/γ-aluminum oxide catalyst systems using chromium, iron, and manganese luminescence. 2496

Poulsen, **J. C.** Electronic spectra of aromatic hydrocarbon anions and cations in the CNDO/S [complete neglect of differential overlap using spectroscopically determined parameters] model. 1420

Price, **D.** Forst fall-off procedures utilizing direct count state densities. 2326

Priesand, **M. A.** Ultrasound propagation in binary mixtures of dimethyl sulfoxide and water. 2611

Prigogine, **M.** Mechanism of the hydrolysis of treithylethoxysilane at the silica-carbon tetrachloride interface. Comments. 757

Pruetz, **W. A.** Chemiluminescent reactions after pulse radiolysis of aqueous dye solutions. Absolute yields. 1251

Prusazcyk, **J.** Stop-flow time-of-flight mass spectrometry kinetics study. Reaction of ozone with nitrogen dioxide and sulfur dioxide. 1775

Pruss, **F.** Direct identification of the reactive channels in the reactions of oxygen atoms and hydroxyl radicals with acetylene and methylacetylene. 311

Pruss, **F. J. Jr.** Extending the use of the atomic oxygen + nitrogen dioxide → nitric oxide + molecular oxygen reaction for measuring low oxygen atom concentrations. 208

Pruss, **F. J. Jr.** Determination of branching ratios for the reaction of oxygen atoms with ethylene. 663

Purcell, **J. M.** Nuclear magnetic resonance studies of frozen aqueous solutions. 807

Pysh, **E. S.** Time-dependent Hartree calculations of the sequence dependence of DNA hypochromism. 444

Querry, **M. R.** Infrared optical constants of aqueous solutions of electrolytes. Alkali halides. 238

Querry, **M. R.** Infrared optical constants of aqueous solutions of electrolytes. Acids and bases. 1405

Quick, **E. E.** Effects of intramolecular hydrogen bonds on intermolecular hydrogen bonding. 2236

Quinney, **P. R.** Solubility measurements of aromatic hydrocarbons and carbon disulfide in liquid sulfur by gas chromatography. 2635

Rabani, **J.** Yields of radiation products in sodium metaphosphate glasses. 752

Rabani, **J.** Pulse radiolysis of cyclopentane in aqueous solutions. 1049

Rabani, **J.** Pulse radiolysis of the aqueous ferro-ferricyanide system. II. Reactions of hydrogen atoms and hydrated electrons with ferrocyanide and ferricyanide ions. 1368

Rabani, **J.** Pulse radiolytic investigations of $OHCH_2O_2$ radicals. 2089

Rabinovitch, **B. S.** Fall-off behavior of a thermal unimolecular system in the presence of a weak collider inert bath gas. 863

Rabinovitch, **B. S.** Transfer of vibrational energy from highly excited butyl radicals. Relative collision diameters of homologous n-perfluoroalkane bath molecules. 1979

Rabinovitch, **B. S.** Transfer of vibrational energy from highly excited butyl radicals. Structural effects on the magnitudes of relative collision diameters. 1984

Rabinovitch, **B. S.** Intramolecular vibrational energy relaxation. Decomposition of a series of chemically activated fluoroalkyl cyclopropanes. 2535

Radovic, **J.** Cation radical salts of N-methylphenothiazine and its analogs. Synthesis and characterization. 1750

Rai, **A. P.** Heats of transport of gases. III. Thermoosmosis of ternary gaseous mixtures. 2693

Ramirez, **J. E.** Nuclear magnetic resonance studies of frozen aqueous solutions. 807

Rampazzo, **L.** Charge dependence of free energy of adsorption at the electrode-solution interface. 417

Rao, **K. V. S.** Radicals formed during the radiolysis of a range of oxysulfur and oxyphosphorus compounds. 576

Rao, **K. V. S.** Electron paramagnetic resonance study of sulfur dioxide(1-) and tetraoxosulfate(1-) ions on vanadium oxide supported on silica gel. 649

Rao, **P. S.** Interaction of hydrated electrons with the peptide linkage. 1193

Rapiejko, **R. J.** Thermochemistry of carbonyl addition reactions. II. Enthalpy of addition of dimethylamine to formaldehyde. 599

Rard, **J. A.** Electrical conductances of some aqueous rare earth electrolyte solutions at 25°. I. Rare earth perchlorates. 1435

Rastogi, **R. P.** Heats of transport of gases. III. Thermoosmosis of ternary gaseous mixtures. 2693

Ratkje, **S. K.** Raman spectra of molten mixtures containing aluminum fluoride. I. Lithium fluoride-trilithium hexafluoroaluminate eutectic mixture. 1499

Ratnasamy, **P.** Surface acidity of cobalt-molybdenum-aluminum oxide catalysts. Comments. 2069

Rauch, **F. C.** Kinetics of gas-phase thermal decomposition of tris(difluoroamino)methyl compounds. 2189

Rawlins, **W. T.** Rate constant for carbon monoxide + molecular oxygen = carbon dioxide + atomic oxygen from 1500 to 2500° K. Reevaluation of induction times in the shock-initiated combustion of hydrogen-oxygen-carbon monoxide-argon mixtures. 497

Reeves, **R. R.** Dual photon effects in nitrogen dioxide photolysis. 1583

Reidler, **J.** Metal ion association in alcohol solutions. III. Erbium chloride in aqueous methanol. 424

Reimschussel, **W.** Self-diffusion in liquid binary solutions. 2307

Renner, **T. A.** Computer-recorded Gouy interferometric diffusion and the Onsager-Gosting theory. 2050

Renner, **T. A.** Electrolyte diffusion in acetonitrile. Harned conductometric technique. 1667

Renouprez, **A.** Structure and texture of a crushed sodium-yttrium zeolite. 1959

Resing, **H. A.** Kinetics of surface reactions from nuclear magnetic resonance relaxation times. 1279

Rhine, **P.** Infrared optical constants of aqueous solutions of electrolytes. Alkali halides. 238

Rhine, **P.** Infrared optical constants of aqueous solutions of electrolytes. Acids and bases. 1405

Ricci, **R. W.** Fluorescence quenching of the indole ring system by lanthanide ions. 1953

Rice, **S. A.** Ultraviolet spectrum and photophysical properties of trimethylenecyclopropane. 568

Rieke, **R. D.** Ion association between naphtho[b]cyclobutene radical anion and alkali metal ions. 723

Roberts, **J. D.** Nitrogen-15 nuclear magnetic resonance spectroscopy. Nitrogen-15 chemical shifts determined from natural-abundance spectra. 2507

Roberts, **J. H.** Raman spectroscopic study of binary systems. I. Molecular association in the ammonia hexadeuteriobenzene liquid system. 2106

Roberts, **R.** Vaporization of reactive salts. 1433

Robertson, **K. S.** Effects of intramolecular hydrogen bonds on intermolecular hydrogen bonding. 2236

Rockley, **M. G.** Photophysics of isolated molecules. Disubstituted benzenes. 7

Rodewald, **R. F.** Transition state enthalpies of transfer in aqueous dimethyl sulfoxide solutions. Alkaline hydrolysis of ethyl acetate. 1509

Rodgers, **A. S.** Thermochemistry of gas-phase equilibrium 1,1,1-trifluoroethane + molecular iodine = 2,2,2-trifluoroethyl iodide + hydriodic acid. Carbon-hydrogen bond dissociation energy in 1,1,1-trifluoroethane and the heat of formation of the 2,2,2-trifluoroethyl radical. 2315

Rogers, **D. W.** Heats of hydrogenation of sixteen terminal monoolefins. Alternating effect. 2569

Rogers, **F. E.** Thermochemistry of carbonyl addition reactions. II. Enthalpy of addition of dimethylamine to formaldehyde. 599

Rome, **K. A.** External heavy-atom effect on the photoisomerization of cyanine dyes. 16

Roncin, **J.** Electron capture in γ-irradiated methylcyclohexane glass. 867

Ronfard-Haret, **J. C.** Electron spin resonance of γ irradiation induced free radicals in polyvinylpyridines. 899

Rorabacher, **D. B.** Mathematical approach for stopped-flow kinetics of fast second-order reactions involving inhomogeneity in the reaction cell. 305

Rosano, **H. L.** Surface drag viscosity of bovine serum albumin monolayers. 2266

Rosenberg, **H. S.** Solubility of mercury in polar gases. 186

Rosenfeld, **T.** Role of the triplet state in the photoisomerization of retinal isomers 336

Roth, **H. D.** Chemically induced polarization of fluorine-19 nuclei. Fluorinated phenoxyl and anilinyl radicals. 1837

Roth, **N. J. L.** Predicted observable fluorescent lifetimes of several cyanines. 1154

Rowland, **F. S.** Isotope effect in energy losses for deactivating collisions of tetrafluoromethane with chemically activated fluoroethyl radicals $CH_2{}^{18}FCH_2$ and $CD_2{}^{18}FCD_2$. 850

Rowland, **F. S.** Relative reaction rate involving thermal fluorine-18 atoms and thermal fluoroethyl radicals with oxygen, nitric oxide, sulfur dioxide, nitrogen, carbon monoxide, and hydrogen iodide. 857

Russell, **M. E.** Energetics of formation of some structural isomers of gaseous $C_2H_5O^+$ and $C_2H_6N^+$ ions. 1268

Russell, **R. L.** Solvent and temperature effects in the photoionization of tetramethyl-p-phenylenediamine. 2128

Rytter, **E.** Raman spectra of molten mixtures containing aluminum fluoride. I. Lithium fluoride-trilithium hexafluoroaluminate eutectic mixture. 1499

Sabbatini, **N.** Intersystem crossing efficiency in the hexacyanochromate(III) ion. 541

Saboungi, **M. L.** Phase diagrams of reciprocal molten salt systems. Calculations of liquid-liquid miscibility gaps. 1091

Safarik, **I.** Model calculations of the hydrogen/deuterium kinetic isotope effect in the atomic hydrogen + disilane reaction. 398

Sakurai, **T.** Comparison of the fluorinations of uranium dioxide by bromine trifluoride and elemental fluorine. 1140

Saleh, **J. M.** Oxidation of titanium, tantalum, and niobium films by oxygen and nitrous oxide. 2486

Salomon, **M.** Complex solubilities of the silver halides in 3-methyl-2-oxazolidone 1817

Sambrook, **T. E. M.** Radiolysis of liquid nitrous oxide. 28

Sambrook, T. E. M. Radiolysis of liquid nitrous oxide. Hydrocarbon additives. 32
Sambrook, T. E. M. Radiolysis of liquid hydrocarbon-nitrous oxide solutions. Precursors of nitrogen. 102
Samlaska, J. A. Extending the use of the atomic oxygen + nitrogen dioxide → nitric oxide + molecular oxygen reaction for measuring low oxygen atom concentrations. 208
Sargent, F. P. Direct electron spin resonance detection of free radicals produced in electron-irradiated liquid alcohols. 1977
Sarr, M. Cyclopentene decomposition in shock waves. 436
Sartorio, R. Cation exchange diffusion experiments. 2292
Sauer, M. C. Jr. Excited state production by nonionic processes in the pulse radiolysis of gaseous systems containing naphthalene. 22
Scandola, F. Wavelength dependence of nitropentaamminecobalt(III) photochemistry. Charge transfer and ligand field excited-state behavior. 572
Scandola, F. Mechanism of photosubstitution reactions of square-planar platinum(II) complexes. II. Effect of the leaving ligand on the photosubstitution mechanism of diethylenetriamineplatinum(II) complexes. 2349
Scandola, M. A. Intersystem crossing efficiency in the hexacyanochromate(III) ion. 541
Scandola, M. A. Wavelength dependence of nitropentaamminecobalt(III) photochemistry. Charge transfer and ligand field excited-state behavior. 572
Schellman, J. A. Theory of circularly polarized emission from molecules displaying rotary Brownian motion. 387
Schelly, Z. A. Solvent-jump relaxation kinetics of the association of rhodamine type laser dyes. 1891
Schelly, Z. A. Dissociation field effect and temperature-jump kinetics of ethanolic and aqueous phenolphthalein. 2450
Scheps, R. Ultraviolet spectrum and photophysical properties of trimethylenecyclopropane. 568
Scheraga, H. A. Intermolecular potentials from crystal data. III. Determination of empirical potentials and application to the packing configurations and lattice energies in crystals of hydrocarbons, carboxylic acids, amines, and amides. 1595
Scheraga, H. A. Intermolecular potentials from crystal data. IV. Application of empirical potentials to the packing configurations and lattice energies in crystals of amino acids. 1621
Scheraga, H. A. Empirical intermolecular potential energy function for water. 909
Scheraga, H. A. Structure of liquid water. II. Improved statistical thermodynamic treatment and implications of a cluster model. 1531
Scheraga, H. A. Vibrational frequencies of water clusters. 1844
Scheraga, H. A. Variation of disulfide bond stretching frequencies with disulfide dihedral angle in dimethyl disulfide. 1848
Scheraga, H. A. Structure, energetics, and dynamics of the water dimer. 2055
Scherer, J. R. Raman spectra and structure of water from -10 to 90°. 1304
Schiff, R. Dye laser flash photolysis kinetics study of the reaction of ground-state atomic oxygen with hydrogen peroxide. 463
Schmidt, P. P. Theory of electron transfer reactions in simple dielectric fluids. 1684
Schnipelsky, P. Molecular structure effect on the diffusion of heptane isomers. 1428
Schnuelle, G. W. Statistical thermodynamic consideration of solvent effects on conformational stability. Supermolecule-continuum model. 2064
Schnyders, H. Phase diagrams of reciprocal molten salt systems. Calculations of liquid-liquid miscibility gaps. 1091
Schrader, M. E. Ultrahigh vacuum techniques in the measurement of contact angles. III. Water on copper and silver. 87
Schreiber, H. D. Potential function model of weak and strong hydrogen bonds. 1415
Schrier, E. E. Experimental determination and scaled particle theory calculation of the activity coefficients of benzene and cyclohexane in aqueous sodium chloride solutions. 165
Schrier, M. Y. Experimental determination and scaled particle theory calculation of the activity coefficients of benzene and cyclohexane in aqueous sodium chloride solutions. 165
Schug, J. C. Approximate molecular orbital study of organic positron and positronium complexes. 2683
Schuler, M. A. Radiation chemical studies on systems related to ascorbic acid. Radiolysis of aqueous solutions of α-bromotetronic acid. 1063
Schuler, R. H. Radiolysis of aqueous solutions of cyclopentane and cyclopentene. 1052
Schuler, R. H. Radiation chemical studies on systems related to ascorbic acid. Radiolysis of aqueous solutions of α-bromotetronic acid. 1063
Schuler, R. H. Oxidation of hydroxycyclohexadienyl radical by metal ions. 2335
Schulman, E. M. Optimal determination of relaxation times of fourier transform nuclear magnetic resonance. Determination of spin-lattice relaxation times in chemically polarized species. 1971
Schulte-Frohlinde, D. Laser flash photolysis of substituted stilbenes in solution. 446
Schulte-Frohlinde, D. Evidence for the triplet route in the photochemical trans → cis isomerization of nitrostilbenes in solution. 451
Schulte-Frohlinde, D. Effects of photoselection on decomposition kinetics in frozen solutions using unpolarized light. 782
Schwartz, S. E. Determination of the equivalence point of the nitrogen + nitric oxide titration reaction by electrical conduction. 1120
Schwarz, H. A. Pulse radiolysis study of thallium(II) in aqueous perchloric acid solutions. 488
Schwarz, H. A. Pulse radiolysis studies of chloride complexes of thallium(II). Absorption spectra and stability constants of thallium chloride(1+) ion, thallium dichloride, and thallium trichloride(1-) ion. 892
Scibona, G. Electrical liquid membrane potential. Biionic isothermal potential. 2370
Scuppa, B. Electrical liquid membrane potential. Biionic isothermal potential. 2370
Searcy, A. W. Transition state theory for vaporization and condensation. 1298
Sears, P. G. Conductance behavior of some ammonium and partially substituted ammonium tetraphenylborates in 3-methyl-2-oxazolidone and 3-tert-butyl-2-oxazolidone at 25°. 2687
Sears, P. G. Conductance behavior of tetraalkyammonium salts in 3-tert-butyl-2-oxazolidone at 25°. 2689
Seebach, G. L. Electronic structure of oxovanadium(IV) and copper(II) dicyclohexyldithiophosphinate complexes. 962
Sekhar, M. V. C. Kinetics of the shock-induced competitive dehydrofluorinations of 1,1,2-trifluoroethane. 472
Setser, D. W. Unimolecular reactions and energy partitioning. Three- and four-centered elimination reactions of chemically activated 1,1,2-trichloroethane-d_0-d_1, and -d_2. 2166
Sevilla, M. D. Radicals formed after electron attachment to 5-halouracils in aqueous glasses. 696
Sharma, D. K. Surface acidity of cobalt-molybdenum-aluminum oxide catalysts. Comments. 2069
Sharma, H. D. Isotopic exchange reactions between nitrogen oxides and oxyhalides. 402
Sharma, L. D. Surface acidity of cobalt-molybdenum-aluminum oxide catalysts. Comments. 2069
Shelef, M. Nitric oxide and carbon monoxide chemisorption on cobalt-containing spinels. 2490
Shepherd, J. R. Kinetics of the reaction between iron(II) and silver(I) catalyzed by silver nuclei on titanium dioxide surfaces. 2580
Shida, T. Kinetic studies of photobleaching of trapped electrons in protiated and deuterated methanol and ethanol glasses at 77°K. 232
Shida, T. Electronic absorption spectra of ion radicals and their molecular orbital interpretation. IV. Anion radicals of aromatic and unsaturated aliphatic carbonyl compounds. 741
Shiloh, K. I. Theory of ion-complexing effects in ion-exchange column performance. 926
Shimamori, H. Competitive and noncompetitive electron capture of nitrous oxide with sulfur hexafluoride and electron thermalization in the gas-phase radiolysis of xenon. 954
Shimokoshi, K. Electron spin resonance study of chlorine dioxide adsorbed on the alkali-cation-exchanged X-type zeolites. 1770
Shioshita, D. T. Solvation of extracted complex metal acids. VII. Improved model. 2572
Shipman, L. L. Empirical intermolecular potential energy function for water. 909
Shipman, L. L. Variation of disulfide bond stretching frequencies with disulfide dihedral angle in dimethyl disulfide. 1848
Shipman, L. L. Structure, energetics, and dynamics of the water dimer. 2055
Shiraishi, H. Electron spin polarization effects in a study of transient hydrogen atoms in acidic ices under electron irradiation. 1336
Shortridge, R. G. Chemical lasers produced from O(^{3}P) atom reactions. IV. Carbon monoxide laser emission from the oxygen atom + cyanogen reaction. 1451
Silber, H. B. Metal ion association in alcohol solutions. III. Erbium chloride in aqueous methanol. 424
Silber, H. B. Metal ion association in alcohol solutions. IV. Existence of an inner-sphere complex between erbium(III) and perchlorate. 1940
Silver, B. L. Oxygen-17 anisotropic dipolar interaction in the carbonyl group of semiquinones. 2140
Simic, M. Pulse radiolysis of cyclopentane in aqueous solutions. 1049
Simmons, E. L. Rate of the photochemical reaction of a thin powdered layer. 1265
Simon, M. S. Carcinogenicity of bis(chloromethyl) ether and chloromethyl methyl ether. Comments. 2696
Simonaitis, R. Reaction of hydroperoxyl radicals with nitric oxide and nitrogen peroxide. 653
Simonaitis, R. Reactions of methylperoxy radicals with nitric oxide and nitrogen dioxide. 2417
Simonetta, M. Geometry and electronic structure of nitrostyrene molecules and anions. 49
Simons, G. Virial theorem decomposition of molecular force fields. 989
Simpson, G. A. Mechanism of direct and rubrene enhanced chemiluminescence during α-peroxylactone decarboxylation. 2559
Singh, R. D. CNDO [complete neglect of differential overlap]/2 study of NH...O hydrogen bonds in ions, zwitterions, and neutral molecules. 970
Singhal, T. C. Nonequilibrium thermodynamic studies of electrokinetic effects. V. Onsager's reciprocity relations. 2302
Skanupong, S. Heats of hydrogenation of sixteen terminal monoolefins. Alternating effect. 2569
Skerjanc, J. Thermodynamics of polycarboxylate aqueous solutions. I. Dilatometry and calorimetry of protonation and copper(II) binding. 607
Slagle, I. R. Extending the use of the atomic oxygen + nitrogen dioxide → nitric oxide + molecular oxygen reaction for measuring low oxygen atom concentrations. 208
Slagle, I. R. Determination of branching ratios for the reaction of oxygen atoms with ethylene. 663
Sloth, E. N. Effect of anionic constituents on the surface ionization of lithium salts. 820
Smith, P. Electron paramagnetic resonance study of radicals formed from allyl compounds. 117
Smith, S. R. Thermal decomposition of lithium perchlorate. I. Initiation rate. 773
Smith, S. R. Thermal decomposition of lithium perchlorate. II. Chloride catalysis. 776

Smith, W. S. Consecutive unimolecular decomposition following recoil tritium activation of 1,1-difluoroethane. 2186
Snir, J. Theory of circularly polarized emission from molecules displaying rotary Brownian motion. 387
Snow, R. L. Singlet-triplet separation in helium. 1334
Solka, B. H. Energetics of formation of some structural isomers of gaseous $C_2H_5O^+$ and $C_2H_6N^+$ ions. 1268
Solomon, J. J. Negative temperature dependence of slow ion-molecule reactions. 1773
Solsky, J. F. Vapor pressure measurements of 4,4'-dimethoxyazoxybenzene. 275
Somsen, G. Hydrophobic interactions in mixtures of N,N-dimethylformamide and water. Model calculations and enthalpies of solution. 1719
Sonnabend, L. F. Kinetic studies of bis(chloromethyl)ether hydrolysis by mass spectrometry. 1096
Sood, S. P. Isotopic exchange reactions between nitrogen oxides and oxyhalides. 402
Soylemez, T. Radiolysis of aqueous solutions of cyclopentane and cyclopentene. 1052
Spedding, F. H. Apparent molal volumes of some dilute aqueous rare earth salt solutions at 25°. 1106
Spedding, F. H. Electrical conductances of some aqueous rare earth electrolyte solutions at 25°. I. Rare earth perchlorates. 1435
Spencer, J. N. Potential function model of weak and strong hydrogen bonds. 1415
Spencer, J. N. Effects of intramolecular hydrogen bonds on intermolecular hydrogen bonding. 2236
Sprague, E. D. Effects of photoselection on decomposition kinetics in frozen solutions using unpolarized light. 782
Srinivasan, R. Role of trifluoromethyl radicals in the photochemical iodine laser. 951
Stacey, M. Laser Raman spectra of species adsorbed on oxide surfaces. II. 300
Stearns, C. A. Identification and dissociation energy of gaseous hafnium mononitride. 273
Stedman, D. H. Chemiluminescent reactions of disulfur monoxide. 1248
Stein, F. P. Effect of iron impurities on the thermal decomposition of α-lead azide. 478
Stein, G. Natural and experimental fluorescence lifetimes of benzene in various solvents. 1904
Stein, G. Photolysis of benzene in cyclohexane at 2537 Ang. 1909
Stein, G. Reaction of the hydrated electron with benzene studied by pulse radiolysis. 1987
Stern, J. H. Thermodynamics of caffeine and the 1-1 caffeine-salicylate complex in water at 25°. 1922
Stern, K. H. Equilibrium vaporization rates and vapor pressures of solid and liquid sodium chloride, potassium chloride, potassium bromide, cesium iodide, and lithium fluoride. 1998
Stevenson, G. R. Electron spin resonance study of the effect of electron-releasing groups upon the molecular orbitals of substituted cyclooctatetraene anion radicals. 90
Stevenson, G. R. Equilibrium studies by electron spin resonance. VIII. Use of time averaged coupling constants to determine free ion-ion pair equilibrium constants. 1771
Stigter, D. Micelle formation by ionic surfactants. II. Specificity of head groups, micelle structure. 2480
Stockmayer, W. H. Effect of urea on magnetic relaxation in aqueous solutions of poly(ethylene oxide). 1528
Stoecklin, G. Pressure and phase dependence of the stereochemical course in hot tritium for hydrogen and chlorine-38 for chlorine substitution in meso- and rac-1,2,-dichloro-1,2-difluoroethane. 658
Stoecklin, G. Stereochemistry of the decay-induced gas-phase halogen exchange in diastereomeric 2,3-dichlorobutanes. 1043
Stoklosa, H. J. Electronic structure of oxovanadium(IV) and copper(II) dicyclohexyldithiophosphinate complexes. 962
Stone, J. A. Flash photolysis of aqueous solutions of cysteine. 1130
Stork, W. H. J. Studies of compound formation on alkali/γ-aluminum oxide catalyst systems using chromium, iron, and manganese luminescence. 2496
Strasberger, B. Linear dichroism. XI. Determination of the polarization of electronic transitions in coronene and penta- and hexahelicene. 1400
Strauss, U. P. Counterion binding by poly(vinyl sulfonate). 1013
Strausz, O. P. Photolysis of hydrogen sulfide in the presence of dimethylsilane. 203
Strausz, O. P. Model calculations of the hydrogen/deuterium kinetic isotope effect in the atomic hydrogen + disilane reaction. 398
Studier, M. H. Effect of anionic constituents on the surface ionization of lithium salts. 820
Sturm, J. Ultrasonic absorption in aqueous solutions of nucleotides and nucleosides. II. Kinetics of proton exchange in adenosine 5'-monophosphate. 80
Sturtevant, J. M. Thermodynamics of transfer of molecules and groups from nonpolar to aqueous environments. I. Method. Butyric acid at 25°. 2363
Su, Y. Y. Ring opening in 1,1-dimethylcyclopropane by recoil tritium atoms. 2531
Suess, G. N. Absolute quenching cross sections of $Hg(^3P_1)$ with various molecules. 482
Sugai, S. Polymer concentration dependence of surface electric potential of cylindrical polyelectrolyte in aqueous salt solutions. 1189
Sugihara, H. Electron spin resonance study of chlorine dioxide adsorbed on the alkali-cation-exchanged X-type zeolites. 1770
Sullivan, P. D. Activation parameters for the restricted rotation of the hydroxyl group in the duroquinol cation radical as determined from the electron spin resonance spectra. 130
Sunder, S. Temperature dependence of limiting heat capacities of dissolution of tetrabutylphosphonium bromide, tetraphenylphosphonium bromide, and tetraphenylarsonium chloride in water and hydrophobic hydration. 738
Sundheim, B. R. Electron paramagnetic resonance spectra of tetrachloromanganate(II) in molten tetrabutylammonium tetrachlorocadmate. 1957
Suzuki, K. Effect of pressure on the thermodynamically reversible gelation of 12-hydroxystearic acid in carbon tetrachloride. 759
Suzuki, K. Electron spin resonance study of the formation of anion radicals over titanium exchanged Y-zeolite. 218
Symons, M. C. R. Radicals formed during the radiolysis of a range of oxysulfur and oxyphosphorus compounds. 576
Symons, M. C. R. Low-temperature studies of photolyses of transition-metal complexes. Ferricyanide ion. 1335
Tabata, Y. Electron spin polarization effects in a study of transient hydrogen atoms in acidic ices under electron irradiation. 1336
Tagawa, S. Low-temperature pulse radiolysis. I. Negative ions of halogenated compounds. 519
Takenaka, T. Infrared attenuated total reflection spectra of adsorbed layers at the interface between a germanium electrode and an aqueous solution of sodium laurate. 941
Takeshita, K. Transition metal ions on molecular sieves. II. Catalytic activities of transition metal ions on molecular sieves for the decomposition of hydrogen peroxide. 1653
Takeshita, T. Electron spin resonance study of photosensitized radical formation in n-hexane by benzoic acid. 105
Takezaki, Y. Isomerizaton of chemically activated propenyl radicals. 2543
Tamai, Y. Optical microscopic study on the catalytic hydrogenation of graphite. 2254
Tanaka, I. Emission of imino radicals in the $c^1\pi$ state formed from the photolysis of ammonia, methylamine, and ethylenimine at 123.6 nm. 1784
Tanaka, K. Intermediate of oxygen exchange reaction over illuminated titanium dioxide. 555
Tanaka, K. Intermediate oxygen species of homomolecular oxygen exchange and the oxidation of carbon monoxide over zinc oxide under illumination. 2303
Tanford, C. Theory of micelle formation in aqueous solutions. 2469
Tang, Y. N. Consecutive unimolecular decomposition following recoil tritium activation of 1,1-difluoroethane. 2186
Tang, Y. N. Ring opening in 1,1-dimethylcyclopropane by recoil tritium atoms. 2531
Taniguchi, Y. Effect of pressure on the thermodynamically reversible gelation of 12-hydroxystearic acid in carbon tetrachloride. 759
Tao, S. J. Positron annihilation in amino acids and proteins. 1261
Tapping, R. L. Structural and solvent effects on the rate of reaction between heterocyclic bases and copper(II) bis(diethyldithiocarbamate). 316
Tardy, D. C. Behavior of collisional efficiencies in external activation systems. 612
Tardy, D. C. Homoallylic isomerization of 1-penten-4-yl and the critical energy for methyl + 1,3-butadiene. 1245
Tardy, D. C. Ring opening of chemically activated cyclopentyl and methylcyclobutyl radicals. 1573
Tardy, D. C. Analysis of external activation systems with multiple isomerizations and decompositions. 1579
Tardy, D. C. Reactions of chemically activated pentenyl radicals. Kinetic parameters of 1,4 hydrogen shifts and the cis-trans isomerization of homoallylic radicals. 2201
Taylor, L. D. Carcinogenicity of bis(chloromethyl) ether and chloromethyl methyl ether. Comments. 2696
Terrin, B. Thermodynamics of transfer of molecules and groups from nonpolar to aqueous environments. I. Method. Butyric acid at 25°. 2363
Testa, A. C. Solvent effects on the fluorescence lifetime of 2-aminopyridine. 201
Thibault, R. M. Charge scavenging in γ radiolysis of cyclohexane solutions of carboranes. 788
Thomas, J. K. Luminescence decay of hydrophobic molecules solubilized in aqueous micellar systems. Kinetic model. 190
Thomas, J. K. Equilibria between triplet states of aromatic hydrocarbons. 196
Thomas, J. K. Formation of ions and excited states in the pulse radiolysis of benzonitrile. 2094
Thomas, J. K. Laser photoionization in micellar solutions. Fate of photoelectrons. 2248
Thomas, S. G. Jr. Condensed-phase photochemistry of cyclobutanone. 1461
Thomas, T. F. Photochemistry of 7-ketonorbornane in vapor phase and solution. 2637
Thornton, S. J. Isotope effect in diffusion of carbon-14-substituted benzenes in benzene, n-heptane, n-octane, and cyclohexane at 25°. 846
Thyrion, F. C. Flash photolysis of aromatic sulfur molecules. Reply to comments. 1442
Tilquin, B. Disproportionation and recombination of cyclopentyl radicals. 462
Timmons, R. B. Mechanism of the hydrolysis of triethylethoxysilane at the silica-carbon tetrachloride interface. Reply to comments. 758
Timmons, R. B. Kinetic isotope effects in the reactions of hydrogen and deuterium atoms with dimethyl ether and methanol. 2650
Tobias, C. W. Conductance studies of the alkali metal chlorides in aluminum chloride-propylene carbonate solution. 2521
Tobias, C. W. Thermodynamics of ion solvation of the alkali metal chlorides in aluminum chloride-propylene carbonate solution. 2576
Tomar, M. S. Skeletonized films and measurements of their optical constants. 947
Tomazic, B. Growth of calcium phosphate on hydroxyapatite crystals. Effect of supersaturation and ionic medium. 2218
Tomita, A. Optical microscopic study on the catalytic hydrogenation of graphite. 2254
Tou, J. C. Kinetic studies of bis(chloromethyl)ether hydrolysis by mass spectrometry. 1096

Toukubo, K. Determination of cross-term diffusion coefficients in ternary systems by the capillary cell method. 2281

Toyoda, S. Electron nuclear double resonance study of 9-arylxanthyl radicals. 2512

Traficante, D. D. Carbon-13 chemical shifts of the carbonyl carbon. VII. Phenol-acetone system. 124

Trumbore, C. N. Radiolysis and photolysis of the hydrogen peroxide-p-nitrosodimethylaniline-oxygen system. 888

Truong, T. B. Electron capture in γ-irradiated methylcyclohexane glass. 867

Tschuikow-Roux, E. Kinetics of the shock-induced competitive dehydrofluorinations of 1,1,2-trifluoroethane. 472

Tschuikow-Roux, E. Modified semi-ion-pair model for the evaluation of activation energies of four-center reactions of hydrogen halides to olefins. 1035

Tschuikow-Roux, E. Temperature dependence of the reactions of hydroxy and hydroperoxy radicals with ozone. 1447

Tsuji, K. Electron spin resonance study of photosensitized radical formation in n-hexane by benzoic acid. 105

Tsunoda, M-a. Electric and nonelectric interactions of a nonionic-cationic micelle. 1086

Tsuruya, S. Copper complexes as catalysts of the oxidative coupling reaction of phenol derivatives. 811

Tuazon, E. C. Gauche-trans rotational isomerism in ethylamine. Far-infrared spectra of ethylamine-d_2. 803

Tucker, E. E. Hydrogen bonding of phenol in carbon tetrachloride. Use of activity data to evaluate association models. 1443

Tucker, J. Dependence of the glass transition temperature on heating and cooling rate. 2673

Tucker, J. C. Heat capacities and fusion entropies of the tetrahydrates of calcium nitrate, cadmium nitrate, and magnesium acetate. Concordance of calorimetric and relaxational ideal glass transition temperatures. 278

Tung, T-L. Flash photolysis of aqueous solutions of cysteine. 1130

Turner, D. L. Reactions of nitrogen oxide (NO^+) ion with methanol. 501

Turner, I. D. M. Laser Raman spectra of species adsorbed on oxide surfaces. II. 300

Vadasdi, K. Determining the composition of species presence in a system from potentiometric data. 816

Van-Catledge, F. A. Comparison of approximate INDO [intermediate neglect of differential overlap] and ab initio wave functions. 763

Van Deventer, E. H. Lithium-lithium hydride system. 1933

Van Leirsburg, D. A. Interaction of matrix-isolated nickel fluoride and nickel chloride with carbon monoxide, molecular nitrogen, nitric oxide, and molecular oxygen and of calcium fluoride, chromium(II) fluoride, manganese(II) fluoride, copper(II) fluoride, and zinc(II) fluoride with carbon monoxide in argon matrixes. 134

Van Tiggelen, P. J. Ions in ammonia flames. 2320

Van Wart, H. E. Cation exchange in mixed solvent media. I. Equilibrium swelling of polystyrenesulfonate resins in dimethyl sulfoxide-water media. 411

Van Wart, H. E. Variation of disulfide bond stretching frequencies with disulfide dihedral angle in dimethyl disulfide. 1848

Vedrine, J. C. Temperature dependence of hyperfine coupling for copper complexes in sodium Y zeolite. 531

Veleckis, E. Lithium-lithium hydride system. 1933

Vermeulen, T. Theory of ion-complexing effects in ion-exchange column performance. 926

Vertes, A. Effect of surface-active materials in water on ortho-positronium lifetime and its connection to the bubble model. 2526

Vidoczy, T. Sequence studies in liquid phase hydrocarbon oxidation. II. Mechanism of the alcohol-ketone transition in the oxidation of ethylbenzene. 828

Vijh, A. K. Effects of anions on the potentials of zero charge of metals. 2240

Vitagliano, V. Cation exchange diffusion experiments. 2292

Von Sonntag, C. Radiation chemistry of ethers. V. Solvated electrons from excited (λ 185 nm) p-dioxane. 2181

Voss, A. J. R. Effects of photoselection on decomposition kinetics in frozen solutions using unpolarized light. 782

Waghorne, W. E. Coordination and ionic solvation. 1731

Wahlbeck, P. G. Effect of anionic constituents on the surface ionization of lithium salts. 820

Walker, M. S. Electrochemical studies and molecular energy levels in furanquinones 1714

Wall, S. N. Kinetics of step-wise micelle association. 1024

Wallace, R. M. A method for the determination of rank in the analysis of absorption spectra of multicomponent systems (correction). 2698

Walling, C. Optimal determination of relaxation times of fourier transform nuclear magnetic resonance. Determination of spin-lattice relaxation times in chemically polarized species. 1971

Wang, F. M. Fall-off behavior of a thermal unimolecular system in the presence of a weak collider inert bath gas. 863

Wang, H-C. Ultrasonic relaxation of aqueous yttrium nitrate. 261

Wang, P. S. Electron-electron double resonance investigations of irradiated malonic acid-d_4 single crystals. 1839

Ward, G. K. Isothermal compressibility of aqueous sodium chloride, magnesium chloride, sodium sulfate, and magnesium sulfate solutions from 0 to 45° at 1 atm. 1636

Warren, J. P. Nitrogen-15 nuclear magnetic resonance spectroscopy. Nitrogen-15 chemical shifts determined from natural-abundance spectra. 2507

Wasson, J. R. Electron spin resonance spectra of manganese (II)-doped powder samples of hexakis(pyridine N-oxide)mercury(II) perchlorate complexes. 45

Wasson, J. R. Electronic structure of oxovanadium(IV) and copper(II) dicyclohexyldithiophosphinate complexes. 962

Watanabe, T. New asymmetric dielectric relaxations in two liquid triacetates. 1078

Waters, P. F. High-voltage electroosmosis. Pressure-voltage behavior in the system γ-alumina-2-propanol. 65

Watkins, A. R. Short-lived intermediates formed by the interaction between electronically excited molecules and inorganic ions. 1885

Watkins, A. R Kinetics of fluorescence quenching by inorganic anions. 2555

Wei, L. Y. Ion-molecule reactions in methanol and hydrogen sulfide. 2527

Weinberg, M. S. Generation of radicals in the charge-transfer photochemistry of coordination complexes of colbalt(III) in aqueous solution. 686

Wen, W. Y. Second-order diffusion-controlled reaction. Decay of allyl free radicals in irradiated polyethylene. 1798

West, D. X. Low-temperature studies of photolyses of transition-metal complexes. Ferricyanide ion. 1335

West, J. C. Uncoupled representations in hydrogen isotope exchange reactions. 984

Westover, L. B. Kinetic studies of bis(chloromethyl)ether hydrolysis by mass spectrometry. 1096

Whisnant, C. C. Hyperfine models for piperidine nitroxides. 1410

Whitehead, H. C. Chlorine Kβ x-ray emission spectra of several solid organic chlorine compounds. 2592

Whitehead, R. Forst fall-off procedures utilizing direct count state densities. 2326

Whittam, J. H. Surface drag viscosity of bovine serum albumin monolayers. 2266

Whitten, G. Photolysis of nitric acid vapor. 1

Wilder, J. Dependence of the glass transition temperature on heating and cooling rate. 2673

Wilhoit, R. C. Thermodynamic properties of systems with specific interactions calculated from the hard-sphere equation of state. I. Binary systems with one inert component. 1961

Wilkins, R. A. Jr. Kinetics of nitric oxide catalyzed decomposition of nitryl chloride and its related nitrogen isotope exchange reactions. 2073

Wilkinson, J. G. Low-temperature studies of photolyses of transition-metal complexes. Ferricyanide ion. 1335

Willard, J. E. Reversible trap to cabanion electron transfer in γ-irradiated hydrocarbon glasses. 1135

Willard, J. E. Decay kinetics of sorbed methyl radicals generated by photodecomposition and radiolysis of methyl halides on silica gel. 1391

Willard, J. E. Radical pairs, electron spin resonance relaxation times, and limiting radical concentrations in γ-irradiated 3-methylpentane glass. 2233

Willard, J. E. Chemical states of sulfur-35 formed by the $^{35}Cl(n,p)^{35}S$ process in potassium chloride. 372

Williams, D. Infrared optical constants of aqueous solutions of electrolytes. Alkali halides. 238

Williams, D. Infrared optical constants of aqueous solutions of electrolytes. Acids and bases. 1405

Williams, D. J. Mechanism of fluorescence quenching by acids in poly(N-vinylcarbazole). 2009

Williams, F. Methyl radical-methanesulfenate anion pairs formed by dissociative electron capture in γ-irradiated crystalline dimethyl-d_6 sulfoxide at 77°K. 1882

Williams, R. L. Relative reaction rate involving thermal fluorine-18 atoms and thermal fluoroethyl radicals with oxygen, nitric oxide, sulfur dioxide, nitrogen, carbon monoxide, and hydrogen iodide. 857

Winer, A. M. Electron paramagnetic resonance absorption in oriented phosphorescent 2,3-benzocarbazole and 1,2,3,4-tetrahydroanthracene at magnetic fields below 65 G. 692

Winzor, D. J. Difference gel chromatography of kinetically controlled systems. Irreversible polymerization. 460

Wojciechowska, E. Scavenging of electrons in 3-methylpentane glass at 77°K. 2696

Woltermann, G. M. Electron spin resonance spectra of manganese (II)-doped powder samples of hexakis(pyridine N-oxide)mercury(II) perchlorate complexes. 45

Wong, M. M. Solvent-jump relaxation kinetics of the association of rhodamine type laser dyes. 1891

Wong, W. Dye laser flash photolysis kinetics study of the reaction of ground-state atomic oxygen with hydrogen peroxide. 463

Woo, J. W. High-voltage electroosmosis. Pressure-voltage behavior in the system γ-alumina-2-propanol. 65

Wood, P. B. Electron paramagnetic resonance study of radicals formed from allyl compounds. 117

Wood, R. H. Heats of mixing aqueous electrolytes. XI. Charge-asymmetric limiting law at low concentrations. Barium chloride with sodium chloride and sodium sulfate with sodium chloride. 1924

Wood, R. H. Interactions of aqueous electrolytes with nonelectrolytes. Enthalpy of dilution of urea and tert-butyl alcohol in salt solutions. 2460

Wood, R. H. Heat of mixing aqueous nonelectrolytes at constant molality. Sucrose, urea, and glycine. 2465

Woolley, E. M. Complex solubility of silver iodide in ethanol-water, methanol-water, acetone-water, and dioxane-water mixtures. 2244

Wrenn, S. Interfacial and micellar properties of bolaform electrolytes. 1387

Wright, L. D. Self-association and solvent-association of cholesterol and other 3β-hydroxysteroids in nonpolar media. 250

Wrighton, M. S. Technique for the determination of absolute emission quantum yields of powdered samples. 2229

Wu, C. H. Rate constants for the reaction of ozone with olefins in the gas phase. 2318

Wu, E. C. Thermochemistry of gas-phase equilibrium 1,1,1-trifluoroethane + molecular iodine = 2,2,2-trifluoroethyl iodide + hydriodic acid. Carbon-hydrogen bond dissociation energy in 1,1,1-trifluoroethane and the heat of formation of the 2,2,2-trifluoroethyl radical. 2315

Wyatt, W. V. Hydrocarbon surface species on cobalt. 618

Wychick, D. Electrochemical studies and molecular energy levels in furanquinones 1714

Yaacobi, M. Effects of solutes on the strength of hydrophobic interaction and its temperature dependence. 170

Yaacobi, M. Solvophobic interaction. 175

Yadava, B. P. Relative *cis-trans* isomerization rates. Another test of the energy randomization hypothesis. 770

Yamabe, T. Behavior of the excess electron in methane. 148

Yamada, Y. Electron nuclear double resonance study of 9-arylxanthyl radicals. 2512

Yamanaka, S. Role of interlayer cations in the formation of acrylonitrile-montmorillonite complexes. 42

Yamaoka, K. Diffuse reflectance spectra of metachromatic dyes. Existence of a long wavelength band in solid states. 1040

Yamashita, M. Optical saturation and quenching effects in the triplet state of Rhodamine 6G at 77°K. 2006

Yandell, J. K. Pulse radiolysis study of thallium(II) in aqueous perchloric acid solutions. 488

Yang, J. T. Conformation of N-acetyl-L-alanine-N'-methylamide in 1,2-dichloroethane by circular dichroism and optical rotatory dispersion. 1127

Yankwich, P. E. Three-element reaction coordinates. III. Barrier curvature effects on intramolecular kinetic isotope effects. 544

Yany, F. Mechanism of direct and rubrene enhanced chemiluminescence during α-peroxylactone decarboxylation. 2559

Yao, H. C. Nitric oxide and carbon monoxide chemisorption on cobalt-containing spinels. 2490

Yasumori, I. Electron spin resonance study of chlorine dioxide adsorbed on the alkali-cation-exchanged X-type zeolites. 1770

Yasumori, I. Radiochemical study of active sites on palladium. Behavior of preadsorbed carbon-14-labeled acetylene and carbon-14-labeled carbon monoxide in acetylene hydrogenation. 583

Yavuz, O. Thermodynamics of caffeine and the 1-1 caffeine-salicylate complex in water at 25°. 1922

Yeager, H. L. Conductance measurements of alkali metal trifluoroacetates in propylene carbonate. 1380

Yeh, C-Y. Theoretical treatment of the circular dichroism of N-acetyl amino sugars. 1829

Yogev, A. Linear dichroism. XI. Determination of the polarization of electronic transitions in coronene and penta- and hexahelicene. 1400

Yokozeki, A. Reinvestigation of the structure of perfluoroethane by electron diffraction. 2389

Yonezawa, T. Copper complexes as catalysts of the oxidative coupling reaction of phenol derivatives. 811

Yoshioka, K. Electric birefringence of potassium polystyrenesulfonate in aqueous solution as a function of molecular weight, concentration, and field strength (correction). 2698

Young, F. Mechanism of hydroxyapatite dissolution. Synergistic effects of solution fluoride, strontium, and phosphate. 1273

Young, S. L. Titrimetric applications of multiparametric curve fitting. III. Evaluation of the parameters characterizing acidimetric potentiometric titrations of laurate ion. 2626

Yu, T-Y. Ion-molecule reactions in disilane. 1184

Zambonin, P. G. Redox mechanism in an ionic matrix. IV. Catalytic effects of peroxide and superoxide on the oxidation of nitrite by molecular oxygen in molten alkali nitrates. 1693

Zambonin, P. G. Electron paramagnetic resonance identification of molten salt produced superoxide ions. 1294

Zana, R. Comparative ultrasonic absorption studies of association in solutions of ethanol and of 2,2,2-trifluoroethanol. 529

Zana, R. Partial molal volumes of ions in organic solvents from ultrasonic vibration potential and density measurements. I. Methanol. 627

Zana, R. Partial molal volumes of irons in organic solvents from ultrasonic vibration potentials and density measurements. II. Ethanol and dimethylformamide. 1099

Zana, R. Ultrasonic absorption in aqueous solutions of nucleotides and nucleosides. II. Kinetics of proton exchange in adenosine 5'-monophosphate. 80

Zehavi, D. Pulse radiolysis of the aqueous ferro-ferricyanide system. II. Reactions of hydrogen atoms and hydrated electrons with ferrocyanide and ferricyanide ions. 1368

Zehe, M. J. Reinvestigation of the symmetric stretching mode of matrix-isolated dialuminum monoxide. 236

Zimmerman, G. L. Catalyzed and uncatalyzed dissolution of anhydrous chromic chloride in aqueous solutions. 1993

Zipp, A. P. Solvation numbers in nonaqueous solvents. 556

Zorman, G. Radicals formed after electron attachment to 5-halouracils in aqueous glasses. 696

KEYWORD INDEX to Volume 78, 1974

Absorption methane zeolite IR 2180
Absorption optical aq electrolyte 1405
Absorption optical nitrofluorenone THF 1395
Absorption oxide laser Raman 300
Absorption spectra multicomponent systems analysis 2698
Absorption ultrasound aq acetate 1913
Abstraction alkene radical 347
Abstraction hydrogen ether methanol 2650
Acceptor donor nitrofluorenone THF 1395
Acetaldehyde reaction nitrate radical 1337
Acetate aq ultrasound absorption 1913
Acetate ethyl enthalpy soln 1509
Acetate fluoro mobility propylene carbonate 1380
Acetate liq dielec relaxation 1078
Acetic fluoroacetic acid dimer 1709
Acetone aq silver iodide 2244
Acetone fluoro fluorescence 671
Acetone fluoro relaxation vibrational 679
Acetone halo photochem spectra 665
Acetone mercury vapor concn 186
Acetone phenol hydrogen bond 124
Acetonitrile benzoate transfer water 839
Acetonitrile diffusion electrolyte conductometry 1667
Acetonitrile irradn nitrobenzyl 112
Acetonitrile water hydrogen bond 1727
Acetophenone anion absorption spectrum 1473
Acetylene cobalt surface hydrogen 618
Acetylene hydrogenation palladium catalyst 583
Acetylene reaction methylene 1344
Acetylene reaction oxygen hydroxyl 311
Acetylene silane ion mol reaction 2645
Acetylene sulfur dioxide photolysis 325
Acid fluorescence quenching polyvinylcarbazole 2009
Acid frozen aq soln NMR 807
Acid nitric alpha radiolysis 211
Acid nitric vapor UV photolysis 1
Acid pH micelle effect 1490
Acid sulfoxide hydrogen bonding 1662
Acid transfer enthalpy detn 2363
Acidic ice electron spin polarization 1336
Acidity benzoic acid deriv 839
Acidity cobalt molybdenum alumina catalyst 2069 2070
Acidity dimethylsulfoxide aq 421
Acidity silica detn spectra 2376
Acidity surface Raman detn 300
Acoustic method max density 2305
Acriflavin radiolysis chemiluminescence 1251
Acrolein reactivity MO 1874
Acrylonitrile chemisorption montmorillonite cation 42
Activated complex collisional reaction 1773
Activated radical energy loss collision 850
Activation energy addn reaction 1035
Activation energy collision 612
Active site palladium hydrogenation catalyst 583
Activity coeff amino acid 1197
Activity coeff transfer benzoate 839
Activity detn gas chromatog 1644
Activity electrolyte acetonitrile diffusion 1667
Activity nonelectrolyte aq salt 165
Activity osmotic coeff electrolytes ions 2698
Activity phenol hydrogen bond model 1443
Addn alkene radical 347
Addn heat dimethylamine formaldehyde 599
Addn reaction activation energy 1035
Adduct ether hydrogen chloride 432
Adduct isotope effect deuterium 429
Adsorbed alkyl ketone photolysis 2442
Adsorbed butyl nitroxide silica EPR 200
Adsorbed butylamine silica alumina IR 704
Adsorbed chlorine dioxide zeolite 1770
Adsorbed ketone photolysis 2446
Adsorbed layer IR reflection 941
Adsorbed mol silica NMR 38
Adsorbed sulfur dioxide vanadium oxide 649
Adsorption anion metal electrode 2240
Adsorption carbon dioxide uranium 2117
Adsorption chromia alumina IR 588
Adsorption diazine silica IR 2376
Adsorption free energy electrode charge 417
Adsorption gas water surface tension 2262
Adsorption isotherm helium group gas 405
Adsorption mercaptan nickel IR 1648
Adsorption multilayer sticking coeff 748
Adsorption multilayer theory significant structure 2600
Adsorption nitroxide silica EPR 2110
Adsorption oxygen titanium zeolite 218
Adsorption pyrazine pyridine mercury electrode 1226
Adsorption solid carbon 622
Adsorption water copper silver 87
Adsorption water zinc oxide 1116
Alanine acetyl conformation 1127
Albumin monolayer viscosity pressure 2266
Alc amine molal vol aq 1030
Alc amine solvation electron 792
Alc aq silver iodide 2244
Alc butyl heat diln 2460
Alc butyl proton diffusion 70
Alc glass trapped electron photobleaching 232
Alc hydrogen bond perchlorate 168
Alc irradiated radical detection 1977
Alc polaron relaxation visible spectra 393
Alc radiolysis electron scavenging 504
Alc solvation nonpolar solvent dielec 1203
Alc spectra solvated electron 514
Alc water hydrogen bond 1723
Alk earth metal binding 1013
Alk earth salt ammonia Raman 143
Alkali chloride cerium chloride mixing 178
Alkali chloride cond soln 2521
Alkali chloride ion soln 2576
Alkali chloride lanthanum chloride mixing 181
Alkali fluoroacetate cond propylene carbonate 1380
Alkali halide aq IR 238
Alkali halide vaporization rate 1998
Alkali metal binding polysulfonate 1013
Alkali metal halide compressibility soln 2367
Alkali metal redn naphthocyclobutene 723
Alkali nitrate liq ammonia Raman 708
Alkali nitrate melt superoxide ESR 1294
Alkali salt ammonia Raman 143
Alkane interaction solvophobic 175
Alkane polaron IR alc amine 792
Alkane polyisobutylene interaction parameter 60
Alkane reaction hot hydrogen 559
Alkane reactivity oxygen atom 1457
Alkanoate cholesteryl liq crystal 1740
Alkene abstraction addn radical 347
Alkene heat hydrogenation 2569
Alkene kinetics isomerization 770
Alkene maleic acid copolymer 607
Alkene ozone reaction kinetics 2085 2318
Alkyl ketone adsorbed photolysis 2442
Alkyl radical cross disproportionation 1586
Alkylamine hydrobromide aq soln thermodn 1217
Alkylammonium carboxylate hydrophobicity 1759
Alkylammonium fluoroacetate cond propylene carbonate 1380
Alkylammonium hydrophobic interaction 1719
Alkylammonium salt cond oxazolidone 2689
Alkylammonium salt liq membrane 2370
Alkylammonium salt micellization 2469
Alkylbenzene chloroform diffusion liq 2297
Allyl compd radical EPR 117
Allyl radical decay polyethylene 1798
Alpha radiolysis nitric acid 211
Alumina chromia catalyst IR 588
Alumina cobalt molybdenum acidity 2069 2070
Alumina diazine adsorption UV 2376
Alumina IR butylamine adsorbed 704
Alumina nitroxide adsorption EPR 2110
Alumina silica adsorbed nitroxide 200
Aluminum alkali chloride cond 2521
Aluminum alkali metal oxide structure 2496
Aluminum oxide IR matrix 236
Aluminum oxide propanol electroosmosis pressure 65
Aluminum propylene carbonate solvation 2576
Amide nitrogen 15 NMR 2507
Amide packing lattice energy 1595
Amide solvation electron IR 2631
Amine alc molal vol aq 1030
Amine alc solvation electron 792
Amine aq water structure 714
Amine chloropalladate complex ESR 2136
Amine nitrogen 15 NMR 2507
Amine org cation heat formation 1268
Amine oxide micellization 1086
Amine packing lattice energy 1595
Amine photolysis imidogen fluorescence 1784
Amine solvation electron IR 2631
Amine substitution hydroxide copper 305
Amino acid activity coeff 1197
Amino acid frozen aq soln NMR 807
Amino acid lattice energy 1621
Amino acid positron annihilation 1261
Amino radical ESR 2047
Aminobenzoic caffeine complex thermodn 1922
Aminopyridine fluorescence lifetime solvent 201
Ammine cobalt complex photoredn 686
Ammine copper EPR zeolite 531
Ammine halo ruthenium EPR 700
Ammine rhodium complex photoaquation 1144
Amminecobalt nitro photolysis 572
Ammonia benzene soln Raman 2106
Ammonia discharge ESR 2047
Ammonia flame chemiionization 2320
Ammonia liq alkali nitrate Raman 708
Ammonia photolysis imidogen 1784
Ammonia Raman alk earth salt 143
Ammonia solvation ammonium ion 1482
Ammonia sulfur dioxide thermodn dissocn 1378
Ammonium arom interaction 1490
Ammonium chloride soln diffusion 2292
Ammonium ion solvation ammonia 1482
Ammonium perchlorate vaporization 1483
Ammonium tetramethyl ion diffusion gel 735
Ammonium thiocyanate liq ammonia Raman 708
AMP protonation dimerization kinetics 80
Analysis absorption spectra multicomponent systems 2698
Aniline benzophenone irradn 1837
Aniline hydroxy radical reaction 523
Anilinyl fluorine hyperfine coupling 1837
Anion adsorption metal electrode 2240
Anion arom ketone spectrum 1473
Anion exchange membrane noise 761
Anion lithium surface ionization 820
Anion quenching excited hydrocarbon 1885
Anion radical carbonyl compd spectra 741
Anion radical dimerization 295
Anion radical electron transfer solvent effect 285
Anion radical titanium zeolite 218
Anisotropic rotational relaxation ESR 1324
Anthracene iodide fluorescence quenching 2555
Anthranilic acid radiolysis chemiluminescence 1251
Appearance potential org cation 1268
Aq max density temp expansibility 1041
Aq soln heat mixing 2465
Aq soln ions disulfides hydroxyl 282
Aq soln magnetic relaxation 1002
Aquation photo hexaamminerhodium complex 1144
Aqueous soln mol wt concn field strength 2698
Argon chemiluminescence sulfur oxide 1248

Argon pulse radiolysis excitation 22
Arom carboxylic acid reaction hydroxyl 1521
Arom compd reaction hydroxyl polarog 160
Arom fluorescence quenching 2555
Arom halogen compd radiolysis 519
Arom hydrocarbon ion electronic spectra 1420
Arom hydrocarbon quenching excited 1885
Arom hydrocarbon triplet equil 196
Arom ketone anion spectrum 1473
Arom radical cation hectorite metal 994
Arom sulfur flash photolysis polemic 1441 1442
Arsenic phosphide bond energy 603
Arsonium chloride soln thermodn 738
Ascorbic acid radiation chemistry 1063
Assocn erbium chloride aq methanol 424
Assocn ethanol solvent effect 529
Assocn fluoranthene org solvent NMR 1330
Assocn ion relaxation Onsager Provencher 1431
Assocn kinetics micelle 1024
Assocn lanthanum potassium chloride melt 1134
Assocn rhodamine dye kinetics 1891
Atom recombination wall 465
Atomic beam adsorption sticking coeff 748
Azide lead thermal decompn 478
Azobenzene deriv polarog 1825
Azoxyanisole vapor pressure chromatog 275
Barium binding polyacid thermodn 1486
Barium chloride soln heat mixing 1924
Barium stearate film ellipsometry 947
Barrier rotation benzophenone ketyl 2144
Barrier rotation borane trimethylamine 1503
Barrier rotation ESR fluoroalkyl 2014
Barrier rotation hexafluoroethane 2389
Barrier rotation thiourea ditertbutyl 961
Base frozen aq soln NMR 807
Base heterocyclic reaction copper complex 316
Base transfer enthalpy detn 2363
Basic dye metachromasia 536
Basicity ether 432
Behenate barium film ellipsometry 947
Benzene ammonia soln Raman 2106
Benzene cyclopentane film cathodoluminescence 2081
Benzene deriv activity haloalkane 1644
Benzene deriv liq membrane 2370
Benzene deriv soly sulfur 2635
Benzene diffusion binary liq 2307
Benzene diffusion isotope effect 846
Benzene electron scavenging radiolysis 504
Benzene fluorescence energy transfer 2407
Benzene fluorescence lifetime 1904
Benzene hydrated electron reaction 1987
Benzene hydroxylation metal irradn 2335
Benzene hydroxylation phenylation irradn 1795
Benzene photolysis benzvalene prodn 1909
Benzene polyisobutylene interaction parameter 60
Benzene soly aq sodium chloride 165
Benzenediazonium photolysis photoselection effect 782
Benzoate caffeine complex thermodn 1922
Benzoate dimer irradn hexane 105
Benzoate transfer water acetonitrile 839
Benzocarbazole EPR 692
Benzonitrile radiolysis pulse 2094
Benzophenone anion absorption spectrum 1473
Benzophenone irradn diphenylamine ESR 2225
Benzophenone ketyl rotation barrier 2144
Benzophenone phenol aniline irradn 1837
Benzoquinone potassium ion pair 1771
Benzoyl peroxide decompn NMR 1971
Benzvalene prodn benzene photolysis 1909
Biionic liq membrane potential 2370
Binary liq system diffusion 2307
Binary system diffusion 2307
Binding counterion polyvinyl sulfonate 1013
Binding energy chlorine metal 107
Biochem model micelle luminescence decay 190
Biol oxidn singlet oxygen 1681
Biphenyl electron scavenging methylpentane 2696
Biphenyl fluorescence quenching perchlorate 2555
Biphenyl halo radiolysis spectra 519
Bipyridine rhodium complex 727
Bipyridine ruthenium complex phosphorescence quenching 1374
Bipyridine ruthenium sensitized phosphorescence 541
Bismuth phosphide bond energy 603
Boiling point element 115 1945
Bolaform electrolyte interface micelle 1387
Bond angle disulfide IR correlation 855
Bond energy arsenic bismuth phosphide 603
Bond force const transition state 544
Bond hydrogen lactam 2341
Bond length dimethyl disulfide 1848
Bond stability double 2569
Bonding hydrogen energy 1415
Borane trimethylamine IR Raman 1503
Borate tetramethylammonium hydrogen bond 2585
Borate tetraphenyl enthalpy soln 1509
Boride activity diffusion acetonitrile 1667
Borohydride tetramethylammonium hydrogen bond 2585
Boron oxide mol force field 989
Bromide alkylammonium cond oxazolidone 2689
Bromide fluorescence quenching naphthalene 2555
Bromide hydrogen exchange deuterium 2549
Bromide lithium surface ionization 820
Bromide photosubstitution platinum complex 2349
Bromide potassium excited scattering 2438
Bromide potassium transport DMSO 2405
Bromide propylammonium heat soln 1719
Bromide silver soly oxazolidone 1817
Bromide silver soly ozazolidone 1817
Bromide sodium enthalpy soln 1509
Bromine chloride emission spectrum 1833
Bromine fluoride fluorination uranium oxide 1140
Bromine scavenger perfluorocyclohexane radiolysis 360
Bromine 81 quadrupolar relaxation 1002
Bromoacetic acid fluorescence quenching 2009
Bromotetronic acid radiolysis 1063
Brownian motion rotary fluorescence 387
Bubble bursting drag 1949
Bubble soln diffusion detn 2516
Bursting bubble drag 1949
Bursting surfactant film purity 234
Butadiene addn methyl 1245
Butadiene cycloaddn methylene MO 1167
Butanol paramagnetic solute NMR 851
Butene methyl photolysis mechanism 98
Butyl alc proton diffusion 70
Butyl nitroxide EPR adsorbed 200
Butyl nitroxide isotropic splitting 1313
Butyl radical excited energy transfer 1979 1984
Butylamine IR adsorbed silica alumina 704
Butylphosphonium bromide soln thermodn 738
Butyric acid transfer thermodn 2363
Cadmium chloro Raman coordination 595
Cadmium nitrate hydrate thermodn 278
Caffeine heat soln complexation 1922
Calcium acetate ultrasound absorption 1913
Calcium alkali fluoride enthalpy 1478
Calcium hydroxide phosphate growth 2218
Calcium nitrate hydrate thermodn 278
Calcium phosphate hydrate pyrolysis 1631
Calcium potassium nitrate relaxation 639
Calcium transport cation membrane 1805
Calorimeter expanding solid 1701
Capacitance cond aq isopentylammonium nitrate 1431
Capacity heat ammonium halide analog 738
Capacity heat org compd mixt 1961
Capacity heat salt hydrate 278
Capture electron methylcyclohexane radiolysis 867
Capture electron nitrous oxide radiolysis 954
Carbanion electron transfer trap 1135
Carbazole spectroscopy photoselection 1512
Carbon adsorption solid 622
Carbon compd mol force field 989
Carbon dioxide poisoning catalyst 2110
Carbon dioxide uranium IR 2117
Carbon disulfide soly sulfur 2635
Carbon monoxide chem laser 1451
Carbon monoxide chemisorption cobalt spinel 2490
Carbon monoxide chromia catalyst IR 588
Carbon monoxide compressed IR 1968
Carbon monoxide matrix interaction 134
Carbon monoxide MO calcn 763
Carbon monoxide oxidn catalysis 2303
Carbon monoxide oxygen kinetics 497
Carbon monoxide reaction methylene 1344
Carbon NMR silica adsorption 38
Carbon sulfide dissocn 634
Carbon tetrachloride cyclohexane photolysis 1899
Carbon tetrachloride diffusion binary liq 2283
Carbon tetrachloride fluoroacetic acid 1709
Carbon tetrachloride gelation hydroxystearic acid 759
Carbon tetrachloride phenol hydrogen bond 1443
Carbon tetrafluoride collision radical 850
Carbon 13 shift carbonyl assocn 124
Carbonate cupric oxide reaction 2670
Carbonate potassium glass photocond 2454
Carbonate propylene solvation 2576
Carbonate radical tryptophan reaction 2099
Carbonyl assocn carbon 13 shift 124
Carbonyl compd radical anion spectra 741
Carbonyl group semiquinone dipole interaction 2140
Carbonyl sulfide reaction sulfur atom 1137
Carborane radiolysis energy transfer 788
Carboxylate alkylammonium hydrophobicity 1759
Carboxylate proton exchange octanol 2339
Carboxylic acid arom reaction hydroxyl 1521
Carboxylic cobalt complex photoredn 686
Carboxylic packing lattice energy 1595
Carcinogen chloromethyl methyl ether polemic 2696
Catalase kinetics model intermediate 1919
Catalysis dissoln chromic chloride 1993
Catalyst platinum hydrogenation 875
Catalyst poisoning zeolite nitroxide 2110
Cathodoluminescence benzene cyclopentane film 2081
Cathodoluminescence octane 2077
Cation binding polyvinyl sulfonate 1013
Cation coordination solvation 1731
Cation diffusion polystyrenesulfonate gel 735
Cation exchange complexing 926
Cation exchange equil unequal charge 1110
Cation exchange heat zirconium phosphate 152
Cation exchange membrane interface 1805
Cation exchange zirconium phosphate 1150
Cation exchanger solvent uptake 411
Cation mobility DMSO 2405
Cation montmorillonite chemisorption acrylonitrile 42
Cation radical arom hectorite metal 994
Cation zeolite chlorine dioxide ESR 1770
CD deoxyacetamidohexose transition 1829
CD dihydrogen disulfide 1554
Cellulose morphol ESR 308
Cephalosporin electron configuration MO 2604
Cerium chloride alkali chloride mixing 178
Cerium radiation chemistry hydroperoxyl 2330
Cesium alumina catalyst structure 2496
Cesium hydrogen heat exchange 1812
Cesium iodide vaporization rate 1998
Chain length cyanine fluorescene 1154
Chalcogenide trialkoxyphosphine iodine UV 1657
Charge distribution molecule 763
Charge electrode adsorption free energy 417
Charge neutrality electrolyte soln 2060
Charge transfer cobalt complex 686
Charge transfer complex UV 980
Charge transfer photopolymn methylstyrene 341
Chem induced dynamic polarization 1971
Chem system compn detn potentiometry 816
Chemiionization ammonia flame 2320
Chemiluminescence dye radiolysis 1251
Chemiluminescence Grignard reaction 1896
Chemiluminescence singlet oxygen 1681
Chemiluminescent reaction sulfur oxide 1248
Chemiluminesence peroxy decarboxylation 2559
Chemisorption acrylonitrile montmorillonite cation 42
Chemisorption carbon dioxide uranium 2117
Chemisorption chlorine metal surface 107
Chloranil anion radical ESR 2140
Chloranilic acid radical ESR 2140
Chlorate thermal decompn 773
Chloride alkali aluminum cond 2521
Chloride alkali cerium heat mixing 178
Chloride alkali lanthanum heat mixing 181
Chloride anion exchange noise 761
Chloride bromine emission spectrum 1833
Chloride catalysis lithium perchlorate decompn 776
Chloride chromic dissoln catalysis 1993
Chloride diffusion sodium polyacrylate 1756

Chloride erbium assocn aq methanol 424
Chloride fluorescence quenching terphenyl 2555
Chloride interaction matrix IR 134
Chloride iron extn ether 2572
Chloride lanthanide aq molal vol 1106
Chloride lanthanum potassium melt Raman 1134
Chloride lithium surface ionization 820
Chloride magnesium aq compressibility 1636
Chloride mobility propylene carbonate 1380
Chloride nitrate membrane potential 2370
Chloride nitrosyl nitrogen exchange 402
Chloride nitryl reaction nitric oxide 2073
Chloride silver soly oxazolidone 1817
Chloride sodium soln diffusion 2292
Chloride soln heat mixing 1924
Chlorine compd mol force field 989
Chlorine dioxide ESR zeolite 1770
Chlorine reaction metal 107
Chlorine substitution dichlorodifluoroethane 658
Chlorine x ray emission org 2592
Chloro cadmium Raman coordination 595
Chloro complex thallium 2 892
Chloroacetic acid fluorescence quenching 2009
Chloroferrate extn chloroethyl ether 2572
Chloroform alkylbenzene diffusion liq 2297
Chloromethyl ether hydrolysis 1096
Chloromethyl methyl ether carcinogen polemic 2696
Chloropalladate amine complex ESR 2136
Cholesterol dimerization solvation NMR 250
Cholesteryl alkanoate liq crystal 1740
Chromate cyano intersystem crossing 541
Chromate cyanocobaltate energy transfer 2122
Chromatog azoxyanisole vapor pressure 275
Chromatog gas activity detn 1644
Chromatog gas interaction parameter 60
Chromatog gel irreversible polymn 460
Chromatog method diffusion liq 2297
Chromatog perfluorocyclobutane photolysis 2071
Chromia alumina catalyst IR 588
Chromic chloride dissoln catalysis 1993
Chromium oxide crystn 2621
Chromous ion dissoln catalyst 1993
CI tetragonal energy matrix 2678
Circular polarization light fluorescence 387
Cis trans isomerization thiacarbocyanine 2355
Cluster model liq water structure 1531
CNDO MO dimethyl disulfide 1848
Cobalt ammine complex photoredn 686
Cobalt chemisorption acetylene ethylene 618
Cobalt molybdenum alumina acidity 2069 2070
Cobalt nitropentaammine photolysis 572
Cobalt oxalato complex photolysis 1361
Cobalt spinel chemisorption oxide vapor 2490
Cobaltate cyanochromate luminescence 2122
Coion cond polyelectrolyte soln 1242
Collision excitation reaction 612
Collision fluoroethyl radical tetrafluoromethane 850
Collisional reaction rate temp 1773
Compensation effect oxidn kinetics 2486
Complex activated collisional reaction 1773
Complex cobalt ammine photoredn 686
Complex copper maleic copolymer 607
Complex yttrium nitrate formation 261
Complexing ion exchange 926
Compn detn chem system potentiometry 816
Compressibility aq amine 714
Compressibility isothermal ion pair 1636
Compressibility transfer salt soln calcn 2367
Computer program glycosidation 1918
Computer program isomerization 1579
Cond alkylammonium carboxylate 1759
Cond capacitance aq isopentylammonium nitrate 1431
Cond elec molten salt 639
Cond elec perylene complex 215
Cond equiv polyelectrolyte soln 1242
Cond lithium perchlorate THF 917
Cond magnesium oxide defect hydrogen 758
Cond methyl sulfoxide iodine 1744
Condensation germanium oxygen 1763
Condensation transition state theory 1298
Conductance equation Justice derivation 1383
Conduction elec detn atomic nitrogen 1120
Conductometry electrolyte diffusion acetonitrile 1667
Configuration triiodide dil soln 2306
Conformation acetylalanine 1127
Conformation dimethyl disulfide 1848
Conformation ESR fluoro alkyl radical 2030
Conformation ethylamine far IR 803
Conformation mol electron diffraction 2380
Conformation phenyl vinyl ether 440
Contact angle water copper silver 87
Cooling rate transition temp 2673
Coordinate reaction isotope effect 544
Coordination cadmium chloro Raman 595
Coordination complex ion pair phosphorescence 1374
Coordination solvation ion 1731
Copper complex maleic copolymer 607
Copper complex MO model 1235
Copper complex reaction heterocyclic base 316
Copper complex UV ESR 811
Copper complex zeolite EPR 531
Copper contact angle water 87
Copper cupric electrode nitrate melt 2670
Copper dicyclohexyldithiophosphinate electron structure 962
Copper dithiolate perylene complex 215
Copper glycinate cellulose ESR 308
Copper hydroperoxyl radical reaction 779
Copper hydroxide amine substitution 305
Copper reaction chlorine 107
Core charge nitroarom MO 1868
Coronene linear dichroism UV 1400
Correlation rotational time estn 1321
Counterion binding polyvinyl sulfonate 1013
Counterion cond polyelectrolyte soln 1242
Coupling singlet triplet formaldehyde 2270
Cresol hydroxyl radiolytic polarog 160
Crit temp fluid intermol energy 1241
Critical micelle concn fatty acid 2626
Cross section quenching triplet 482
Crystal org intermol potential 1595
Crystn chromium oxide 2621
Cupric formate thermal decompn 2664
Cupric oxide carbonate reaction 2670
Cyanate radiolysis radical ESR 1074
Cyanide nitrous oxide soln radiolysis 2660
Cyanine dye fluorescent lifetime 1154
Cyanine dye photoisomerization 16
Cyano chromate intersystem crossing 541
Cyanobenzene complex methylstyrene 341
Cyanochromate cobaltate luminescence 2122
Cyanogen reaction oxygen laser 1451
Cyclic anhydride complex 980
Cycloaddn methylene butadiene MO 1167
Cyclobutane hot decompn mechanism 2309
Cyclobutanone photolysis matrix mechanism 1461
Cyclobutyl methyl ring cleavage 1573
Cyclohexadienyl hydroxy pulse radiolytic polarog 160
Cyclohexane benzene diffusion 846
Cyclohexane diffusion binary liq 2307
Cyclohexane nitrous oxide radiolysis 102
Cyclohexane photolysis 1899
Cyclohexane polyisobutylene interaction parameter 60
Cyclohexane radiolysis iodine effect 366
Cyclohexane soly aq sodium chloride 165
Cyclohexane toluene film cathodoluminescence 2081
Cyclohexene recoil tritium reaction 347
Cyclooctatetraene anion radical ESR 90
Cyclopentane benzene cathodoluminescence film 2081
Cyclopentane cyclopentene aq radiolysis 1052
Cyclopentane radiolysis water 1049
Cyclopentene cyclopentane aq radiolysis 1052
Cyclopentene dehydrogenation shock wave 436
Cyclopentyl radical disproportionation recombination 462
Cyclopentyl ring cleavage 1573
Cyclopentyl spectrum decay 1049
Cyclopentylperoxy spectrum decay 1049
Cyclopropane fluoroalkyl decompn kinetics 2535
Cyclopropane nitrous oxide radiolysis 102
Cysteine aq soln photolysis 1130
Deactivating collision isotope effect 850
Decane cathodoluminescence 2077
Decarboxylation chemiluminesence peroxy 2559
Decay polaron soln detn 2103
Decay radical irradiated polyethylene 1798
Decompn chlorate perchlorate 773
Decompn cupric formate thermal 2664
Decompn fluoroalkyl cyclopropane kinetics 2535
Decompn hot cyclobutane mechanism 2309
Decompn isomerization theory 1579
Decompn kinetics excited propylene 1348
Decompn nitryl chloride catalysis 2073
Defect magnesium oxide interaction hydrogen 758
Dehydration calcium phosphate 1631
Dehydrochlorination trichloroethane mechanism 2166
Dehydrofluorination trifluoroethane shock 472
Dehydrogenation cyclopentene shock wave 436
Density max aq solute expansibility 1041
Density max temp soln 2305
Density pentyl alc 652
Density state unimol kinetics 2326
Deoxyacetamidohexose CD transition 1829
Desorption surface kinetics 1298
Detn rank analysis spectra multicomponent systems 2698
Deuterium effect magnetic resonance 221
Deuterium exchange hydrogen bromide 2549
Deuterium isotope effect 398
Deuterium isotope effect adduct 429
Deuterium proton transfer methane 93
Deuteron quadrupole coupling water 1674
Dialuminum oxide IR matrix 236
Diazine adsorption silica IR 2376
Diazopropane photolysis gas phase 1348
Dibenzophenothiazine oxidn 1750
Dichlorobutane halogen exchange stereochem 1043
Dichlorodifluoroethane substitution tritium chlorine 658
Dichroism linear disklike mol 1400
Dicyclohexyldithiophosphinate complex electron structure 962
Dielec const liq sulfur 1670
Dielec const molten salt 639
Dielec const pentanol water 652
Dielec const thioamide solvent 1018
Dielec methyl sulfoxide iodine 1744
Dielec relaxation liq acetate 1078
Dielec response time domain 1440
Diffraction electron gas structure 2380
Diffusion binary gas 1564
Diffusion binary liq 2283
Diffusion cation polystyrenesulfonate gel 735
Diffusion chloride sodium polyacrylate 1756
Diffusion controlled radical decay 1798
Diffusion cetn bubble soln 2516
Diffusion electrolyte acetonitrile conductometry 1667
Diffusion interferometric detn 2050
Diffusion iodine atom helium 878
Diffusion isomer heptane helium 1428
Diffusion isotope effect benzene 846
Diffusion liq binary system 2307
Diffusion liq chromatog method 2297
Diffusion proton butyl alc 70
Diffusion sodium liq 2275
Diffusion ternary electrolyte soln 2292
Diffusion ternary system 2281
Diffusivity polymer membrane permeability 408
Difluoroamino compd pyrolysis 2189
Difluoroethane radiolysis 2183
Difluoroethane tritium hot atom reaction 2186
Dilatometry maleic acid copolymer 607
Diln heat alc urea 2460
Diln heat propylammonium chloride 77
Dimer dye ionic spectra 380
Dimer fluoroacetic acetic acid 1709
Dimer water energy structure 2055
Dimerization AMP kinetics 80
Dimerization cholesterol solvation NMR 250
Dimerization kinetics rhodamine dye 1891
Dimerization radical anion kinetics 295
Dimethoxyazoxybenzene vapor pressure 275
Dimethyl disulfide CNDO MO 1848
Dimethyl sulfoxide enthalpy transfer 1509
Dimethylamine formaldehyde heat addn 599
Dimethylcyclopropanes recoil tritium reaction 2531
Dimethylsilane hydrogen sulide photolysis 203
Dimethylsilane photolysis hydrogen sulfide 203
Dimethylsulfoxide aq soln pH 421
Dinitrostilbene photoisomerization mechanism 45
Dioxane aq silver iodide 2244

Dioxane photolysis solvated electron 2181
Dioxide carbon poisoning catalyst 2110
Dioxide carbon uranium IR 2117
Dioxide nitrogen photolysis photon 1583
Dioxide nitrogen reaction ozone 1775
Dioxide selenium force field 989
Dioxide sulfur adsorbed vanadium oxide 649
Dioxide sulfur adsorption zeolite 218
Diphenylamine irradn benzophenone ESR 2225
Diphenylhydroxymethyl photochem formation 1837
Dipole interaction semiquinone 2140
Dipole moment borane trimethylamine 1503
Dipole moment nitrostyrene 49
Dipole moment thioamide solvent 1018
Dipyridyl rhodium complex voltammetry 727
Disilane ion mol reaction 1184
Disilane reaction hydrogen atom 398
Disklike mol linear dichroism 1400
Displacement disilane hydrogen 398
Disproportionation alkyl radical 1586
Disproportionation recombination cyclopentyl radical 462
Disproportionation thallium 2 488 892
Dissociative vaporization reaction kinetics 1298
Dissocn carbon sulfide 634
Dissocn catalyst transition metal 1653
Dissocn const pyridinyl radical 2211
Dissocn energy arsenic bismuth phosphide 603
Dissocn energy fluoroethyl hydrogen 2315
Dissocn energy hafnium nitride 273
Dissocn nitrous oxide rutile 870
Dissocn thermodn ammonia sulfur dioxide 1378
Dissoln catalysis chromic chloride 1993
Disulfide carbon soly sulfur 2635
Disulfide dimethyl CNDO MO 1848
Disulfide IR correlation bond angle 855
Disulfide reaction hydroxyl radical 282
Dithiolate metal perylene complex 215
DMF ion molal vol 1099
DMF potassium chloride electroosmosis 2302
DMF solvation propylammonium bromide 1719
DMSO cation mobility 2405
DMSO water hydrogen bond 1723 1727
DMSO water ultrasound propagation 2611
DNA hypochromism Hartree detn 444
Documentation service review 1339
Dodecyl sulfate positronium lifetime 2526
Donor acceptor nitrofluorenone THF 1395
Double bond stability 2569
Double resonance irradiated malonic acid 1839
Drag bursting bubble 1949
Drift mobility electron alk ice 2454
Duroquinol radical rotation ESR 130
Dye cyanine fluorescent lifetime 1154
Dye cyanine photoisomerization 16
Dye ionic spectra dimer 380
Dye mercuric chloride metachromasia 536
Dye metachromatic reflectance spectra 1040
Dye radiolysis chemiluminescence 1251
Dye thiacarbocyanine stereoisomer 2355
Eigenvalue chem system compn detn 816
Elec cond aq lanthanide perchlorate 1435
Elec cond ethylammonium phenylborate 2687
Elec cond ion solvation 556
Elec cond Justice equation 1383
Elec cond low polarity electrolyte 1210
Elec cond perylene complex 215
Elec cond viscosity mixed solvent compn 907
Elec conduction detn atomic nitrogen 1120
Elec field liq crystal 1740
Elec noise anion exchange membrane 761
Elec potential metal anion 2240
Elec relaxation molten salt 639
Elec surface potential polyelectrolyte 1189
Electric birefringence potassium polystyrenesulfonate aq soln 2698
Electrochem ESR kinetics detn 290
Electrochem reaction furanquinone solvent 1714
Electrochem redn rhodium dipyridyl complex 727
Electrode adsorption anion 2240
Electrode charge adsorption free energy 417
Electrode copper cupric nitrate melt 2670
Electrode germanium interface aq 941
Electrode mercury adsorption pyrazine pyridine 1226
Electrode tubular simulation model 718
Electrodeposition alkali metal 2521
Electrokinetics nonaq contamination water 65
Electrolyte aq hydrophobic interaction 170
Electrolyte aq IR reflection 1405
Electrolyte bolaform interface micelle 1387
Electrolyte diffusion acetonitrile conductometry 1667
Electrolyte entropy nonaq solvent 1000
Electrolyte low polarity field dissocn 1210
Electrolyte mixing thermodn 1927
Electrolyte soln charge neutrality 2060
Electrolyte ternary diffusion soln 2292
Electron affinity furanquinone MO 1714
Electron capture nitrous oxide radiolysis 954
Electron configuration cephalosporin MO 2604
Electron configuration tetragonal system 2678
Electron detn time hydrated 2103
Electron diffraction gas structure 2380
Electron double resonance radical 1839
Electron exchange theory 1684
Electron formation pyrene photoionization 2248
Electron hydrated benzene reaction 1987
Electron hydrated peptide 1193
Electron impact excitation methane 2077
Electron methylcyclohexane gamma radiolysis 867
Electron radiolysis nickel soln 882
Electron scavenging alc radiolysis 504
Electron scavenging liq neopentane 853
Electron scavenging methylpentane glass 2696
Electron solvated dioxane photolysis 2181
Electron solvated IR 2414
Electron solvated optical absorption 2631
Electron solvated reaction 796
Electron solvated spectra alc 514
Electron solvation alc amine 792
Electron spin polarization hydrogen 1336
Electron spin resonance irradiated alc 1977
Electron transfer org solvent effect 285
Electron transfer pyridinyl formation 2211
Electron transfer quantum theory 2148
Electron transfer rutile nitrous oxide 870
Electron transfer trap carbanion 1135
Electron trapped energy structure 2454
Electron trapped EPR hydroxide 221
Electron trapped photobleaching alc glass 232
Electronic spectra arom hydrocarbon ion 1420
Electronic spectra radical anion 741
Electronic structure dihydrogen disulfide 1554
Electronic structure MO calcn 763
Electroosmosis high voltage nonaq 65
Electroosmosis Onsager reciprocity relation 2302
Electrostatic potential solute solvent 1853
Electrostriction ion methanol 627
Electrostriction ion org solvent 1099
Element 115 property 1945
Elimination dichlorodifluoroethane tritium chlorine 658
Ellipsometry barium stearate film 947
Emission spectrum bromine chloride 1833
Emission x ray chlorine org 2592
ENDOR trapped electron hydroxide 221
ENDOR xanthyl radical 2512
Energy bond arsenic bismuth phosphide 603
Energy density unimol kinetics 2326
Energy dissocn hafnium nitride 273
Energy free surfactant micellization 1086
Energy hydrogen bond MO 970
Energy hydrogen bonding 1415
Energy intermol fluid crit temp 1241
Energy level ligand field tetragonal 2678
Energy level octahedral ligand field 56
Energy level ruthenium ammine 700
Energy loss collision activated radical 850
Energy loss electron methane 2077
Energy matrix tetragonal CI 2678
Energy transfer carborane radiolysis 788
Energy transfer chromate cyanocobaltate 2122
Energy transfer excited butyl radical 1979 1984
Energy transfer external activation 612
Energy transfer fluorescence benzene 2407
Energy transfer ketone photolysis 2446
Energy water dimer 2055
Enthalpy activation salt cond 639
Enthalpy detn micelle formation 1442
Enthalpy mixing molten fluoride 1478
Enthalpy polyelectrolyte binding metal 1486
Enthalpy solvation ammonium ion 1482
Enthalpy transfer aq dimethyl sulfoxide 1509
Enthalpy transfer detn acid base 2363
Entropy element 115 1945
Entropy fluoroiodoethane 2315
Entropy fusion salt hydrate 278
Entropy ionic nonaq soln 1000
Entropy sodium hydroxide hydrate 1701
Entropy solvation ion 2576
Entropy transfer butyric acid 2363
Enzyme oxidn singlet oxygen 1681
EPR allyl compd radical 117
EPR benzocarbazole tetrahydroanthracene 692
EPR butyl nitroxide adsorbed 200
EPR copper complex zeolite 531
EPR nitroxide silica adsorption 2110
EPR photoreaction hydroperoxyl radical 779
EPR potassium nitrosodisulfonate radical 375
EPR ruthenium halo ammine 700
EPR silver nitrosyl 1174
EPR sulfur oxide ion 649
EPR tetrachloromanganate fused salt 1957
EPR trapped electron hydroxide 221
Equation state adsorbed noble gas 405
Equil cation exchange unequal charge 1110
Equil fluoroethane iodination 2315
Equil reaction wetting 1178
Equiv cond polyelectrolyte soln 1242
Erbium chloride assocn aq methanol 424
Erbium perchlorate inner sphere complex 1940
ESR amino radical 2047
ESR anisotropic rotational relaxation 1324
ESR benzophenone irradn diphenylamine 2225
ESR cellulose morphol 308
ESR chloranil anion radical 2140
ESR chlorine dioxide zeolite 1770
ESR conformation fluoro alkyl radical 2030
ESR copper complex 811
ESR copper complex model 1235
ESR cyclooctatetraene anion radical 90
ESR detn radical anion dimerization 295
ESR duroquinol radical rotation 130
ESR electrochem kinetics detn 290
ESR hydrogen acidic ice 1336
ESR hydroxycyclohexadienyl radical 1521
ESR inertia slow tumbling 935
ESR ion pair formation 1771
ESR IR dicyclohexyldithiophosphinate metal 962
ESR irradiated malonic acid 1839
ESR manganese mercury complex 45
ESR nitrostyrene anion radical 49
ESR palladium mixed complex 2136
ESR photolysis ferricyanide glass 1335
ESR piperidine nitroxide 1410
ESR polyvinylpyridine 899
ESR radical cyanate radiolysis 1074
ESR radical fluoroketone photolysis 2036
ESR radical methyl sulfoxide 1882
ESR radical uracil 696
ESR relaxation methylpentane irradn 2233
ESR Rhodamine 6G triplet 2006
ESR rotation barrier fluoroalkyl 2014
ESR rotational correlation time 1321
ESR satn recovery theory 1155
ESR silver diethyl phosphate 958
ESR superoxide alkali nitrate melt 1294
ESR titanium Y zeolite 218
Ethane nitrous oxide radiolysis 102
Ethane thermodn soln electrolyte 170
Ethane thermodn soln solvophobicity 175
Ethanediol radiolysis electron scavenging 504
Ethanol aq ion pair 1759
Ethanol assocn solvent effect 529
Ethanol glass photobleaching electron 232
Ethanol ion molal vol 1099
Ethanol potassium bromide scattering 2438
Ethanol radiolysis electron scavenging 504
Ether adduct hydrogen chloride 432
Ether chloromethyl hydrolysis 1096
Ether conformation MO 440
Ether extn iron chloride 2572
Ether hydrolysis mechanism 2658
Ether iodine complex stability 557
Ethyl acetate enthalpy soln 1509
Ethyl oxide amine cation energy 1268
Ethylamine conformation far IR 803
Ethylammonium phenylborate elec cond 2687
Ethylene cobalt surface hydrogen 618
Ethylene photolysis 1254
Ethylene reaction oxygen branching 663
Ethyleneamineplatinum photosubstitution 2349
Ethylenediamine complex catalyst 1653
Ethylenimine photolysis imidogen 1784

Ethylpentane glass gamma irradn 1135
Ethylthiocarbamato copper 316
Eutectic fluoride Raman 1499
Exchange cation membrane interface 1805
Exchange deuterium hydrogen bromide 2549
Exchange electron theory 1684
Exchange halogen dichlorobutane stereochem 1043
Exchange heat hydrogen cesium 1812
Exchange kinetics detn hydrogen 984
Exchange nitrogen oxide oxychloride 402
Exchange oxygen catalysis 2303
Exchange oxygen photocatalysis titania 555
Exchange proton carboxylate octanol 2339
Exchange water keratin zeolite 1279
Exchange zirconium phosphate heat cation 152
Exchanger cation solvent uptake 411
Excitation naphthalene pulse radiolysis 22
Excitation reaction collision 612
Excited arom hydrocarbon quenching 1885
Excited butyl radical energy transfer 1979 1984
Excited oxygen atoms nitrous oxide 2698
Excited potassium bromide scattering 2438
Excited propylene decompn kinetics 1348
Excited state disulfide 1554
Expanding solid calorimeter 1701
Expansibility solute aq max density 1041
Explosion difluoroamino compd 2189
Fast reaction kinetics stopped flow 305
Fatty acid potentiometry soly product 2626
Ferricyanide glass photolysis ESR 1335
Ferricyanide pulse radiolysis 1368
Ferrocyanide pulse radiolysis 1368
Ferrous redn silver catalytic 2580
Field dissocn low polarity electrolyte 1210
Film benzene cyclopentane cathodoluminescence 2081
Film bursting drag 1949
Film oxidn transition metal 2486
Film skeletonized optical property 947
Film surfactant bursting purity 234
Flame ammonia chemiionization 2320
Flash photolysis arom sulfur polemic 1441 1442
Flash photolysis hydrazine vapor 1356
Flow reactor analysis oxygen 208
Flowing soln tubular electrode 718
Fluid intermol energy crit temp 1241
Fluoranthene assocn org solvent NMR 1330
Fluoranthene fluorescence quenching thiocyanate 2555
Fluorene fluorescence quenching nitrate 2555
Fluorescein radiolysis chemiluminescence 1251
Fluorescence benzene energy transfer 2407
Fluorescence carbazole deriv 1512
Fluorescence circular polarization light 387
Fluorescence fluorinated toluene xylene 7
Fluorescence fluoro acetone 671
Fluorescence halogenated acetone 665
Fluorescence imidogen photolysis amine 1784
Fluorescence lifetime aminopyridine solvent 201
Fluorescence lifetime benzene 1904
Fluorescence quenching arom 2555
Fluorescence quenching fluoro acetone 682
Fluorescence quenching indole lanthanide 1953
Fluorescence quenching polyvinylcarbazole acid 2009
Fluorescence rhodamine dimer 380
Fluorescence thiacarbocyanine dye 2355
Fluorescence trimethylenecyclopropane photoproduct 568
Fluorescent lifetime cyanine dye 1154
Fluoride effect hydroxylapatite dissoln 1273
Fluoride hexafluoroaluminate lithium Raman 1499
Fluoride hydrogen MO calcn 763
Fluoride interaction matrix IR 134
Fluoride molten mixing enthalpy 1478
Fluorination uranium oxide 1140
Fluorine compd mol force field 989
Fluorine fluorination uranium oxide 1140
Fluorine hot atom reaction 857
Fluoro acetone fluorescence quenching 682
Fluoro acetone relaxation vibrational 679
Fluoro alkyl radical ESR conformation 2030
Fluoroacetate alkali cond propylene carbonate 1380
Fluoroacetic acetic acid dimer 1709
Fluoroalkyl radical rotation barrier 2014
Fluoroammonium fluoromethylsulfonate vaporization 1433
Fluoroethane iodination thermodn 2315
Fluoroethyl radical collision tetrafluoromethane 850
Fluoroiodomethane photolysis laser emission 951
Fluoroisopropanol heat soln 454
Fluoroketone ESR photolysis radical 2036
Force const borane trimethylamine 1503
Force const transition state bond 544
Force field mol virial theorem 989
Force theory intermol 1961
Formaldehyde dimethylamine heat addn 599
Formaldehyde intersystem coupling 2270
Formate cupric thermal decompn 2664
Formation const calcn mol complex 557
Formation heat fluoroethyl 2315
Formation yttrium nitrate complex 261
Fourier transform magnetic relaxation 1971
Free energy adsorption electrode charge 417
Free energy formation thallium 2 488
Free energy ion pair 1759
Free energy ion transfer 1731
Free energy lithium hydride 1933
Free energy micellization 2469
Free energy mixing electrolyte 1927
Free energy mixing org compd 1961
Free energy polyelectrolyte binding metal 1486
Free energy solvation ammonium ion 1482
Free energy solvation ion 2576
Free energy surfactant micellization 1086
Free energy transfer butyric acid 2363
Free energy triplet equil 196
Free radical hydrocarbon crystals irradn 2698
Frozen aq soln NMR 807
Furanquinone electrochem reaction solvent 1714
Fusion heat salt hydrate 278
Fusion heat sodium hydroxide 1701
Gamma irradn hydrocarbon glass 1135
Gamma irradn hydroxide ice 221
Gamma irradn phosphate ESR 958
Gamma irradn polyvinylpyridine 899
Gamma radiolysis methylcyclohexane electron 867
Gamma radiolysis nickel soln 882
Gas adsorption water surface tension 2262
Gas binary transport model 1564
Gas chromatog activity detn 1644
Gas chromatog interaction parameter 60
Gas electron diffraction structure 2380
Gas phase solvation mass spectrometry 1482
Gas quenching mercury triplet 482
Gel polystyrenesulfonate diffusion cation 735
Gelatin membrane permeability 408
Gelation hydroxystearic acid pressure solvent 759
Germanium difluoride mol force field 989
Germanium electrode interface aq 941
Germanium oxygen reaction condensation 1763
Glass hydrocarbon gamma irradn 1135
Glass molten salt cond 639
Glass transition salt hydrate 278
Glass transition temp heating rate 2673
Glassy sodium metaphosphate irradn 752
Glucose glycosidation mechanism calcn 1918
Glyceryl triacetate dielec relaxation 1078
Glycine soln heat mixing 2465
Glycosidation glucose mechanism calcn 1918
Gold reaction chlorine 107
Graphite hydrogenation metal catalysis 2254
Grignard reaction chemiluminescence 1896
Grinding zeolite structure transformation 1959
Growth calcium hydroxide phosphate 2218
Hafnium nitride dissocn energy 273
Halide alkali aq IR 238
Halide alkali compressibility soln 2367
Halide alkali vaporization rate 1998
Halide expansibility aq max density 1041
Halide hydrogen bonding energy 1415
Halide phosphonium soln thermodn 738
Halide silver soly oxazolidone 1817
Halide tetramethylammonium hydrogen bond 2585
Halo acetone photochem spectra 665
Halo ammine ruthenium EPR 700
Haloalkane arom activity 1644
Haloalkene isomerization shock tube 1469
Halogen compd arom radiolysis 519
Halogen exchange dichlorobutane stereochem 1043
Halomethane irradn silica gel 1391
Halostannate tetramethylammonium hydrogen bond 2585
Hammett const azobenzene redn 1825
Hartree detn DNA hypochromism 444
Heat addn dimethylamine formaldehyde 599
Heat capacity fusion sodium hydroxide 1701
Heat capacity mixing org compd 1961
Heat capacity soln alkylamine hydrobromide 1217
Heat cation exchange zirconium phosphate 152
Heat diln alc urea 2460
Heat diln mixing propylammonium chloride 77
Heat dissocn hafnium nitride 273
Heat exchange hydrogen cesium 1812
Heat fluoroethyl iodide 2315
Heat formation org cation 1268
Heat hydrogen bond ether 432
Heat hydrogenation terminal alkene 2569
Heat mixing alkali cerium chloride 178
Heat mixing alkali lanthanum chloride 181
Heat mixing aq soln 2465
Heat mixing electrolyte 1927
Heat mixing salt soln 1924
Heat salt hydrate 278
Heat silane cation 1184
Heat soln ammonium halide analog 738
Heat soln complexation caffeine 1922
Heat soln model solvent effect 454
Heat soln propylammonium bromide 1719
Heat transfer soln micelle 834
Heat transport ternary gas 2693
Heating rate transition temp 2673
Heavy atom isotope effect 544
Heavy water quadrupole coupling 1674
Heavy water Raman structure 1304
Hectorite metal arom radical cation 994
Helium diffusion heptane isomer 1428
Helium group gas adsorption isotherm 405
Helium singlet triplet sepn 1334
Heptane activity haloalkane 1644
Heptane benzene diffusion 846
Heptane isomer diffusion helium 1428
Heptylammonium salt liq membrane 2370
Heteroconjugation inorg anion alc 168
Heterocycle nitrogen redn kinetics 2615
Heterocycle nitrogen 15 NMR 2507
Heterocyclic base reaction copper complex 316
Hexacyanochromate intersystem crossing 541
Hexadecane irradn radical pair 2233
Hexafluoroaluminate fluoride lithium Raman 1499
Hexafluoroethane mol structure 2389
Hexahelicene linear dichroism UV 1400
Hexane benzene film luminescence 2081
Hexane diffusion binary liq 2283
Hexane irradn benzoate dimer 105
Hexane irradn proton trapping 91
Hexane pulse radiolysis excitation 22
Hexanetriyl triacetate dielec relaxation 1078
Hexose acetylamino CD 1829
Hot atom reaction fluorine 857
Hot atom reaction tritium 2186
Hot atom sulfur 35 372
Hueckel MO insertion compd 2399
Hydrate calcium phosphate pyrolysis 1631
Hydrate sodium hydroxide thermodn 1701
Hydrated electron benzene reaction 1987
Hydrated electron detn time 2103
Hydration hydrophobic magnetic relaxation 1002
Hydration lanthanide perchlorate elec cond 1435
Hydrazine vapor flash photolysis 1356
Hydride lithium system 1933
Hydride transfer methyl silane 2429
Hydrobromide alkylamine aq soln thermodn 1217
Hydrocarbon arom ion electronic spectra 1420
Hydrocarbon arom quenching excited 1885
Hydrocarbon crystals irradn free radical 2698
Hydrocarbon effect nitrous oxide radiolysis 32
Hydrocarbon glass gamma irradn 1135
Hydrocarbon nitrous oxide radiolysis 102
Hydrocarbon packing lattice energy 1595
Hydrocarbon reaction oxygen kinetics 1780
Hydrocarbon soly liq sulfur 2635
Hydrochloric acid IR reflection 1405
Hydrocyanic acid soln radiolysis 2660
Hydrogen adduct nitrone irradn alkane 91
Hydrogen atom alkane reaction 559
Hydrogen atom disilane reaction 398
Hydrogen atom recombination wall 465
Hydrogen bond acetone phenol 124
Hydrogen bond ammonia 2106

Hydrogen bond aq org 1727
Hydrogen bond cholesterol nonpolar soln 250
Hydrogen bond fluoroacetic acid 1709
Hydrogen bond gelation hydroxystearic acid 759
Hydrogen bond intramol intermol 2236
Hydrogen bond isotope effect 429
Hydrogen bond lactam 2341
Hydrogen bond MO peptide 970
Hydrogen bond model phenol activity 1443
Hydrogen bond perchlorate alc 168
Hydrogen bond tetramethylammonium salt 2585
Hydrogen bond water org 1723
Hydrogen bonding acid sulfoxide 1662
Hydrogen bonding energy 1415
Hydrogen bromide deuterium exchange 2549
Hydrogen cesium heat exchange 1812
Hydrogen chemiluminescence sulfur oxide 1248
Hydrogen chloride ether adduct 432
Hydrogen compd mol force field 989
Hydrogen electron spin polarization 1336
Hydrogen exchange kinetics detn 984
Hydrogen interaction magnesium oxide defect 758
Hydrogen ion binding polysulfonate 1013
Hydrogen ion exchange 1150
Hydrogen migration quinone rearrangement 1820
Hydrogen MO calcn 763
Hydrogen oxygen combustion 497
Hydrogen peroxide decompn catalyst 1653
Hydrogen peroxide nitrosodimethylaniline photolysis 888
Hydrogen peroxide reaction oxygen atom 463
Hydrogen reaction ether methanol 2650
Hydrogen reaction ferrocyanide ferricyanide 1368
Hydrogen sulfide MO 1554
Hydrogen sulfide photolysis dimethylsilane 203
Hydrogen sulfide proton affinity 2527
Hydrogen sulide dimethylsilane photolysis 203
Hydrogen transfer silane ion mol 2195
Hydrogenation catalyst palladium active site 583
Hydrogenation graphite metal catalysis 2254
Hydrogenation heat terminal alkene 2569
Hydrogenation platinum catalyst 875
Hydrolysis chloromethyl ether 1096
Hydrolysis ether mechanism 2658
Hydrolysis ethyl acetate 1509
Hydrolysis triethylethoxysilane polemic 757 758
Hydroperoxy ozone reaction kinetics 1447
Hydroperoxyl radiation chemistry 2330
Hydroperoxyl radical reaction copper 779
Hydroperoxyl reaction nitrogen oxide 653
Hydrophobic hydration magnetic relaxation 1002
Hydrophobic interaction alkylammonium 1719
Hydrophobic interaction proton relaxation 851
Hydrophobicity alkylammonium carboxylate 1759
Hydrophobicity electrolyte aq 170
Hydroxide copper amine substitution 305
Hydroxide EPR trapped electron 221
Hydroxide photosubstitution platinum complex 2349
Hydroxide sodium enthalpy soln 1509
Hydroxide sodium hydrate thermodn 1701
Hydroxide sodium IR reflection 1405
Hydroxyapatite crystal growth 2218
Hydroxycyclohexadienyl oxidn metal ion 2335
Hydroxycyclohexadienyl radical deriv radiolytic polarog 160
Hydroxycyclohexadienyl radical ESR 1521
Hydroxyl ozone reaction kinetics 1447
Hydroxyl radical phenol reaction 523
Hydroxyl radical reaction disulfide 282
Hydroxyl reaction acetylene 311
Hydroxyl reaction arom carboxylic acid 1521
Hydroxyl reaction arom compd polarog 160
Hydroxyl zinc oxide adsorption water 1116
Hydroxylapatite dissoln strontium effect 1273
Hydroxylation benzene irradn 1795
Hydroxylation benzene metal irradn 2335
Hydroxymethylperoxy radical UV 2089
Hydroxystearic acid gelation pressure solvent 759
Hyperfine coupling chloranil radical 2140
Hyperfine interaction perturbed nitroxide 1313
Hyperfine model piperidine nitroxide 1410
Hypochromism DNA Hartree detn 444
Ice acidic electron spin polarization 1336
Ice hydroxide gamma irradn 221
Ice intermol frequency spectrum 1844
Imidogen photolysis amine fluorescence 1784
Imino radical amine photolysis 1784
Indole fluorescence quenching lanthanide 1953
Inertia ESR slow tumbling 935
Information explosion review 1339
Insertion compd transition sulfide 2399
Interaction matrix IR 134
Interaction parameter polyisobutylene solvent 60
Interface adsorbed layer IR 941
Interface aq germanium electrode 941
Interface bolaform quaternary ammonium 1387
Interface cation exchange membrane 1805
Interfacial tension reaction equil nonequil 1178
Interferometric detn diffusion 2050
Intermol energy fluid crit temp 1241
Intermol force theory 1961
Intermol frequency spectrum ice 1844
Intermol potential energy water 909
Intermol potential org crystal 1595
Intermol potential polar compd 1862
Intersystem coupling formaldehyde 2270
Intersystem crossing hexacyanochromate 541
Iodide fluorescence quenching anthracene 2555
Iodide iodine atom reaction 1698
Iodide iodine soln Raman 2306
Iodide lithium surface ionization 820
Iodide silver complex soly 2244
Iodination fluoroethane thermodn 2315
Iodine atom iodide reaction 1698
Iodine atom recombination kinetics 878
Iodine effect cyclohexane radiolysis 366
Iodine ether complex stability 557
Iodine iodide soln Raman 2306
Iodine laser fluoromethyl radical 951
Iodine methyl sulfoxide electronic 1744
Iodine scavenger perfluorocyclohexane radiolysis 360
Iodine trialkoxyphosphine chalcogenide UV 1657
Iodoethane entropy 2315
Iodoplatinum photosubstitution 2349
Ion ammonium solvation ammonia 1482
Ion assocn relaxation Onsager Provencher 1431
Ion equil cond modulation 1210
Ion exchange complexing 926
Ion exchange equil unequal charge 1110
Ion exchange zirconium phosphate 1812
Ion irradn sodium metaphosphate 752
Ion mol reaction acetylene silane 2645
Ion mol reaction disilane 1184
Ion mol reaction mass spectra 2433
Ion mol reaction methylsilane 2422
Ion mol reaction rate 1773
Ion mol reaction silane 2195
Ion molal vol org solvent 1099
Ion pair alkylammonium carboxylate 1759
Ion pair chloranil radical 2140
Ion pair coordination complex phosphorescence 1374
Ion pair ethylammonium salt 2687
Ion pair formation ESR 1771
Ion pair isothermal compressibility 1636
Ion pair magnesium sulfate aq 246 1287
Ion partition membrane water 2259
Ion radical salt 1750
Ion recombination triplet polemic 309 310
Ion solvation coordination 1731
Ion solvation methanol 627
Ion solvation org solvent cond 556
Ion solvation Walden product 907
Ionic dissocn methylstyrene complex 341
Ionic entropy nonaq soln 1000
Ionic nuclei magnetic relaxation 1002
Ionization ammonia flame 2320
Ionization energy element 115 1945
Ionization potential dihydrogen disulfide 1554
Ionization sulfonephthalein isotope effect 1021
Ionization surface lithium anion 820
Ions disulfides hydroxyl aq soln 282
IR acetylene ethylene cobalt 618
IR alkali halide aq 238
IR amide solvation electron 2631
IR aq org solvent 1727
IR aq urea soln 1754
IR arom halogen radiolysis 519
IR arom radical anion 741
IR borane trimethylamine 1503
IR butylamine adsorbed silica alumina 704
IR carbon dioxide uranium 2117
IR chromia alumina catalyst 588
IR compressed carbon monoxide 1968
IR copper complex zeolite 531
IR dialuminum oxide matrix 236
IR diazine adsorption silica 2376
IR disulfide correlation bond angle 855
IR ESR dicyclohexyldithiophosphinate metal 962
IR far ethylamine conformation 803
IR matrix interaction 134
IR mercaptan adsorption nickel 1648
IR methane absorption zeolite 2180
IR methyl sulfoxide iodine 1744
IR microemulsion 256
IR polaron alc amine alkane 792
IR polaron soln 2414
IR reflection adsorbed layer 941
IR reflection aq electrolyte 1405
IR silver nitrosyl 1174
IR solvated electron alc 514
IR tetramethylammonium salt 2585
IR trimethylenecyclopropane photoproduct 568
IR water org solvent 1723
Iridium chloro ruthenium bipyridine phosphorescence 1374
Iron chloride extn ether 2572
Iron doped lead azide decompn 478
Iron hectorite arom radical cation 994
Iron reaction chlorine 107
Iron thallium kinetics aq soln 488
Irradiated polyethylene radical decay 1798
Irradn alkane proton trapping 91
Irradn benzene hydroxylation phenylation 1795
Irradn benzophenone diphenylamine ESR 2225
Irradn benzophenone phenol aniline 1837
Irradn biphenyl methylpentane glass 2696
Irradn deuterated malonic acid 1839
Irradn gamma hydrocarbon glass 1135
Irradn halomethane silica gel 1391
Irradn hexane benzoate dimer 105
Irradn hydroxylation benzene metal 2335
Irradn methylpentane radical pair 2233
Irradn nitrobenzyl acetonitrile 112
Irradn phosphate gamma ESR 958
Irradn radical formation polyvinylpyridine 899
Irradn sodium metaphosphate ion 752
Isocyanide methyl isomerization 863
Isomer heptane diffusion helium 1428
Isomerization alkene kinetics 770
Isomerization calcn multiple 1579
Isomerization haloalkene shock tube 1469
Isomerization methyl isocyanide 863
Isomerization pentenyl methylbutenyl 1245
Isomerization pentenyl radical 2201
Isomerization photo cyanine dye 16
Isomerization photo thiacarbocyanine dye 2355
Isomerization propenyl radical mechanism 2543
Isopentylammonium nitrate aq cond capacitance 1431
Isothermal compressibility ion pair 1636
Isotope effect benzene diffusion 846
Isotope effect deactivating collision 850
Isotope effect deuterium 398
Isotope effect deuterium adduct 429
Isotope effect kinetic 544
Isotope effect sulfonephthalein ionization 1021
Isotope exchange kinetics detn 984
Isotope oxygen photocatalytic exchange 555
Isotropic splitting butyl nitroxide 1313
Junction potential liq electrolyte 2060
Justice conductance equation derivation 1383
Keratin zeolite exchange water 1279
Ketene formation oxygen ethylene 663
Ketone adsorbed photolysis 2446
Ketone alkyl adsorbed photolysis 2442
Ketone arom anion spectrum 1473
Ketonorbornane photochemistry 2637
Kinetic electron scavenging neopentane 853
Kinetics alkene isomerization 770
Kinetics assocn surfactant micelle 1024
Kinetics catalase model intermediate 1919
Kinetics chemiluminescence sulfur oxide 1248
Kinetics decompn excited propylene 1348
Kinetics decompn fluoroalkyl cyclopropane 2535
Kinetics dissociative vaporization reaction 1298
Kinetics electron transfer solvent effect 285
Kinetics erbium complex formation 1940

Kinetics glucose glycosidation 1918
Kinetics micelle formation 1676
Kinetics micelle luminescence decay 190
Kinetics ozone alkene reaction 2085 2318
Kinetics particle formation photolysis 325
Kinetics pentane radiolysis 508
Kinetics phenylalanine polaron 1790
Kinetics phenylmethanol oxidn 828
Kinetics photolysis photoselection effect 782
Kinetics radical decay polyethylene 1798
Kinetics radiolysis arom halogen 519
Kinetics reaction hydroxyl ozone 1447
Kinetics reaction positronium nitrobenzene 1881
Kinetics redn nitrogen heterocycle 2615
Lactam hydrogen bond 2341
Lanthanide fluorescence quenching indole 1953
Lanthanide perchlorate aq elec cond 1435
Lanthanide salt aq molal vol 1106
Lanthanum chloride alkali chloride mixing 181
Lanthanum potassium chloride melt Raman 1134
Laser carbon monoxide chem 1451
Laser dye dimerization 1891
Laser emission fluoroiodomethane photolysis 951
Laser excitation Rhodamine 6G 2006
Laser photolysis ionic polymn 341
Laser photolysis micelle luminescence decay 190
Laser radiation pyrene photoionization 2248
Laser Raman absorption oxide 300
Lattice energy amino acid 1621
Lattice energy packing org 1595
Laurate sodium adsorption electrode 941
Lead azide thermal decompn 478
Least squares linear mol complex 557
Lerolat N300 positronium lifetime 2526
Lifetime fluorescence aminopyridine solvent 201
Lifetime positronium surface active soln 2526
Ligand field excitation hexaamminerhodium 2698
Ligand field octahedral energy level 56
Ligand field tetragonal energy level 2678
Light circular polarization fluorescence 387
Linear dichroism disklike mol 1400
Linear least squares mol complex 557
Liq crystal cholesteryl alkanoate 1740
Liq crystal mol assocn 1206
Liq crystal vapor pressure 275
Liq membrane potential biionic 2370
Literature science review 1339
Lithium alumina catalyst structure 2496
Lithium calcium fluoride enthalpy 1478
Lithium chloride soln heat mixing 77
Lithium fluoride hexafluoroaluminate Raman 1499
Lithium fluoride vaporization rate 1998
Lithium fluoroacetate cond propylene carbo= nate 1380
Lithium lithium hydride system 1933
Lithium perchlorate cond THF 917
Lithium perchlorate decompn catalysis 776
Lithium surface ionization anion 820
Luminescence cyanochromate cobaltate 2122
Luminescence decay micelle hydrophobic mol 190
Luminescence hexane benzene film 2081
Luminescence propane electron impact 2077
Luminescence quantum yield powder 2229
Magnesium acetate hydrate thermodn 278
Magnesium acetate ultrasound absorption 1913
Magnesium chloride aq compressibility 1636
Magnesium oxide defect interaction hydrogen 758
Magnesium sulfate assocn aq Raman 246
Magnesium sulfate ion pair aq 1287
Magnetic relaxation Fourier transform 1971
Magnetic relaxation hydrophobic hydration 1002
Maleic acid copolymer binding metal 1486
Maleic copolymer copper complex 607
Malonic acid deuterated irradn 1839
Manganese ESR mercury complex 45
Margarate barium film ellipsometry 947
Mass spectra ion mol reaction 2433
Mass spectra methylsilane 2429
Mass spectra oxygen nitrogen ethyl 1268
Mass spectrometry gas phase solvation 1482
Mass spectroscopy vaporization oxide 266
Mass UV dicyclohexyldithiophosphinate metal 962
Matrix interaction IR 134
Max density temp soln 2305
Mechanism catalase intermediate 1919
Mechanism decompn hot cyclobutane 2309
Mechanism dehydrochlorination trichloroe= thane 2166
Mechanism detn radical ion reaction 290
Mechanism glucose glycosidation calcn 1918
Mechanism hydrolysis ether 2658
Mechanism isomerization propenyl radical 2543
Melting point element 115 1945
Melting point solid adsorption carbon 622
Membrane anion exchange noise 761
Membrane cation exchange interface 1805
Membrane gelatin permeability 408
Membrane water ion partition 2259
Mercaptan adsorption nickel IR 1648
Mercuric chloride dye metachromasia 536
Mercuric iodide soln photolysis 1698
Mercury electrode adsorption pyrazine pyri= dine 1226
Mercury electrode anion adsorption 2240
Mercury pyridine oxide ESR 45
Mercury soly polar gas 186
Mercury triplet quenching gas 482
Metachromasia dye mercuric chloride 536
Metachromatic dye reflectance spectra 1040
Metal alkali binding polysulfonate 1013
Metal catalysis graphite hydrogenation 2254
Metal dicyclohexyldithiophosphinate ESR IR 962
Metal dithiolate perylene complex 215
Metal reaction chlorine 107
Metaphosphate sodium irradn ion 752
Methane absorption zeolite IR 2180
Methane electron impact excitation 2077
Methane proton transfer deuterium 93
Methane thermodn soln electrolyte 170
Methane thermodn soln solvophobicity 175
Methane trapped electron MO 148
Methanetriamine hexafluoro pyrolysis 2189
Methanol aq assocn erbium chloride 424
Methanol benzoate transfer acetonitrile 839
Methanol glass photobleaching electron 232
Methanol ion solvation 627
Methanol mercury vapor concn 186
Methanol nitrogen oxide reaction 501
Methanol phenyl oxidn kinetics 828
Methanol potassium chloride electroosmosis 2302
Methanol proton affinity 2527
Methanol reaction hydrogen atom 2650
Methyl addn butadiene 1245
Methyl decay silica gel 1391
Methyl disulfide hydroxyl reaction 282
Methyl ether reaction hydrogen atom 2650
Methyl isocyanide isomerization 863
Methyl silane hydride transfer 2429
Methyl sulfoxide iodine electronic 1744
Methyl sulfoxide radical ESR 1882
Methyl sulfoxide water exchange 411
Methylacetylene reaction oxygen hydroxyl 311
Methylamine photolysis imidogen 1784
Methylammonium salt hydrogen bond 2585
Methylbutene photolysis mechanism 98
Methylbutenyl isomerization pentenyl 1245
Methylcyclohexane gamma radiolysis electron 867
Methylcyclohexene recoil tritium reaction 354
Methylcyclopentane nitrous oxide radiolysis 102
Methylene cycloaddn butadiene MO 1167
Methylene reaction small mol 1344
Methylpentane glass electron scavenging 2696
Methylpentane glass gamma irradn 1135
Methylpentane irradn proton trapping 91
Methylpentane irradn radical pair 2233
Methylperoxy reaction nitrogen oxide photo= lysis 2417
Methylpiperidine oxyl anisotropic splitting 1313
Methylsilane ion mol reaction 2422
Methylstyrene photopolymn charge transfer 341
Micellar soln pyrene photoionization 2248
Micelle assocn kinetics 1024
Micelle bolaform quaternary ammonium 1387
Micelle effect pH acid 1490
Micelle formation kinetics model 1676
Micelle formation nucleation Monte Carlo 1423
Micelle hydrophobic mol luminescence decay 190
Micelle soln transfer heat 834
Micelle structure ionic surfactant 2480
Micellization size effect 2469
Micellization surfactant free energy 1086
Microemulsion water surfactant IR NMR 256
Miscibility calcn quaternary salt system 1091
Mixing electrolyte thermodn 1927
Mixing enthalpy molten fluoride 1478
Mixing heat alkali cerium chloride 178
Mixing heat aq soln 2465
Mixing heat lanthanum alkali chloride 181
Mixing heat propylammonium chloride 77
Mixing heat salt soln 1924
Mixing org compd thermodn 1961
MO benzophenone ketyl 2144
MO calcn wave function 763
MO CNDO dimethyl disulfide 1848
MO electron configuration cephalosporin 2604
MO electronic spectra radical 741
MO energy hydrogen bond 970
MO furanquinone electron affinity 1714
MO hydrocarbon ion spectra 1420
MO hydrogen sulfide 1554
MO methane trapped electron 148
MO methylene cycloaddn butadiene 1167
MO model copper complex 1235
MO nitroarom core charge 1868
MO nitrostyrene 49
MO phenyl vinyl ether 440
MO position org complex 2683
MO reactivity oxirane acrolein 1874
MO splitting cyclooctatetraene 90
MO theory x ray emission 2592
Mobility cation DMSO 2405
Mobility drift electron alk 2454
Model atom recombination cylinder 465
Model catalase kinetics intermediate 1919
Model simulation tubular electrode 718
Model transport binary gas 1564
Mol assocn liq crystal 1206
Mol complex linear least squares 557
Mol force field virial theorem 989
Mol interaction gas chromatog 1644
Mol ion reaction rate 1773
Mol motion ESR polyglutamate 1324
Mol motion microemulsion 256
Mol orientation water adsorbate mercury 1226
Mol sieve transition metal catalyst 1653
Mol structure diffraction thermodn 2380
Mol structure diffusion heptane isomer 1428
Mol structure hexafluoroethane 2389
Mol structure spectra polaron 514
Mol wt distribution polymer 1083
Molal vol alc amine aq 1030
Molal vol aq amine 714
Molal vol aq lanthanide salt 1106
Molal vol aq magnesium sulfate 1287
Molal vol ion org solvent 1099
Molar volume ion methanol 627
Molecule charge distribution 763
Molten fluoride Raman 1499
Molten salt elec relaxation 639
Molten salt reciprocal miscibility calcn 1091
Molten salt superoxide model 1294
Molybdenum cobalt alumina acidity 2069 2070
Molybdenum cyano ruthenium bipyridine phosphorescence 1374
Monoxide carbon chem laser 1451
Monoxide carbon matrix interaction 134
Monoxide carbon MO calcn 763
Montmorillonite cation chemisorption acryl= onitrile 42
Morphol cellulose ESR 308
Multilayer adsorption theory significant structure 2600
Multiple isomerization calcn 1579
Naphthalene fluorescence quenching bromide 2555
Naphthalene halo radiolysis spectra 519
Naphthalene radiolysis singlet triplet 22
Naphthocyclobutene redn alkali metal 723
Nematic mol assocn optical reflection 1206
Neopentane liq electron scavenging 853
Neopentane nitrous oxide radiolysis 102
Neutralization maleic acid copolymer 607
Neutron irradn potassium chloride 372
Nickel adsorption mercaptan IR 1648
Nickel binding polyacid thermodn 1486
Nickel dithiolate perylene complex 215
Nickel reaction chlorine 107
Nickel soln gamma radiolysis 882
Nitrate alkali liq ammonia Raman 708
Nitrate alkali melt superoxide ESR 1294
Nitrate alkylammonium cond oxazolidone 2689
Nitrate chloride membrane potential 2370

Nitrate fluorescence quenching fluorene 2555
Nitrate isopentylammonium aq cond capacitance 1431
Nitrate lanthanide aq molal vol 1106
Nitrate melt copper cupric electrode 2670
Nitrate mobility propylene carbonate 1380
Nitrate potassium calcium relaxation 639
Nitrate radical acetaldehyde propene 1337
Nitrate yttrium ultrasonic relaxation 261
Nitric acid alpha radiolysis 211
Nitric acid vapor UV photolysis 1
Nitric oxide chemisorption cobalt spinel 2490
Nitric oxide chromia catalyst IR 588
Nitric oxide complex silver 1174
Nitric oxide neg ion polemic 1445 1446
Nitric oxide reaction methylene 1344
Nitric oxide reaction nitryl chloride 2073
Nitric oxide reaction oxygen 1780
Nitric oxide titrn atomic nitrogen 1120
Nitride hafnium dissocn energy 273
Nitrite oxidn oxide catalysis 1693
Nitrite palladium pyridine ESR 2136
Nitroarom core charge MO 1868
Nitrobenzene deriv UV 494
Nitrobenzene positronium reaction kinetics 1881
Nitrobenzene solvent heat soln 454
Nitrobenzyl irradn acetonitrile 112
Nitrofluorenone THF photocond 1395
Nitrogen atomic detn elec conduction 1120
Nitrogen chemiluminescence sulfur oxide 1248
Nitrogen compd mol force field 989
Nitrogen dioxide photolysis photon 1583
Nitrogen dioxide reaction ozone 1775
Nitrogen dioxide titrn oxygen detn 208
Nitrogen heterocycle redn kinetics 2615
Nitrogen hydrogen bonding energy 1415
Nitrogen hyperfine interaction nitroxide 1313
Nitrogen matrix interaction IR 134
Nitrogen MO calcn 763
Nitrogen oxide methanol reaction 501
Nitrogen oxide oxychloride exchange 402
Nitrogen oxide oxychloride reaction 2073
Nitrogen oxide reaction hydroperoxyl 653
Nitrogen oxide reaction methylperoxy photolysis 2417
Nitrogen oxygen ammonia flame 2320
Nitrogen 15 NMR chem shift 2507
Nitromethane potassium bromide scattering 2438
Nitromethane water hydrogen bond 1723
Nitromethoxystilbene photoisomerization mechanism 451
Nitropentaamminecobalt photolysis 572
Nitrosodimethylaniline hydrogen peroxide photolysis 888
Nitrosodisulfonate potassium radical EPR 375
Nitrostilbene photoisomerization triplet mechanism 451
Nitrostilbene photolysis triplet transient 446
Nitrostyrene UV dipole ESR 49
Nitrosyl chloride nitrogen exchange 402
Nitrosyl silver IR EPR 1174
Nitrous oxide cyanide soln radiolysis 2660
Nitrous oxide dissocn rutile 870
Nitrous oxide excited oxygen atoms 2698
Nitrous oxide hydrocarbon radiolysis 102
Nitrous oxide liq radiolysis 28 32
Nitrous oxide oxidn film 2486
Nitrous oxide xenon radiolysis 954
Nitroxide butyl EPR adsorbed 200
Nitroxide EPR silica adsorption 2110
Nitroxide ESR inertial effect 935
Nitroxide ESR satn recovery 1155
Nitroxide hyperfine interaction perturbed 1313
Nitroxide piperidine hyperfine model 1410
Nitroxide rotational correlation time 1321
Nitryl chloride reaction nitric oxide 2073
NMR acetone phenol assocn 124
NMR assocn fluoranthene org solvent 1330
NMR butanol paramagnetic solute 851
NMR chem 15 nitrogen 2507
NMR cholesterol dimerization solvation 250
NMR deoxyacetamidohexose CD 1829
NMR detn surface reaction kinetics 1279
NMR fluorinated phenoxyl anilinyl 1837
NMR frozen aq soln 807
NMR hydrogen bonding 1662
NMR induced dynamic polarization 1971
NMR ion solvation 1731
NMR microemulsion 256
NMR mol adsorbed silica 38
NMR oxygen effect 1747
NMR perchlorate alc hydrogen bond 168
NMR polyoxyethylene urea 1528
Noise anion exchange membrane 761
Nonaq soln ionic entropy 1000
Nonelectrolyte activity aq salt 165
Nonequil reaction wetting 1178
Nonlinear least squares mol complex 557
Nonpolar solvent solvation alc dielec 1203
Nucleation micelle Monte Carlo 1423
Oblate ellipsoid micelle 2469
Octadecane arom activity 1644
Octahedral ligand field energy level 56
Octane benzene diffusion 846
Octane cathodoluminescence 2077
Octanol proton exchange carboxylate 2339
Onsager Provencher ion assocn relaxation 1431
Onsager reciprocity relation electroosmosis 2302
Optical absorption aq electrolyte 1405
Optical absorption nitrofluorenone THF 1395
Optical absorption solvated electron 2631
Optical reflection nematic mol assocn 1206
Optical spectra complex theory 2678
Orbit spin octahedral ligand field 56
Orbital redn factor ruthenium 700
Org chlorine x ray emission 2592
Org compd mixing thermodn 1961
Org crystal intermol potential 1595
Org electron transfer solvent effect 285
Org mol sorption micelle heat 834
Organonickel compd electron radiolysis 882
Orientation water pyrazine pyridine mercury 1226
Oscillator strength dihydrogen disulfide 1554
Osmosis reverse membrane thickness 2259
Osmosis thermal ternary mixt 2693
Osmotic activity coeff electrolytes ions 2698
Outer sphere electron transfer 1684
Oxalate thiocyanate palladium ESR 2136
Oxalato cobalt complex photolysis 1361
Oxazolidone alkylammonium salt cond 2689
Oxazolidone ethylammonium salt cond 2687
Oxazolidone soly silver halide 1817
Oxide absorption laser Raman 300
Oxide alkyl disulfide hydroxyl 282
Oxide carbon compressed IR 1968
Oxide chromium crystn 2621
Oxide dialuminum IR matrix 236
Oxide nitric complex silver 1174
Oxide nitric titrn atomic nitrogen 1120
Oxide nitrogen reaction hydroperoxyl 653
Oxide nitrogen reaction methylperoxy photolysis 2417
Oxide nitrogen titrn oxygen detn 208
Oxide nitrous dissocn rutile 870
Oxide nitrous liq radiolysis 28 32
Oxide oxychloride nitrogen exchange 402
Oxide phosphine trialkoxy iodine 1657
Oxide pyridine mercury ESR 45
Oxide sulfur chemiluminescent reaction 1248
Oxide sulfur ion EPR 649
Oxide vaporization mass spectroscopy 266
Oxide zinc catalysis 2303
Oxidn biol singlet oxygen 1681
Oxidn carbon monoxide catalysis 2303
Oxidn hydroxycyclohexadienyl metal ion 2335
Oxidn nitrite oxide catalysis 1693
Oxidn phenothiazine dibenzophenothiazine 1750
Oxidn phenylmethanol kinetics 828
Oxidn thallium chloro complex 892
Oxidn transition metal film 2486
Oxirane reactivity MO 1874
Oxychloride nitrogen oxide reaction 2073
Oxychloride oxide nitrogen exchange 402
Oxygen adsorption titanium zeolite 218
Oxygen ammonia nitrogen flame 2320
Oxygen atom reaction acetylene 311
Oxygen atom reaction hydrogen peroxide 463
Oxygen atom reactivity alkane 1457
Oxygen carbon monoxide kinetics 497
Oxygen chemiluminescence sulfur oxide 1248
Oxygen compd mol force field 989
Oxygen detn flow reactor 208
Oxygen effect NMR 1747
Oxygen exchange catalysis 2303
Oxygen exchange photocatalysis titania 555
Oxygen germanium reaction condensation 1763
Oxygen hydrogen bonding energy 1415
Oxygen hyperfine interaction nitroxide 1313
Oxygen matrix interaction IR 134
Oxygen org cation heat formation 1268
Oxygen reaction cyanogen laser 1451
Oxygen reaction ethylene branching 663
Oxygen reaction hydrocarbon kinetics 1780
Oxygen reaction methylene 1344
Oxygen singlet biol oxidn 1681
Oxyl methylpiperidine anisotropic splitting 1313
Oxyphosphorus compd radiolysis 576
Oxysulfur compd radiolysis 576
Ozone alkene reaction kinetics 2085 2318
Ozone hydroxyl reaction kinetics 1447
Ozone mol force field 989
Ozone nitric oxide nitrogen dioxide rate 2698
Ozone reaction nitrogen dioxide 1775
Ozonolysis alkene kinetics 2318
Packing configuration amino acid 1621
Packing lattice energy org 1595
Palladium dithiolate perylene complex 215
Palladium hydrogenation catalyst active site 583
Palladium mixed complex ESR 2136
Palladium reaction chlorine 107
Palmitate barium film ellipsometry 947
Paramagnetic solute NMR butanol 851
Particle formation kinetics photolysis 325
Partition ion membrane water 2259
Pentahelicene linear dichroism UV 1400
Pentane radiolysis kinetics 508
Pentanol water dielec const 652
Pentenyl chem activated reaction 2201
Pentenyl isomerization methylbutenyl 1245
Peptide hydrated electron 1193
Peptide hydrogen bond MO 970
Peptide pulse radiolysis 1790
Perchlorate alkylammonium cond oxazolidone 2689
Perchlorate ammonium vaporization 1433
Perchlorate erbium inner sphere complex 1940
Perchlorate fluorescence quenching biphenyl 2555
Perchlorate hydrogen bond alc 168
Perchlorate lanthanide aq elec cond 1435
Perchlorate lanthanide aq molal vol 1106
Perchlorate lithium cond THF 917
Perchlorate lithium decompn catalysis 776
Perchlorate tetramethylammonium hydrogen bond 2585
Perchlorate thermal decompn 773
Perfluorocyclobutane photolysis 2071
Perfluorocyclohexane radiolysis iodine effect 366
Perfluorocyclohexane radiolysis radical scavenger 360
Permeability gelatin membrane 408
Peroxide catalysis nitrite oxidn 1693
Peroxide hydrogen decompn catalyst 1653
Peroxide hydrogen nitrosodimethylaniline photolysis 888
Peroxide hydrogen reaction oxygen atom 463
Peroxy chemiluminesence decarboxylation 2559
Perylene complex elec cond 215
PH dimethylsulfoxide aq soln 421
Phase transition cholesteryl alkanoate 1740
Phenol acetone hydrogen bond 124
Phenol benzophenone irradn 1837
Phenol hydrogen bond 2236
Phenol hydrogen bond isotope effect 429
Phenol hydrogen bond model activity 1443
Phenol hydrogen bond perchlorate 168
Phenol hydroxyl radical reaction 523
Phenol hydroxyl radiolytic polarog 160
Phenol solid adsorption carbon 622
Phenolphthalein proton transfer 2450
Phenothiazine oxidn 1750
Phenoxyl fluorine hyperfine coupling 1837
Phenyl vinyl ether conformation 440
Phenylalanine polaron kinetics 1790
Phenylation benzene irradn 1795
Phenylborate alkylammonium cond oxazolidone 2689
Phenylborate ethylammonium elec cond 2687
Phenylmethanol oxidn kinetics 828
Phenylphosphonium halide soln thermodn 738
Phosphate anion exchange noise 761
Phosphate calcium hydrate pyrolysis 1631
Phosphate calcium hydroxide growth 2218
Phosphate effect hydroxylapatite dissoln 1273
Phosphate ESR gamma irradn 958
Phosphate zirconium cation exchange 1150
Phosphate zirconium heat cation exchange 152
Phosphate zirconium ion exchange 1812
Phosphide arsenic bismuth bond energy 603
Phosphine oxide trialkoxy iodine 1657
Phosphonium halide soln thermodn 738

Phosphonium tetraphenyl enthalpy soln 1509
Phosphor powder quantum yield 2229
Phosphorescence carbazole deriv 1512
Phosphorescence halogenated acetone 665
Phosphorescence hexacyanochromate intersystem crossing 541
Phosphorescence quenching ruthenium bipyridine complex 1374
Phosphorescence sulforhodamine dimer 380
Phosphorescence transition metal 2496
Phosphorothioic triamide methyl solvent property 1018
Photoaquation hexaamminerhodium complex 1144
Photobleaching trapped electron alc glass 232
Photocatalysis oxygen exchange titania 555
Photochem acetone halo 665
Photochem reaction solid rate 1265
Photochem rhodium complexes 2698
Photochemistry ketonorbornane 2637
Photocond nitrofluorenone THF 1395
Photocond potassium carbonate glass 2454
Photogenerated charge carrier aq glass 2454
Photoionization pyrene micellar soln 2248
Photoionization tetramethylphenylenediamine dielec liq 2128
Photoisomer quinone polarog 1820
Photoisomerization cyanine dye 16
Photoisomerization nitrostilbene triplet mechanism 451
Photoisomerization retinal triplet state 336
Photoisomerization thiacarbocyanine dye 2355
Photolysis adsorbed alkyl ketone 2442
Photolysis adsorbed ketone 2446
Photolysis amine imidogen fluorescence 1784
Photolysis benzene benzvalene prodn 1909
Photolysis cobalt oxalato complex 1361
Photolysis cyclobutanone matrix mechanism 1461
Photolysis cyclohexane 1899
Photolysis cysteine aq soln 1130
Photolysis diazopropane gas phase 1348
Photolysis dioxane solvated electron 2181
Photolysis ethylene 1254
Photolysis ferricyanide glass ESR 1335
Photolysis flash arom sulfur polemic 1441 1442
Photolysis flash hydrazine vapor 1356
Photolysis fluoroiodomethane laser emission 951
Photolysis fluoroketone ESR radical 2036
Photolysis hydrogen peroxide nitrosodimethylaniline 888
Photolysis hydrogen sulfide dimethylsilane 203
Photolysis hydrogen sulide dimethylsilane 203
Photolysis kinetics photoselection effect 782
Photolysis laser ionic polymn 341
Photolysis mercuric iodide soln 1698
Photolysis methylbutene mechanism 98
Photolysis methylperoxy reaction nitrogen oxide 2417
Photolysis micelle luminescence decay 190
Photolysis nitrogen dioxide photon 1583
Photolysis nitropentaamminecobalt 572
Photolysis nitrostilbene triplet transient 446
Photolysis perfluorocyclobutane 2071
Photolysis sulfur dioxide acetylene 325
Photolysis UV nitric acid vapor 1
Photon two photolysis 1583
Photopolymn charge transfer methylstyrene 341
Photoproduct trimethylenecyclopropane spectra 568
Photoreaction hydroperoxyl radical 779
Photoredn cobalt ammine complex 686
Photoselection carbazole spectroscopy 1512
Photoselection effect kinetics photolysis 782
Photoselection relaxation circular polarization 387
Photosubstitution platinum complex 2349
Picrate alkylammonium cond oxazolidone 2689
Piperidine nitroxide hyperfine model 1410
Platinum catalyst hydrogenation 875
Platinum chloro ruthenium bipyridine phosphorescence 1374
Platinum complex photosubstitution 2349
Poisoning catalyst nitroxide zeolite 2110
Polar compd potential intermol 1862
Polarization acrylonitrile montmorillonite cation 42
Polarization circular light fluorescence 387
Polarization dipole alc nonpolar solvent 1203
Polarization electron spin hydrogen 1336
Polarization transition disklike mol 1400
Polarog azobenzene deriv 1825
Polarog quinone photoisomer 1820
Polarog radiolytic hydroxycyclohexadienyl radical deriv 160
Polaron alc relaxation visible spectra 393
Polaron IR alc amine alkane 792
Polaron phenylalanine kinetics 1790
Polaron reaction ferrocyanide ferricyanide 1368
Polaron reaction rate const 2631
Polaron spectra mol structure 514
Polemic nitric oxide neg ion 1445 1446
Polyacrylate sodium diffusion chloride 1756
Polyacrylate sodium soln diffusion 2292
Polyacrylic acid surface potential 1189
Polyelectrolyte binding metal thermodn 1486
Polyelectrolyte soln equiv cond 1242
Polyelectrolyte surface elec potential 1189
Polyethylene irradiated radical decay 1798
Polyglutamate mol motion ESR 1324
Polyglutamic acid surface potential 1189
Polyiodide formation soln Raman 2306
Polyisobutylene solvent interaction parameter 60
Polymer mol wt distribution 1083
Polymerization disilane ion mol 1184
Polymn irreversible chromatog gel 460
Polyoxyethylene urea NMR 1528
Polypeptide frozen aq soln NMR 807
Polystyrenesulfonate exchanger solvent selectivity 411
Polystyrenesulfonate gel diffusion cation 735
Polyvinyl alc membrane permeability 408
Polyvinyl sulfonate counterion binding 1013
Polyvinylcarbazole acid fluorescence quenching 2009
Polyvinylpyridine irradn radical formation 899
Position org complex MO 2683
Positron annihilation protein 1261
Positronium lifetime surface active soln 2526
Positronium nitrobenzene reaction kinetics 1881
Potassium alumina catalyst structure 2496
Potassium benzoquinone ion pair 1771
Potassium bromide excited scattering 2438
Potassium bromide transport DMSO 2405
Potassium calcium fluoride enthalpy 1478
Potassium calcium nitrate relaxation 639
Potassium carbonate glass photocond 2454
Potassium chloride neutron irradn 372
Potassium chloride soln heat mixing 77
Potassium halide vaporization rate 1998
Potassium hydroxide IR reflection 1405
Potassium lanthanum chloride melt Raman 1134
Potassium nitrosodisulfonate radical EPR 375
Potassium polystyrenesulfonate aq electric birefringence 2698
Potassium radiolysis hydroxylaminedisulfonate 375
Potassium tetrachloroaluminate Raman cadmium 595
Potential adsorption solid carbon 622
Potential biionic liq membrane 2370
Potential copper cupric electrode 2670
Potential electrostatic solute solvent 1853
Potential energy adsorbed noble gas 405
Potential energy borane trimethylamine 1503
Potential energy hydrogen bonding 1415
Potential energy intermol water 909
Potential energy trapped electron 2454
Potential function mol 989
Potential intermol amino acid 1621
Potential intermol org crystal 1595
Potential intermol polar compd 1862
Potential internal rotation ethylamine 803
Potential ionization dihydrogen disulfide 1554
Potential liq junction electrolyte 2060
Potential surface elec polyelectrolyte 1189
Potential 6 dimensional water dimer 2055
Potentiometry compn detn chem system 816
Potentiometry sodium laurate acid 2626
Powd solid photochem reaction rate 1265
Pressure dependence unimol kinetics 2326
Pressure electroosmosis propanol aluminum oxide 65
Pressure gelation hydroxystearic acid 759
Pressure surface albumin monolayer 2266
Pressure thermoosmotic ternary mixt 2693
Pressure water relaxation time 1674
Propane luminescence electron impact 2077
Propane nitrous oxide radiolysis 102
Propane potassium bromide scattering 2438
Propanol aluminum oxide electroosmosis pressure 65
Propanol radiolysis electron scavenging 504
Propene reaction nitrate radical 1337
Propenyl radical isomerization mechanism 2543
Propylammonium bromide heat soln 1719
Propylene carbonate chloride cond 2521
Propylene carbonate cond alkali fluoroacetate 1380
Propylene carbonate solvation 2576
Propylene excited decompn kinetics 1348
Protein frozen aq soln NMR 807
Protein positron annihilation 1261
Proton affinity methanol hydrogen sulfide 2527
Proton diffusion butyl alc 70
Proton exchange carboxylate octanol 2339
Proton relaxation hydrophobic interaction 851
Proton transfer methane deuterium 93
Proton transfer phenolphthalein 2450
Protonation AMP kinetics 80
Protonation maleic acid copolymer 607
Pulse radiolysis ferrocyanide ferricyanide 1368
Pulse radiolysis naphthalene excitation 22
Pulse radiolytic polarog hydroxycyclohexadienyl 160
Purine methyl ultrasound relaxation 848
Pyrazine mercury electrode adsorption 1226
Pyrene photoionization micellar soln 2248
Pyridine adsorbed oxide Raman 300
Pyridine amino fluorescence solvent 201
Pyridine copper EPR zeolite 531
Pyridine deriv reaction copper complex 316
Pyridine mercury electrode adsorption 1226
Pyridine nitrite palladium ESR 2136
Pyridine oxide mercury ESR 45
Pyridineplatinum photosubstitution 2349
Pyridinyl radical spectrum 2211
Pyrolysis difluoroamino compd 2189
Pyromellitic anhydride complex methylstyrene 341
Quadrupolar relaxation bromine 81 1002
Quadrupole coupling deuteron water 1674
Quadrupole moment carbon monoxide 1968
Quantum theory electron transfer 2148
Quantum yield hydroperoxyl reaction 653
Quantum yield luminescence powder 2229
Quaternary ammonium bolaform interface micelle 1387
Quenching excited arom hydrocarbon 1885
Quenching fluorescence arom 2555
Quenching fluorescence fluoro acetone 682
Quenching fluorescence indole lanthanide 1953
Quenching fluorescence polyvinylcarbazole acid 2009
Quenching mercury triplet gas 482
Quinone photoisomer polarog 1820
Radiation chemistry ascorbic acid 1063
Radiation chemistry hydroperoxyl 2330
Radical allyl compd EPR 117
Radical anion carbonyl compd spectra 741
Radical anion dimerization 295
Radical anion electron transfer solvent effect 285
Radical carbonate tryptophan reaction 2099
Radical cation arom hectorite metal 994
Radical cyanate radiolysis ESR 1074
Radical cyclopentyl disproportionation recombination 462
Radical decay irradiated polyethylene 1798
Radical detection irradiated alc 1977
Radical electron double resonance 1839
Radical ESR inertial effect 935
Radical ESR methyl sulfoxide 1882
Radical ESR phosphate irradn 958
Radical ESR satn recovery 1155
Radical fluoro alkyl ESR conformation 2030
Radical fluoroethyl collision tetrafluoromethane 850
Radical formation irradn polyvinylpyridine 899
Radical hydroperoxyl reaction copper 779
Radical hydroxycyclohexadienyl ESR 1521
Radical hydroxyl phenol reaction 523
Radical hydroxymethylperoxy UV 2089
Radical ion reaction mechanism detn 290
Radical ion salt 1750
Radical pair methylpentane irradn 2233
Radical prodn cobalt complex photoredn 686
Radical propenyl isomerization mechanism 2543
Radical rotation barrier fluoroalkyl 2014
Radical scavenger perfluorocyclohexane radiolysis 360

Radical scavenging cyclohexane radiolysis 366
Radical uracil ESR 696
Radical xanthyl ENDOR 2512
Radiolysis alc electron scavenging 504
Radiolysis alpha nitric acid 211
Radiolysis aq cyclopentane cyclopentene 1052
Radiolysis arom halogen compd 519
Radiolysis benzonitrile pulse 2094
Radiolysis bromotetronic acid 1063
Radiolysis carborane energy transfer 788
Radiolysis cyanate radical ESR 1074
Radiolysis cyanide nitrous oxide soln 2660
Radiolysis cyclohexane iodine effect 366
Radiolysis cyclopentane water 1049
Radiolysis difluoroethane 2183
Radiolysis dye chemiluminescence 1251
Radiolysis gamma methylcyclohexane electron 867
Radiolysis gamma nickel soln 882
Radiolysis hydrogen peroxide nitrosodimethylaniline 888
Radiolysis liq nitrous oxide 28 32
Radiolysis naphthalene singlet triplet 22
Radiolysis nitrous oxide hydrocarbon 102
Radiolysis nitrous oxide xenon 954
Radiolysis oxyphosphorus oxysulfur 576
Radiolysis pentane kinetics 508
Radiolysis perfluorocyclohexane radical scavenger 360
Radiolysis potassium hydroxylaminedisulfonate 375
Radiolysis pulse ferrocyanide ferricyanide 1368
Radiolysis pulse peptide 1790
Radiolytic polarog hydroxycyclohexadienyl radical deriv 160
Radius atomic element 115 1945
Raman alkali nitrate liq ammonia 708
Raman ammonia alk earth salt 143
Raman *ammonia benzene* soln 2106
Raman borane trimethylamine 1503
Raman cadmium chloro coordination 595
Raman iodide iodine soln 2306
Raman lanthanum potassium chloride melt 1134
Raman laser absorption oxide 300
Raman lithium fluoride hexafluoroaluminate 1499
Raman magnesium sulfate aq 246
Raman water structure temp 1304
Rate collisional reaction temp 1773
Rate heating transition temp 2673
Rayon morphol ESR 308
Reaction coordinate isotope effect 544
Reaction electrochem furanquinone solvent 1714
Reaction equil nonequil wetting 1178
Reaction kinetics hydroxyl ozone 1447
Reaction kinetics positronium nitrobenzene 1881
Reaction rate const polaron 2631
Reaction vaporization kinetics 1298
Reactivity oxirane acrolein MO 1874
Reactor flow analysis oxygen 208
Rearrangement quinone hydrogen migration 1820
Reciprocal molten salt miscibility calcn 1091
Recoil tritium reaction dimethylcyclopropanes 2531
Recombination disproportionation cyclopentyl radical 462
Recombination hydrogen atom wall 465
Recombination ion triplet polemic 309 310
Recombination kinetics iodine atom 878
Redn azobenzene Hammett const 1825
Redn naphthocyclobutene alkali metal 723
Redn nitrogen heterocycle kinetics 2615
Redn silver catalytic ferrous 2580
Redn thallium chloro complex 892
Redox hydroxycyclohexadienyl deriv 160
Redox potential thioamide solvent 1018
Redox rhodium dipyridyl complex 727
Reflectance spectra metachromatic dye 1040
Reflectance spectra phosphor powder 2229
Reflection IR adsorbed layer 941
Reflection IR alkali halide 238
Reflection IR aq electrolyte 1405
Refraction alkali halide aq 238
Refraction skeletonized film 947
Refractive index aq electrolytes 1405
Relaxation anisotropic rotational ESR 1324
Relaxation dielec liq acetate 1078
Relaxation elec cond 1210
Relaxation elec molten salt 639
Relaxation ESR methylpentane irradn 2233
Relaxation magnetic Fourier transform 1971
Relaxation magnetic hydrophobic hydration 1002
Relaxation polaron alc visible spectra 393
Relaxation time water pressure 1674
Relaxation ultrasonic yttrium nitrate 261
Relaxation ultrasound methyl purine 848
Relaxation vibrational fluoro acetone 679
Response tubular electrode 718
Retinal photoisomerization triplet state 336
Reverse osmosis membrane thickness 2259
Review information explosion 1339
Rhodamine B radiolysis chemiluminescence 1251
Rhodamine dimer fluorescence 380
Rhodamine dye dimerization kinetics 1891
Rhodamine 6G triplet ESR 2006
Rhodium ammine complex photoaquation 1144
Rhodium complexes photochem 2698
Rhodium dipyridyl complex voltammetry 727
Ring cleavage cyclopentyl methylcyclobutyl 1573
Rotary Brownian motion fluorescence 387
Rotation barrier benzophenone ketyl 2144
Rotation barrier borane trimethylamine 1503
Rotation barrier ESR fluoroalkyl 2014
Rotation barrier hexafluoroethane 2389
Rotation barrier thiourea ditertbutyl 961
Rotation duroquinol radical ESR 130
Rotation ethylamine potential internal 803
Rotation vibration formaldehyde 2270
Rotational anisotropic relaxation ESR 1324
Rotational correlation time estn 1321
Rotational excitation imidogen photolysis 1784
Rubidium 87 quadrupolar relaxation 1002
Ruthenium bipyridine complex phosphorescence quenching 1374
Ruthenium bipyridine sensitized phosphorescence 541
Ruthenium halo ammine EPR 700
Rutile dissocn nitrous oxide 870
Safety chloromethyl methyl ether 2696
Safety sodium hydroxide storage 1701
Salicylate caffeine complex thermodn 1922
Salt frozen aq soln NMR 807
Salt molten elec relaxation 639
Salt molten reciprocal miscibility calcn 1091
Salt soln heat mixing 1924
Salt soln transfer compressibility calcn 2367
Satn recovery theory ESR 1155
Scattering potassium bromide excited 2438
Scavenger radical perfluorocyclohexane radiolysis 360
Scavenging electron alc radiolysis 504
Scavenging electron liq neopentane 853
Scavenging electron methylpentane glass 2696
Scavenging radical cyclohexane radiolysis 366
Science publishing literature review 1339
Seed crystal hydroxyapatite growth 2218
Selectivity solvent polystyrenesulfonate exchanger 411
Selenide hydrogen force field 989
Selenium dioxide force field 989
Semiconductor perylene complex 215
Semicontinuum model polaron alc 393
Semiquinone dipole interaction 2140
Serum albumin monolayer viscosity pressure 2266
Shock dehydrofluorination trifluoroethane 472
Shock tube isomerization haloalkene 1469
Shock wave cyclopentene dehydrogenation 436
Significant structure theory multilayer adsorption 2600
Silane acetylene ion mol reaction 2645
Silane hydrogen transfer 2195
Silane hydrolysis polemic 757
Silane ion mol reaction 1184
Silane methyl hydride transfer 2429
Silica adsorption nitroxide EPR 2110
Silica alumina adsorbed nitroxide 200
Silica diazine adsorption IR 2376
Silica gel irradn halomethane 1391
Silica IR butylamine adsorbed 704
Silica NMR mol adsorbed 38
Silver complex nitric oxide 1174
Silver contact angle water 87
Silver diethyl phosphate ESR 958
Silver halide soly oxazolidone 1817
Silver iodide complex soly 2244
Silver reaction chlorine 107
Silver redn catalytic ferrous 2580
Simulation electrochem ESR kinetics detn 290
Simulation model tubular electrode 718
Singlet ketonorbornane photochemistry 2637
Singlet oxygen biol oxidn 1681
Singlet triplet naphthalene radiolysis 22
Singlet triplet sepn helium 1334
Size distribution chromium oxide 2621
Size effect micellization 2469
Skeletonized film optical property 947
Soap film bursting drag 1949
Sodium calcium fluoride enthalpy 1478
Sodium cation exchange heat 152
Sodium chloride aq compressibility 1636
Sodium chloride soln diffusion 2292
Sodium chloride soln heat mixing 77 1924
Sodium chloride vaporization rate 1998
Sodium dodecyl sulfate film bursting 234
Sodium hydroxide bromide enthalpy soln 1509
Sodium hydroxide hydrate thermodn storage 1701
Sodium hydroxide IR reflection 1405
Sodium ion diffusion gel 735
Sodium ion exchange 1150
Sodium laurate adsorption electrode 941
Sodium laurate potentiometry acid 2626
Sodium liq diffusion 2275
Sodium metaphosphate irradn ion 752
Sodium polyacrylate diffusion chloride 1756
Sodium sulfate soln heat mixing 1924
Sodium *transport* cation *membrane* 1805
Sodium zeolite structure grinding 1959
Sodium zinc cation exchange equil 1110
Solid adsorption carbon 622
Solid powder photochem reaction rate 1265
Soln alkali chloride ion 2576
Soln entropy nonaq ionic 1000
Soln heat alkylamine hydrobromide 1217
Soln heat ammonium halide analog 738
Soln heat complexation 1922
Soln heat model solvent effect 454
Soln micelle transfer heat 834
Soln structure supermol continuum 2064
Soln temp max density 2305
Soln thermodn phosphonium halide 738
Solute expansibility aq max density 1041
Solute solvent electrostatic potential 1853
Solute solvent statistical thermodn 2064
Solvated electron dioxane photolysis 2181
Solvated electron IR 2414
Solvated electron optical absorption 2631
Solvated electron reaction 796
Solvated electron spectra alc 514
Solvation alc nonpolar solvent dielec 1203
Solvation alk earth cation ammonia 143
Solvation alkali salt liq ammonia 708
Solvation ammonium ion ammonia 1482
Solvation chloride propylene carbonate 2521
Solvation cholesterol dimerization NMR 250
Solvation coordination ion 1731
Solvation electron alc amine 792
Solvation ion methanol 627
Solvation ion org solvent cond 556
Solvation ion Walden product 907
Solvent compn mixt Walden product 907
Solvent effect assocn alc 529
Solvent effect cyanine isomerization 16
Solvent effect heat soln model 454
Solvent effect org electron transfer 285
Solvent effect tetramethylphenylenediamine photoionization 2128
Solvent fluorescence lifetime aminopyridine 201
Solvent polyisobutylene interaction parameter 60
Solvent solute electrostatic potential 1853
Solvent solute statistical thermodn 2064
Solvent thioamide redox potential 1018
Solvent uptake cation exchanger 411
Solvophobic interaction alkane 175
Soly fatty acid potentiometry 2626
Soly hydrocarbon liq sulfur 2635
Soly product fatty acid potentiometry 2626
Soly silver halide oxazolidone 1817
Soly water pentanol 652
Sound absorption aq acetate 1913
Spectra copper complex model 1235
Spectroscopic const bromine chloride 1833
Spectroscopy time domain dielec 1440
Spectrum arom ketone anion 1473
Spectrum hydrogen bond isotope effect 429
Spectrum pyridinyl radical 2211
Spectrum thallium chloro complex 892
Spin density nitroxide 1313
Spin electron polarization hydrogen 1336
Spin lattice relaxation time 1971
Spin orbit octahedral ligand field 56
Spinel cobalt chemisorption oxide vapor 2490
Splitting zero field benzocarbazole 692
Stability double bond 2569
Stannate tetramethylammonium hydrogen bond 2585

Statistical thermodn liq water 1531
Statistical thermodn solute solvent 2064
Statistics Monte Carlo micelle 1423
Stearate barium film ellipsometry 947
Stereochem halogen exchange dichlorobutane 1043
Sticking coeff multilayer adsorption 748
Stopped flow kinetics fast reaction 305
Streaming potential potassium chloride 2302
Stretching frequency dimethyl disulfide 1848
Strontium effect hydroxylapatite dissoln 1273
Structure dealuminated zeolite 1550
Structure electronic dihydrogen disulfide 1554
Structure electronic MO calcn 763
Structure gas electron diffraction 2380
Structure liq water 1531
Structure mol diffusion heptane isomer 1428
Structure mol force field 989
Structure mol hexafluoroethane 2389
Structure mol spectra polaron 514
Structure thallium exchanged zeolite 2395
Structure transformation zeolite grinding 1959
Structure water dimer 2055
Structure water Raman temp 1304
Styrenesulfonate polymer exchanger 411
Sublimation energy element 115 1945
Substitution amine hydroxide copper 305
Substitution dichlorodifluoroethane stereochem 658
Sucrose effect water structure 1754
Sucrose soln heat mixing 2465
Sugar acetylamino CD 1829
Sulfate dodecyl positronium lifetime 2526
Sulfate lithium surface ionization 820
Sulfate magnesium aq compressibility 1636
Sulfate magnesium ion pair 246
Sulfate magnesium ion pair aq 1287
Sulfate sodium soln heat mixing 1924
Sulfide carbon dissocn 634
Sulfide carbonyl reaction sulfur atom 1137
Sulfide hydrogen MO 1554
Sulfide phosphine trialkoxy iodine 1657
Sulfide transition insertion compd 2399
Sulfonate fluoromethyl ammonium vaporization 1433
Sulfonate polyvinyl counterion binding 1013
Sulfonephthalein ionization isotope effect 1021
Sulforhodamine dimer phosphorescence 380
Sulfoxide acid hydrogen bonding 1662
Sulfoxide dimethyl enthalpy transfer 1509
Sulfoxide methyl iodine electronic 1744
Sulfoxide methyl radical ESR 1882
Sulfoxide methyl water exchange 411
Sulfur arom flash photolysis polemic 1441 1442
Sulfur atom reaction carbonyl sulfide 1137
Sulfur compd mol force field 989
Sulfur dioxide acetylene photolysis 325
Sulfur dioxide adsorption zeolite 218
Sulfur dioxide ammonia thermodn dissocn 1378
Sulfur dioxide reaction ozone 1775
Sulfur hexafluoride cyclohexane photolysis 1899
Sulfur hexafluoride electron capture 954
Sulfur hydrogen bonding energy 1415
Sulfur liq dielec const 1670
Sulfur liq hydrocarbon soly 2635
Sulfur oxide chemiluminescent reaction 1248
Sulfur oxide ion EPR 649
Sulfur 35 hot atom 372
Sulide hydrogen dimethylsilane photolysis 203
Supermol continuum soln structure 2064
Superoxide catalysis nitrite oxidn 1693
Superoxide ESR alkali nitrate melt 1294
Surface acidity Raman detn 300
Surface active soln positronium lifetime 2526
Surface desorption kinetics 1298
Surface elec potential polyelectrolyte 1189
Surface ionization lithium anion 820
Surface pressure albumin monolayer 2266
Surface reaction kinetics detn NMR 1279
Surface tension water gas adsorption 2262
Surfactant film bursting purity 234
Surfactant ionic micelle structure 2480
Surfactant micelle assocn kinetics 1024
Surfactant micellization free energy 1086
Surfactant water microemulsion IR NMR 256
Susceptibility copper complex model 1235
Temp crit fluid intermol energy 1241
Temp max density soln 2305
Temp rate collisional reaction 1773
Temp transition heating rate 2673
Terminal alkene heat hydrogenation 2569
Ternary electrolyte soln diffusion 2292
Ternary system diffusion 2281
Terphenyl fluorescence quenching chloride 2555
Tetraalkylammonium activity coeff 1197
Tetrachloroaluminate potassium Raman cadmium 595
Tetrachloromanganate EPR fused salt 1957
Tetrafluoride carbon collision radical 850
Tetragonal energy matrix CI 2678
Tetrahydroanthracene EPR 692
Tetramethylammonium ion diffusion gel 735
Tetramethylphenylenediamine photoionization dielec liq 2128
Tetraphenylboride activity diffusion 1667
Thallium exchanged zeolite structure 2395
Thallium 2 chloro complex 892
Thallium 2 reaction aq soln 488
Thermal decompn chlorate perchlorate 773
Thermal decompn cupric formate 2664
Thermal decompn lead azide 478
Thermal decompn lithium perchlorate 776
Thermal diffusion binary gas 1564
Thermodn cation exchange unequal charge 1110
Thermodn dissocn ammonia sulfur dioxide 1378
Thermodn electrolyte mixing 1927
Thermodn electrolytes 2698
Thermodn gas electron diffraction 2380
Thermodn mixing fluoroacetic acid 1709
Thermodn statistical liq water 1531
Thermodn trialkoxyphosphine chalcogenide iodine 1657
Thermoosmosis ternary mixt 2693
THF lithium perchlorate cond 917
THF nitrofluorenone photocond 1395
THF water hydrogen bond 1727
Thiacarbocyanine dye isomerization 16
Thiacarbocyanine dye stereoisomer 2355
Thioamide solvent redox potential 1018
Thiocyanate alkali liq ammonia Raman 708
Thiocyanate fluorescence quenching fluoranthene 2555
Thiocyanate palladium oxalate ESR 2136
Thioformamide methyl solvent property 1018
Thiolate metal perylene complex 215
Thiourea ditertbutyl rotation barrier 961
Thorium radiation chemistry hydroperoxyl 2330
Time domain dielec response 1440
Titania photocatalysis oxygen exchange 555
Titanium oxide catalysis redn 2580
Titanium Y zeolite ESR 218
Toluene cyclohexane film cathodoluminescence 2081
Toluene diffusion binary liq 2283 2307
Toluene fluorinated fluorescence 7
Tortuosity polymer membrane permeability 408
Transfer compressibility salt soln calcn 2367
Transfer electron quantum theory 2148
Transfer energy carborane radiolysis 788
Transfer enthalpy aq dimethyl sulfoxide 1509
Transfer enthalpy detn acid base 2363
Transfer heat soln micelle 834
Transient response tubular electrode 718
Transient triplet nitrostilbene photolysis 446
Transition heat salt hydrate 278
Transition metal catalysts 2254
Transition metal complex spectra 2678
Transition metal film oxidn 2486
Transition metal mol sieve catalyst 1653
Transition metal phosphorescence 2496
Transition polarization carbazole deriv 1512
Transition polarization disklike mol 1400
Transition state bond force const 544
Transition state collisional reaction 1773
Transition state enthalpy hydrolysis 1509
Transition state theory vaporization condensation 1298
Transition sulfide insertion compd 2399
Transition temp heating rate 2673
Transport heat ternary mixt 2693
Trap carbanion electron transfer 1135
Trapped electron EPR hydroxide 221
Trapped electron photobleaching alc glass 232
Trialkoxyphosphine chalcogenide iodine UV 1657
Trichloroethane dehydrochlorination mechanism 2166
Triethylethoxysilane polemic hydrolysis 757 758
Trifluoroethane dehydrofluorination shock 472
Trifluoroethanol assocn solvent effect 529
Triiodide configuration dil soln 2306
Trimethylamine borane IR Raman 1503
Trimethylenecyclopropane spectra photoproduct 568
Triple ion lithium perchlorate THF 917
Triplet equil arom hydrocarbon 196
Triplet ion recombination polemic 309 310
Triplet ketonorbornane photochemistry 2637
Triplet mechanism photoisomerization nitrostilbene 451
Triplet mercury quenching gas 482
Triplet Rhodamine 6G ESR 2006
Triplet singlet naphthalene radiolysis 22
Triplet singlet sepn helium 1334
Triplet state retinal photoisomerization 336
Triplet transient nitrostilbene photolysis 446
Tritium hot atom reaction 2186
Tritium recoil cyclohexene reaction 347
Tritium recoil methylcyclohexene reaction 354
Tritium recoil reaction dimethylcyclopropanes 2531
Tritium substitution dichlorodifluoroethane 658
Tryptophan carbonate radical reaction 2099
Tubular electrode simulation model 718
Tungsten vanadium oxide vaporization 266
Two photon photolysis 1583
Ultrasonic absorption AMP soln 80
Ultrasonic relaxation yttrium nitrate 261
Ultrasound absorption aq acetate 1913
Ultrasound absorption electrolyte methanol 627
Ultrasound alc assocn 529
Ultrasound erbium perchlorate 1940
Ultrasound ion molal vol org solvent 1099
Ultrasound lithium perchlorate THF 917
Ultrasound propagation DMSO water 2611
Ultrasound relaxation methyl purine 848
Unimol kinetics pressure dependence 2326
Uracil radical ESR 696
Uranium dioxide carbon IR 2117
Uranium oxide fluorination 1140
Uranium radiation chemistry hydroperoxyl 2330
Urea effect water structure 1754
Urea heat diln 2460
Urea nitrogen 15 NMR 2507
Urea polyoxyethylene NMR 1528
Urea soln heat mixing 2465
Urethane nitrogen 15 NMR 2507
UV absorption disklike mol 1400
UV alumina diazine adsorption 2376
UV arom halogen radiolysis 519
UV carbazole deriv 1512
UV charge transfer complex 980
UV copper complex 811
UV dihydrogen disulfide 1554
UV fluoranthene assocn org solvent 1330
UV hydroxymethylperoxy radical 2089
UV mass dicyclohexyldithiophosphinate metal 962
UV max disulfide correlation UV 855
UV nitrobenzene deriv 494
UV nitrostyrene 49
UV photolysis nitric acid vapor 1
UV potassium nitrosodisulfonate radical 375
UV trialkoxyphosphine chalcogenide iodine 1657
UV trimethylenecyclopropane photoproduct 568
Vacuum adsorption contact angle water 87
Valence sulfur potassium chloride 372
Vanadium oxide adsorbed sulfur dioxide 649
Vanadium oxydichloride cellulose ESR 308
Vanadium tungsten oxide vaporization 266
Vanadyl dicyclohexyldithiophosphinate electron structure 962
Vanadyl hectorite arom radical cation 994
Vapor concn mercury methanol 186
Vapor pressure dimethoxyazoxybenzene 275
Vaporization oxide mass spectroscopy 266
Vaporization rate alkali halide 1998
Vaporization reaction kinetics 1298
Vaporization reactive salt 1433
Vibration rotation formaldehyde 2270
Vibrational energy fluorinated methylbenzene decay 7
Vibrational frequency water cluster 1844
Vibrational relaxation fluoro acetone 679
Vinylcarbazole polymer fluorescence quenching 2009

Vinylpyridine gamma irradn 899
Virial coeff intermol energy fluid 1241
Virial coeff mercury polar org 186
Virial theorem mol force field 989
Viscosity binary liq 2283
Viscosity elec cond mixed solvent compn 907
Viscosity pentyl alc 652
Viscosity serum albumin monolayer 2266
Viscosity water quadrupole coupling 1674
Visible arom halogen radiolysis 519
Visible reflection solid dye 1040
Visible spectra halogenated acetone 665
Visible spectra ionic dye 380
Visible spectra polaron alc relaxation 393
Visible spectra radical anion 741
Visible spectra solvated electron 514
Vol molal aq lanthanide salt 1106
Vol molal ion org solvent 1099
Voltammetry rhodium dipyridyl complex 727
Volume mixing org compd 1961
Volume molal alkylamine hydrobromide 1217
Walden product ion solvation 907
Wall recombination hydrogen atom 465
Water adsorption zinc oxide 1116
Water cluster vibrational frequency 1844
Water contact angle copper silver 87
Water deuteron quadrupole coupling 1674
Water dimer energy structure 2055
Water DMSO ultrasound propagation 2611
Water exchange keratin zeolite 1279
Water hydrogen bond org 1723
Water intermol potential energy 909
Water liq statistical thermodn 1531
Water membrane ion partition 2259
Water orientation mercury electrode 1226
Water pentanol dielec const 652
Water Raman structure temp 1304
Water structure aq amine 714
Water structure electrolyte nonelectrolyte 170
Water structure frozen aq soln 807
Water structure IR halide 238
Water structure urea effect 1754
Water surface tension gas adsorption 2262
Water surfactant microemulsion IR NMR 256
Wave function MO calcn 763
Wetting reaction equil nonequil 1178
X irradn potassium hydroxylaminedisulfonate 375
X ray emission org chlorine 2592
Xanthyl radical ENDOR 2512
Xenon nitrous oxide radiolysis 954
Xylene fluorinated fluorescence 7
Yttrium nitrate ultrasonic relaxation 261
Zeeman effect formaldehyde 2270
Zeolite chlorine dioxide ESR 1770
Zeolite copper complex EPR 531
Zeolite dealuminated structure 1550
Zeolite keratin exchange water 1279
Zeolite methane absorption IR 2180
Zeolite nitroxide catalyst poisoning 2110
Zeolite silver nitrosyl IR 1174
Zeolite structure transformation grinding 1959
Zeolite thallium exchanged structure 2395
Zeolite transition metal catalyst 1653
Zeolite Y titanium ESR 218
Zero field splitting benzocarbazole 692
Zinc oxide adsorption water 1116
Zinc oxide catalysis 2303
Zinc sodium cation exchange equil 1110
Zirconium phosphate cation exchange 1150
Zirconium phosphate heat cation exchange 152
Zirconium phosphate ion exchange 1812

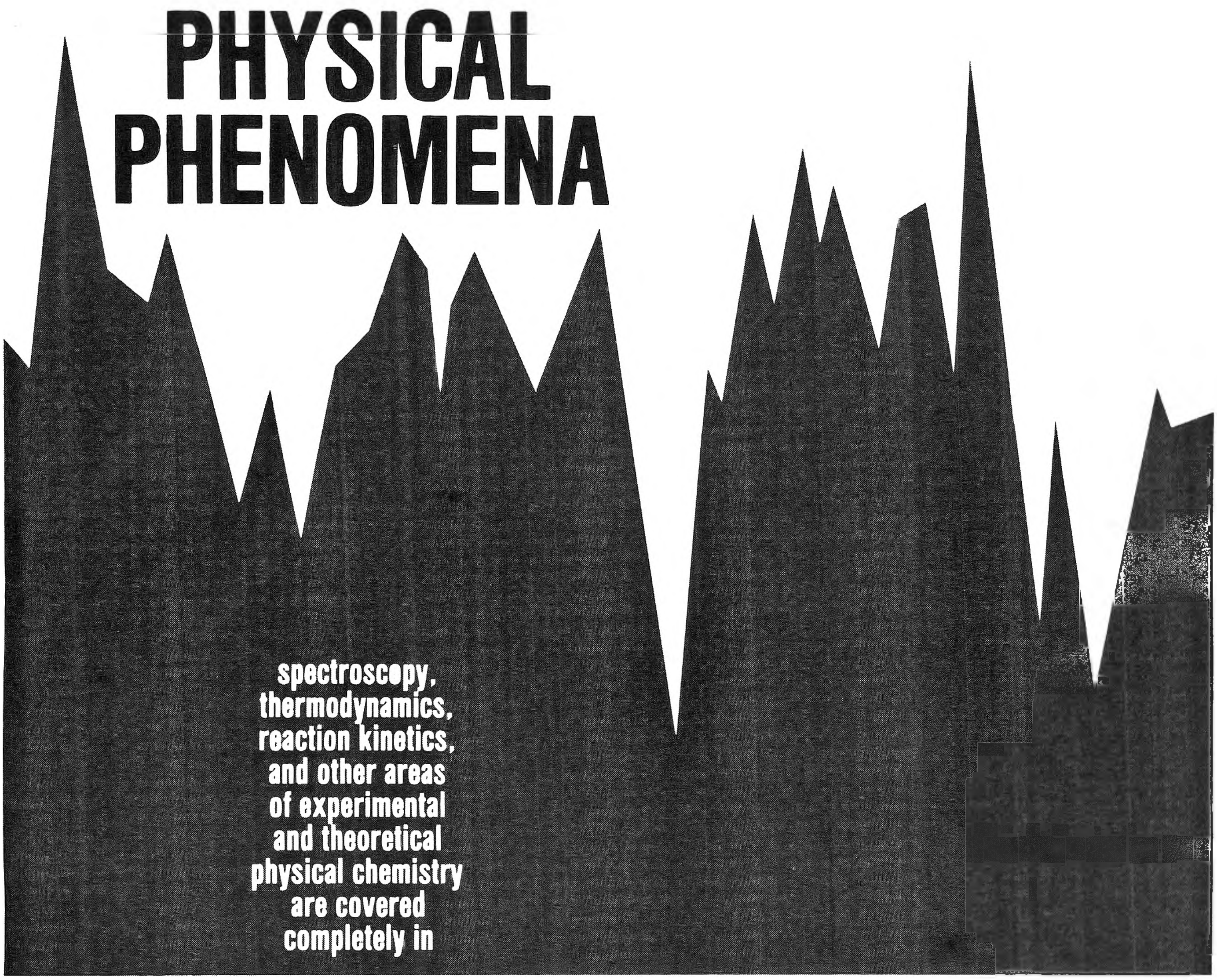
PHYSICAL
PHENOMENA
spectroscopy,
thermodynamics,
reaction kinetics,
and other areas
of experimental
and theoretical
physical chemistry
are covered
completely in

THE JOURNAL OF PHYSICAL CHEMISTRY

The biweekly JOURNAL OF PHYSICAL CHEMISTRY includes over 25 papers an issue of original research by many of the world's leading physical chemists. Articles, communications, and symposia cover new concepts, techniques, and interpretations. A "must" for those working in the field or interested in it, the JOURNAL OF PHYSICAL CHEMISTRY is essential for keeping current on this fast moving discipline. Complete and mail the coupon now to start your subscription to this important publication.

The Journal of Physical Chemistry
American Chemical Society
1155 Sixteenth Street, N.W.
Washington, D.C. 20036

1975

Yes, I would like to receive the JOURNAL OF PHYSICAL CHEMISTRY at the one-year rate checked below:

	U.S.	*Canada***	*Latin America***	*Other Nations***
ACS Member One-Year Rate*	☐ $20.00	☐ $24.50	☐ $24.50	☐ $25.00
Nonmember	☐ $80.00	☐ $84.50	☐ $84.50	☐ $85.00

Bill me ☐ Bill company ☐ Payment enclosed ☐

Air freight rates available on request

Name

Street Home ☐ Business ☐

City State Zip

Journal subscriptions start on January '75

*NOTE: Subscriptions at ACS member rates are for personal use only. **Payment must be made in U.S. currency, by international money order, UNESCO coupons, U.S. bank draft, or order through your book dealer.

Chemical Reaction Engineering—II

ADVANCES IN CHEMISTRY SERIES No. 133

A symposium co-sponsored by the American Chemical Society, the American Institute of Chemical Engineers, the Canadian Society for Chemical Engineering, and the European Federation of Chemical Engineering.

Here's an excellent source to bring you up-to-date on the continually changing state of the art in chemical reaction engineering. Fifty-one contributed papers concentrate on direct process applications and outline specific current processes and reaction types.

Subject areas include:

- novel reactor types; physical processes
- kinetics and mechanisms; heterogeneous catalytic reactors
- design models; optimal policies of operation; and more

698 pages (1974) Cloth bound $35.00. Postpaid in U.S. and Canada, plus 40 cents elsewhere.

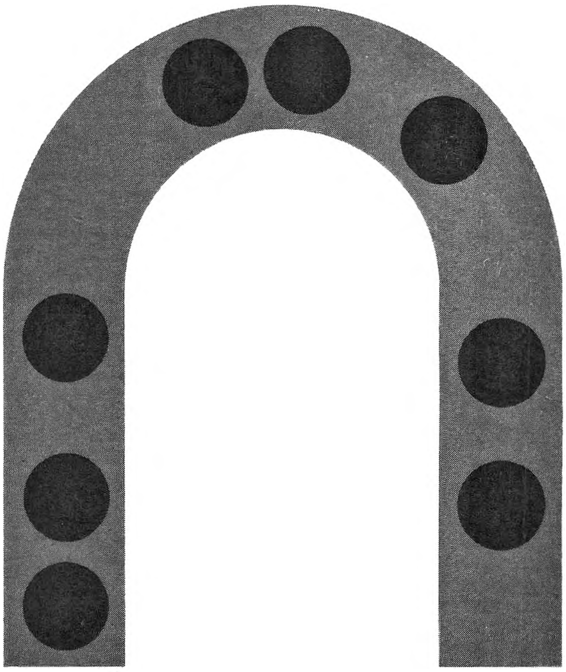

Other ACS books on chemical engineering include:

Annual Reviews of Industrial and Engineering Chemistry, Vol. 2
Fifteen reviews survey current work in industrial and engineering chemistry, focusing on new subject areas such as crystallization from melts, continuous crystallization from solution, chemical thermodynamics, and synthetic fibers. Ten topics are continued from Vol. 1. Over 5,600 references.
537 pages. Cloth. (1972) $19.95

Applied Kinetics and Chemical Reaction Engineering
Fifteen articles survey the application of kinetics to phenomena involved in a chemical conversion process and the synthesis of a descriptive, theoretical framework suitable for design, control, and optimization of a reaction. Topics include mixing and contacting, surface catalysis, photochemical reactions, oscillating reactions, turbulent heat transfer and others.
224 pages. Cloth. (1967) $7.50, plus 25¢ in Canada, PUAS, 40¢ foreign.

No. 121 Molecular Sieves
Fifty-five papers from the Third International Conference on Molecular Sieves report on scientific and industrial progress in five sections: structure, crystallization, ion exchange and modification, sorption, and catalysis.

No. 118 Chemical Engineering in Medicine
Seventeen papers focus on such topics as blood oxygenation, inert gas exchange, oxygen transport in the brain, pharmacokinetics, infant oxygenators, thermal control, erythropoiesis blood gas partial pressures, placental oxygen transfer, and placental glucose metabolism.
365 pages. Cloth. (1973) $16.75

No. 109 Chemical Reaction Engineering
Fixed and fluid bed reactors, polymerization kinetics and reactor design, optimization of reactor performance, catalysis in gas-solid surface reactions, two-phase and slurry reactors, industrial process kinetics, and transient operation.
685 pages. Cloth. (1972) $16.50

No. 105 Anaerobic Biological Treatment Processes
Nine papers survey the state of the art of this natural process for waste treatment, with three papers on methane fermentation, others on process control and design. Considers volatile acid formation, toxicity, synergism, antagonism, pH control, heavy metals, light metal cations.
196 pages. Cloth. (1971) $9.00

No. 89 Isotope Effects in Chemical Processes
Methods of separating isotopes and labeled molecules—chemical exchange, electromigration, photochemical processes, and distillation—are examined, along with factors that suit a process to isotope separation—single stage fractionation, exchange rate, and reflux.
278 pages. Cloth. (1969) $13.00

No. 80 Chemical Reactions in Electrical Discharges
A wide range of topics is covered in 37 papers by chemists, physicists, and engineers—treatments of decomposition and dissociation reactions, ion-molecule reactions, chemical syntheses, and chemical engineering aspects and physics of reactions in electrical discharges.
514 pages. Cloth. (1969) $15.00

Order from: **Special Issues Sales/American Chemical Society**
1155 Sixteenth Street, N.W., Washington, D.C. 20036